UNIVERSITY OF TURIN

Phd School in life and Health Sciences
Molecular Medicine

**The blood-brain barrier/glioblastoma stem cells interaction
is a key factor determining tumor chemoresistance:
new therapeutic strategies to improve the pharmacological
treatment of glioblastoma multiforme**

Iris Chiara Salaroglio

UNIVERSITY OF TURIN
Department of Oncology

Phd School in life and Health Sciences
Molecular Medicine
XXIX Cycle
Academic Years: 2014-2017

**The blood-brain barrier/glioblastoma stem cells interaction
is a key factor determining tumor chemoresistance:
new therapeutic strategies to improve the pharmacological
treatment of glioblastoma multiforme**

Tutor: Prof.ssa Chiara Riganti   Candidata: Iris Chiara Salaroglio

Coordinator: Prof. Francesco Novelli

ABSTRACT

Glioblastoma Multiforme (GB) is a central nervous system tumor with high aggressiveness and chemoresistance due to the presence of cancer stem cells (SCs). Low delivery of many anticancer drugs across the blood–brain barrier (BBB) further limits the success of chemotherapy in GB. This is because of the presence of tight junctions (TJs) and the high levels of ATP-binding cassette transporters like P-glycoprotein (Pgp/ABCB1), which effluxes drugs back to the bloodstream.

In the first part of thesis, I investigated if the 'canonical' Wnt pathway (Wnt/GSK3β/β-catenin axis), and the 'non-canonical' Wnt pathway (Wnt/RhoA/RhoAK axis) cooperate to control the expression of Pgp in BBB cells. By analyzing human primary brain microvascular endothelial cells constitutively activated for RhoA, silenced for RhoA or treated with the RhoAK inhibitor Y27632, I found that RhoAK phosphorylated and activated the protein tyrosine phosphatase 1B (PTP1B), which dephosphorylated tyrosine 216 of GSK3β, decreasing inhibition of β-catenin. By contrast, the inhibition of RhoA/RhoAK axis prevented the activation of PTP1B, enhanced the GSK3β -induced phosphorylation and ubiquitination of β-catenin, reduced the β-catenin-driven transcription of Pgp. RhoAK inhibition increased the delivery of Pgp substrates like doxorubicin across the BBB and improved doxorubicin efficacy against GB cells co-cultured under BBB monolayer. These data demonstrate that in human BBB cells the expression of Pgp is controlled by a crosstalk between canonical and non-canonical Wnt pathways.

Temozolomide (TMZ), the first line GB chemotherapy, crosses the BBB but its effects on BBB cells permeability and Pgp activity are not known. I found that TMZ, at therapeutic concentration, increased the transport of Pgp substrates across BBB cells and decreased the expression of Pgp. By methylating the promoter of *Wnt3* gene, TMZ decreased the synthesis of Wnt3 in BBB cells, disrupting the Wnt3/GSK3β/β-catenin signaling and reducing the binding of β-catenin on the promoter of *mdr1* gene, which encodes for Pgp. In co-culture models of BBB cells and human GB cells, pre-treatment with TMZ increased the delivery, cytotoxicity, and antiproliferative effects of doxorubicin, vinblastine, and topotecan, three substrates of Pgp that are usually poorly delivered across BBB. Thus, TMZ increases the BBB permeability of drugs that are normally effluxed by Pgp back to the bloodstream, opening the way to new combinatorial chemotherapy schemes in GB.

BBB is disrupted in presence of GB but it has never been investigated whether the grade of differentiation/or stemmness of GB cells at the tumor-BBB interface influences the permeability of BBB cells. To address this issue, in the second part of my thesis I set co-culture of BBB cells in the absence or presence of GB cells, cultured as SCs and as differentiated cells (AC). GB cells co-cultured with BBB increased the permeability to doxorubicin and dextran-70, indexes of Pgp and TJs functions, respect to BBB cells cultured alone. This effect was stronger with GB AC than with GB SCs and was due to changes in the expression of Pgp and TJ proteins. Also conditioned medium obtained from GB cell cultures induced increased doxorubicin and dextran-70. AC-conditioned medium was more effective than SC-conditioned medium. Of note, GB AC clones stably overexpressing Wnt3a acquired stemness properties and modified BBB permeability as GB SCs. This work suggests that the degree of GB cells differentiation or stemness modulates BBB permeability and that soluble Wnt3a may be a key actor in this process. GB AC produces a leaker BBB than GB SCs. This feature may explain the great difficulty encountered by chemotherapy to fully eradicate SC-enriched GB.

The presence of Pgp in both BBB and GB SCs dramatically reduces the success of chemotherapy against this tumor, limiting the therapeutic efficacy of chemotherapy in eradicating GB SCs.

Finding effective and safe inhibitors of Pgp that improve drug delivery across BBB and target GB SCs is still an open field.

In the last part of my thesis, I analyzed new types of molecules or formulations able to inhibit Pgp on BBB cells and/or GB cells: thiosemicarbazones compounds, carbonic anhydrase XII (CAXII) inhibitors and SLN-carried drugs.

I investigated the efficacy of three thiosemicarbazone derivatives in bypassing the Pgp-mediated drug efflux in primary human BBB cells. At 10 nM concentration, the compounds were not cytotoxic for BBB cells, but they significantly increased the permeability of the Pgp-substrate doxorubicin across BBB monolayer. Thiosemicarbazone derivatives increased doxorubicin uptake in GB grown under BBB monolayer, with greater effects in the Pgp-rich SCs clones than in the differentiated clones derived from the same tumor. All the compounds increased intratumor doxorubicin delivery and cytotoxicity in BBB-GB co-cultures, producing a significant killing of GB SC.

CAXII protein maintains optimum Pgp activity and is specifically expressed in drug-resistant solid tumors. I found that CAXII had higher expression in SCs than in AC. Selective CAXII inhibitors reduced Pgp activity, as the last-generation direct Pgp inhibitor tariquidar. Co-treatment of GB SCs with CAXII inhibitor and TMZ as well as a range of different second-line chemotherapeutic drugs for GB treatment, substrates of Pgp, restored the intracellular retention and cytotoxicity of the drugs. Furthermore, CAXII-knocked out SCs became as sensitive as AC to TMZ, indicating that CAXII plays a crucial role in TMZ resistance. The strongest CAXII inhibitor of the library tested, compound **1 -** at nanomolar concentration - rescued the efficacy of TMZ in orthotopic models of primary GB derived from SCs of patients resistant to TMZ, without detectable signs of systemic toxicity. These findings suggest new combinatorial chemotherapy schemes in GB to eradicate SCs.

To improve the drug transport across BBB, I finally employed solid lipidic nanoparticles (SLNs) conjugated with ApoE chimeric peptide binding ApoE-receptor that is abundant on BBB cells. Preliminary biodistribution experiments showed that these ApoE-SLNs loaded with a methotrexate derivative, a drug that does not cross BBB, enhanced the drug brain accumulation *in vivo* and decreased the growth of ortrotopically implanted gliomas, resistant to TMZ.

Overall, the three approaches used - thiosemicarbazone compounds, CAXII inhibitors and SLNs functionalized with ApoE - can be proposed as adjuvant tools in new combinatorial treatments to eradicate GB, in particular the stemmness component that expresses Pgp and is resistant to chemotherapuetic drugs, including TMZ.

1. INTRODUCTION

1.1 Glioblastoma multiforme

The word 'glioma' comprises all forms of tumor that have a glial cell origin. Each year, about 5–6 cases out of 100,000 people are diagnosed with primary central nervous system (CNS) tumors, of which about 80% are malignant gliomas [Alifieris, 2015]. Gliomas include astrocytomas, oligodendroglioma, ependymomas and mixed gliomas, graded from I to IV by World Health Organization (WHO) classification, based on histological features, cell type origins, prognostic and survival factors, degree of malignancy. Glioblastoma multiforme (GB) is classified as IV/IV grade tumor [Brown, 2016].

GB is considered the most common, aggressive and lethal brain tumor in adult due to high degree of tumor cell infiltration into surrounding brain tissue. GB usually occurs within the white matter in the form of heterogeneous lesion, but it spreads rapidly into the surrounding brain tissue [Ellor, 2014]. While 90%–95% of GBs develops *de novo* (primary glioblastoma multiforme), 5%–10% is the result of the malignant progression from a low-grade glioma (secondary glioblastoma multiforme). Primary and secondary GBs have a similar morphology, despite the different molecular pathways beyond their developments [Kim, 2015].

The mean age of primary and secondary GB patients is 62 and 45, respectively, although there is a greater variation in age distribution within the secondary type. Primary GB is rarely seen in younger patients, constituting only 8.8% of all childhood CNS tumors. GBs of children and adults do not usually show morphological differences; the only difference is the proliferative activity of the glioma cells, which is higher in children. Primary GB develops more frequently in males than in females (M:F ratio = 3:1), whereas for secondary GB there is the opposite trend [Urbanska, 2014].

The exact etiology of GB has not been clarified up to now. GB is expected to be a spontaneous tumor, although 1% of all GB cases can be associated with familial form. The potential risk factors for glioma are not well understood but exposure to ionizing radiation, electromagnetic fields and certain metals, as well as some pesticides, polycyclic aromatic compounds and solvents, can increase the likelihood of developing GB [Alifieris, 2015].

Unfortunately, even when treated, the tumor tends to spread rapidly and to recur, resulting in a very poor prognosis. GB is an incurable malignancy, wherein the median survival of patients is about 18 months [Carlsson, 2014]. Only 30% of patients achieve 2- year survival and fewer than 10% survive more than 3 years. Exceptionally, a small number of patients can survive for a longer period [Auffinger, 2015]. According to a population-based study, survival rates do not differ between men and women, but they are higher for younger patients and in patients diagnosed for more than 2 years compared with newly diagnosed patients. The risk of death is higher during the first quarter of the second year of GB post-diagnosis, whereas the mortality decreases to half of its rate at 2.5 years [Thakkar, 2014].

1.2 Glioblastoma multiforme therapy

GB standard therapy involves surgical resection, followed by radiotherapy plus concomitant chemotherapy with temozolomide (TMZ).

Surgical resection occurs within few days after diagnosis and requires a craniotomy to removes as much of the tumor as possible. The surgery usually alleviates symptoms, decreases the dependence of corticosteroids and can extend patients' survival. However, it cannot remove the entire tumor, because of GB infiltrating property. Some GB cells extend several centimeters into the surrounding brain tissue, inducing GB recurrence.

Radiation helps eradicate these cells: standard radiotheraphy regimen includes fractionated focal irradiation in daily fractions of 2 Gray units (Gy), five times a week for 6 weeks (30 treatment days in total), for a total irradiation charge of 60 Gy. During these 6 weeks, the patient simultaneously receives daily TMZ (Temodar) at a dosage of 75 mg/m^2/day [Anjum, 2017].

The treatment with TMZ, in association with radiotherapy, provides the highest median survival time in patients from 12.1 to 14.6 months and an increase in the 2-year survival rate from 10% to 27% than other alkylating agents such as carboplatin, procarbazine, carmustine and lomustine. Until 1970, these alkylating agents were used as first line agents in GB treatment, but their use was suspended for their toxicity and inferior results when compared with TMZ [Urbanska, 2014]. Radiotherapy facilitates the passage of TMZ through the blood-brain barrier (BBB) and promotes the spontaneous conversion of the drug into the active metabolite [Stupp, 2010]. In addition radiotherapy reduces the DNA-repair enzyme O^6 methylguanine-DNA methyltransferase (MGMT), increasing the long term survival rate of patients [Tolcher, 2003].

After these cycles of radio/chemiotherapy the patients, 4 weeks later, enter a maintenance phase which consists of 6 cycles of TMZ: 150-200 mg/m^2/day of TMZ for 5 days, followed by 23 days of drug suspension, with a 28 days cycle [Anjum, 2017].

1.2.1 Temozolomide

TMZ is an alkylating agent prodrug, able to cross the BBB, easy to administrate (oral and injectable form) and well tolerable. Once it is converted into its active metabolite 5-(3-methyltriazen-1-yl)-imidazole-4-carboxamide (MTIC), TMZ methylates O^6 on guanine with the formation of O^6-methylguanine (O^{6}MeG) in DNA, leading to subsequent DNA damage, tumor cell G2/M phase arrest and cell death [Anjum, 2017] (Figure 1).

TMZ, despite its lipophilic properties and small molecular size (194 Da), has 20% penetration across the normal BBB, due to its short half-life and to efflux mechanisms on BBB. For this reason, TMZ requires high systemic doses to reach therapeutic levels in the brain [Hendricks, 2015]. Although generally well-tolerated, there are evidences that TMZ can cause nerve damage, nausea, hair loss, vomiting, infertility, diarrhea, skin rash, myelosuppression, irreversible thrombocytopenia, aplastic anaemia, and even death, raising some concerns about its use [Alifieris, 2015].
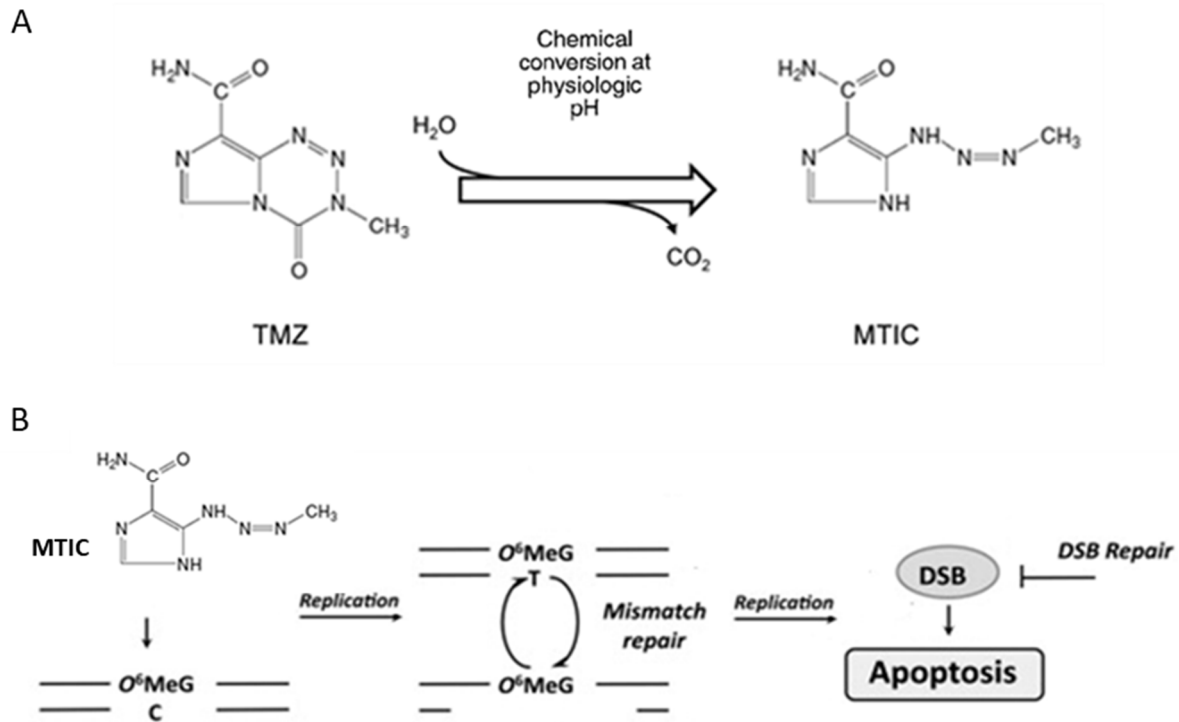
Figure 1. Structure and action of Temozolomide. A. Chemical structure of temozolomide (TMZ) that is converted into its metabolite 3-methyl-(triazen-1-yl)imidazole-4-carboxamide (MTIC). **B.** MTIC is the active metabolite that induces guanine methylation on O^6, determining a mismatch repair with thymine and consequent DNA damage, tumor cell G2/M phase arrest and cell death [Anjum, 2017]. DSB: double strand break.

1.3 Challenges in glioblastoma multiforme treatment

Despite advanced molecular and genetic knowledge in GB biology, the majority of successful preclinical therapies have failed to provide meaningful results when tested on GB patients. Since GB is a highly vascularized tumor, with a high proliferative activity and infiltrative nature a complete resection of the tumor through surgery is not possible. Radiotherapy and chemotherapy are not always efficient to completely eradicate tumor stem cells (SCs) that contribute to initiation, progression and recurrence of the tumor [Stupp, 2015; Pourgholi, 2016]. These cells show a multidrug resistance (MDR) phenotype that prevents cellular accumulation and efficacy of TMZ and other antineoplastic drugs. One of the main reasons for TMZ-resistance in GB SCs is the over-expression of O^6–methylguanine-DNA-methyltransferase (MGMT), which de-methylates guanine [Eramo, 2006]. Other known reasons for poor outcomes of TMZ treatment include altered activity of DNA-repairing systems, the persistence of cancer stem cell sub-populations, aberrant activation of cell survival and anti-apoptotic pathways, microenvironment factors such as hypoxic niches and/or niches rich of growth factors and showing protective autophagy mechanisms [Beier, 2011] (Figure 2).

In addition, GB is difficult to treat because of the presence of BBB, the natural barrier in the brain, and of the blood brain tumor barrier (BBTB) that tumor forms [Urbanska, 2014].

Inter- and intra-tumor heterogeneity, along with the presence of BBB and treatment resistance, make GB one of the most lethal tumors.
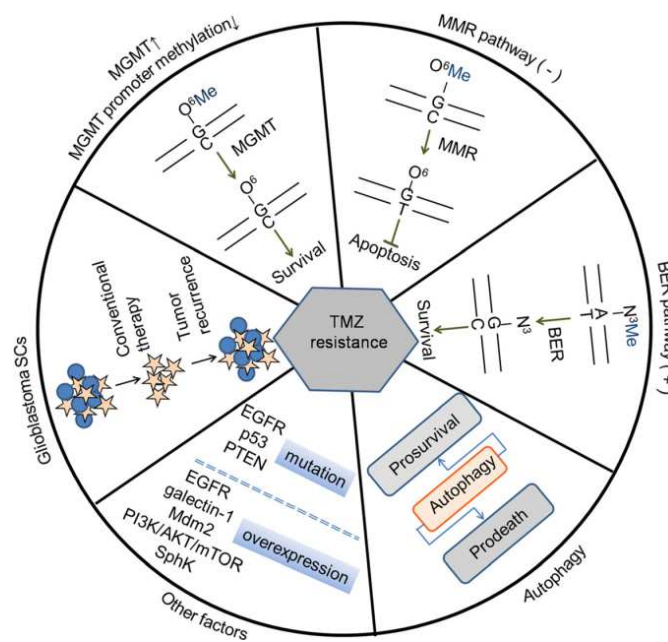
Figure 2. Schematic illustration of the most well known resistance mechanisms to TMZ in GB. Natural barriers, DNA repair mechanisms, deregulated signaling pathways, GB stem cells and autophagy induce resistance to TMZ, but also represent valuable targets for GB, enabling more specific and effective treatments [Miranda, 2017].

1.3.1 Cancer stem cells

The presence of SCs within GB is one of the main reasons for chemoresistance [Yamada, 2012]. GB SCs are believed to originate from the transformation of neural stem cells of the embryonic matrix and the neurogenic zones of the adult brain or from the dedifferentiation of hemispheric astrocytes or tumor cells. The latter reacquires stemness through embryonic regression upon the progressive accumulation of mutations [Shiffer, 2015].

GB SCs were isolated from adult human GB for the first time in 2004 by Galli and colleagues using the same isolation protocol of human neural stem cells. These cells grew in suspension as neurospheres (NS) and showed *in vitro* stem-cell characteristics such as extensive self-renewal, multipotency and the ability to differentiate in astrocytes, oligodendrocytes, neurons and even endothelial cells. Most importantly, they generate new tumors when transplanted into the striatum of adult immunodeficient mice [Galli, 2004].

GB SCs share with neural stem cells stemness antigens, such as CD133, Musashi1, Nestin, and Sox2, and share with primary tumors the same genetic alterations. Until now, it is known that activity of transforming growth factor/bone morphogenetic protein (TGF/BMP), Notch, Wnt, and sonic Hedgehog homolog pathways, are involved in self-renewal, proliferation, and invasion [Yang, 2015].

The molecular basis of chemoresistance in GB SCs is under intensive investigation. Some mechanisms of intrinsic resistance to chemotherapy are the (i) resistance to redox stress, (ii) the capacity to rapidly repair damaged DNA, (iii) the ability to adapt to a hyper-inflammatory or nutritional-stressing microenvironment, (iv) the ability of metabolic reprogramming, and (v) the ability to expel anticancer drugs through ATP-binding cassette transporters. These characteristics allow GB SCs to continue to differentiate into rapidly proliferating progenitor-like and more differentiated tumor cells and to be refractory to current treatment strategies [Yoshida, 2017].

Normal tissue stem cells are located within or adjacent to a microenvironment, known as the "niche," that is favorable for the maintenance of their stemness. GB SCs have a synergistic, codependent relationship with the tumor environment, residing in specialized niches in which GB SCs and non-tumoral cells reciprocally promote tumorigenesis. GB niche is a cellular heterogeneous microenviroment consisting of GB SCs, differentiated SCs, endothelial cells (EC), microglia/tumor-associated macrophages (TAMs), astrocytes, and neurons (Figure 3).

GB SCs are most frequently found in the perivascular and hypoxic regions of tumors [Filatova, 2013] (Figure 3). The perivascular niche surrounds the blood vessels infiltrating the tumor, which are frequently poorly formed, leaky and friable. Vessels with poor integrity create a microenvironment with high interstitial pressure and poor delivery of oxygen and other nutrients. Drug penetration into the tumor is therefore limited [Rosso, 2009]. GB SCs have a complex relationship with tumor-associated ECs, mutually supporting each other through intercellular signaling. GB SCs promote tumorigenesis by secreting vascular endothelial growth factor (VEGF) that induces EC migration and subsequent angiogenesis, a key step to support and maintain rapid tumor growth. VEGF secretion is induced by the chemokine CXCL12 (SDF1), whose receptor CXCR4 is highly expressed by GB SCs. In response to CXCL12, GB SCs upregulate VEGF production in a PI3K/Akt-dependent manner [Ping, 2011]. GB SCs can transdifferentiate into endothelial-like cells that directly and substantially contribute to the formation of tumor blood vessels [Filatova, 2013]. Conversely, ECs secrete several factors that confer prosurvival (L1CAM,

attivation of Sonic Hedgehog pathway, mTor pathway, NFkB) and invasive (Angiopoietin1, N-cadherin, Integrin β, Notch1) properties to GB SCs [Roos, 2017].

A relatively low tissue oxygen tension is a characteristic in GB as a function of the poor vasculature and dense cellularity. The hypoxic niche, called also perinecrotic niche, supports GB SCs survival and proliferation *via* the hypoxia-inducible factor (HIF) transcription factors HIF-1 and HIF-2. GB SCs utilize HIF signaling to maintain stemness and promote their own survival and expansion [Seidel, 2010]. HIF enacts these changes *via* induction of GB SC-associated genes (c-Myc, Oct4, Nestin, Nanog) and upregulation of downstream effectors (Notch, Prostatic Acid Phosphatase, Akt). Hypoxia has a direct role in chemotherapeutic resistance as well, inducing MGMT expression in GB SC cell lines [Filatova, 2013].

TAMs constitute the dominant tumor-infiltrating inflammatory cells in GB and are correlate with poor prognosis and high malignancy grade in glioma [Roggendorf, 1996]. GB SCs recruit TAMs, induce polarization of TAMs into the immunosuppressive M2 phenotype and enhance the capacity of TAMs to inhibit T cell proliferation. The factors involved in the activation of M2 TAMs included VEGF, SDF1, and TGFβ1. TAMs, in turn, secrete a variety of cytokines and signaling molecules including TGFβ, SDF1, basic fibroblast growth factor (bFGF), and nitric oxide (NO) that could promote the cancer stem cell phenotype [Wei, 2010]. In addition, direct GB SC-mediated induction of effector T cell death and Treg proliferation further limits the potential host response [Roos, 2017].

A better knowledge of the interaction of GB SCs and niches will provide new insights to develop new therapeutic strategies for GB patients. Targeting GB SC niches may represent a novel strategy for treating GB.
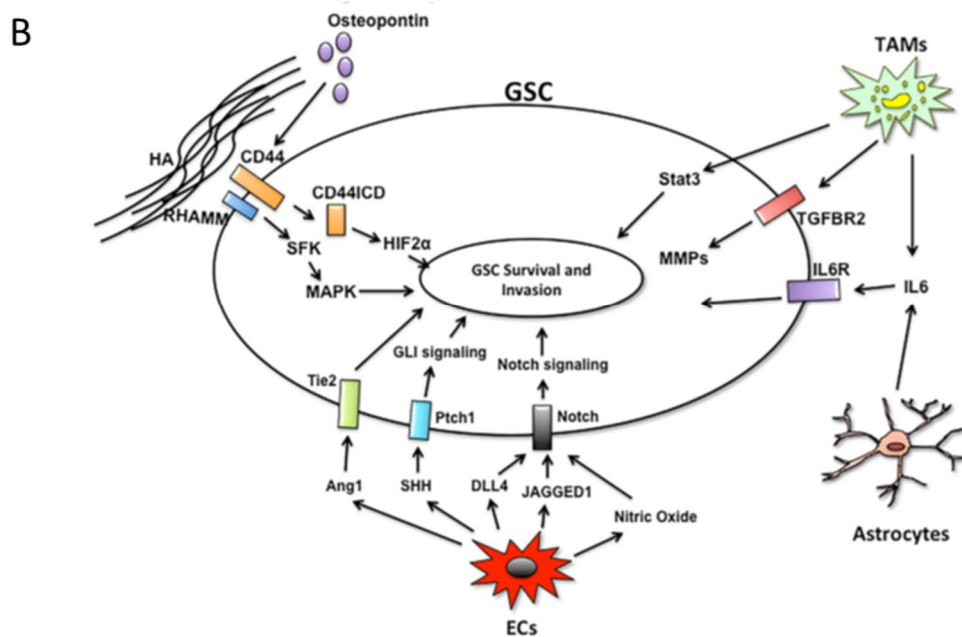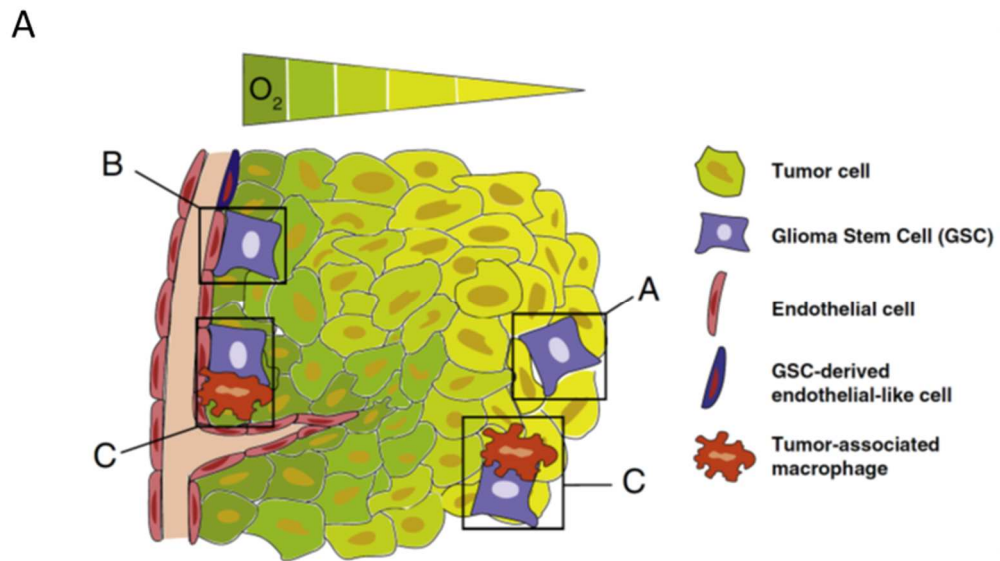
Figure 3. GB SCs and their niches. A. GB SCs reside in hypoxic (A) and perivascular (B) niches. Both niches provide GB SCs with signaling that promote GB SCs maintenance and survival. GB SCs, on the other hand, produce factors that control the formation of blood vessels. Immune cells, in particular tumor-associated macrophages (TAMs), reside in both GB niches (C) and crosstalk with GB SCs [Filatova, 2013].
B. Paracrine pathways facilitating GB SCs invasion. Non-tumor cells within the niche support GB SCs survival and invasion by secreting factors that activate key signaling pathways in GSCs to maintain self-renewal and survival [Roos, 2017].

1.3.2 Blood-brain barrier and blood-brain tumor barrier

GB chemotherapy fails because of the lack of successful drug delivery across the physiologic barriers, BBB and blood-brain tumor barrier BBTB [Pourgholi, 2016].

The BBB is a dynamic interface that separates the brain parenchyma from the circulatory system and protects CNS from the passage of foreign and harmful substances through the blood stream, preventing brain injuries. In addition, the BBB also maintains CNS fluid homeostasis.

The complete surface area of the BBB comprises approximately 20 m^2, with a total length of capillaries in the brain of approximately 600,000 m. The pivotal component of the BBB (Figure 4) is a monolayer of ECs which are connected by tight junctions (TJs) and adherens junctions (AJs). Absence of fenestration also contributes to the barrier properties of brain ECs to regulate paracellular transport. Thus, for a small molecule, free diffusion across the BBB requires both lipophilicity and a molecular mass smaller than 400-500 Da. Most large molecules such as immunoglobulins need a transcellular pathway across the BBB, forming a small number of pinocytic vesicles in ECs. In addition, pericytes, astrocytes and neurons are involved in controlling permeability and other functions of the BBB.

The TJs between ECs are composed of proteins such as occludins, claudins and junctional adhesion molecules, and limit the intercellular leakage. The ECs are also covered by a specialized extracellular matrix and basement membrane which is composed of collagen (particularly type IV), fibronectin, laminin, tenascin and proteoglycans [van Tellingen, 2015].

The BBB isolates both CNS and systemic fluid contents using different defense mechanisms, including transport barrier (para-cellular and transcellular), enzymatic barrier, immunologic barrier and efflux transport systems [Hendricks, 2015].

The presence of several intra- and extracellular enzymes in the ECs, such as phosphatase, peptidase, esterase, monoamine oxidase, nucleotidase, and cytochrome P450, provides a metabolic obstacle responsible for degradation of various drugs and neurotoxins. Moreover, BBB have several drug efflux transporters, belonging to a superfamily of membrane proteins called ATP-binding cassette (ABC) transporters that extrude a large number of drugs from the brain constituting a major obstacle for chemotherapy.

BBB is compromised within the core of the high-grade brain tumors, but intact in the so called Brain Adjacent to Tumor (BAT) area where the invasive tumor cells may reside and generate a tumor relapse. In this area, the brain parenchyma is not transformed and as a consequence of the intact BBB, the delivery of chemotherapeutic drugs to tumor cells is limited [Agarwal, 2011].

The pathological disruptions of the BBB induced by tumor is defined blood-brain tumor barrier (BBTB). The BBTB consists of existing and newly formed blood vessels, which allow oxygen and nutrients delivery to the tumor and its subsequent growth and survival in the brain. In low-grade gliomas, the normal vascularization and the function of the BBTB remain mostly intact and resemble the BBB under normal conditions; high-grade brain tumors typically exhibit a dysfunctional BBTB with enhanced permeability. According to this enhanced permeability, it could be plausible to consider that accumulation of therapeutic agents in the tumor tissues is favoured, but this phenomenon does not happen since other mechanisms, such as high expression of efflux transporters and altered dynamics of cerebral fluid flow not well known, continue to carry out their defense functions [Hendricks, 2015].

Hence, the presence of BBTB in tumor bulk and the presence of intact BBB in BAT represent major obstacles for the drug delivery and the effective treatment in GB [van Tellingen, 2015; Jue, 2016].
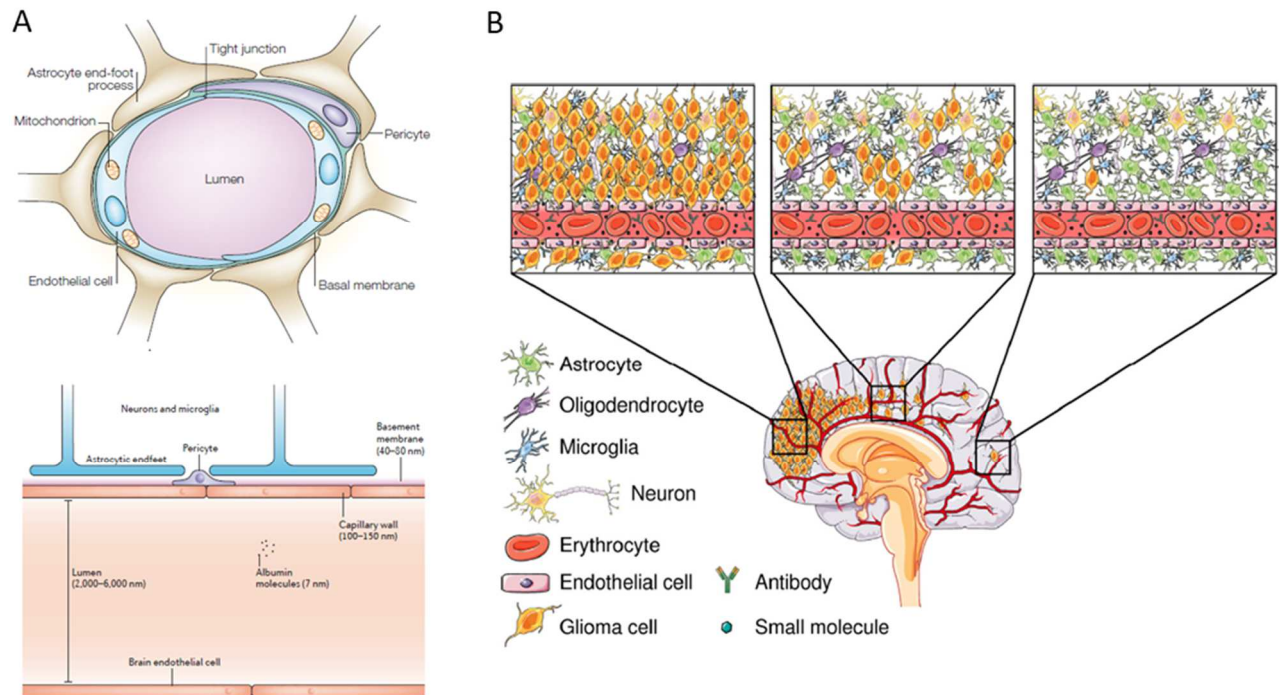
Figure 4. Schematic illustration of the BBB and BBTB. A. BBB comprises endothelial cells, astrocyte endfeet and pericytes. Brain capillary endothelial cells and pericytes are surrounded by a basal membrane. Tight junctions between the cerebral endothelial cells form a diffusion barrier, which selectively excludes most blood-borne substances from the brain. Astrocytic end-feet tightly ensheath the vessel wall and seem to be crucial for the induction and maintenance of the endothelial barrier [Banks, 2016; Löscher, 2005].
B. Glioblastomas consist of different regions characterized by various degrees of BBTB integrity. Heterogeneous BBTB integrity can be found throughout a glioblastoma, varying from completely compromised in bulky tumor areas (left panel) to slightly leaky in more invasive peripheral regions (middle panel) or even completely intact insparsely invaded regions distant from the tumor bulk (right panel). Where the BBTB is compromised macromolecules (e.g. antibodies) and compounds that are normally efficiently restricted from the brain by efflux transporters can extravasate and engage glioma cells, while an intact BBTB protects isolated invaded tumor cells against efficient delivery of therapeutics and often give rise to recurrent tumors [van Tellingen, 2015].

1.3.3 Multidrug resistance transporters on blood-brain barrier and glioblastoma multiforme

Poor responses or resistances to drug treatment limit the effectiveness of GB therapies. MDR is a generic term describing the variety of strategies that cancer cells use to avoid the cytotoxic and immunogenic effects of anticancer drugs. The MDR phenotype involves different mechanisms highly regulated during the cancer progression and treatment [Yang, 2015]. Unresponsiveness of the tumor can be intrinsic or acquired after the exposure to chemotherapy. Mechanisms of drug resistance in brain diseases include (i) genome variability (gene polymorphisms leading to alterations in drug metabolism, drug targets or drug transporters), (ii) disease-related mechanisms (etiology of the disease, disease progression despite treatment, structural brain alterations and/or network changes, alterations in drug targets or alterations in drug uptake into the brain) and (iii) drug-related mechanisms (induction of drug-metabolizing enzymes or drug transporters, ineffective mechanisms of drug action) [Löscher, 2005].

Drug resistance can, therefore, be considered a complex phenomenon that involves many mechanisms, none of which is completely known. Enhanced understanding of these underlying mechanisms is a prerequisite for improving drug therapy by preventing or reversing resistance.

One of the main mechanisms of MDR is the overexpression of ABC transporters. These pumps, using the energy of ATP hydrolysis, actively efflux drugs from tumor cells, causing reduction in intracellular drug levels in cancer cells. Consequently, these cells survive the cytotoxic insult and become drug resistant [Uribe, 2017]. P-glycoprotein (Pgp/ABCB1), multidrug-resistance related proteins (MRPs/ABCCs), and breast cancer resistance protein (BCRP/ABCG2) are the main ABC transporters. They are highly expressed in GB SCs, either derived directly from primary tumors or obtained *in vitro* by growing GB differentiated cells in the SCs-generating medium [Riganti, 2013]. For this reason, GB SCs are resistant to a wide range of chemotherapeutic drugs, like paclitaxel, carboplatin, etoposide, vincristine, irinotecan, doxorubicin, substrates of Pgp used as second line GB treatment [Jiang, 2014].

BBB expresses high level of ABC transporters, involved in the physiological protection against xenobiotics and cellular catabolites. Pgp and BCRP are the main transporters present on the luminal side of BBB and are involved in the efflux of different substrates chemotherapeutic agents back into the bloodstream (e.g. anthracyclines like doxorubicin, taxanes, Vinca alkaloids, epipodophyllotoxins, imatinib, dasatinib, lapatinib, gefitinib, sorafenib, erlotinib for Pgp; mitoxantrone, topotecan, methotrexate and sulfated conjugates for BCRP). Regarding MRP family members, MRP1, 2, 4 are present on the luminal side of BBB and MRP3, 5, 6 on the abluminal side. They are capable of transporting structurally diverse lipophilic drugs such as anthracyclins, Vinca alkaloids, methotrexate and camptothecins (Figure 5).

Pgp, BCRP and MRPs family play a crucial role in drug efflux transport through BBB and drug uptake in GB SCs. New strategies of drug delivery have been developed, to increase drug uptake by BBB cells and reduce backward efflux. Common approaches include the osmotic opening of the TJs, regional drug delivery by local catheters, drug enriched wafers and conventionally-enhanced delivery devices, the use of carrier systems like antibody-conjugated drugs, nanoparticle (NP)-carried drugs or liposome-carried drugs [Pinzón-Daza, 2013].
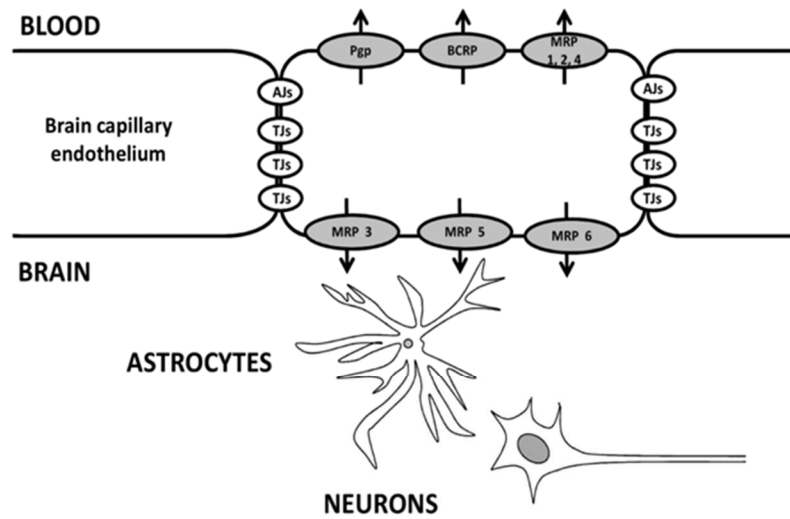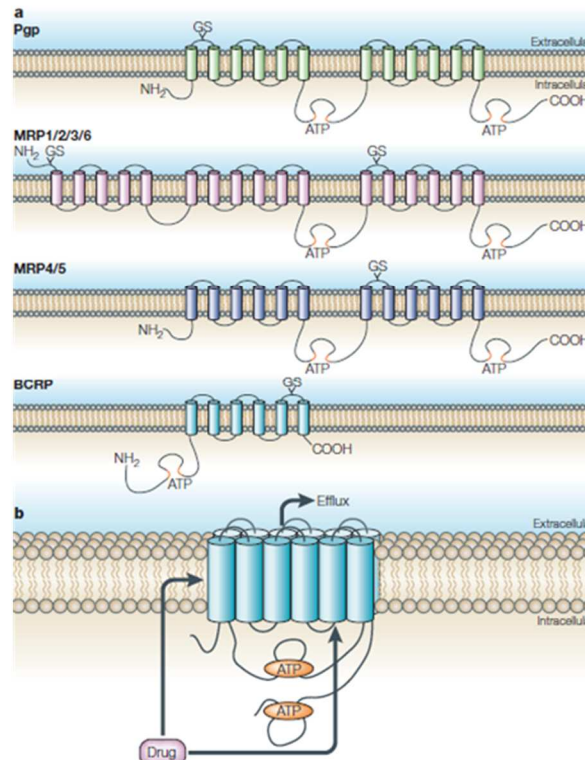
Figure 5. A. Schematic representation of ABC transporters in the blood-brain barrier (BBB). P-glycoprotein (Pgp), breast cancer resistance protein (BCRP) and multidrug-resistance related protein 1-2-4 (MRP1-2-4) are present on luminal side. MRP 3-5-6 in abluminal side [Pinzón-Daza, 2013].

B. Schematic representation of transmembrane structural organization of multidrug transporters. The models indicate the transmembrane domains, glycosylation sites (GS) and ATP binding sites. Two general structures have been described for members of MRP family. Compared with MRP4 and 5, MRP1, 2, 3 and 6 have an additional amino (N)-terminal domain, with five transmembrane domains. Except for the location of their glycosylation sites, their structure is similar to that of Pgp. BCRP consists of only six transmembrane domains, and has only one nucleotide-binding domain Löscher, 2005].

1.3.3.1 P-glycoprotein

P-glycoprotein was identified in 1976 by Ling et al. as a 170-kDa membrane glycoprotein overexpressed in colchicine resistant cell lines able to reduce drug permeability [Juliano, 1976]. Pgp is encoded by the MDR1 gene located on chromosome 7 (q21.12) and abundantly expressed on the intestine mucosal membrane, kidney proximal tubule epithelia, liver, placenta, and luminal BBB, where it functions to protect against xenobiotics and cellular catabolites.

Pgp has two homologous regions, each containing two hydrophobic transmembrane domains (TMD, of six α-helices), and two nucleotide binding domains (NBD, located on the cytoplasmic side) (Figure 6). NBD contains the structural motif called "ABC signature" that couples the hydrolysis of ATP to the transport of the substrate. TMD contain the drug specific binding sites determining the substrate specificity. The drug, binding TMD with high affinity, induces a conformational change in Pgp that allows the binding between ATP and NBD. ATP hydrolysis causes a second conformational change: Pgp loses affinity for drugs and the binding site releases the drug in the extracellular environment. Only after release of ADP and/or Pi, Pgp returns to its original configuration with high binding affinity for the substrate, restoring for the next catalytic cycle. It can be considered a flippase that removes its substrates while they cross the lipid bilayer [Higgins, 1997].

Pgp is able to bind and excrete a large variety of hydrophobic, neutral or positive substrates, with different chemical structures. The main anticancer drugs are anthracyclines (doxorubicin, epirubicin, daunorubicin), Vinca alkaloids (vinblastine and vincristine), taxanes (paclitaxel, docetaxel), colchicine, epipodophyllotoxins (etoposide, teniposide), but also some of the most recent anticancer drugs such as imatinib, dasatinib, erlotinib, gemtuzumab [Jiang, 2014].
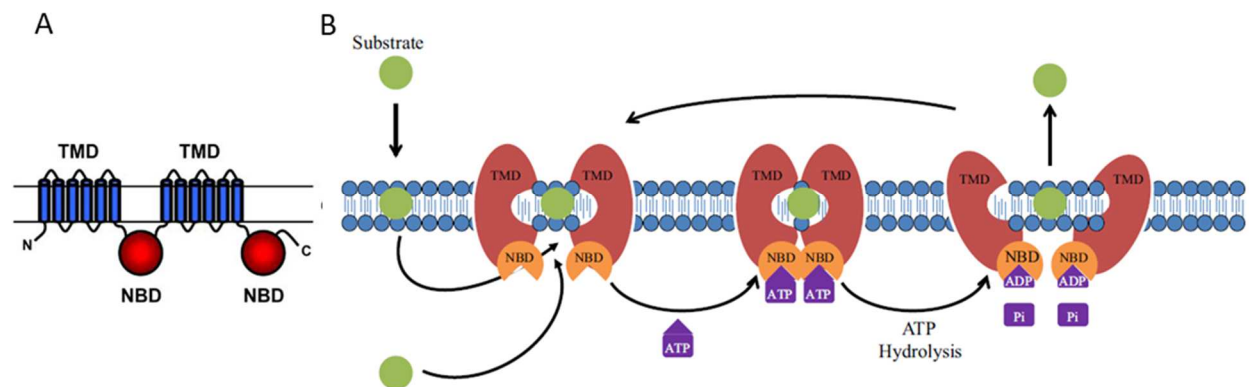
Figure 6. Schematic representation of the human Pgp. A. The upper part represents the extracellular side, the lower site intracellular space. TMD contains six α-helices; NBD binds ATP [Higgins, 1997]. **B.** Model of the multidrug transporter Pgp in a cell membrane. Pgp extrude compounds entered the membrane from the cytoplasm outside the cell. The two TMD of Pgp form a chamber that seems to be open to the extracellular space, and might be accessible for drugs from the lipid phase at the interfaces between the transmembrane domains. Binding or cleavage of ATP provides the energy to induce a conformational change, which is associated with a reduction in drug-binding affinity, thereby probably favouring drug efflux to the extracellular space [Löscher, 2005].

1.3.4. Strategies to improve chemotherapy efficacy in glioblastoma multiforme

Despite multiple efforts over the past decades to develop new strategies to treat GB, none of them led to a better prognostic or an enhanced quality of life for GB patients, when compared to the current standard of care [van Tellingen, 2015].

Some strategies to improve chemotherapy efficacy in GB include physical approaches, nanotherapeutic strategies and chemosensitizing agents to improve drug delivery trough BBB and GB targeting.

1.3.4.1 Physical therapy

Overcoming BBB delivery issues by directly administering the drug into the brain has been one of the key goals in neuroscience. Pharmaceutical agents can be delivered directly into the tumor brain by intrathecal delivery, intraventricular delivery, intranasal delivery, or a catheter convection system for drug delivery [Hendrick, 2015]. Gliadel® wafers or polifeprosan 20 wafer are biodegradable polymer wafers inserted into the tumor cavity after surgical removal of high grade glioma, used for a slow release of drugs like carmustine (BCNU) or TMZ [Panigrahi, 2011]. Different studies have supported the benefit of combining Gliadel® wafers with TMZ, revealing a survival improvement of patients by 3 to 4 months without an increase in toxicity, compared with those who received Gliadel® wafers or TMZ/radiotherapy separately. Unfortunately, the high cost of treatment, the high risk of infection, which hinders the recruitment of patients, limited the progress of clinical trials [Ellor, 2014]. Convection-enhanced delivery (CED) represents a good alternative approach to the Gliadel® wafers, since it does not rely on diffusion. This technique is based on a catheter placed in the tumor tissue, which is connected to a syringe pump, allowing the continuous positive-pressure infusion of a solute containing the drug. Since CED constitutes a form of localized delivery, with direct administration of the drug into the brain, it is possible to obtain a higher drug concentration in the target tissue, with minimal systemic secondary effects. Although this technique is advantageous in brain drug delivery, it is not widely used, due to its backflow that leads to drug release in brain healthy tissue [Vogelbaum, 2015]. Other alternative therapeutic approach includes the use of devices, such as the Novo-TTF-100A (OptuneTM). OptuneTM is a portable device that generates tumor treating fields (TTFields) directly to the patient's scalp, being able to disrupt mitosis in tumor cells with consequent cellular death. The use of this device with TMZ treatment provides a remarkable prolongation of progression-free and overall survival in patients with GB, conferring a better quality of life [Stupp, 2015].

The hyperthermia treatment has received increasing attention from clinicians, due to its potential to eradicate cancer cells. This method consists of generating heat (41–46 °C) on the region of the tumor, through microwaves, infrared irradiation or ultrasound, thereby triggering the activation of multiple intracellular and extracellular degradation mechanisms [Pourgholi, 2016].

New therapeutic approaches consisting of hyperthermia technique combined with nanoparticles have been introduced for GB in recent years [Glaser, 2017]. Radiotherapy associated with hyperthermia in GB enhances the radio-sensitivity and TMZ-sensitivity of GB SCs, thus reducing tumor growth [Man, 2015]. Nevertheless, hyperthermia use is limited since healthy cells are damaged by exposure to high temperatures and the lethal heat dose for all subpopulation cells within the tumor is difficult to define. All techniques showed promising results, but they need to be improved for optimizing GB treatment.

1.3.4.2 Nanomedicine

Rapid advances in protein engineering and materials sciences has recently permitted considerable progress in the field of nanomedicine to develop novel nanoscale strategies for cancer diagnosis and treatment. The main requisites that nanocarriers must have when they are administered systemically are: 1) the preservation of their structural integrity in the bloodstream; 2) their escape from sequestration in reticulo-endothelial cells; 3) the absence of "first passage" effect and hepatic catabolism and 4) the absence of important urinary clearance. Furthermore, they must not induce side effects, such as liver or kidney toxicity or abnormal immunoreactivity [Kim, 2015].

Until now, the most commonly used carriers for drug delivery within the CNS included polymeric NPs and liposomes because of their increased cellular uptake and reduced efflux through ABC transporters through BBB. NPs are solid colloidal particles made with a broad spectrum of materials: sugar derivatives such as malto-dextrins or chitosan; fatty acids such as beenic acid and palmitic acid that are assembled in the so-called solid lipidic NPs (SLNs); proteins such as human albumin (HA) and type B gelatin. They can be divided into nanospheres, if they are entirely made of solid components, and nanocapsules, if made of a solid shell surrounding a central cavity containing hydrophilic or hydrophobic solvents. Liposomes are lipid vesicles with a wide range of sizes, from 20 nm to 1 µm of diameter. They are made by one or multiple phospholipid bilayers with the typical structural organization of cell membranes, loaded with hydrophobic, hydrophilic or amphipathic drugs [Pinzòn-Daza, 2013]. NPs and liposomes, currently used in solid tumor treatment, usually are subjected to the enhanced permeability and retention (EPR) effect [Peer, 2007]: drug loaded-nanocarriers, administered intravenously, passively extravasate into tumor tissue through the leaky vasculature (defective angiogenesis), accumulate in the tumor and release therapeutic cargo near tumor cells. However, the EPR effect depends entirely on the diffusion of drugs and it is difficult to control that diffusion is uniform in all the tumor. In the case of brain tumors, the EPR effect is not so efficient due to the dense brain matrix impeding diffusion and the elevated interstitial fluid pressure [Séhédic, 2015]. To overcome the above limitations, nanocarriers are manipulated on charge, size of NPs, hydrophobicity properties, coating as well as specificity of targeting [Pourgholi, 2016]. For example, conjugation of NPs with polysorbate (Tween®) or other hydrophilic coatings, such as polyethylene glycol (PEG), human serum albumin (HSA), poloxamers (Pluronic® F68) and poly-vinylalcohol (PVA), has been shown to enhance drug transport through BBB [Karim, 2016].

Furthermore, their surface can be manipulated with BBB or GB-specific ligands such as antibodies, peptides, aptamers that bind to antigens or receptors on the target cells, enhancing tumor permeability and thereby improving treatment efficacy. While glucose transporters, insulin receptors, and transferrin receptors (TfR) normally existing on the BBB are have been reported to facilitate transcytosis of NPs *via* binding to these receptors on BBB endothelial cells, CD133, epidermal growth factor receptor (EGFR), transferrin receptors (TfR) could be direct targets anti-GB SCs [Kim, 2015]. The reticuloendothelial system (RES), a part of the immune system presenting cells with high phagocytic capacity, can sequester nanocarriers and remove them from the systemic circulation, with their subsequent destruction. Overall, strategies to overcome this issue include the nanocarrier size control, which should be lower than 100 nm, and the use of PEG-coating, which avoid their opsonisation and RES uptake. Smaller nanocarriers have another advantage, since they can easily penetrate through the leaky BBTB by EPR effect, thus attacking GB tumor bulk more efficiently [Pourgholi, 2016].
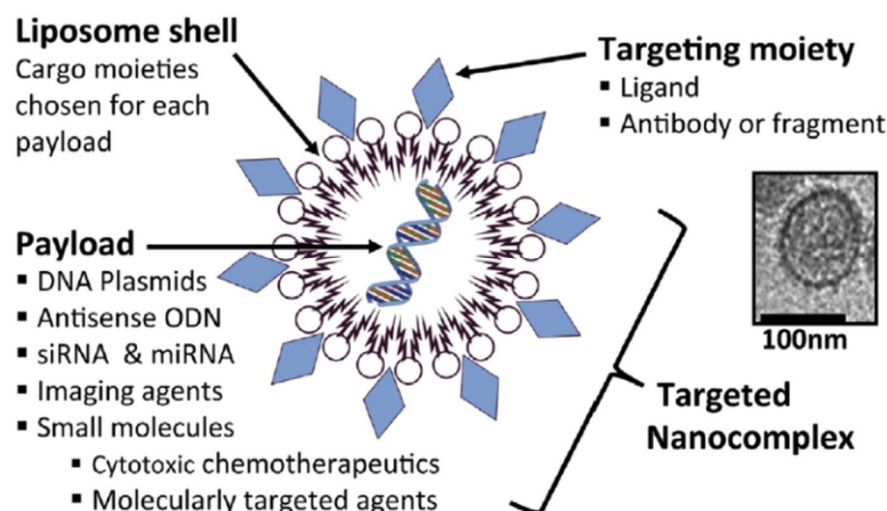
Figure 7. Schematic representation of targeted nanocarrier comprised of a targeting and cargo moiety. Various payloads can be packaged inside a cargo moiety made of liposome shell. A representative electron microscopic image of liposome is shown. The scale bar represents 100 nm [Kim, 2015].

1.3.4.3 Chemosensitizers

The development of the MDR phenotype is associated with elevated expression levels of ABC transporters in the cancer cells. The first approach to overcome drug resistance was through the association of cytotoxic drugs with an ABC-transporter inhibitor. The inhibition of ABC transporters can act blocking drug-binding site(s) either competitively, non-competitively or allosterically, interfering with ATP hydrolysis or altering integrity of cell membrane lipids (Figure 8). Usually these compounds show presence of a basic nitrogen atom and two planar aromatic domains, lipid solubility and cationic charge [Ankit, 2014].

Great efforts have been made to find selective inhibitors of Pgp, BCRP and MRPs family, but their low tissue specificity and subsequent high toxicity limit their clinical use. This leads to investigations and development of more effective and safe ABC transporters inhibitors [Chen, 2016].

The first generation of Pgp inhibitors was composed of drugs that were developed for other indications but they had also been shown to inhibit Pgp. Such drugs include immunosuppressants (cyclosporin A), calcium channel blockers (verapamil), anti-hypertensives, and anti-estrogens. However, at dosages that would effectively prevent MDR, these agents are highly toxic. Second generation inhibitors, such as dexverapamil, dexniguldipine, valspodar and biricodar, showed a higher affinity and specificity for Pgp, making them more effective at lower concentrations but, they produced side effects because they are substrates for cytochromes P450 (CYP450) and acted on more than one transporter. A third generation of inhibitors was created to overcome these problems. They reverted resistant phenotype at lower doses with high selectivity towards Pgp and had reduced susceptibility for metabolic biotransformation by the CYP system. These agents, as

elacridar (GF120918), tariquidar (XR9576), zosuquidar (LY335979) and OC144-093 (ONT-093), are effective at the nanomolar concentration range 2-100 nM and require low doses to achieve effective MDR reversal *in vivo* [Akhtar, 2011]. Tariquidar and elacridar block also BCRP. Furosemide, glibenclamide, MK-571, probenecid are inhibitors of MRP protein family [Saneja, 2014].

In the search for P-glycoprotein inhibitors, it was sometimes overseen that Pgp-expressing tumor cells retain sensitivity to local anesthetics, detergents, antimetabolites, alkylating agents, platinum compounds as well as natural products such as saponins or flavonoid. This finding opened the opportunity to bypass MDR by treatment with non-cross-resistant drugs, exploiting the sensitivity to these agents (the so-called "collateral sensitivity", CS) [Szakács, 2014].

Most of the studies on ABC transporter inhibitors were performed in animals, making it difficult to translate some promising results obtained in animal models into clinical applications in humans. Overall, the routine use of ABC transporter inhibitors to enhance the drug delivery across the BBB *in vivo* is still controversial. However, targeting ABC efflux transporters with new chemosensitizers and novel approaches - such as RNA interference and epigenetic regulation - is still seen as a good strategy to improve drug delivery and overcome MDR [Chen, 2016].
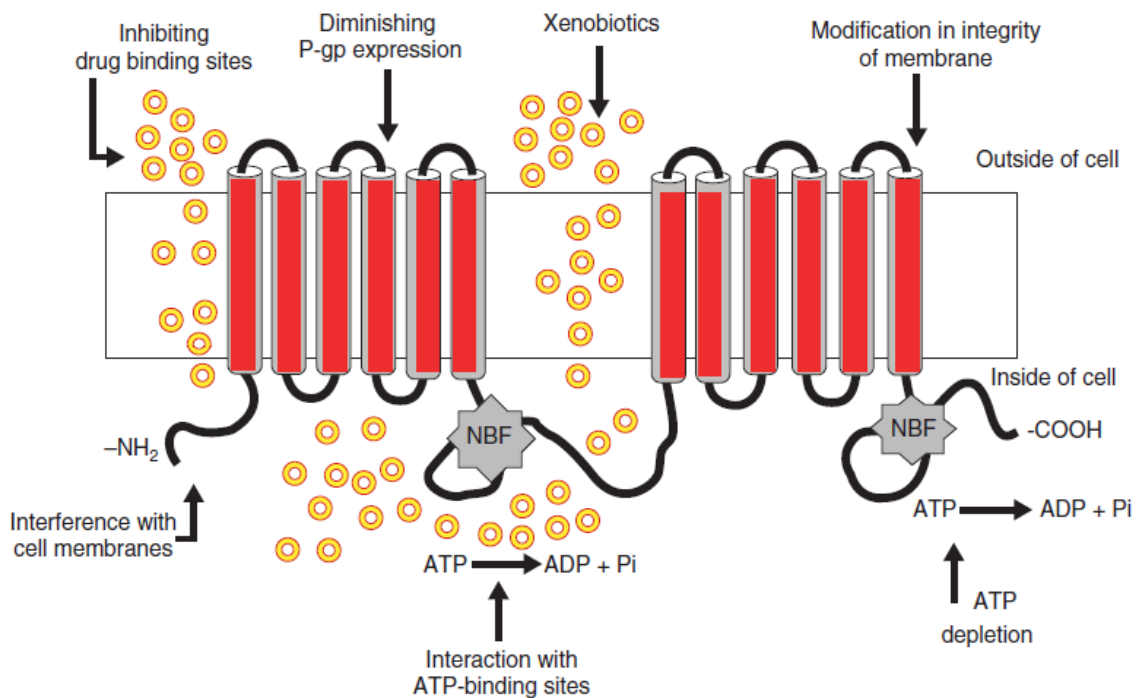
Figure 8. Overview of inhibitory mechanisms of P-glycoprotein [Bansal, 2009].

2. AIM

The general aim of this thesis was to investigate the molecular and cellular basis of interaction between GB and BBB that affect drug delivery and GB targeting, in particular GS SCs targeting. At first I analyzed the molecular mechanisms that determine low drug delivery across BBB, focusing my attention on Pgp. Then I investigated how GB differentiated cells or SCs may influence BBB drug permeability. Finally, I validated new strategies to improve drug delivery across BBB and efficient targeting of GB SCs.

This thesis can be divided in the following three specific aims:

1) <u>Molecular mechanisms determining low drug delivery across BBB.</u>

GB chemotherapy almost universally fails because of low delivery of chemotherapeutic drugs across BBB, due to the presence of ABC efflux pump such as Pgp. In the first part of my thesis, I investigated the biochemical mechanisms regulating Pgp activity at the BBB-GB interface. The Wnt canonical pathway (Wnt/GSK3/β-catenin axis) has a central role in regulating the expression of Pgp in BBB cells [Lim, 2008] but it is unknown whether the Wnt non-canonical pathway (Wnt/RhoA/ RhoAK axis) controls also the Pgp expression and cooperated with Wnt canonical pathway in regulating the Pgp levels in BBB cells.

Also temozolomide (TMZ), the first-line GB therapy, has a regulator effect on Pgp expression, not yet investigated before. I found that this potent chemotherapeutic drug is also a potential chemosensitizers that downregulates Pgp expression, by disrupting Wnt/GSK3/β-catenin axis.

2) <u>Influence of the interaction between GB and BBB on drug delivery across BBB.</u>

Since the BBB is disrupted in presence of GB [van Tellingen, 2015] and GB SCs are more chemoresistant than GB differentiated cells [Riganti, 2013], I investigated if the grade of differentiation and/or stemness of GB cells may influence drug permeability across BBB. The aim of this second part was to develop *in vitro* model of BBB-GB with different grades of differentiation of tumor cells (including GB SCs and differentiated cells), in order to obtain standardized model which mimic *in vitro* the complex situation existing *in vivo* at the GB-BBB interface and to better understand what effects GB induces on BBB.

3) <u>Development of new strategies to improve drug delivery by targeting BBB-dependent and GB SCs-dependent mechanisms.</u>

BAT area is a critical zone for targeting chemotherapy because it contains GB cells that can spread to other areas of the CNS or cause local relapse. Since BAT is surrounded by a competent BBB the delivery of chemotherapeutic drugs to this area is difficult.

In the last part of my thesis, I developed and validated *in vitro* and *in vivo* new chemical inhibitors selective for BBB (thiosemicarbazone-derivatives; aim 3a) and GB SCs (carbonic anhydrase XII - CAXII – inhibitors; aim 3b) and new NPs formulations able to bypass ABC transporters efflux present at BBB-GB interface (aim 3c).

3. MATERIALS AND METHODS

3.1 Chemicals

The plasticware for cell cultures was from Falcon (Becton Dickinson, Franklin Lakes, NJ). 0.4-µm diameter pores-size Transwells were from (Corning Life Sciences, Chorges, France). WntA [2-amino-4-(3,4-(methylenedioxy)benzylamino)-6-(3- methoxyphenyl)pyrimidine] was purchased from Calbiochem (San Diego, CA, USA). Human recombinant Dickkopf- 1 (Dkk-1) was from R&D Systems (Minneapolis, MN, USA). [^{14}C]-sucrose, [^{14}C]-inulin, [^{3}H]-vinblastine were from PerkinElmer (Waltham, MA, USA). Sodium dodecyl sulfate (SDS) was from Fluka (Buchs, Switzerland). TRIS, phosphoric acid, hydrochloric acid, sodium hydroxide and sodium phosphate monobasic from Merck (Darmstadt, Germany). Br-dodecane, dichlorometane, chloroform, methanol and ethanol from Carlo Erba (Val De Reuil, France). ApoE chimera peptide was from Genscript (NJ, USA). Deionized water was obtained by a MilliQ system (Millipore, MO, USA).

When not otherwise specified, all the other reagents were purchased from Sigma Chemicals Co. (St. Louis, MO). The electrophoresis reagents were obtained from Bio- Rad Laboratories (Hercules, CA). The protein content of cell lysates was assessed with the BCA kit from Sigma Chemicals Co.

3.2 Cells

The immortalized hCMEC/D3 cells, a primary human brain microvascular endothelial cell line that retains the BBB characteristics *in vitro*, were cultured as reported [Weksler, 2005]. Cells were seeded at 50,000/cm^2 density and were grown for 7 days up to confluence in Petri dishes and Transwells. Primary human brain microvascular endothelial cells (HBMECs) were purchased from PromoCell GmbH (Heidelberg, Germany) and cultured in the endothelial cell growth medium MV (PromoCell GmbH), supplemented with 5 % v/v fetal calf serum (FCS), 0.4 % v/v endothelial cell growth supplement (PromoCell GmbH), 10 ng/ml EGF, 90 µg/ml heparin, and 1 µg/ml hydrocortisone. Primary human GB cells (CV17, 0101010627, No3, namely Unknown Patient Number UPN 1-2-3 in the part 3 of this thesis) were obtained from surgical samples of patients from the Department of Neuroscience, Neurosurgical Unit, University of Turin, Italy. The pathological diagnosis was performed according to WHO guidelines. Cells were cultured as SC-enriched populations (neurospheres, NS) or differentiated/adherent cells (AC). For NS, surgical samples were cut into 1mm^3-pieces, digested with 30 µg/ml collagenase and 50 µg/ml hyaluronidase and seeded in Dulbecco's modified Eagle's medium (DMEM)–F12 medium, supplemented with 1 M HEPES (4-(2-hydroxyethyl)-1-piperazine ethanesulfonic acid), 0.3 mg/ml glucose, 75 mg/ml NaHCO$_3$, 2mg/ml heparin, 2 mg/ml bovine serum albumin, 2 mM progesterone, 20 ng/ml EGF, and 10 ng/ml bFGF. AC were generated by dissociating NS in single cell suspension by repeated pipetting, centrifuging cells at 12,000 g for 5 min and seeding them in DMEM supplemented with 10% fetal bovine serum (FBS; Lonza). U87-MG cells (ATCC, Rockville, MD) were used as GB reference cell line for both NS and AC and cultured as reported above. Morphological analysis and phenotypic characterization of differentiation and stemness markers, *in vitro* clonogenicity and self-renewal, in *vivo* tumorigenicity properties are detailed in [Riganti, 2013]. Rat F98 glioma cells were obtained from LGC Standards S.r.l. (Sesto San Giovanni, MI, Italy) and cultured in DMEM supplemented with 10% FBS and 100 U/ml penicillin and 100 mg/ml streptomycin.

3.3 Co-culture model

500,000 (for intracellular doxorubicin accumulation, PCR and cytotoxicity assays) or 1,000 (for proliferation assay) GB cells were added in the lower chamber of Transwell 4 days after seeding hCMEC/ D3 cells or HBMECs in Transwell inserts. After 3 days of co-culture the medium of the upper and lower chamber was replaced, and cells were used for the experimental assays as detailed in Results.

3.4 Animals

Fischer male rats (Charles River, MA, USA), weighing 200–250 g, nude Balb/C mice (Charles River, MA, USA), weighing 20-21 g, were housed in standard facilities, handled and maintained according to our Institutional Animal Care and Use Committee ethical regulations. Animals were kept under controlled environmental conditions (23 ± 1°C, 50–60% humidity, 12 h light and dark cycles, lights on at 7:00 a.m.). Animals were given *ad libitum* access to food and water. The procedures conformed to the Ethics Committee of University of Turin's institutional guidelines on animal welfare (DL 116/92) as well as International Guidelines, and all efforts were done to minimize the number of animals and their discomfort. All experiments on animal models were performed according to an experimental protocol approved by the University Bioethical Committee and the Italian Ministry of Health (Prot. No. 0135/2015).

3.5 Synthesis and characterization of carbonic anhydrase XII inhbitors

Detailed synthesis of CAXII inhibitors, namely compounds **1-5**, performed at Griffith Institute for Drug Discovery, Griffith University, Brisbane, Australia, is reported in [Mujundar, 2016]. The activity of CA was measured as reported in [Morris, 2011].

To test the stability in plasma, mouse plasma (Animal Resource Centre, Perth, Australia, pooled from multiple mice) was stored frozen at -80 °C. Compound **1** was spiked into plasma to a nominal concentration of 1000 ng/ml (final DMSO and acetonitrile concentrations were 0.2 and 0.4% v/v, respectively), vortex mixed and then aliquoted (50 µl). Spiked plasma aliquots were incubated at 37°C for 4 h, and at various time points, triplicate plasma samples were taken and immediately snap-frozen in dry ice. All plasma samples were stored frozen (-20 °C) until analysis by LC-MS (using a Micromass Xevo triple quadrupole mass spectrometer, Waters Co., Milford, MA) relative to calibration standards (**1** and diazepam as internal standard) prepared in blank mouse plasma. At each sample time, the average concentration of test compound (based on triplicate samples) was expressed as a % compound remaining relative to the sample quenched at time = 5 min. Studies were performed by Centre for Drug candidate Optimisation, Monash University, Melbourne, Australia.

The metabolic stability assay was performed in mouse liver microsomes (Xenotech, Tokyo, Japan, lot#1510043). Compound **1** (1 µmol/l) was incubated in liver microsomes at a final protein concentration of 0.4 mg/ml at 37°C. The metabolic reaction was initiated by the addition of a NADPH-regenerating system, and subsequently quenched with acetonitrile (containing diazepam as internal standard) at 2 min, 30 min and 60 min. Compounds were also incubated in the absence of NADPH cofactor to monitor the non-cytochrome P450-mediated metabolism in the microsomal matrix. A species scaling factor [Ring, 2011] was used to convert the *in vitro* clearance (CL_{int}) (µl/min/mg) to an *in vivo* CL_{int} (ml/min/kg). Hepatic blood clearance and the corresponding hepatic extraction ratio (E_H) were calculated using the well-stirred model of hepatic extraction

according to the "in *vitro* $T_{1/2}$" approach described in [Obach, 1999]. The E_H was then used to classify compounds as low (< 0.3), intermediate (0.3 – 0.7), high (0.7 – 0.95) or very high (> 0.95) extraction compounds. Studies were performed by Centre for Drug candidate Optimisation, Monash University, Melbourne, Australia.

3.6 Synthesis and characterization of thiosemicarbazone compounds

The thiosemicarbazone-derivatives compounds **8a**, **10a** and **17a** were synthesized at the Department of Pharmacy, University of Bari, as detailed in [Pati, 2015]. The Pgp activity in the presence of compounds was evaluated by the Calcein-acetoxy methylester (AM) assay and the bioluminescent ATP assay, as described in [Pati, 2015].

3.7 Synthesis of didoceylmethotrexate

Didoceylmethotrexate (ddMTX) was synthesized according to literature [Rosowsky, 1984; Moura, 2011] by Department of Drug Science and Technology, University of Torino (Figure 9).

3.8 SLNs preparation, characterization and functionalization with ApoE

2% behenic acid (BA) and 4% PVA 9000 SLNs were prepared according to the coacervation method [Nelson, 1977]. Briefly, SLN was dispersed in water with PVA 9000 and the mixture was then heated (80°C) under stirring (300 rpm) to obtain a clear solution. 2 mg of ddMTX was dissolved in 300 μl ethanol at 65°C, prior to be added to 2.5 ml of 2% SB and 4% PVA 9000 micellar solution. The acidifying solutions (coacervating solutions – 0.4 ml 1 M sodium dihydrogen phosphate and 0.6 ml 1 M hydrochloric acid) were added dropwise to the mixture until complete BA precipitation occurred. The obtained suspension was cooled under stirring at 300 rpm until 15°C temperature was reached (Annovazzi, 2017). The suspensions were then concentrated under nitrogen steam to a final volume of 2.5 ml.

SLN particle size and polydispersity index were determined 1 h after preparation using dynamic light scattering technique (Brookhaven, NY, USA). Size measurements were obtained at an angle of 90° at 25°C. All data were determined in triplicate. ddMTX concentration was determined in suspension just after preparation and after SLNs purification from unentrapped drug, obtained as previously described for ApoE. ddMTX entrapment efficiency (EE [%]) of SLNs was determined as follows: 0.5 ml SLNs suspension was diluted with 0.5 ml water and centrifuged for 15 min at 62,000× *g* (Allegra 64R centrifuge, Beckmann Coulter, CA, USA); the precipitate was washed with 1 ml of 30:70 v/v ethanol:water to eliminate the adsorbed drug. The lipophilic prodrug was extracted from the solid residue in 1 ml dichloromethane and injected into silica-HPLC (photodiode array [PDA] detector at 302 nm). Based on EE%, the drug loading (mg drug/mg lipid) was calculated. Moreover, the final prodrug content in SLNs suspension was also determined with fluorescence reverse phase (RP)-HPLC after 500-fold water dilution and derivatization.

2.5 ml of SLNs were incubated at room temperature for 1 h with a concentrated aqueous solution of ApoE to have 0.1 mg/ml final concentration in SLNs suspension. The purification from unbound protein was then performed as follows: by gel filtration, using a matrix of crosslinked agarose (Sepharose CL 4B – size exclusion 100,000 Da) as stationary phase; by gel centrifugation, using crosslinked poliacrylamide (Biogel P-6 – size exclusion 6000 Da), and by dialysis (14,000 Da membrane cutoff). Since sample dilution occurs after gel filtration, the opalescent fractions containing the purified SLNs were concentrated under nitrogen steam up to 1 ml final volume.

Chimera peptide binds to SLNs surface by simple electrostatic interaction. The effective functionalization was assessed by SDS gel electrophoresis (12% poliacrylamide) performed in non-denaturing conditions, followed by staining with 10 ml Coomassie Blue solution (0.2% w/v Coomassie Blue, 7.5% v/v acetic acid and 50% v/v ethanol), for 1 h at room temperature, and by overnight de-staining with deionized water. The amount of ApoE associated with SLNs was quantified at the same time with the BCA kit.

The amount of ddMTX was measured by HPLC analysis, using a YL9100 HPLC system equipped with a YL9110 quaternary pump, a YL9101 vacuum degasser and a YL9160 PDA detector and/or a Shimadzu RF-10A fluorescence detector (Shimadzu, Tokyo, Japan), linked to YL-Clarity software for data analysis (Young Lin, Hogye-dong, Anyang, Korea). The RP-HPLC method was developed for the determination of both MTX and ddMTX in biological samples, starting from a literature method (Nelsen, 1977). Briefly, 0.25 ml of samples were added to 0.1 ml of 10% SDS aqueous solution, in order to promote ddMTX dissolution; samples were deproteinized with 0.08 ml of 10% trichloroacetic acid (TCA) and then centrifuged. 0.2 ml of the supernatant was added to 0.05 ml of 5 M pH 5.0 acetate buffer. MTX or ddMTX were oxidized to fluorescent pterydin carboxyilc acid with 0.05 ml of 5% $KMnO_4$. HPLC analysis was performed with Teknokroma Mediterranea Sea RP 2.5 μm 125 × 4.6 mm column. Here, 0.05 M pH 6.7 TRIS buffer (adjusted with phosphoric acid) was used as a mobile phase at 1 ml/min flow. After peak elution, gradient was performed with 30% acetonitrile in order to clean the column from reaction subproducts. Retention time was 12 min. For ddMTX analysis, Teknokroma Kromosil 100™, 250 × 4.6 mm, of 2.5 μm particle size was employed. HPLC-grade dichloromethane/methanol (95/5 v/v) was used as a mobile phase with a flow rate of 1 ml/min. The PDA detector was set at 302 nm. Retention time was 10 min.

3.9 Biodistribution studies of SLNs

ddMTX-loaded SLNs, with or without ApoE (1.6 mg/ kg ddMTX corresponding to 1 mg/kg MTX), and disodium MTX (1 mg/kg) solution in normal saline were administered through a catheter surgically positioned in the jugular vein of male Wistar healthy rats (weight, 250 g). ddMTX was not used as control, because of its very low water solubility, that hampers its intravenous administration as a free molecule. At scheduled times (30 and 90 min after administration), rats were sacrificed by CO_2-induced euthanasia; plasma was withdrawn, and organs (liver, spleen, kidneys, lungs, heart and brain) were removed surgically. Each experiment was performed with four rats for each sample administered. A pilot biodistribution experiment was also performed by using 7-day implanted GB models, described below, aiming to detect differences between biodistribution in healthy rats and glioma models. GB-carrying rats were sacrificed 30 min after administration. Organs were homogenized with UltraTurrax® (IKA, Staufen, Germany) for 5 min in water at a tissue concentration of 125 mg/ml; tissue homogenates and plasma underwent the derivatization reaction prior to fluorimetric HPLC detection [Nelson, 1977].

3.10 Permeability coefficient across the blood-brain barrier cells

The permeability to dextran-fluorescein isothiocyanate (DEXT), [14C]-sucrose, [14C]-inulin, was taken as a parameter of tight junction integrity. The permeability to doxorubicin (DOX), [3H]-vinblastine, mitoxantrone (MXR), was taken as index of ABC transporters activity [Weksler,

2005].

hCMEC/D3 cells, seeded at 50,000/cm^2 and grown for 7 days up to confluence in six-multiwell Transwell inserts, were incubated at day 4 with or without TMZ (50 µmol/l for 72 h) or incubated with GB cells or GB-conditioned medium for 24-72 hours. Then the culture medium was replaced in both chambers. 2 µmol/l DEXT, 2 µ Ci/ml [^{14}C]-sucrose, 2 µCi/ml [^{14}C]-inulin, 5 µmol/l DOX, 2 µCi/ml [^{3}H]-vinblastine, or 10 µmol/l MXR, were added to the upper chamber of Transwell. After 3 h, the medium in the lower chamber was collected. The amount of [^{14}C]-sucrose, [^{14}C]-inulin or [^{3}H]-vinblastine was measured using a tri-carb liquid scintillation analyzer (PerkinElmer). Radioactivity was converted in nmol/cm^2, using a calibration curve previously prepared. The amount of DEXT, DOX and MXR present in the lower chamber was measured fluorometrically, using a LS-5 spectrofluorometer (PerkinElmer). Excitation and emission wavelengths were: 494 and 518 nm (DEXT), 475 and 553 nm (DOX), 607 and 684 nm (MXR). Fluorescence was converted in nmol/cm^2, using a calibration curve previously set. The permeability coefficients were calculated as reported [Siflinger-Birnboim, 1987]. In time- and temperature-dependence experiments, the Transwell inserts were incubated at 4, 15, and 37 °C, and treated as reported above; aliquots of the medium from the lower chamber were collected every 30 min up to 3 h. The amount of doxorubicin or vinblastine in the lower chamber was quantified as described earlier. When indicated, a 25 % w/v solution of mannitol, used to increase the leakage of solutes through the BBB tight junctions, was co-incubated in the upper chamber.

For TMZ permeability, hCMEC/D3 cells seeded in Transwell inserts as reported above were incubated for 72 h with 0.7 µCi/ml [^{3}H]-TMZ (Moravek Biochemical Inc., Brea, CA, USA), equivalent to 10 µmol/l TMZ, in the presence of increasing concentrations (50, 100, and 200 µM) of cold TMZ. After this incubation period, the amount of [^{3}H]-TMZ in the lower chamber was measured by liquid count scintillation. The results were expressed as the percentage of [^{3}H]-TMZ recovered in the lower chamber after 72 h *versus* [^{3}H]-TMZ added in the upper chamber at time 0, taking into account the concentration of cold TMZ added in the upper chamber at time 0.

3.11 Intracellular drugs accumulation

After 24 hours or 72 hours of co-culture, 5 µmol/l DOX, 2 µmol/l DEXT, 10 µmol/l MXR were added to the upper chamber of Transwell inserts containing hCMEC/D3 cells monolayer. After 3 hours, the cells in the lower chamber were collected, rinsed with PBS, re-suspended in 0.3 ml ethanol/HCl 0.3 N (1:1 v/v) and sonicated. A 25 µl aliquot was used to measure the protein content and the remaining sample was used to quantify fluorometrically the intracellular drugs content as described above. Results were expressed as nmol DOX/mg cell proteins, ng MXR/mg cell proteins and mg DEXT/mg cell proteins, according to a titration curve previously set. TMZ content was measured by incubating cells with 10 µM [^{3}H]-TMZ (0.7 µCi/ml; Moravek). The amount of [^{3}H]-TMZ in cell lysate was measured by liquid scintillation counting. The results were expressed as nmol [^{3}H]-TMZ/mg cell proteins, according to a titration curve previously set.

3.12 Western blot analysis

Cells were rinsed with ice-cold lysis buffer (50 mmol/l Tris, 10 mmol/l EDTA, 1 % w/v Triton-X100), supplemented with the protease inhibitor cocktail set III (80 µmol/l aprotinin, 5 mmol/l bestatin, 1.5 mmol/l leupeptin, 1 mmol/l pepstatin, 2 mmol/l phenylmethylsulfonyl fluoride PMSF and 1 mmol/l sodium orthovanadate), then sonicated and centrifuged at 13,000 × g for 10

min at 4 °C. 20 µg of protein extracts were subjected to SDS-PAGE and probed with the following antibodies: anti-claudin 3 (Invitrogen Life Technologies, Monza, Italy); anti-claudin 5 (Invitrogen Life Technologies); anti-occludin (Invitrogen Life Technologies); anti-zonula occludens-1 (ZO-1; Invitrogen Life Technologies); anti-Pgp/ABCB1 (clone C219, Cabiochem), anti-MRP1/ABCC1 (Abcam, Cambridge, MA, USA), anti-BCRP/ABCG2 (Santa Cruz Biotechnology Inc., Santa Cruz, CA, USA), anti-Wnt3 (Abcam); anti-GSK3 (BD Biosciences, Franklin Lakes, NJ, USA); antiphospho(Tyr216)GSK3 (BD Biosciences); anti-β-catenin (BD Biosciences); anti-phospho(Ser33/37/Thr41)β-catenin (Cell Signaling Technology Inc., Danvers, MA. USA); anti-protein tyrosine phosphatase 1B (PTP1B; Abcam, Cambridge, UK); anti-phospho(Ser50)PTP1B (Abcam); anti-Caspase-3 (C33, GeneTex, Hsinhu City, Taiwan); anti-CAXII (2C6; Abcam, Cambridge, UK), anti-CAIX (NB100-417; Novus Biologicals, Littleton, CO), anti- β-tubulin (Santa Cruz Biotechnology Inc). This procedure was followed by the exposure to a peroxidase-conjugated secondary antibody (Bio-Rad). The membranes were washed with Tris buffer saline-Tween 0.1 % v/v, and proteins were detected by enhanced chemiluminescence (Bio-Rad).To check the equal control loading in cytosolic fractions, samples were probed with an anti-β-tubulin or anti-GAPDH antibody.

Cytosol/nucleus separation was performed using the Nuclear Extraction Kit (Active Motif, Rixensart, Belgium). 10 µg of cytosolic or nuclear extracts were subjected to Western-blot analysis using the anti-β-catenin antibody. To check the equal control loading in cytosolic and nuclear fractions, samples were probed respectively with an anti-β-tubulin or an anti-TATA -box binding protein (TBP/TFIID) antibody (Santa Cruz Biotechnology Inc). To exclude any cytosolic contamination of nuclear extracts or vice versa, we verified that β-tubulin was undetectable in nuclear samples and TBP was undetectable in cytosolic samples. The densitometric analysis of Western blots was performed with ImageJ software (http://rsb.info.nih.gov/ij/) and expressed as arbitrary units, where "1 unit" is the mean band density in untreated cells.

Plasma membrane-associated proteins, extracted using the Cell Surface Protein Isolation kit (Thermo Fisher Scientific Inc., Waltham, MA), were evaluated as described earlier [De Boo, 2009]. An anti-pancadherin antibody (H-300; Santa Cruz Biotechnology Inc.) was used to confirm equal protein loading.

3.13 Immunoprecipitation

100 µg of proteins from whole-cell extracts (for ubiquitinated β-catenin) or 100 µg of plasma membrane-associated proteins (for co-immunoprecipitation of Pgp/CAXII or Pgp/CAIX) were immunoprecipitated with the anti-β-catenin antibody and the anti-CAXII and anti-CAIX antibodies respectively, using the PureProteome protein A and protein G Magnetic Beads (Millipore, Billerica, MA, USA). The immunoprecipitated proteins were separated by SDS–PAGE and probed with an anti-ubiquitin antibody (Enzo Life Science, Farmingdale, NY, USA) or anti-Pgp antibody, respectively, followed by a peroxidase-conjugated secondary antibody.

3.14 Chromatin immunoprecipitation (ChIP)

ChIP experiments were performed using the Magna ChIP A/G chromatin immunoprecipitation kit (Millipore, Billerica, MA, USA). Samples were immunoprecipitated with 5 µg of anti-β-catenin antibody or with no antibody. The immunoprecipitated DNA was washed and eluted twice with 100 µl of elution buffer (0.1 M NaHCO₃, 1 % w/v SDS), the cross-linking was reversed by

incubating the samples at 65 °C for 6 h. Samples were then treated with 1 µl proteinase K for 1 h at 55 °C. The DNA was eluted in 50 ml of H$_2$O and analyzed by quantitative real-time PCR (qRT–PCR). The putative β-catenin site on *mdr1* promoter was validated by the MatInspector software (http://www.genomatix.de/). As negative control, the immunoprecipitated samples were subjected to PCR with primers matching a region 10,000 bp upstream the *mdr1* promoter, using primers designed with the Primer3 software (http://frodo.wi.mit.edu/primer3).

3.15 Pgp and BCRP activity

Pgp ATPase activity was performed on Pgp-enriched membrane vesicles as detailed in [Kopecka, 2015]. Verapamil (10 µmol/l) was added to the reaction mix to achieve a maximal activation of the Pgp ATPase activity. Results were expressed as nmol hydrolyzed phosphate (Pi)/min/mg proteins, according to the titration curve previously prepared. The Calcein-AM assay, a second assay of Pgp activity, was measured as described [Pati, 2015].

Rhodamine 123 and Hoechst 33342 accumulation in cells were used as further indexes of Pgp activity and BCRP activity, respectively. Cells were washed with PBS, detached with cell dissociation solution (Sigma Chemicals Co), centrifuged at 13,000 × *g* for 5 min and re-suspended in 0.5 ml culture medium containing 5 % v/v FBS. A 50-µl aliquot was taken away, sonicated and used for the measurement of the protein content. Twenty µmol/l of rhodamine 123 or 50 µmol/l Hoechst 33342 were added to the remaining sample. After 10 min at 37 °C, cells were washed three times with PBS and re-suspended in 1 ml PBS. The intracellular fluorescence of rhodamine 123 and Hoechst 33342 was measured fluorimetrically, using a LS-5 spectrofluorometer (PerkinElmer). Excitation and emission wavelengths were: 488 and 520 nm for rhodamine 123, 370 and 450 nm for Hoechst 33342. Fluorescence was converted in nmol/mg cell proteins using a calibration curve previously set.

3.16 Fluorescence microscopy

GBM cells were seeded on sterile glass coverslips in the lower chamber and after 3 days of co-culture, stimolus were added to the upper chamber of Transwell inserts containing hCMEC/D3 cells monolayer. After 24 h GB cells were collected from the lower chamber, were rinsed with PBS, fixed with 4% w/v paraformaldehyde for 15 min, washed three times with PBS and incubated with 4′,6-diamidino-2-phenylindole dihydrochloride (DAPI) for 3 min at room temperature in the dark. Cells were washed three times with PBS and once with water, then the slides were mounted with 4 µl of Gel Mount Aqueous Mounting and examined with a Leica DC100 fluorescence microscope (Leica Microsystems GmbH, Wetzlar, Germany). For each experimental point, a minimum of 5 microscopic fields were examined.

3.17 Proximity ligation assay (PLA)

The CAXII-Pgp interaction was measured with the DuoLink In Situ kit (Sigma Chemicals Co.), using a mouse anti-human Pgp (F4; Sigma Chemical Co.) and a rabbit anti-human CAXII (2310047E01Rik; NovoPro, Shangai, China) antibody, respectively, as per the manufacturer's instructions. Nuclei were counterstained with DAPI. Cells were examined using a Leica TCS SP2 AOP confocal laser-scanning microscope (10× ocular lens; 63× objective lens; Leica Microsystem). For each experimental condition, a minimum of five fields were examined.

3.18 Flow cytometry analysis

Cells were washed with PBS, detached with cell dissociation solution (Sigma Chemical Co.) and re-suspended in medium containing 5 % v/v FBS. Samples were washed with 0.25 % w/v BSA–PBS, permeabilized or not with 0.1% w/v saponin/Hepes, incubated with the primary antibody for Frizzled (Santa Cruz Biotechnology Inc.), LRP6 (Abcam), anti-CAXII (Abcam) or anti-ABCB1/Pgp (MRK16; Kamiya, Seattle, WA) for 45 min at 4 °C, then washed twice and incubated with secondary FITC-conjugated antibody for 30 min at 4 °C. After washing and fixing in paraformaldehyde (PFA) 2 % w/v, the surface amount of Frizzled, LRP6 or anti-CAXII antibody was detected on 100,000 cells by a FACS Calibur system, using the Cell Quest software (Becton–Dickinson) or *Guava® easyCyte* flow cytometer (Millipore), using the InCyte software (Millipore). Control experiments included incubation of cells with non-immune isotypic antibody, followed by the secondary antibody.

3.19 Cell cycle analysis

For cell cycle distribution, the glioblastoma cells were washed twice with fresh PBS, incubated in 0.5 ml of ice-cold 70% v/v ethanol for 15 min, then centrifuged at 1,200 g for 5 min at 4°C and rinsed with 0.3 ml of citrate buffer (50 mmol/l Na_2HPO_4, 25 mmol/l sodium citrate, 1% v/v Triton X-100), containing 10 mg/ml propidium iodide and 1 mg/ml RNAse (from bovine pancreas). After 15 min incubation in the dark, the intracellular fluorescence was detected by a FACS Calibur flow cytometer (Becton Dickinson). For each analysis, 10,000 events were collected and analyzed by the Cell Quest software (Becton Dickinson).

3.20 Proliferation assays of glioblastoma cells in co-culture models

1,000 GB cells were seeded in the lower chamber of Transwell, containing confluent hCMEC/D3 cells in the insert. This time was considered "day 0" in the proliferation assay. After 3 days of co-culture, the upper chamber of the Transwell inserts was filled with fresh medium or medium containing stimulus: 50 μmol/l TMZ for 72 h, 5 μmol/l DOX for 24 h, 50 μmol/l TMZ for 72 h plus 5 μmol/l DOX in the last 24 h, 20 nmol/l vinblastine for 24 h, 50 μmol/l TMZ for 72 h plus 20 nmol/l vinblastine in the last 24 h, 10 μmol/l topotecan for 24 h, 50 μmol/l TMZ for 72 h plus 10 μmol/l topotecan in the last 24 h, 10 mmol/l Y27632 for 3 h, 5 mmol/l DOX for 24 h, 10 mmol/l Y27632 for 3 h followed by 5 mmol/l DOX for 24 h . The treatments were repeated every 7 days, for 4 weeks. At day 7, 14, 21, and 28, GB cells were collected, transferred into a 96-well plate, fixed with 4 % w/v paraformaldehyde, and stained with 0.5 % w/v crystal violet solution for 10 min at room temperature. The plate was washed three times in water, then 100 μl of 0.1 mmol/l sodium citrate in 50 % v/v ethanol was added to each well and the absorbance was read at 570 nm. The absorbance units were converted into cell number, according to a titration curve obtained with serial cells dilutions of each cell line. To check that hCMEC/D3 cells retain BBB properties, the permeability to DEXT and inulin was measured weekly in a parallel set of Transwell.

3.21 Cytotoxicity, viability and apoptosis assays

The release of lactate dehydrogenase (LDH) in cell supernatant is considered an index of cells damage and necrosis (Riganti, 2013). The extracellular medium was centrifuged at 12,000 × g for 15 min to pellet cellular debris, whereas the cells were washed with fresh medium, detached with

0.01% v/v trypsin/EDTA, re-suspended in 0.2 ml of 82.3 mM triethanolamine phosphate-HCl (pH 7.6) and sonicated on ice with two 10 s-bursts. LDH activity was measured in the extracellular medium and in the cell lysate: 50 µl of supernatant from extracellular medium or 5 µl of cell lysate were incubated at 37°C with 5 mmol/l NADH. The reaction was started by adding 20 mmol/l pyruvic acid and was followed for 6 min, measuring absorbance at 340 nm with a Packard EL340 microplate reader (Bio-Tek Instruments, Winooski, VT). The reaction kinetics was linear throughout the time of measurement. Results were expressed as percentage of extracellular LDH *versus* total (intracellular plus extracellular) LDH. Trypan Blue and Neutral Red staining were used as viability assays. For Trypan blue dye exclusion test, cells were plated at a density of 2×10^5 cells in 5 ml medium in a 25 cm^2 flask, allowed to grow for 24 h and then treated with drugs for 72 h at 37°C in a 5% O^2/CO^2 atmosphere. The number of viable cells was determined using a TC20 automated cell counter (Bio-Rad) and cytotoxicity was expressed by the number of surviving cells as percentage of control (untreated cells). All experiments were performed in quadruplicate. For Neutral Red staining, 1×10^5 cells were seeded in 96-well plates and treated as reported in the Results, then incubated 1 h at 37°C with Neutral Red solution diluted 1:50 in complete medium. Cells were washed 3-times in PBS and once in 1:1 solution of citrate buffer (50 mmol/l sodium citrate, pH 7.5)-70% methanol. The absorbance at 540 nm was read using a Packard EL340 microplate reader (Bio-Tek Instruments, Winooski, VT). The absorbance of untreated cells was considered as 100% viability; the results were expressed as percentage of viable cells vs. untreated cells. The apoptosis of GB cells was assessed by analyzing the cleavage of Caspase-3 by western blotting, as described above, and by enzymatic assay, as detailed in (Pinzón-Daza, 2012). Cells were lysed in 0.5 ml of Caspase lysis buffer (20 mmol/l HEPES/KOH, 10 mmol/l KCl, 1.5 mmol/l MgCl$_2$, 1 mmol/l EGTA, 1 mmol/l EDTA, 1 mmol/l DTT, 1 mmol/l PMSF, 10 µg/ml leupeptin; pH 7.5). Then 20 µg cell lysates were incubated for 1 h at 37°C with 20 µmol/l of the fluorogenic substrate of Caspase-3, DEVD-7-amino-4-methylcumarine (DEVD-AMC), in 0.25 ml Caspase assay buffer (25 mmol/l HEPES, 0.1% w/v 3-[(3-cholamidopropyl)dimethylammonio]-1-propanesulfonate CHAPS, 10% w/v sucrose, 10 mmol/l DTT, 0.01% w/v egg albumin; pH 7.5). The reaction was stopped by adding 0.75 ml ice-cold 0.1% w/v trichloroacetic acid and the fluorescence of the AMC fragment released by active Caspase-3 was read using a LS-5 spectrofluorimeter (PerkinElmer). Excitation and emission wavelengths were 380 nm and 460 nm respectively. Fluorescence was converted in pmol/µg cell protein using a calibration curve prepared previously with standard solutions of AMC.The amount of the hydrolyzed DEVD-7-amino-4-methylcumarine, a substrate of Caspase-3, was measured fluorometrically. Results were expressed as nmol/mg cell protein using a calibration curve prepared with standard solutions of amino-4-methylcumarine.

3.22 Quantitative real-time PCR (qRT-PCR)

Total RNA was extracted and reverse-transcribed using the QuantiTect Reverse Transcription Kit (Bio-Rad). qRT-PCR was carried out using IQ SYBR Green Supermix (Bio-Rad), according to the manufacturer's instructions. The same cDNA preparation was used to quantify the genes of interest and the housekeeping genes. Primer sequences were designed with the Primer3 software (http://frodo.wi.mit.edu/primer3). The relative quantification was performed by comparing each PCR product with the housekeeping PCR product using Bio-Rad software gene expression quantitation (Bio-Rad).

3.23 Promoter methylation assay

Genomic DNA (1 μg) was subjected to bisulphite modification using the Methyl Easy Xceed kit (Human Genetics Signatures, Randwick, Australia), following the manufacturer's instructions. *Wnt3* promoter sequence was obtained using the UCSC Genome Browser (http://genome.ucsc.edu/). The CpG islands localization on *Wnt3* promoter and the design of primers for methylation-specific PCR (MSP) were performed with Methprimer software (http://www.urogene.org /methprimer). MSP was performed with AmpliTaq gold DNA polymerase (Applied Biosystems, Carlsbad, CA, USA), including universally methylated (CpGenome, Millipore) and unmethylated DNA samples (Human Genetics Signatures) as control. PCR products were visualized on a 3 % w/v agarose gel, stained with 0.05 % v/v ethidium bromide.

3.24 Generation of Wnt3a overexpressing cells

50,000 adherent 01010627 cells were transfected with 2 μg Wnt3a-pCMV6-AC-GFP (green fluorescence protein) expression vector (Origene Technologies Inc, Rockville, MD) or pCMV6-AC-GFP empty vector (Origene Technologies Inc) as a control, using Turbofectin 8.0 (Origene Technologies Inc). Cells were sorted 24 h after the transfection by detecting the GFP-positive cells (FACSCalibur system, Becton Dickinson). Transfected cells (01010627 AC Wnt3a+) were re-seeded in fresh AC medium and used for experiments. Subcultures of 01010627 AC Wnt3a+ cells stably overexpressing Wnt3a were set up, by selecting cells in neomycin-containing medium.

3.25 Generation of Wnt3-silenced cells

A total of 300,000 hCMEC/D3 cells were treated with Turbofectin 8.0 (Origene Technologies Inc., Rockville, MD, USA) and 1 μg of 29-mer shRNA Wnt3 construct in pGFP-C-shLenti-vector (Origene Technologies Inc.) or non-targeting 29-mer scrambled shRNA cassette in pGFP-C-shLenti Vector (Origene Technologies Inc.), used as control. Twenty-four hours after the transfection, the green fluorescent cells were sorted by flow cytometry analysis. Forty-eight hours after the transfection, the cells were transferred in puromycin-containing medium to select clones stably silenced for Wnt3. The silencing efficacy was controlled every two passages by qRT-PCR and Western blot analysis of Wnt3.

3.26 Generation of RhoA-silenced cells

A quantity of 200,000 cells were transfected with 400 nmol/l of 20 to 25 nucleotide non-targeting scrambled small interfering RNAs (Control siRNAA, Santa Cruz Biotechnology) or specific RhoA siRNAs (Santa Cruz Biotechnology), following the manufacturer's instructions. To verify the silencing efficacy, 48 hours after the transfection, the cells were lysed and checked for the expression of RhoA by western blotting, using an anti-RhoA antibody (Santa Cruz Biotechnology).

3.27 Generation of Pgp- and CAXII-knocked out (KO) clones

5×10^5 cells were transduced with 1μg RNA vector (CRISPR pCas guide vector, Origene, Rockville, MD) targeting *Pgp/ABCB1* or *CAXII*, respectively, or with 1μg not-targeting vector, mixed with 1μg donor DNA vector (Origene), following the manufacturer's instructions. Stable

KO cells were selected in medium containing 1 μg/ml puromycin for three weeks. The efficacy of Pgp and CAXII KO was evaluated by immunoblotting, as reported above.

3.28 RhoA and RhoA kinase activity

To evaluate the RhoA activity, the RhoA-GTP-bound fraction, taken as an index of monomeric G-proteins activation, was measured using the G-LISA RhoA Activation Assay Biochem Kit (Cytoskeleton, Denver, USA), according to the manufacturer's instructions. The absorbance was read at 450 nm, using a Packard EL340 microplate reader (Bio-Tek Instruments, Winooski, VT, USA). For each set of experiments, a titration curve was prepared, using serial dilutions of the Rho-GTP positive control of the kit. The data were expressed as U absorbance/mg cell proteins. The RhoAK activity was measured using the CycLex Rho Kinase Assay Kit (CycLex, Nagano, Japan), following the manufacturer's instructions. For each set of experiments, a titration curve was set, using serial dilutions of recombinant RhoAK (MBL, Woburn, MA, USA). The data were expressed as U absorbance/mg cell proteins.

3.29 Protein tyrosine phosphatase 1B (PTP1B) activity

To measure the activity of endogenous PTB1B in cell lysates, the PTP1B Inhibitor Screening Assay kit (Abcam) was used. Cells untreated or treated with RhoA activator II, Y27632 or both, were washed twice in ice-cold PBS, detached by trypsin/EDTA, rinsed with 0.5 mL of PTP1B assay buffer provided by the kit and sonicated. Cell lysate (200 μl), each containing 100 μg proteins, were transferred into a 96-wells plate, in the presence of 100 mmol/l PTP1B substrate from the kit. The plates were incubated for 30 min at 37°C, then 100 μl of the Red Assay reagent of the kit was added for 20 minu. The absorbance at 620 nm was read using a Packard EL340 microplate reader. The activity of purified PTP1B was measured in a cell-free system: 5 U of human recombinant PTP1B protein (Abcam), diluted in 100 μl of reaction buffer (10 mmol/l Tris/HCl, 50 mmol/l NaCl, 2 mmol/l dithiothreitol, 1 mmol/l $MnCl_2$; pH 7.5), were incubated for 10 min at 37°C, with 10 μg of a recombinant peptide from human GSK3 containing phosphorylated tyrosine 216 (Abcam). To test if RhoAK affects the dephosphorylation of GSK3 by PTP1B, in a parallel set of experiments, PTP1B protein was pre-incubated for 30 min at 37°C with 10 U of human recombinant RhoAK (MBL), diluted in 100 μl of the Rho Kinase buffer (from CycLex Rho Kinase Assay Kit) containing 25 mmol/l ATP. When indicated, 10 μmol/l of the RhoAK inhibitor Y27632 was added. After this preincubation step, a 10 μl aliquot from each sample was removed and used to measure the phosphorylation of PTP1B on serine 50 by western blot analysis. The remaining sample was incubated for 10 min at 37°C with the phospho(Tyr 216)-GSK3 peptide, as reported above. In all samples, the reaction was stopped by adding 100 μl of the Red Assay reagent from the PTP1B Inhibitor Screening Assay kit; the absorbance at 620nm was read after 20 min. For each set of experiments, a titration curve was prepared, using serial dilutions of the phosphate standard from the PTP1B Inhibitor Screening Assay kit. Data were expressed as nmol phosphate/μl. The activity of endogenous PTP1B was then expressed as percentage of the activity of PTP1B of each sample *versus* the activity of PTP1B measured in untreated cells. The activity of purified PTP1B was expressed as percentage of the activity of PTP1B measured after the pre-incubation step with RhoAK *versus* the activity of PTP1B measured without the pre-incubation step with RhoAK.

3.30 *In vivo* glioblastoma models

Syngeneic orthotopic GB rat model. Fischer rats were anesthetized by 1.5–2.5% isoflurane and 0.8 l/min oxygen, and then fixed in a stereotactic apparatus. 100,000 F98 glioma cells in 2 µl DMEM+agar 1% were injected stereotactically into Fischer rats. A 1.2 mm burr hole was drilled into the right side of the skull (2.5 mm anterior and 2 mm lateral to the bregma) to expose the dura mater. Using a microliter syringe equipped with a 26-gauge needle and connected to the manipulating arm of the stereotactic apparatus, glioma cells were injected into the caudate nucleus at a depth of 6 mm from the dura mater over a period of 5 min. A Trypan blue exclusion test was performed to assess cell viability before implantation and cells viability was always greater than 95% (Wyne, 1996). After surgery, animals were treated with ketoprofen (10 mg/ml): 2.5 mg/kg once a day at 48 h intervals for the first and second weeks; 5 mg/kg once a day at 48 h intervals for third week; 5 mg/kg once a day and were housed routinely. At the end of the experiment (11 days after tumor cells' implantation), animals were anesthetized with Zoletil®100 0.1 ml/kg intraperitoneally and euthanized with CO_2. Efficacy of ddMTX-loaded SLNs ApoE toward syngeneic F98/Fischer glioma model was assayed following the administration of SLNs at a 1.6 mg/kg ddMTX dose (corresponding to 1 mg/kg MTX) at days 7 and 9 after implantation (six animals; n=8), according to a modified literature method (Jain, 2015). Intravenous administration was performed by injection in the tail vein. Untreated rats were used as controls (n=8), while positive controls were obtained by administering oral TMZ (current pharmacological adjuvant treatment for GBM) at days 7–10 with a dose of 7 mg/kg (n=4).

Glioma growth in F98/Fisher Rat glioma model was monitored at different times (days 7, 9 and 11 after implantation) through MRI, using a high-field (7 T) horizontal bore magnet (Bruker Pharmascan MRI, Ettingen, Germany). Rats were anesthetized with 2% isoflurane in an oxygen/air mixture (1:1) at a flow rate of 3 l/min and placed in a magnetic resonance probe in the supine position. The respiration rate (typical range, 30–50 breaths/min) of the animals was monitored throughout the whole experiment, using an abdominal pneumatic pillow. T1-weighted images (15 transverse slices with a thickness of 1.5 mm and taken in a field of view of 5.0×5.0 cm^2 with a matrix of 128×128 pixel) were acquired using a multislice spinecho sequence (repetition time/echo time TR/TE: 400/8.4 ms, number of averages: 6 on axial and coronal planes after intravenous injection of 0.5 mmol/kg of gadobenate dimeglumine (MultiHance®, Bracco Imaging, Milan, Italy) in the tail vein (Jain, 2015). Glioma volume was evaluated through Bruker Pharmascan software: the brain was divided in 15 transverse slices of 1.5 mm thickness, and the area evidenced by gadobenate dimeglumine (tumor) was approximated by the software. Final integration was performed between calculated areas and slice thickness.

Subcutaneous patient-derived GB model. As pilot study, 1×10^6 AC or SCs/NS GB cells derived from patients, mixed with 100 µl Matrigel, were injected subcutaneously in 6-8 week olds female BALB/c *nu/nu* mice. When the tumor reached a volume of 50 mm^3, animals were randomized into the following groups (10 animals/group) and treated with 2 cycles of 5 consecutive days (days: 1-5 11-15 after randomization) as follows: 1) control group, treated with 0.2 ml saline solution intravenously (i.v.); 2) compound **1** low dose (LD) group, treated with 38 ng/kg compound **1** (in 0.2 mL saline solution; final concentration: 10 nmol/l) i.v.; 3) **1** high dose (HD) group, treated with 3800 ng/kg compound **1** (in 0.2 ml saline solution; final concentration: 1 µmol/l) i.v.; 4) temozolomide group, treated with 50 mg/kg TMZ per os (p.o.); 5) TMZ + **1** LD group, treated with 50 mg/kg TMZ p.o. and 38 ng/kg compound **1** i.v.; 6) TMZ + **1** HD group, treated with 50

mg/kg TMZ p.o. and 3800 ng/kg compound **1** i.v. This schedule and dosage of TMZ was chosen as the most effective in reducing AC GB tumor growth after a preliminary study on animals with subcutaneously implanted AC GB, treated as it follows: 1) control group treated with 0.2 ml saline solution i.v., 2 cycles of 5 consecutive days (days: 1-5; 11-15 after randomization); 2) TMZ 3 group treated with 50 mg/kg TMZ p.o., for 3 consecutive days (days: 1-3 after randomization); 3) TMZ 3 (X2) group, treated with 50 mg/kg TMZ p.o., 2 cycles of 3 consecutive days (days: 1-3; 7-9 after randomization); 4) TMZ 5 group, treated with 50 mg/kg TMZ p.o., for 5 consecutive days (days: 1-5 after randomization); 5) TMZ 5 (x2) group, treated with 50 mg/kg TMZ p.o., 2 cycles of 5 consecutive days (days: 1-5; 11-15 after randomization). Tumor volumes were monitored daily by caliper and calculated according to the equation $(L \times W^2)/2$, where L = tumor length, W = tumor width. Animals were euthanized by injecting zolazepam (0.2 ml/kg) and xylazine (16 mg/kg) intramuscle (i.m.) at day 30. Tumors were excised and photographed immediately after mice sacrifice.

Orthotopic patient-derived GB model. 1×10^6 SCs/NS cells GB cell, stably transfected with the pGL4.51[luc2/CMV/Neo] vector encoding for luciferase (Promega Corporation, Madison, WI), mixed with 2 µl DMEM+agar 1% were injected stereotactically injected into the right caudatus nucleus into 6-8 week olds female BALB/c *nu/nu* mice (weight: 20.3 g $\pm$ 2.4), anesthetized with sodium phenobarbital (60 mg/kg) intraperitoneally (i.p.). Tumor growth was monitored by *in vivo* bioluminescence (Xenogen IVIS Spectrum, PerkinElmer, Waltham, MA) at day 6, 14 and 24 post-implantation. At day 7, animals were randomized into the following groups (6 animals/group) and treated with 2 cycles of 5 consecutive days (days: 7-11; 17-21 after randomization) as follows: 1) control group, treated with 0.2 ml saline solution i.v.; 2) **1** group, treated with 3800 ng/kg compound **1** (in 0.2 ml saline solution; final concentration: 1 µmol/l) i.v.; 3) temozolomide group, treated with 50 mg/kg TMZ *per os*; 4) TMZ + **1** group, treated with 50 mg/kg TMZ p.o. and 3800 ng/kg compound **1** i.v. Animals were euthanized at day 30, as reported.

3.31 Immunohistochemistry and hematochemical parameters

After euthanasia, all animals were submitted to a complete necropsy. Lungs, heart, liver, kidneys, spleen and brain were collected and stored in 10% neutral buffered formalin for histological evaluation. Slide sections (5 mm thick) were obtained using a microtome (Leica Microsystems, Wetzlar, Germany) and stained with hematoxylin and eosin stain. During brain evaluation, histological features were classified as positive if a tumor mass was present and negative if no tumor was detected. Immunohistochemical staining was also done on selected sections. Primary antibodies included: anti-CAXII; anti-Pgp (Millipore); anti-cleaved Caspase-3 (Asp175, Cell Signaling); anti-Ki-67 (Dako, Glostrup, Denmark); anti-GFAP (Dako), followed by a peroxidase-conjugated secondary antibody (Dako). The nuclei were counterstained with hematoxylin. Positive and negative immunohistochemistry controls were routinely used. *In situ* TUNEL assay was performed using *In situ* Cell Death Detection kit (Roche, Diagnostic Corp.) according to the manufacturer's instructions. All staings were visualized by Olympus Provis AX70 microscope equipped with a digital camera or a Leica DC100 microscope (Leica Microsystems GmbH, Wetzlar, Germany; 10 × ocular lens, 20 × or 63 × objective). Quantification of the staining was done by using an Image Pro Plus analysis system. Each immunohistochemical marker was evaluated in at least ten different fields, and particularly measuring the numbers of positive cells for cleaved Caspase-3 and Ki-67.

The hemocromocytometric analysis was performed with a UniCel DxH 800 Coulter Cellular Analysis System (Beckman Coulter, Miami, FL) on 0.5 ml of blood collected immediately after mice sacrifice; the hematochemical parameters LDH, aspartate aminotransferase (AST), alanine aminotransferase (ALT), alkaline phosphatase (AP), creatinine, CPK were measured on the same bloud samples, using the respective kits from Beckman Coulter Inc.

3.32 Statistical analysis.

All data in the text and figures are provided as means $\pm$ SD. The results were analyzed by a one-way analysis of variance (ANOVA) and Tukey's test, using Statistical Package for Social Science (SPSS) software (IBM SPSS Statistics v.19). The Kaplan-Meier method was used to calculate overall survival of mice. Log rank test was used to compare the outcome of the treatment groups, using MedCalc® software (v.17.4). $p < 0.05$ was considered significant.
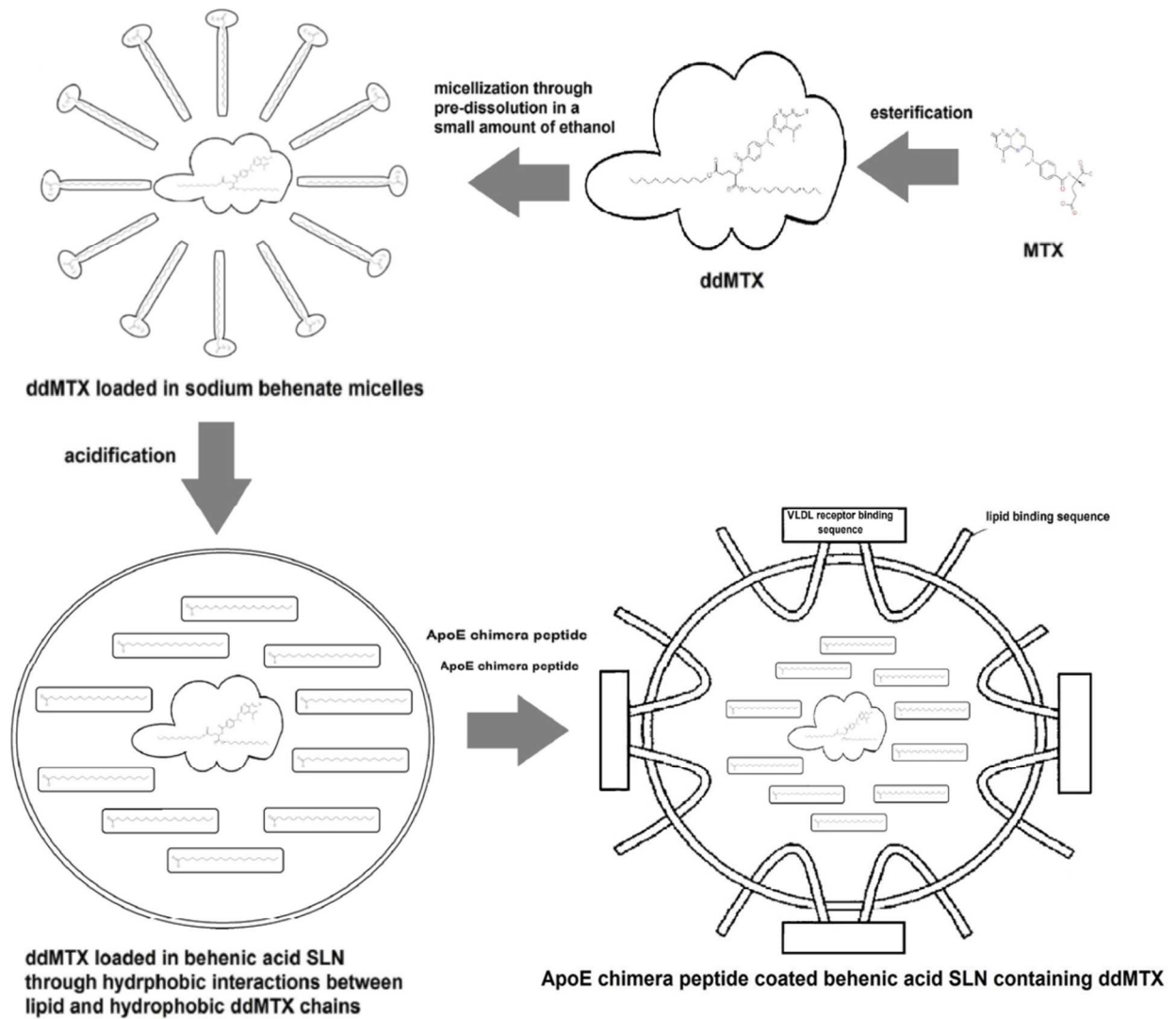
Figure 9. Schematic representation of solid lipid nanoparticles' formulation and functionalization. Didoceylmethotrexate (ddMTX) was synthesized by esterification of Methotrexate (MTX) and loaded in Solid lipid nanoparticle (SLN) by coacervation method [Nelson, 1977]. Then SLN was incubated at room temperature for 1 h with a concentrated aqueous solution of ApoE chimera perptide to obtain ApoE- ddMTX-SLN suspension.

4. RESULTS

4.1 Aim1: Molecular mechanisms determining low drug delivery across BBB

4.1.1 Wnt controls Pgp expression in human BBB cells *via* GSK3/β-catenin and RhoA/RhoA kinase pathways

Human hCMEC/D3 BBB cells exhibited a GSK3 constitutively phosphorylated on tyrosine 216, i.e. activated, and a β-catenin constitutively phosphorylated on serine and threonine (Figure 10A), i.e. primed for ubiquitination. Notwithstanding this pattern, untreated hCMEC/D3 cells had a basal amount of β-catenin translocated into the nucleus (Figure 10B) and bound to the promoter of *mdr1* gene (Figure 10C), which encodes for Pgp. In line with previous findings obtained on hCMEC/D3 cells and primary human brain microvascular endothelial cells [Lopez, 2011], the Wnt activator WntA decreased the phosphorylation/activation of GSK3, strongly reduced the phosphorylation of β-catenin (Figure 10A), increased the nuclear translocation and the binding of β-catenin to the *mdr1* promoter (Figure 10B-C); the Wnt inhibitor Dkk-1 produced opposite effects (Figure 10A-C). In keeping with these results, WntA increased and Dkk-1 decreased the mRNA level of *mdr1* in hCMEC/D3 cells (Figure 10D). In parallel, Wnt modulated the activity of RhoA and RhoA kinase that are effectors of Wnt [Rossol-Allison, 2009]: as shown in Figure 10E, WntA increased and Dkk-1 decreased the GTP binding to RhoA and the activity of RhoA kinase.

These data suggest that both the so-called "canonical" Wnt/GSK3/β-catenin pathway and the "non canonical" Wnt/RhoA/RhoA kinase pathway are active in the hCMEC/D3 cells and vary their activity in response to Wnt activators and inhibitors.

Our findings suggest that Wnt/GSK3/β-catenin axis upregulates Pgp in BBB. It is not known whether:

1) also Wnt/RhoA/RhoA kinase pathway may control Pgp expression in BBB cells;

2) there is a cross-talk between canonical Wnt/GSK3/β-catenin pathway and non canonical Wnt/RhoA/RhoA kinase pathway in modulating Pgp levels.

To clarify this point, I constitutively activated RhoA with the RhoA activator II [Poller, 2010] (Figure 11A) and silenced RhoA in hCMEC/D3 cells (Figure 11B), respectively. The cells with active RhoA showed a reduced phosphorylation of GSK3 and β-catenin (Figure 11C), and an increased β-catenin nuclear translocation (Figure 11D). By contrast, the RhoA-silenced cells exhibited a higher amount of phosphorylated GSK3 and β-catenin (Figure 11C), and a reduced β-catenin nuclear translocation (Figure 11D).

These data suggest that the activity of the Wnt non canonical transducer RhoA controls the activation of the Wnt canonical transducers GSK3/β-catenin in our model.

Moreover, the RhoA activation increased, while the RhoA silencing decreased the binding of β-catenin to *mdr1* promoter (Figure 11E) and the levels of *mdr1* mRNA (Figure 11F) in the hCMEC/D3 cells. The increase of *mdr1* expression induced by WntA or RhoA activator II was not paralleled by an increase in permeability to small molecules, such as sucrose and sodium fluorescein (Figure 12), thus ruling out a Wnt- or RhoA-mediated increase of the monolayer passive permeability.
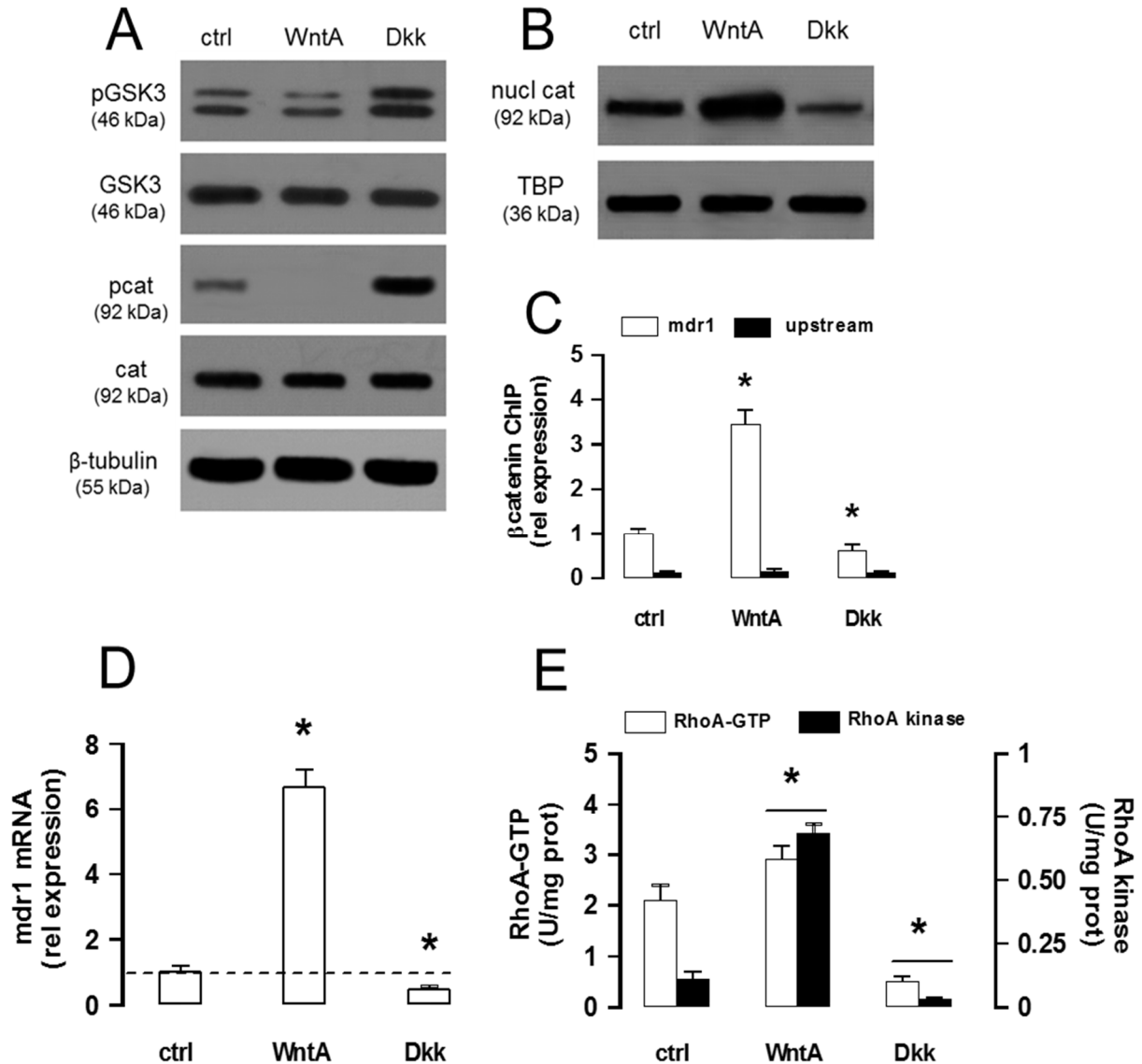
Figure 10. Wnt controls the β-catenin induced transcription of Pgp and RhoA activity in human BBB cells. The hCMEC/D3 cells were grown in fresh medium (*ctrl*), with the Wnt activator 2-amino-4-(3,4-(methylenedioxy)benzylamino)-6-(3-methoxyphenyl)pyrimidine (*WntA*; 20 µmol/l for 24 h) or the Wnt inhibitor Dkk-1 protein (*Dkk*; 1 µg/ml for 24 h) **A.** Western blot analysis of phospho(Tyr216)GSK3 (*pGSK3*), GSK3, phospho(Ser33/Ser37/Thr41)β-catenin (*pcat*), β-catenin (*cat*) in whole cell lysates. The β-tubulin expression was used as a control of equal protein loading. The figure is representative of 3 experiments with similar results. The band density ratio between each protein and β-tubulin was expressed as arbitrary units. *Versus ctrl* cells: * $p < 0.02$. **B**. Nuclear extracts were analyzed for the amount of β-catenin (*nucl cat*). The expression of TBP was used as a control of equal protein loading. The figure is representative of 3 experiments with similar results. The band density ratio between each protein and TBP was expressed as arbitrary units. *Versus ctrl* cells: * $p < 0.02$. **C.** ChIP assay. The genomic DNA was extracted, immunoprecipitated with an anti-β-catenin antibody and analyzed by qRT-PCR, using primers for the β-catenin binding site on *mdr1* promoter (*open bars*) or for an upstream region (*black bars*), chosen as a negative control. Results are presented as means ± SD (n = 4). *Versus ctrl*: * $p < 0.05$. **D.** The *mdr1* expression was detected by qRT-PCR. Data are presented as means ± SD (n = 4). *Versus ctrl*: * $p < 0.02$. **E.** RhoA/RhoA kinase activity. The samples were subjected to ELISA assays to measure the amount of RhoA-GTP (*open bars*) and the activity of RhoA kinase (*black bars*). Data are presented as means ± SD (n = 4). *Versus ctrl*: * $p < 0.05$.
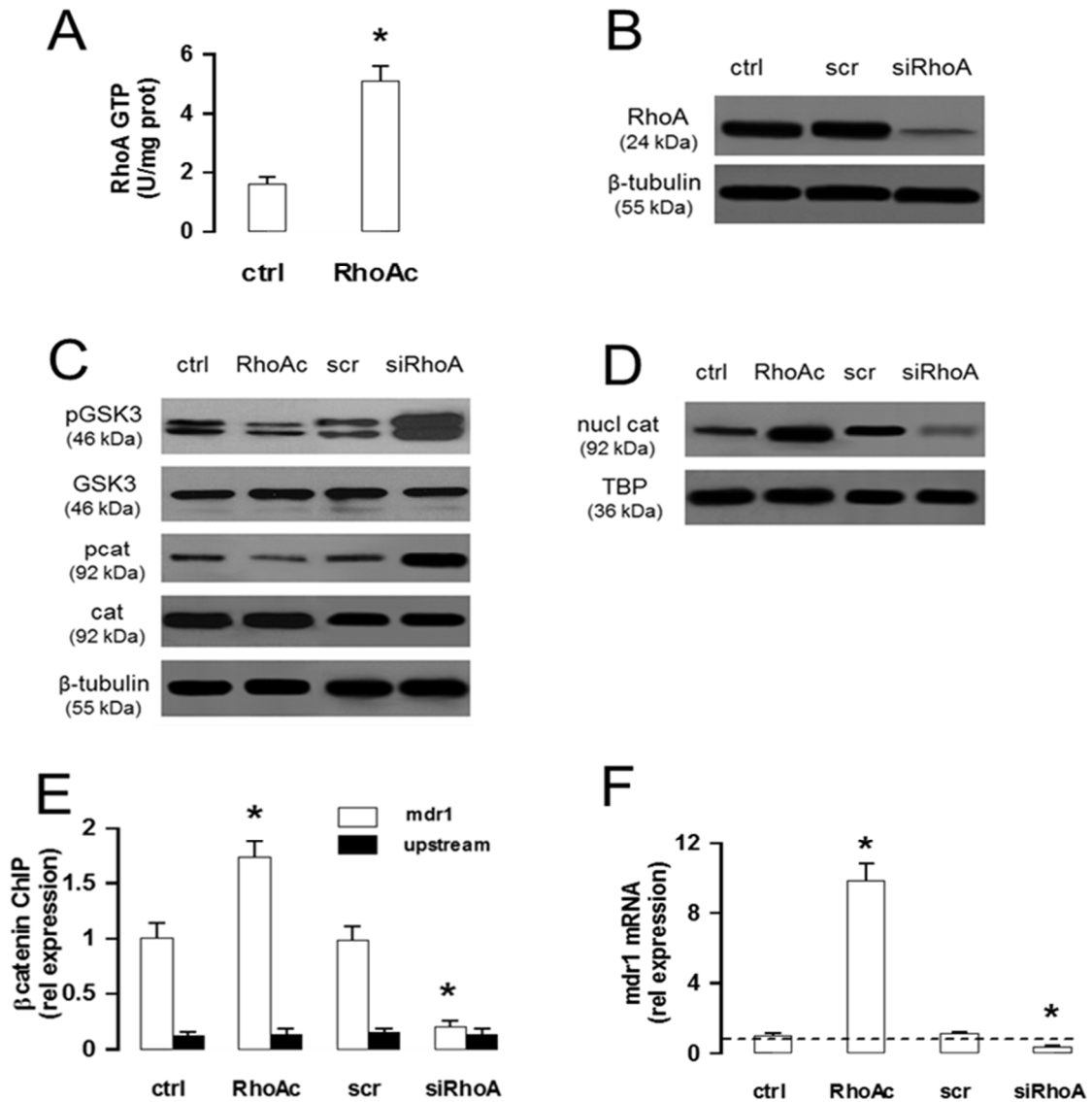
Figure 11. The RhoA activity controls the GSK3/β-catenin-driven transcription of Pgp in human BBB cells.
A. The hCMEC/D3 cells were grown in fresh medium in the absence (*ctrl*) or in the presence of the RhoA activator II (*RhoAc*; 5 μg/ml for 3 h), then the activity of RhoA was measured by an ELISA assay. Data are presented as means ± SD (n = 4). *Versus ctrl*: * p < 0.005. **B.** The cells were cultured for 48 h with fresh medium (*ctrl*), treated with a non targeting scrambled siRNA (*scr*) or a RhoA-targeting specific siRNA pool (*siRhoA*). The expression of RhoA was measured in whole cell lysates by Western blotting. The β-tubulin expression was used as a control of equal protein loading. The figure is representative of 3 experiments with similar results. **C.**Western blot analysis of phospho(Tyr216)GSK3 (*pGSK3*), GSK3, phospho(Ser33/Ser37/Thr41)β-catenin (*pcat*), β-catenin (*cat*) in whole cell lysates of hCMEC/D3 cells treated as described in **A-B**. The β-tubulin expression was used as a control of equal protein loading. The figure is representative of 3 experiments with similar results. **D.** Nuclear extracts from cells treated as described in **A-B** were analyzed for the amount of β-catenin (*nucl cat*). The expression of TBP was used as a control of equal protein loading. **E.** Cells were cultured as reported in **A-B.** After 3 h (for the RhoA activator II-treated cells) or 48 h (for the scrambled- and RhoA-targeting siRNA-treated cells), the genomic DNA was extracted, immunoprecipitated with an anti-β-catenin antibody and analyzed by qRT-PCR, using primers for the β-catenin binding site on the *mdr1* promoter (*open bars*) or for an upstream region (*black bars*), chosen as a negative control. The *ctrl* bars in the figure correspond to the DNA extracted after 48 h from hCMEC/D3 cells; the results were superimposable for the DNA of untreated cells extracted after 3 h (not shown in the figure). Results are expressed as means ± SD (n = 4). *Versus ctrl*: * p < 0.01. **F.** The cells were treated as detailed in **A-B**. After 3 h (for the RhoA activator II-treated cells) or 48 h (for the scrambled- and RhoA-targeting siRNA-treated cells), the *mdr1* expression was detected by qRT-PCR. Data are presented as means ± SD (n = 4). *Versus ctrl*: * p < 0.005.
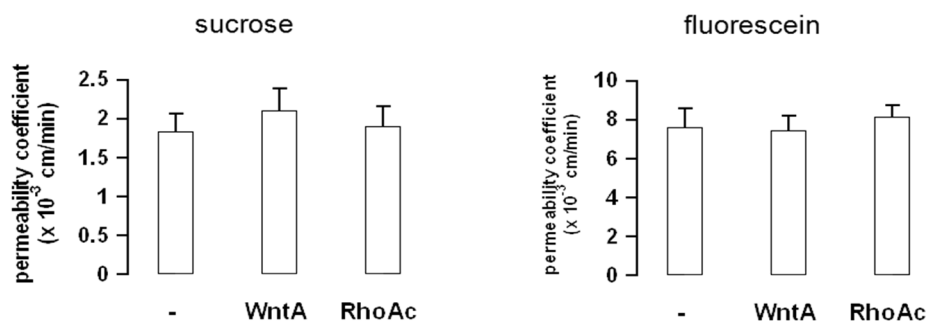
Figure 12. Effects of Pgp inducers on the permeability to small molecules in human BBB cells. The hCMEC/D3 cells were grown for 7 days up to confluence in Transwell inserts, then the medium in the upper chamber was replaced with fresh medium (-) or medium containing the Wnt activator 2-amino-4-(3,4-(methylenedioxy)benzylamino)-6-(3-methoxyphenyl)pyrimidine (*WntA*; 20 µmol/l for 24 h) and the RhoA activator II (*RhoAc*; 5 µg/ml for 3 h), chosen as Pgp inducers. At the end of the incubation period, 2 µCi/ml [^{14}C]-sucrose or 10 µg/ml sodium fluorescein were added in the upper chamber. After 3 h the amount of each compound recovered from the lower chamber was measured by liquid scintillation (for sucrose) or fluorimetrically (for sodium fluorescein). Permeability coefficients were calculated as reported under Materials and methods. Measurements were performed in duplicate and data are presented as means ± SD (n = 3).

## 4.1.2 RhoA kinase inhibition reduces the Pgp transcription in BBB cells, by inhibiting PTP1B activity and increasing the GSK3-mediated phosphorylation and ubiquitination of β-catenin

Since in hCMEC/D3 cells Wnt controls the activity of RhoA and its downstream effector RhoA kinase (Figure 10E), I next investigated whether RhoA kinase mediated the cross-talk between the Wnt/GSK3 canonical pathway and the Wnt/RhoA non canonical pathway. Time-dependence experiments with the RhoA kinase inhibitor Y27632 showed that at 10 µmol/l this compound effectively inhibited the RhoA kinase activity at each time point considered (Figure 13A) and decreased the β-catenin nuclear translocation at the time points from 3 to 24 h (Figure 13B). After 3 h, when the reduction of RhoA kinase activity and β-catenin was maximal, Y27632 did not change the expression of claudin-3, claudin-5, occludin, ZO-1 (Figure 13C) and did not alter the permeability coefficient of DEXT, inulin and sucrose (Figure 13D), suggesting that the RhoA kinase inhibition did not affect the integrity of TJs and the paracellular transport processes. In the light of these results, Y27632 was used at 10 µmol/l for 3 h in all the following experiments: in these conditions, Y27632 increased the phosphorylation of GSK3 and β-catenin (Figure 14A) and reduced the β-catenin nuclear translocation (Figure 14B), also in the presence of a constitutively activated RhoA (Figure 14A-B). The tyrosine phosphatase PTP1B reduces the activity of GSK3 by dephosphorylating tyrosine 216, which is critical for the GSK3 activity [Flahaut, 2009]. PTP1B is in its turn activated by the phosphorylation on serine 50, operated by serine/threonine kinases [Schaich, 2009]. I thus wondered whether RhoA kinase may modulate the GSK3 phosphorylation *via* PTP1B. PTP1B was basally phosphorylated on serine 50 in the hCMEC/D3 cells (Figure 14C). Interestingly, the cells with activated RhoA had increased levels of phospho(Ser50)PTP1B, which was strongly reduced in cells treated with the RhoA kinase inhibitor Y27632. The latter also abolished the phosphorylation of PTP1B induced by active RhoA (Figure 14C). The endogenous activity of PTP1B was significantly increased in cells with activated RhoA and significantly decreased in Y27632-treated cells (Figure 14D). To test whether RhoA kinase, by phosphorylating PTP1B on serine 50, may decrease the phosphorylation of GSK3 on tyrosine 216, I set up a cell-free system and measured the activity of recombinant PTP1B protein, using as a substrate a synthetic peptide derived from GSK3, containing the phosphorylated tyrosine 216 (Figure 14E-F). PTP1B, when pre-incubated with the recombinant RhoA kinase in this cell-free system, was phosphorylated on serine 50, an effect that was prevented by Y27632 (Figure 14E). In keeping with this observation, the pre-incubation with RhoA kinase increased the PTP1B-mediated dephosphorylation of the recombinant phospho(Tyr 216)GSK3 peptide. Such a dephosphorylation was significantly reduced by the RhoA kinase inhibitor Y27632 (Figure 14F).

These data suggest that RhoA kinase activates PTP1B, promotes the tyrosine dephosphorylation of GSK3 and its inhibition, whereas the RhoA kinase inhibition produces opposite effects.
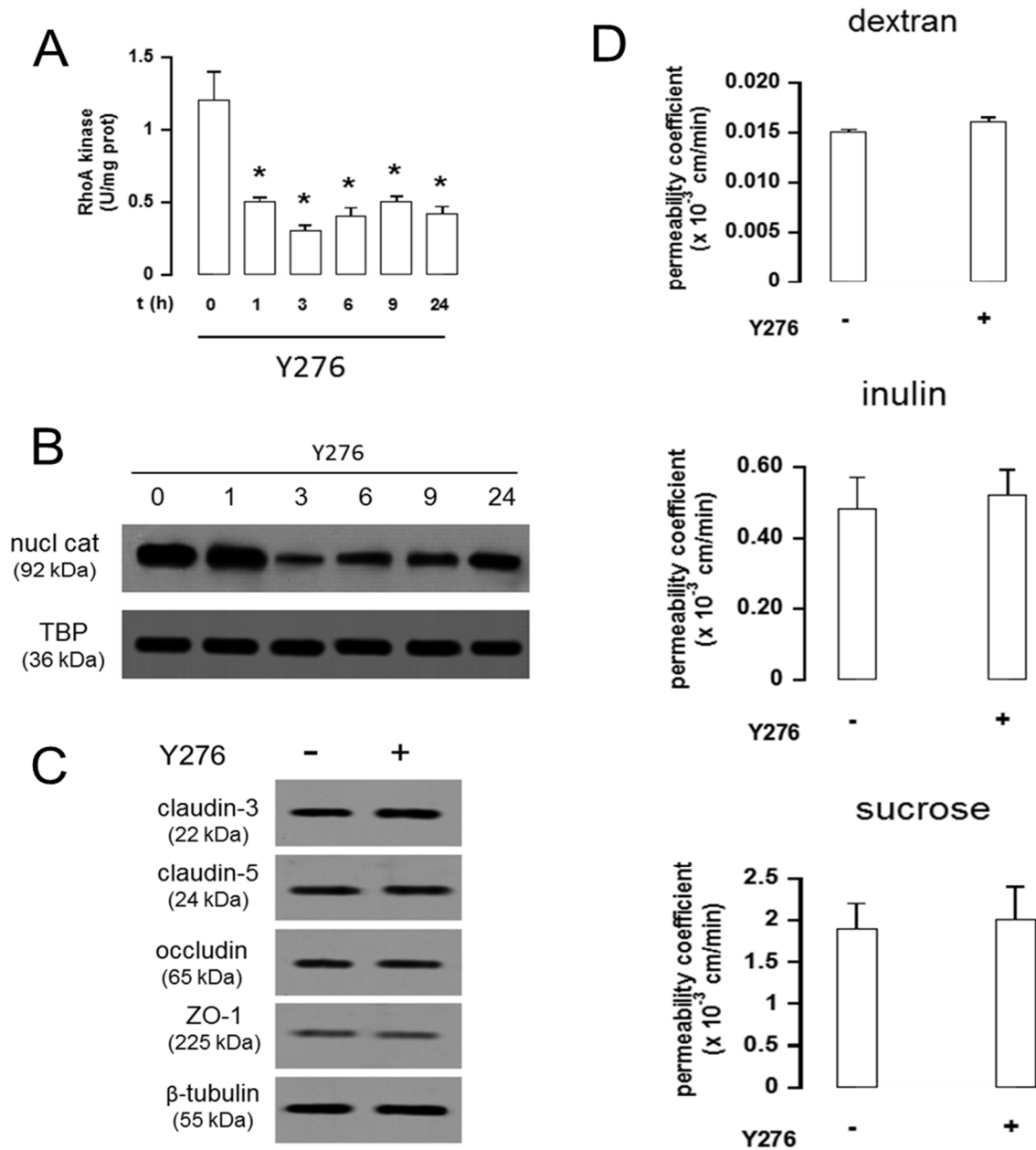
Figure 13. The RhoA kinase inhibition decreases the β-catenin translocation in human BBB cells. The hCMEC/D3 cells were cultured in fresh medium in the absence (*0*) or in the presence of 10 μmol/l RhoA kinase inhibitor Y27632 (*Y276*) for 1, 3, 6, 9, 24 h. **A.** RhoA kinase activity. Samples were subjected to ELISA assays to measure the activity of RhoA kinase. Data are presented as means $\pm$ SD (n = 4). *Versus ctrl*: * p < 0.001. **B.** The nuclear extracts were analyzed for the amount of β-catenin (*nucl cat*). The expression of TBP was used as a control of equal protein loading. The figure is representative of 3 experiments with similar results. **C.** The hCMEC/D3 cells were cultured in fresh medium (-) or in the presence (+) of μmol/l RhoA kinase inhibitor Y27632 (*Y276*) for 3 h, then lysed and subjected to Western blot analysis for claudin-3, claudin-5, occludin, ZO-1. The β-tubulin expression was used as a control of equal protein loading. The figure is representative of 3 experiments with similar results. **D.** The hCMEC/D3 cells were grown for 7 days up to confluence in Transwell inserts, then the medium in the upper chamber was replaced with fresh medium (-) or medium containing (+) 10 μmol/l RhoA kinase inhibitor Y27632 (*Y276*) for 3 h. At the end of the incubation period, 2 μmol/l DEXT-FITC, 2 μCi/ml [^{14}C]-inulin, or 2 μCi/ml [^{14}C]-sucrose were added in the upper chamber. After 3 h the amount of each compound recovered from the lower chamber was measured fluorimetrically (for DEXT-FITC) or by liquid scintillation (for inulin and sucrose). The permeability coefficients were calculated as reported under Materials and methods. Measurements were performed in duplicate and data are presented as means $\pm$ SD (n = 3).
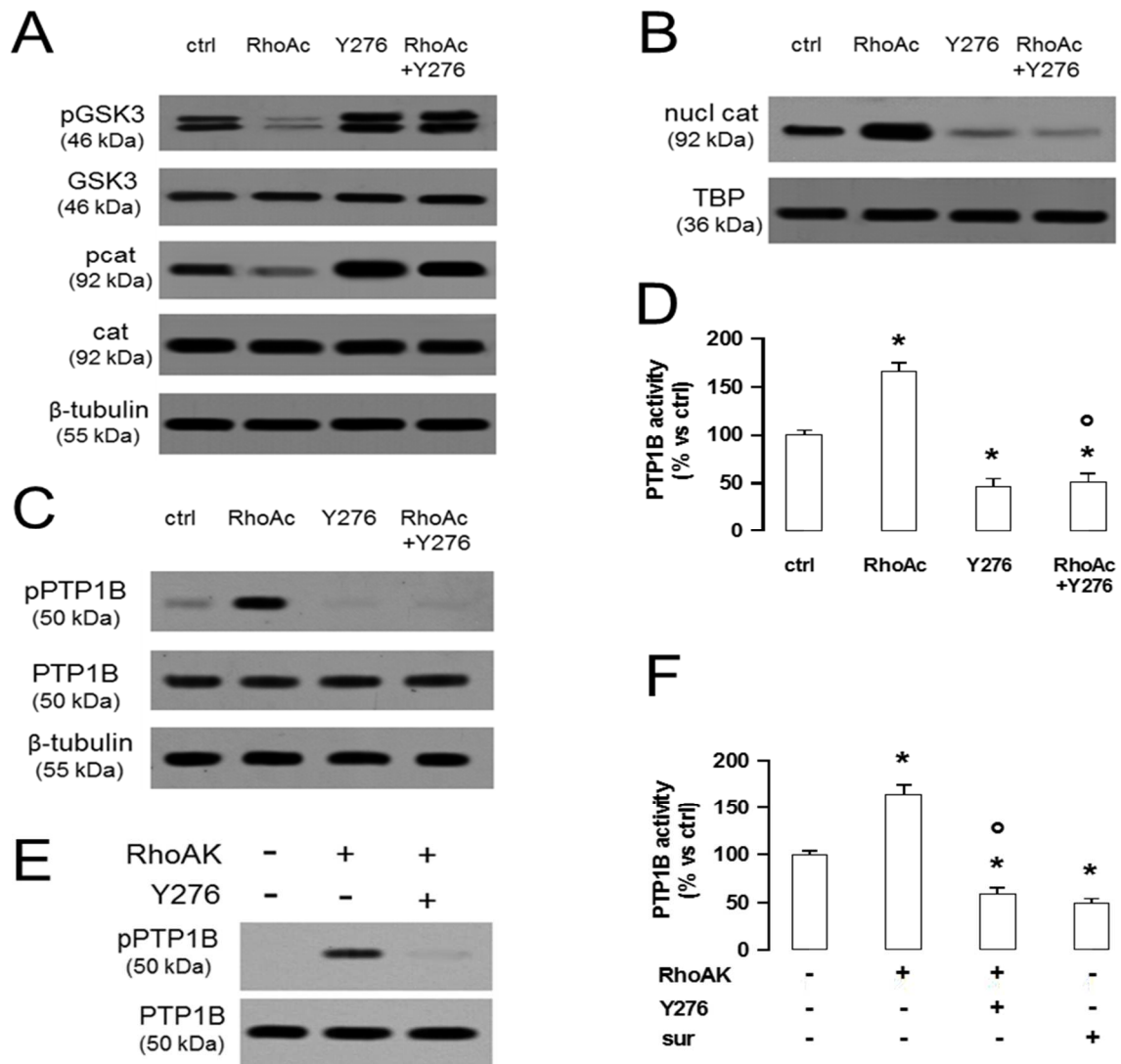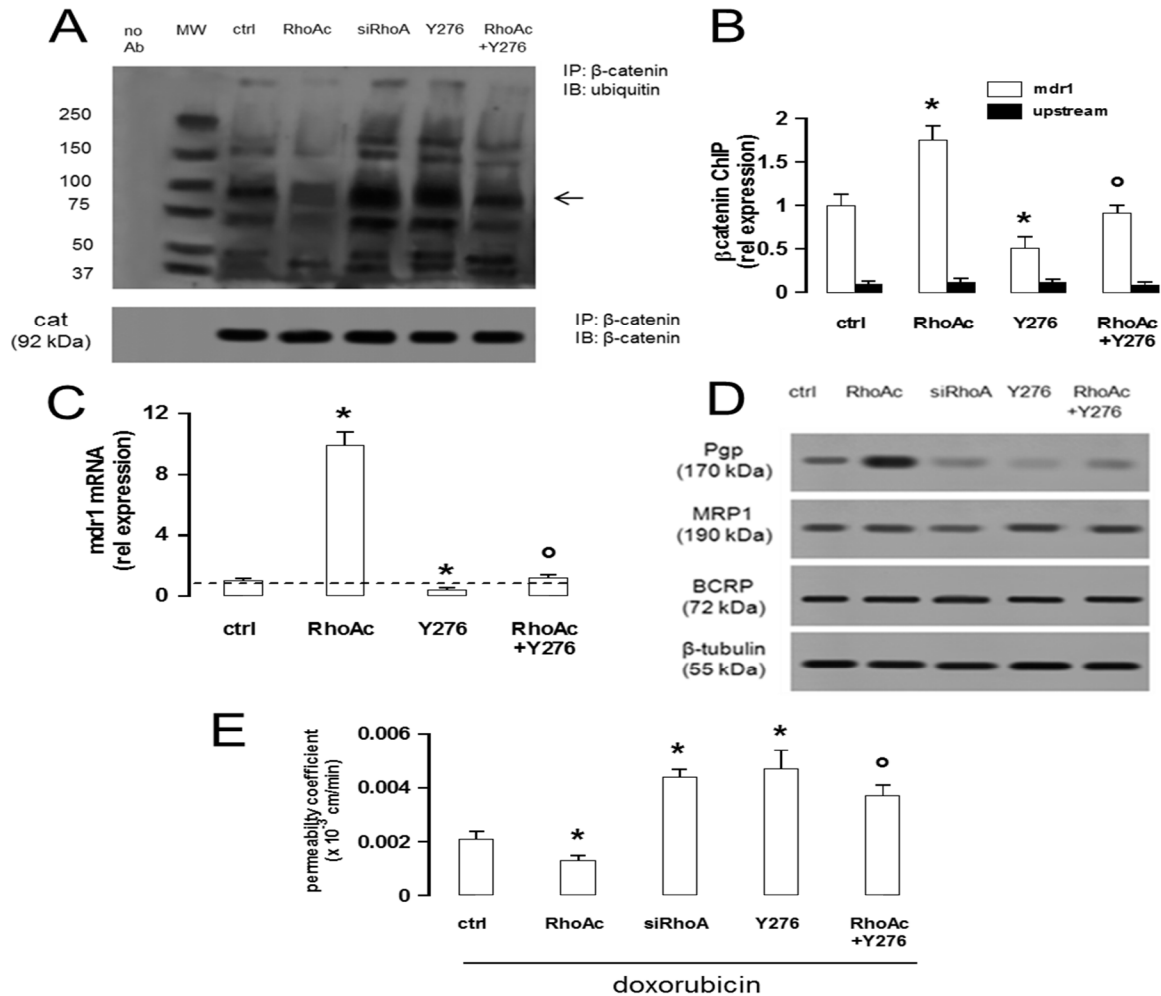
Figure 14. The RhoA kinase inhibition increases the activation of GSK3, by decreasing the activity of PTP1B in human BBB cells. The hCMEC/D3 cells were grown in fresh medium (*ctrl*) or in medium containing the RhoA activator II (*RhoAc*; 5 μg/ml for 3 h) or the RhoA kinase inhibitor Y27632 (*Y276*; 10 μmol/l for 3 h), alone or co-incubated. **A.** Western blot analysis of phospho(Tyr216)GSK3 (*pGSK3*), GSK3, phospho(Ser33/Ser37/Thr41)β-catenin (*pcat*), β-catenin (*cat*) in whole cell lysates. The β-tubulin expression was used as a control of equal protein loading. The figure is representative of 3 experiments with similar results. **B**. The nuclear extracts were analyzed for the amount of β-catenin (*nucl cat*). The expression of TBP was used as a control of equal protein loading. **C**. Western blot analysis of phospho(Ser50)PTP1B (*pPTP1B*) and PTP1B. The β-tubulin expression was used as a control of equal protein loading. The figure is representative of 3 experiments with similar results. **D**. The activity of endogenous PTP1B was measured in cell lysates, as reported under Materials and methods. Data are presented as means $\pm$ SD (n = 3). *Versus ctrl*: * p < 0.002; *versus RhoAc* alone: ° p < 0.001. **E.** *In vitro* phosphorylation of PTP1B in the presence of RhoA kinase and Y27632. 5 U of human recombinant PTP1B were incubated in the absence (-) or in the presence of 10 U of human recombinant RhoA kinase (RhoAK), alone or in the presence of the RhoA kinase inhibitor Y27632 (*Y276*; 10 μmol/l) for 30 min at 37°C, in a reaction buffer containing 25 mmol/l ATP. At the end of this incubation time, samples were resolved by SDS-PAGE and probed with anti-phospho(Ser50)PTP1B (*pPTP1B*) or anti-PTP1B antibodies. The figure is representative of 3 experiments with similar results. **F.** The activity of purified PTP1B was measured in a cell-free system, using a recombinant phospho(Tyr 216)GSK3 peptide as substrate. When indicated, 10 U of RhoA kinase (*RhoAK*), alone or in the presence of Y27632 (*Y276*; 10 μmol/l), were added in the reaction mix 30 min before adding the phospho(Tyr 216)GSK3 peptide. Suramin (*sur*; 10 μmol/l), a known inhibitor of PTP1B, was added together with the phospho(Tyr 216)GSK3 peptide, as internal control. Data are presented as means $\pm$ SD (n = 3). *Versus* PTP1B alone (-): * p < 0.002; *versus RhoAK*: ° p < 0.001.

Since an active GSK3 promotes the phosphorylation of β-catenin, priming it for the subsequent ubiquitination and proteasomal degradation [Vredenburgh, 2011], I next measured the β-catenin ubiquitination in the presence of RhoA/RhoA kinase activators or inhibitors. The untreated hCMEC/D3 cells showed a basal level of β-catenin ubiquitination (Figure 15A), which was in line with the basal phosphorylation of the protein on serine 33, serine 37 and threonine 41 (Figure 10A). The ubiquitination of β-catenin was reduced in cells with active RhoA and increased by the RhoA silencing or the RhoA kinase inhibitor Y27632 (Figure 15A).

These data suggest that an active RhoA kinase prevents the ubiquitination of β-catenin and highlight the possibility to regulate the transcription of β-catenin-target genes by modulating the RhoA kinase activity. As the silencing of RhoA did (Figure 11E-F), also Y27632 decreased the binding of β-catenin to the *mdr1* promoter (Figure 15B) and the levels of *mdr1* mRNA (Figure 15C). Both RhoA silencing and RhoA kinase inhibition reduced the Pgp protein levels, whereas RhoA increased them; by contrast, these treatments did not change the amount of MRP1 and BCRP, two other ABC transporters present on the luminal side of BBB cells [Bai, 2011] (Figure 15D).

To verify whether the inhibition of RhoA and RhoA kinase increases the delivery of Pgp substrates across the BBB, I used DOX [Gottesman, 2002], which exhibited a low permeability across the hCMEC/D3 cell monolayer (Figure 15E), due to the high level of Pgp on the luminal side of these cells [Tai, 2009]. The DOX permeability was further decreased by active RhoA, but it was increased by RhoA silencing or Y27632 (Figure 15E). The latter, which counteracted the effect of RhoA activator II on β-catenin ubiquitination (Figure 15A), also prevented the effects of RhoA activation on β-catenin binding to *mdr1* promoter (Figure 15B), *mdr1* transcription (Figure 15C), Pgp protein levels (Figure 15D) and DOX permeability (Figure 15E).

Figure 15. The RhoA kinase inhibition enhances the ubiquitination of β-catenin, downregulates the β-catenin-induced transcription of Pgp and increases the doxorubicin permeability in human BBB cells. The hCMEC/D3 cells were grown in fresh medium (*ctrl*), or in medium containing the RhoA activator II (*RhoAc*; 5 μg/ml for 3 h) or the RhoA kinase inhibitor Y27632 (*Y276*; 10 μmol/l for 3 h), alone or co-incubated. When indicated, the cells were treated with a non targeting scrambled siRNA or a RhoA-targeting specific siRNA (*siRhoA*) for 48 h (panel **A**) or 72 h (panels **D-E**). **A.** Whole cell lysates were immunoprecipitated (*IP*) with an anti-β-catenin antibody, then immunoblotted (*IB*) with an anti-mono/polyubiquitin antibody or with an anti-β-catenin antibody. Cells treated with non targeting scrambled siRNA had the same level of ubiquitination than untreated (*ctrl*) cells (not shown).The figure is representative of 3 experiments with similar results. *no Ab*: samples immunoprecipitated without anti-β-catenin antibody. *MW*: molecular weight markers. The 92 kDa band corresponding to the native β-catenin protein is indicated by the arrow. **B.** ChIP assay. The genomic DNA was extracted, immunoprecipitated with an anti-β-catenin antibody and analyzed by qRT-PCR, using primers for the β-catenin binding site on the *mdr1* promoter (*open bars*) or for an upstream region (*black bars*), chosen as a negative control. Results are expressed as means ± SD (n = 4). *Versus ctrl*: * $p < 0.05$; *versus RhoAc*: ° $p < 0.01$. **C.** The *mdr1* expression was detected by qRT-PCR. Data are presented as means ± SD (n = 4). *Versus ctrl*: * $p < 0.005$; *versus RhoAc*: ° $p < 0.001$. **D.** Western blot analysis of Pgp, MRP1 and BCRP in the whole cell lysates of hCMEC/D3 cells treated as described above. The β-tubulin expression was used as a control of equal protein loading. The figure is representative of 3 experiments with similar results. **E.** DOX permeability. The cells were grown for 7 days up to confluence in Transwell inserts and incubated as reported above. At the end of the incubation period, DOX (5 μmol/l) was added in the upper chamber. After 3 h the amount of drug recovered from the lower chamber was measured fluorimetrically. The permeability coefficient was calculated as reported under Materials and methods. In cells treated with the non targeting scrambled siRNA the permeability coefficient was 0.0018 ± 0.0002 (not significant *versus ctrl* cells). Measurements were performed in duplicate and data are presented as means ± SD (n = 3). *Versus ctrl*: * $p < 0.05$; *versus RhoAc*: ° $p < 0.02$.

4.1.3 The inhibition of RhoA kinase increases the doxorubicin delivery and cytotoxicity in human glioblastoma cells co-cultured with BBB cells

Since the inhibition of RhoA kinase increased the DOX permeability across the hCMEC/D3 monolayer, I wondered whether priming the BBB cells with Y27632 improves the delivery of doxorubicin to GB cells grown under the BBB monolayer. The DOX accumulation within three primary patient-derived GB cells (CV17, 01010627, Nov3) and the commercial GB U87-MG cell line, all cultured as SCs (i.e. the most TMZ-resistant component [Riganti, 2013]) - co-cultured with hCMEC/D3 cells, was low, as evaluated by fluorimetric assays (Figure 16A) and fluorescence microscope analysis (Figure 16B). The pre-treatment of the hCMEC/D3 cells with Y27632 significantly increased the DOX retention within GB cells (Figure 16A-B). DOX alone did not produce significant cell damages in terms of release of LDH in the extracellular medium of GB cells (Figure 16C), and induced weak signs of apoptosis, as suggested by the low level of cleaved Caspase-3 (Figure 16D). When effective, the drug is expected to induce a G2/M-phase arrest, which was not observed in the 01010627 cells co-cultured under the hCMEC/D3 monolayer exposed to DOX alone (Figure 16E). The exposure to Y27632 followed by DOX strongly increased the release of LDH (Figure 16C), the cleavage of Caspase-3 (Figure 16D), the percentage of cells arrested in G2/M phase (Figure 16E). In parallel such combination increased the amount of cells in pre-G1 phase, an index of apoptotic cells, and decreased the number of cells in S phase (Figure 16E). Of note, used at 10 µmol/l for 3 h, Y27632 alone was not cytotoxic for GB cells (Figure 16C-E). The repeated administration of Y27632 or doxorubicin as single agents on the luminal side of the hCMEC/D3 monolayer did not reduce the proliferation of 01010627 cells growing under this model of BBB (Figure 16F); only the pre-treatment of hCMEC/D3 cells with Y27632 followed by DOX significantly decreased the long-term proliferation of tumor cells (Figure 16F). Interestingly, the pre-treatment with Y27632 produced the same effects of verapamil, a strong inhibitor of Pgp activity in the hCMEC/D3 cells (Figure 17A); when co-incubated with DOX, verapamil increased the drug permeability across the BBB monolayer (Figure 17B) and its accumulation in co-cultured GB cells (Figure 17C), as well as LDH release (Figure 17D), Caspase-3 activation (Figure 17E), G2/M-arrest (Figure 17F) in glioblastoma cells.
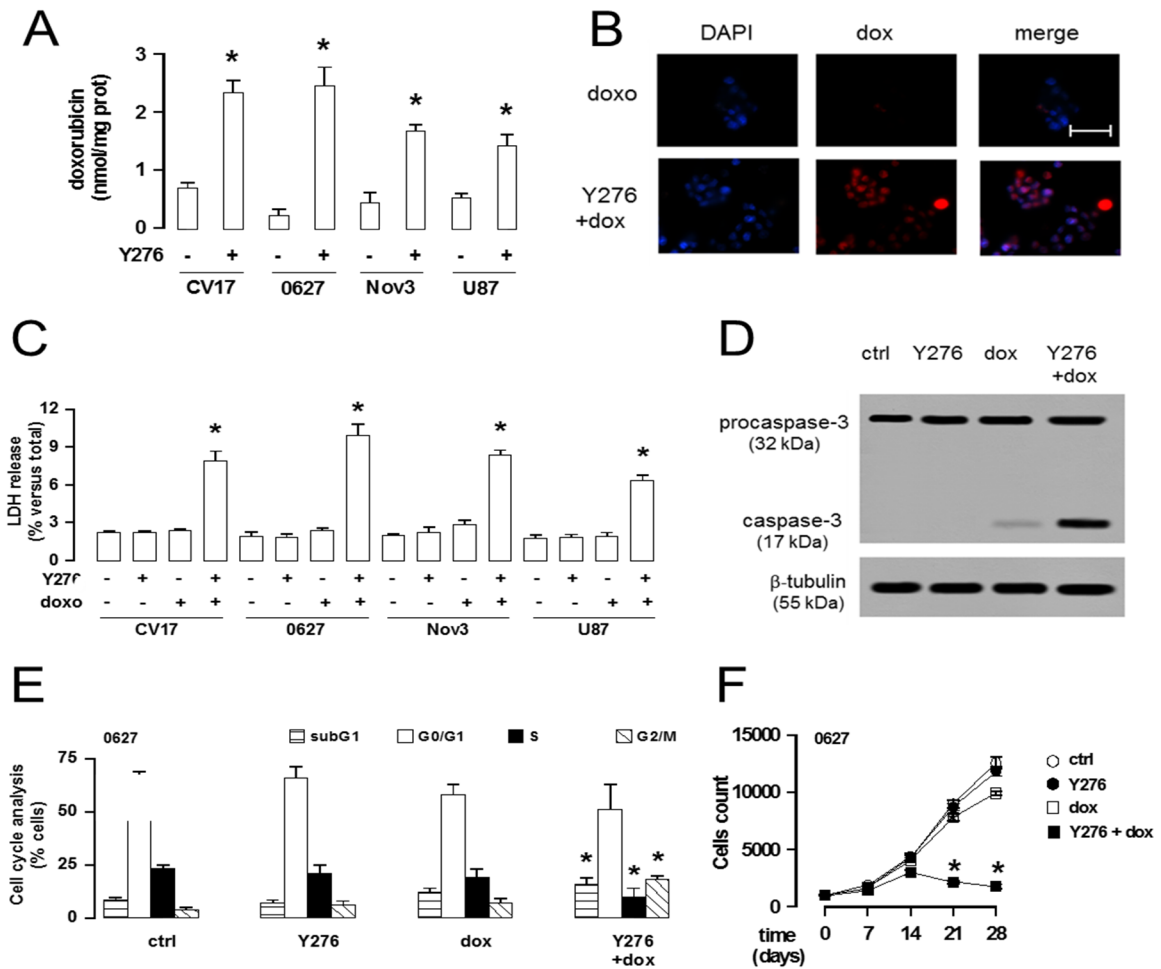
Figure 16. The RhoA kinase inhibitor Y27632 increases the doxorubicin delivery and cytotoxicity in glioblastoma stem cells co-cultured with BBB cells. The hCMEC/D3 cells were grown for 7 days up to confluence in Transwell inserts; CV17, 01010627, Nov3 and U87-MG SCs were seeded at day 4 in the lower chamber. After 3 days of co-culture, the supernatant in the upper chamber was replaced with fresh medium without (- or *ctrl*) or with Y27632 (*Y276*; 10 μmol/l for 3 h). After this incubation time, DOX (*dox*; 5 μmol/l) was added in the upper chamber for 3 h (panels **A-B**) or 24 h (panels **C-F**), then the following investigations were performed. **A.** Fluorimetric quantification of intracellular DOX in GB cells. Data are presented as means $\pm$ SD (n = 4). *Versus* untreated (-) cells: * p < 0.001. **B.** The 01010627 cells were seeded on sterile glass coverslips, treated as reported above, then stained with DAPI and analyzed by fluorescence microscopy to detect the intracellular accumulation of doxorubicin. Magnification: 63 x objective (1.4 numerical aperture); 10 x ocular lens. The micrographs are representative of 3 experiments with similar results. Bar: 20 μm. **C.** The GB cells were checked spectrophotometrically for the extracellular release of LDH activity. Data are presented as means $\pm$ SD (n= 4). *Versus* untreated (-) cells: * p < 0.001. **D.** The whole cell lysates from 01010627 cells were resolved by SDS-PAGE and immunoblotted with an anti-Caspase 3 antibody (recognizing both pro-Caspase and cleaved active Caspase). The β-tubulin expression was used as a control of equal protein loading. The figure is representative of 3 experiments with similar results. **E.** Cell cycle analysis. The distribution of the 01010627 cells in sub-G1, G0/G1, S, G2/M phase was analyzed by flow cytometry, as detailed under Materials and methods. Data are presented as means $\pm$ SD (n=4). *Versus ctrl*: * p < 0.005. **F.** After 3 days of co-culture between hCMEC/D3 and 01010627 cells, the medium of the upper chamber was replaced with fresh medium (*open circles*) or medium containing Y27632 (*Y276*; 10 μmol/l for 3 h, *solid circles*), DOX (*dox*; 5 μmol/l for 24 h, *open squares*), Y27632 (*Y276*; 10 μmol/l for 3 h) followed by DOX (*dox*; 5 μmol/l for 24 h, *solid squares*). Drug treatments were repeated every 7 days, as reported in the Materials and methods section. The proliferation of GB cells was monitored weekly by crystal violet staining. Measurements were performed in triplicate and data are presented as means $\pm$ SD (n= 4). *Versus ctrl*: * p < 0.001.
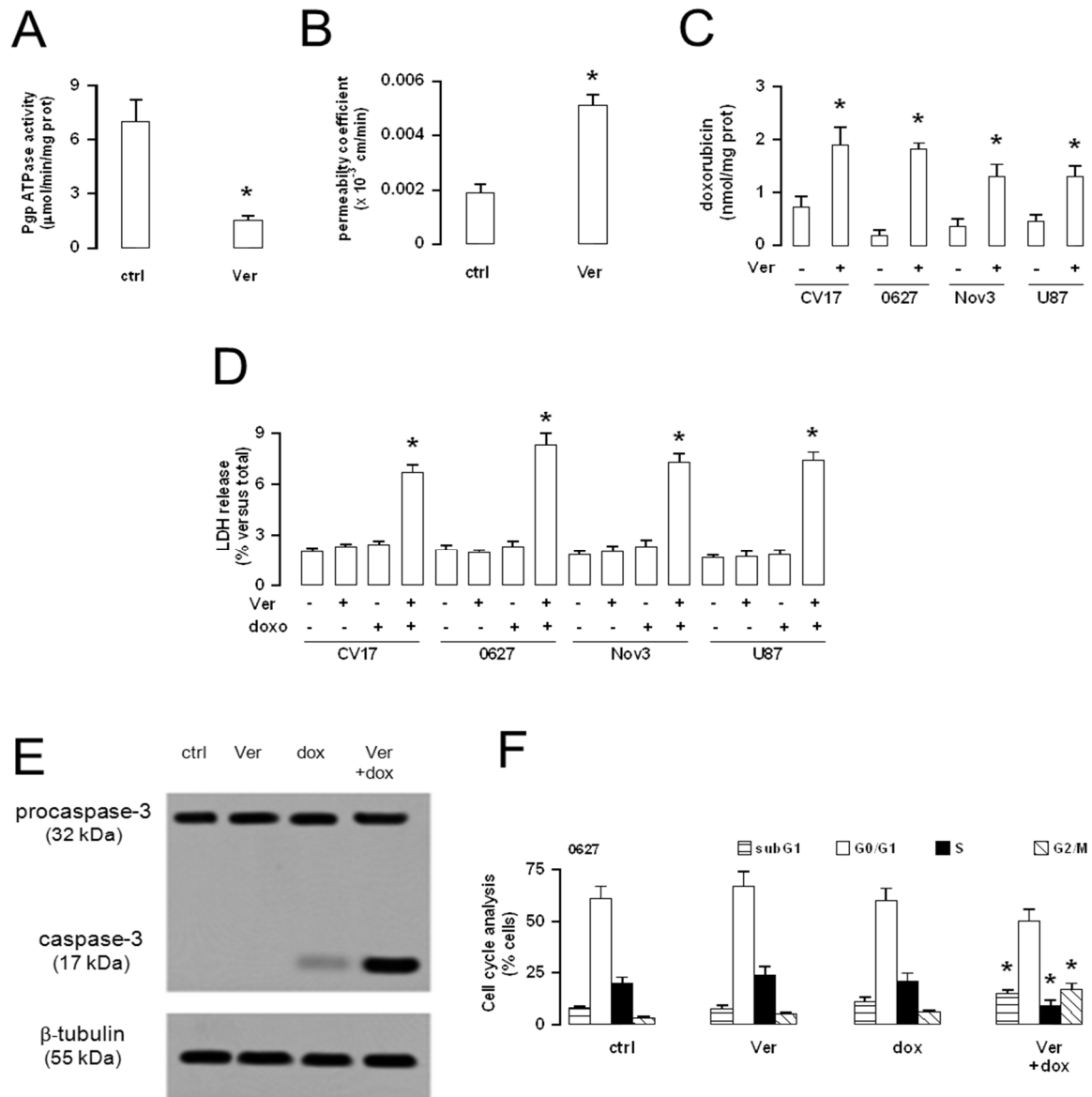
Figure 17. Effects of verapamil on doxorubicin permeability and cytotoxicity in glioblastoma cells co-cultured with BBB cells. The hCMEC/D3 cells were grown for 7 days up to confluence in Transwell inserts; the CV17, 01010627, Nov3 and U87-MG SCs were seeded at day 4 in the lower chamber. After 3 days of co-culture, the supernatant in the upper chamber was replaced with fresh medium without (- or *ctrl*) or with verapamil (*Ver*; 10 µmol/l) for 3 h (panels **A-C**) or 24 h (panels **D-F**). DOX (*dox*; 5 µmol/l) was co-incubated in the upper chamber for 3 h (panels **B-C**) or 24 h (panels **D-F**). **A.** The ATPase activity was measured spectrophotometrically after immunoprecipitation of Pgp from membrane fractions. Measurements were performed in duplicate and data are presented as means $\pm$ SD (n = 3). *Versus ctrl*: * p < 0.005. **B.** The DOX permeability coefficient was calculated as reported under Materials and methods. Measurements were performed in duplicate and data are presented as means $\pm$ SD (n = 3). *Versus ctrl*: * p < 0.001. **C.** Fluorimetric quantification of intracellular doxorubicin in glioblastoma cells. Data are presented as means $\pm$ SD (n = 3). *Versus* untreated (-) cells: * p < 0.01. **D.** GB cells were checked spectrophotometrically for the extracellular release of LDH. Data are presented as means $\pm$ SD (n= 4). *Versus* untreated (-) cells: * p < 0.001. **E.** The whole cell lysates from 01010627 cells were resolved by SDS-PAGE and immunoblotted with an anti-Caspase-3 antibody (recognizing both pro-Caspase and cleaved active Caspase). The β-tubulin expression was used as a control of equal protein loading. The figure is representative of 3 experiments with similar results. **F.** Cell cycle analysis. The distribution of 01010627 cells in sub-G1, G0/G1, S, G2/M phase was analyzed by flow cytometry, as detailed under Materials and methods. Data are presented as means $\pm$ SD (n=4). Vs *ctrl*: * p < 0.01.

4.1.4 Temozolomide increases the delivery of Pgp substrates through BBB cells monolayer by disrupting Wnt/GSK3/β-catenin pathway

Since during my master thesis I found that TMZ, the first-line chemotherapeutic drug in GB, downregulated Wnt/GSK3/β-catenin pathway and Pgp expression in GB SCs [Riganti, 2013], I investigated whether a similar event may occur on BBB cells.

I treated hCMEC/D3 monolayer with 50 µmol/l TMZ (equivalent to 9.7 µg/ml, a concentration that is clinically achievable in blood) [Portnow, 2009]. As shown in Figure 18A (upper panels), the permeability of molecules that have a paracellular diffusion in case of TJs leakage, such as DEXT, inulin and sucrose widely varied in hCMEC/D3 cells, but was compatible with intact TJs [Weksler, 2005]. TMZ did not affect the permeability of these compounds (Figure 18A, upper panels). Also the permeability of ABC transporters substrates displayed major differences: among the substrates of Pgp and MRP1 proteins, DOX was almost 100-fold less transported than vinblastine across the hCMEC/D3 monolayer. Because of their high hydrophobicity, DOX and vinblastine are expected to enter by passive diffusion [Dalmark,1981; Ito, 1999], and then to be effluxed back by Pgp and MRP1. Of note, the permeability of DOX and vinblastine was significantly higher in hCMEC/D3 cells pre-treated with TMZ (Figure 18A, lower panels). By contrast, the permeability of MXR, a substrate of BCRP was unaffected by TMZ (Figure 18A, lower panels).

Congruent with these results, TMZ increased the intracellular accumulation of rhodamine 123, which is effluxed by Pgp and MRP1, and did not change the accumulation of Hoechst 33342, which is effluxed by BCRP (Figure 19).

When I analyzed the expression of typical TJs proteins in cells exposed to TMZ, I detected a small decrease of claudin-3. Claudin-5, occludin and ZO-1 did not change (Figure 18B). hCMEC/D3 cells constitutively expressed Pgp, MRP1 and BCRP (Figure 18C). Of note, TMZ decreased the amount of Pgp, without affecting the other two proteins (Figure 18C). The decrease of Pgp exerted by TMZ was dose-dependent (Figure 20). I next measured the transport of [3H]-TMZ across hCMEC/D3 monolayer, in the presence of increasing concentrations of unlabelled TMZ, sufficient to significantly reduce Pgp: as shown in the Figure 20B, the amount of [3H]-TMZ in the lower chamber of Transwell was about 100% of the amount added in the upper chamber, independently by the decrease of Pgp induced by TMZ itself. These results suggest that Pgp played a minor role in the transport of TMZ across hCMEC/D3 monolayer and that TMZ did not enhance its own delivery by decreasing Pgp. Under our experimental conditions, TMZ (50 µmol/l for 72 h) showed no toxicity on hCMEC/D3 cells, as measured by LDH release (as described below) and Caspase-3 activity (not shown).
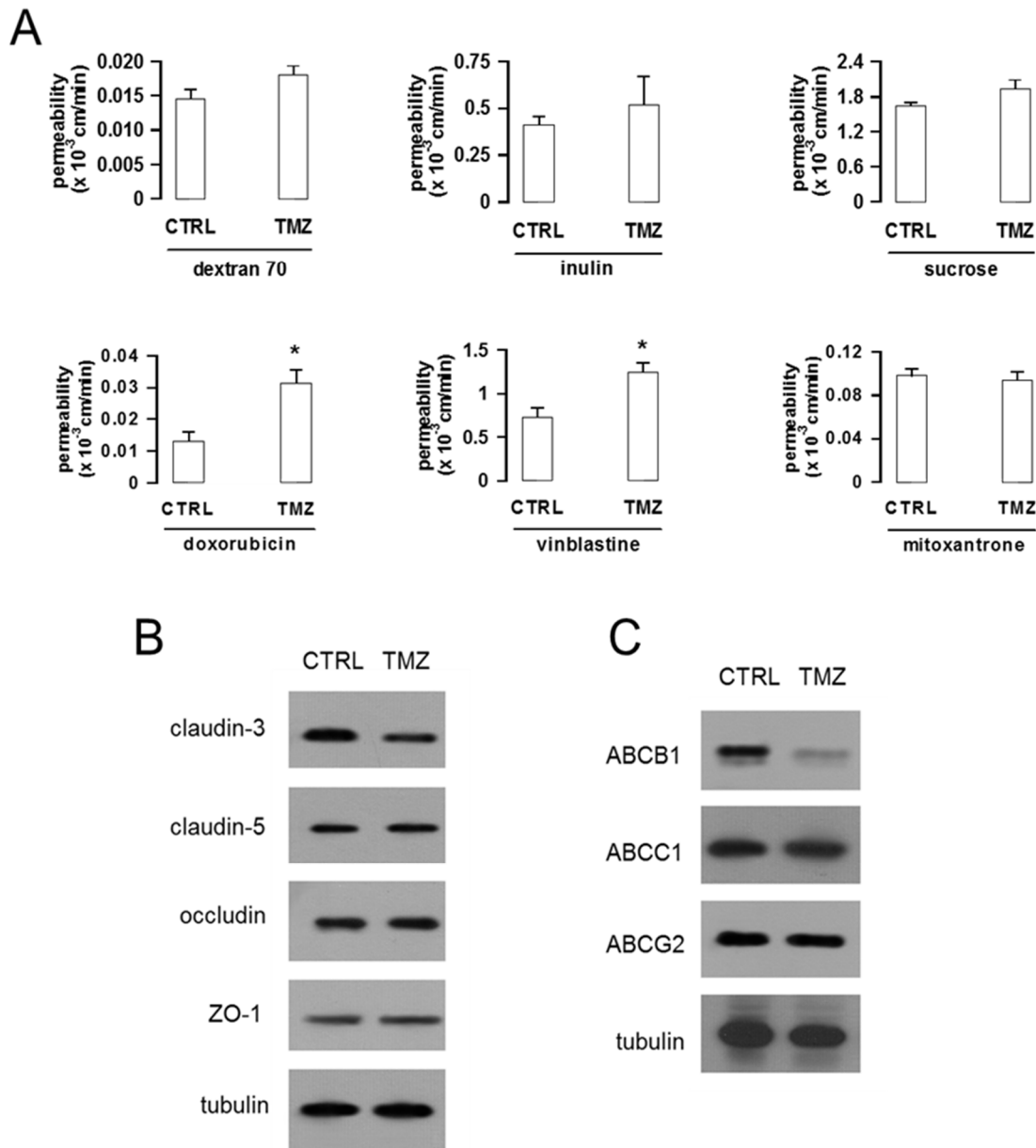
Figure 18. Effects of temozolomide on permeability coefficients, tight junction markers and ABC transporters in blood-brain barrier hCMEC/D3 cells. A. hCMEC/D3 cells were grown for 7 days up to confluence in Transwell inserts, without (*CTRL*) or with TMZ (50 μmol/l for the last 72 h). At the end of the incubation period, 2 μmol/l DEXT-FITC, 2 μCi/ml [^{14}C]-inulin, 2 μCi/ml [^{14}C]-sucrose, 5 μmol/l DOX, 2 μCi/ml [^{3}H]-vinblastine, 10 μmol/l MXR were added in the upper chamber. After 3 h the amount of the drug recovered from the lower chamber was measured fluorimetrically (for DEXT-FITC, DOX, MXR) or by liquid scintillation (for inulin, sucrose, vinblastine). Permeability coefficients were calculated as reported under Materials and methods. Measurements were performed in duplicate and data are presented as means ± SD (n = 3). Vs *CTRL*: * $p < 0.02$. **B.** hCMEC/D3 cells were incubated without (*CTRL*) or with TMZ (50 μmol/l for 72 h), then lysed and subjected to Western blot analysis for claudin-3, claudin-5, occludin, ZO-1. β-tubulin expression was used as control of equal protein loading. The figure is representative of 3 experiments with similar results. **C.** hCMEC/D3 cells, treated as reported in **B**, were subjected to the Western blot analysis for Pgp/ABCB1, MRP1/ABCC1, BCRP/ABCG2. β-tubulin expression was used as control of equal protein loading. The figure is representative of 3 experiments with similar results.
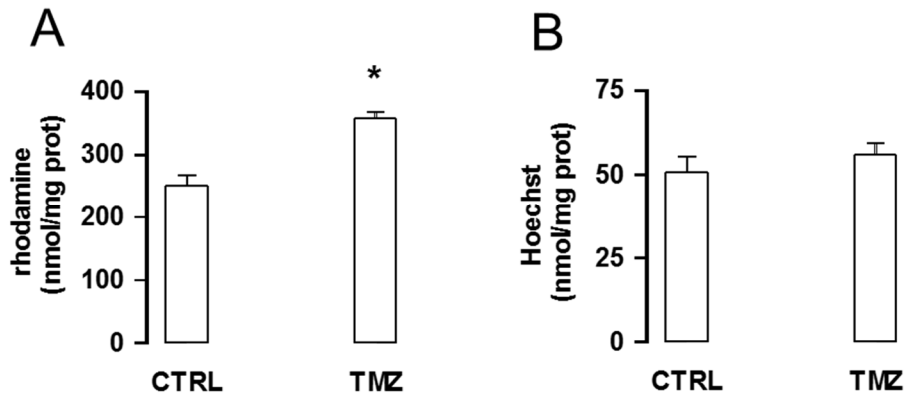
Figure 19. Intracellular accumulation of rhodamine 123 and Hoechst 33342 by hCMEC/D3 cells. hCMEC/D3 cells were grown in fresh medium (*CTRL*) or with 50 μmol/l TMZ for 72 h, then incubated with the Pgp/ABCB1 substrate rhodamine 123 (panel **A**) or the BCRP/ABCG2 substrate Hoechst 33342 (panel **B**). The intracellular retention of rhodamine 123 and Hoechst 33342 was measured in duplicate fluorimetrically, as reported under Materials and methods. Data are presented as means $\pm$ SD (n=4). Vs *CTRL*: * $p < 0.005$.
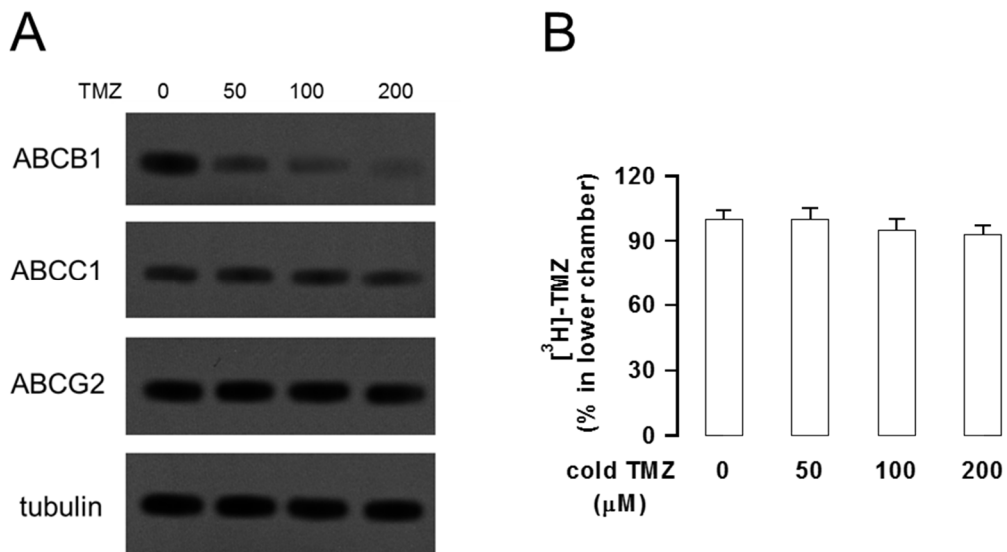
Figure 20. Effect of temozolomide on its own transport across hCMEC/D3 monolayer. A. hCMEC/D3 cells were grown in fresh medium (*0*) or with 50, 100 or 200 μmol/l TMZ for 72 h, then subjected to the Western blot analysis of Pgp/ABCB1, MRP1/ABCC1, BCRP/ABCG2. β-tubulin expression was used as control of equal protein loading. The figure is representative of 3 experiments with similar results. **B.** hCMEC/D3 cells were cultured in Transwell device for 7 days up to confluence, then incubated as reported in **A**, in the presence of 0.7 μC/ml (equivalent to 10 μmol/l) [³H]-TMZ. After this incubation period, the amount of [³H]-TMZ in the lower chamber was measured by liquid count scintillation. Results were expressed as percentage of [³H]-TMZ recovered in the lower chamber *versus* [³H]-TMZ added in the upper chamber at time 0. Data are presented as means $\pm$ SD (n=3).

TMZ lowered the mRNA levels of *mdr1* (Figure 21A) and decreased the binding of β-catenin to the *mdr1* promoter (Figure 21B). In particular, TMZ decreased the amount of β-catenin present in the nucleus of BBB cells (Figure 21C). In parallel the drug increased phospho(Tyr216)GSK3 and serine 33/37/threonine 41-phosphorylated β-catenin (Figure 21D). As a whole, these data suggest that TMZ may reduce the amount of β-catenin active as transcription factor.

It has been already reported in hCMEC/D3 cells that the activity of GSK3 is controlled by the Wnt canonical pathway [Lim, 2008; Kania, 2011].

As shown in Figure 22A, WntA decreased the phosphorylation of GSK3, whereas Wnt antagonist Dkk-1 produced the opposite effect. The phosphorylation of β-catenin, which was low in untreated hCMEC/D3 cells, was not significantly reduced by WntA and was increased by Dkk-1. The GSK3 inhbitor LiCl did not change the phosphorylation of GSK3 on tyrosine 216, but slightly reduced the phosphorylation of β-catenin on serine 33/37/threonine 41, suggesting that it effectively inhibited the activity of GSK3. The nuclear translocation of β-catenin (Figure 22B) and its binding on *mdr1* promoter (Figure 22C) was increased by WntA and LiCl, and reduced by Dkk-1. Indeed, hCMEC/D3 cells treated with Dkk-1 had lower levels of *mdr1* mRNA (Figure 22D) and Pgp protein (Figure 22E). Cells treated with WntA or LiCl had higher amounts of *mdr1* mRNA and Pgp protein (Figure 21D-E). Congruent with this trend, Dkk-1 increased, and WntA and LiCl decreased the permeability of DOX across the hCMEC/D3 monolayer (Figure 22F). Interestingly, TMZ mimicked the effects of Dkk-1 and counteracted the effects of WntA and LiCl on β-catenin phosphorylation (Figure 22A), nuclear translocation (Figure 22B) and *mdr1* promoter binding (Figure 22C), on *mdr1* mRNA (Figure 22D) and Pgp levels (Figure 22E) and on doxorubicin permeability (Figure 22F).

These findings suggested that TMZ reduced *mdr1* transcription by inhibiting the Wnt/GSK3/β-catenin axis.
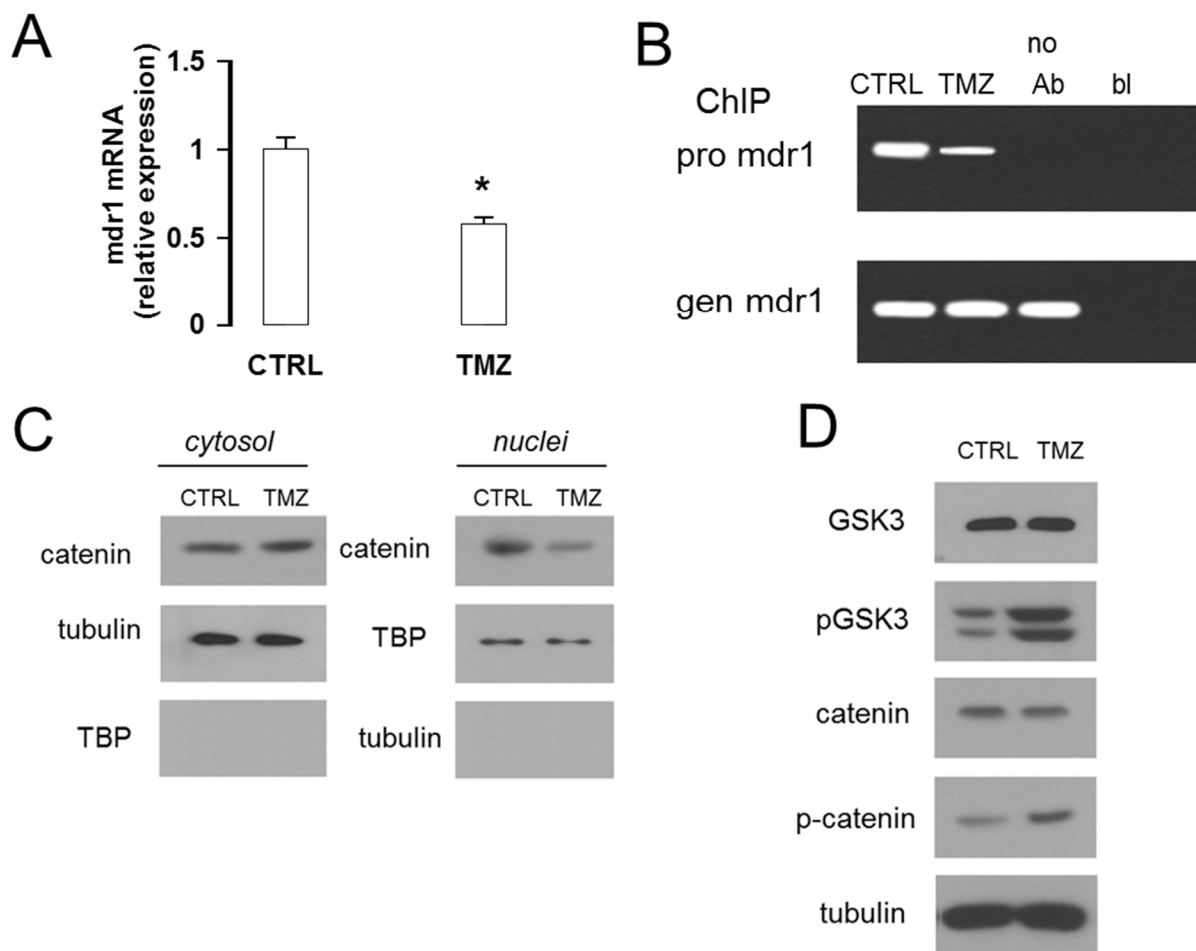
Figure 21. Effects of temozolomide on *mdr1* expression and GSK3/β-catenin pathway in hCMEC/D3 cells. hCMEC/D3 cells were grown in fresh medium (*CTRL*) or in the presence of TMZ (50 μmol/l for 48 h), then subjected to the following investigations. **A.** Total RNA was extracted and reverse-transcribed, the expression of *mdr1* gene was detected by qRT-PCR. The expression level in untreated cells was considered "1". Data are presented as means $\pm$ SD (n = 3). Vs *CTRL*: * p < 0.002. **B.** Chromatin immunoprecipitation of β-catenin on *mdr1* promoter (*pro*) in hCMEC/D3 cells. *gen*: PCR product from genomic DNA. *no Ab*: precipitated samples without anti-β-catenin antibody. *bl*: blank. The figure is representative of 3 experiments with similar results. **C.** Nuclear and cytosolic extracts were analyzed for the amount of β-catenin. The expression of β-tubulin and TBP was used as control of equal protein loading for cytosolic and nuclear samples respectively, and to verify the efficacy of the nucleus-cytosol separation. The figure is representative of 3 experiments with similar results. **D.** Western blot analysis of phospho(Tyr216)GSK3, GSK3, phospho(Ser33/37/Thr41)β-catenin, β-catenin in whole cell lysates. β-tubulin expression was used as control of equal protein loading. The figure is representative of 3 experiments with similar results.
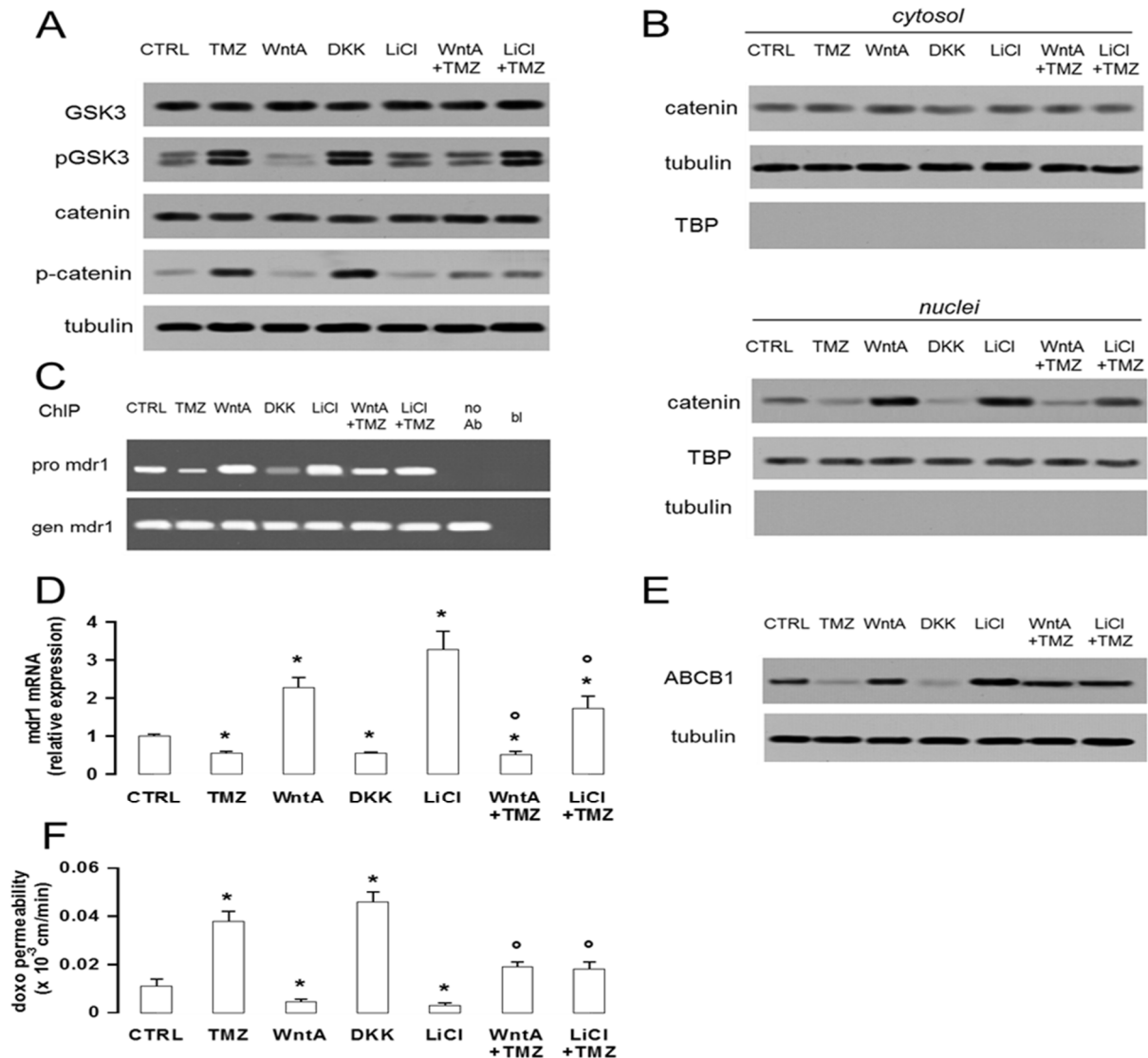
Figure 22. Effects of temozolomide and Wnt modulators on *mdr1* expression in hCMEC/D3 cells. hCMEC/D3 cells were grown in fresh medium (*CTRL*) or with TMZ (50 µmol/l for 48 h), Wnt activator 2-amino-4-(3,4-(methylenedioxy)benzylamino)-6-(3-methoxyphenyl)pyrimidine (*WntA*; 20 µmol/l for 24 h), Wnt inhibitor recombinant Dkk-1 protein (*DKK*; 1 µg/ml for 24 h), GSK3 inhibitor LiCl (*LiCl*; 10 mmol/l for 24 h). When co-incubated, WntA and LiCl were added to TMZ in the last 24 h. **A.** Western blot analysis of phospho(Tyr216)GSK3, GSK3, phospho(Ser33/37/Thr41)β-catenin, β-catenin in whole cell lysates. β-tubulin expression was used as control of equal protein loading. The figure is representative of 3 experiments with similar results. **B.** Nuclear and cytosolic extracts were analyzed for the amount of β-catenin. The expression of β-tubulin and TBP was used as control of equal protein loading for cytosolic and nuclear samples respectively, and to verify the efficacy of the nucleus-cytosol separation. The figure is representative of 3 experiments with similar results. **C.** ChIP of β-catenin on *mdr1* promoter (*pro*) in hCMEC/D3 cells. *gen*: PCR product from genomic DNA. *no Ab*: precipitated samples without anti-β-catenin antibody. *bl*: blank. The figure is representative of 3 experiments with similar results. **D.** *mdr1* expression was detected in triplicate by qRT-PCR. Data are presented as means $\pm$ SD (n = 4). Vs *CTRL*: * $p < 0.02$; vs *WntA* or *LiCl*: ° $p < 0.05$. **E.** Western blot analysis of Pgp/ABCB1. β-tubulin expression was used as control of equal protein loading. The figure is representative of 3 experiments with similar results. **F.** Doxorubicin permeability. hCMEC/D3 cells were grown for 7 days up to confluence in Transwell inserts and treated as reported above. At the end of the incubation period, 5 µmol/l DOX was added in the upper chamber. After 3 h the amount of the drug recovered from the lower chamber was measured fluorimetrically. Permeability coefficient was calculated as reported under Materials and methods. Measurements were performed in duplicate and data are presented as means $\pm$ SD (n = 3). Vs *CTRL*: * p < 0.001; vs *WntA* or *LiCl* alone: ° p < 0.005.

60

## 4.1.5 Temozolomide lowers the synthesis of Wnt3 in BBB cells by modifying the promoter methylation status

TMZ did not change the surface amount of the Wnt receptor Frizzled and Wnt co-receptor LRP6 (Figure 23), leading to exclude interference with the Wnt-signaling on the surface.

The presence of Wnt proteins in endothelial cells is restricted to some antigens of the large Wnt family, such as Wnt2b, Wnt3, Wnt4 and Wnt5 [Goodwin, 2006]. The first three ones are associated to the canonical GSK3/β-catenin pathway [Fu, 2011; Liebner, 2008; Bernardi, 2011].

I asked then if TMZ downregulated the endogenous synthesis of one or more Wnts proteins. I did not detect Wnt2b and Wnt4 in hCMEC/D3 cells (data not shown). Wnt3 was instead detectable at protein (Figure 24A) and mRNA (Figure 24B) level. Notably, TMZ reduced both Wnt3 protein and mRNA (Figure 24A-B).

Since TMZ is an alkylating agent that methylates DNA [Wick, 2009], I investigated whether it might cause the methylation of the *Wnt3* promoter. *Wnt3* promoter has indeed several CpG islands (Figure 25), i.e. regions of promoters that are methylated in infrequently transcribed genes and unmethylated in highly transcribed ones. MSP PCR assays showed that Wnt3 promoter was fully unmethylated in hCMEC/D3 cells (Figure 24C). TMZ decreased the amount of unmethylated promoter and induced the appearance of a methylated band (Figure 24C), thus appearing to be a good candidate for the epigenetic downregulation of Wnt3.

To confirm that Wnt3 was a critical controller of *mdr1* expression in our model, I permanently silenced Wnt3 in hCMEC/D3 cells: silencing produced a 90% reduction in *Wnt3* mRNA (Figure 26A) and made the Wnt3 protein undetectable by Western blotting (Figure 26B). The depletion of the Wnt3 protein significantly increased the amount of phospho(Tyr216)GSK3 and phospho(Ser33/37/Thr41)β-catenin (Figure 26C), prevented the binding of β-catenin on *mdr1* promoter (Figure 26D) and reduced Pgp/ABCB1 protein (Figure 26E). Moreover, hCMEC/D3 cells showed a higher permeability to DOX than wild-type cells (Figure 26F).
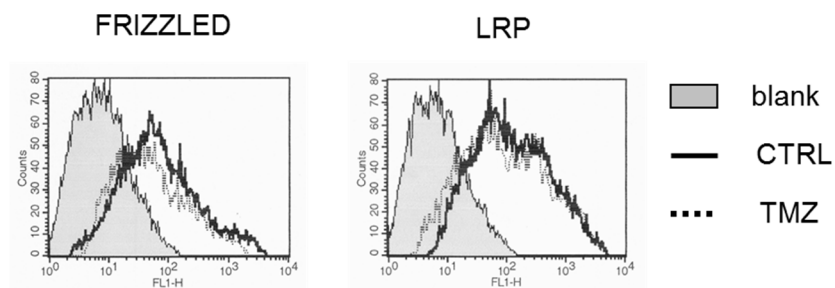
Figure 23. Effects of temozolomide on the expression of Frizzled and LRP6 in hCMEC/D3 cells. hCMEC/D3 cells were incubated for 48 h in fresh medium (*CTRL*) or with 50 μmol/l TMZ. Flow cytometry analysis of surface Frizzled (left panel) and LRP6 (right panel) in cells untreated (*continuous line*) or treated with temozolomide (*dotted line*). *Grey peak*: cells treated with anti-isotypic antibody. The figures shown here are representative of 3 similar experiments, performed in triplicate.
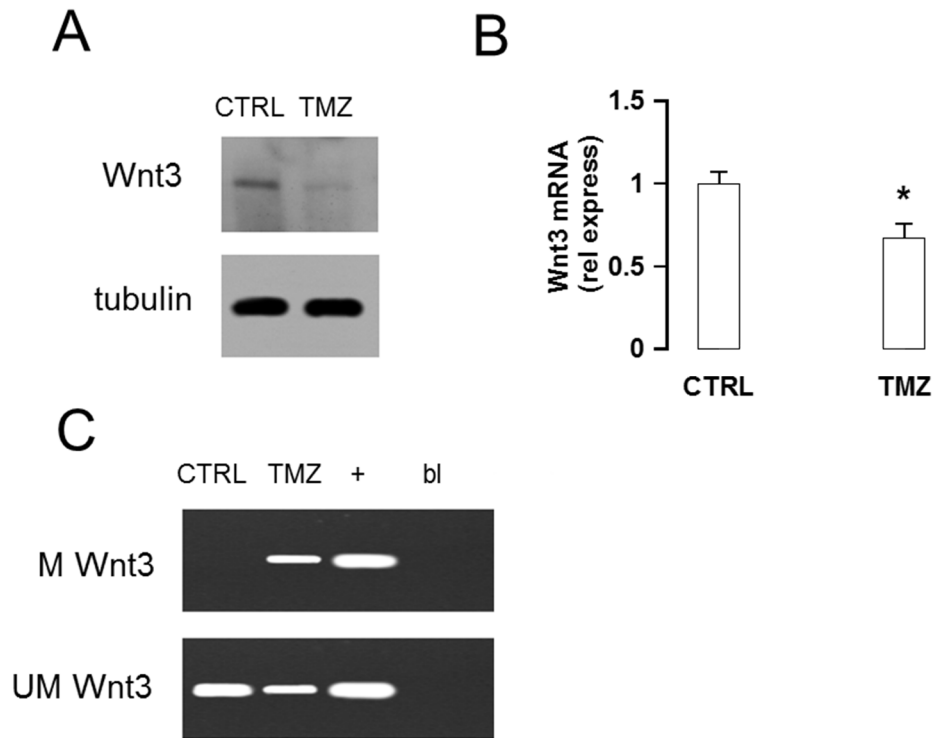
Figure 24. Effects of temozolomide on Wnt3 synthesis in hCMEC/D3 cells. hCMEC/D3 cells were grown in the absence (*CTRL*) or in the presence of TMZ (50 μmol/l for 48 h in Western blot experiments, 24 h in qRT-PCR and MSP experiments), then subjected to the following investigations. **A.** Western blot analysis of Wnt3 in whole cell lysates. β-tubulin expression was used as control of equal protein loading. The figure is representative of 3 experiments with similar results. **B.** Total RNA was extracted and reverse-transcribed, then the expression of *Wnt3* gene was detected by qRT-PCR. The expression level in untreated cells was considered "1". Data are presented as means $\pm$ SD (n = 3). Vs *CTRL*: * $p < 0.05$. **C**. Methylation of *Wnt3* promoter. Genomic DNA was subjected to bisulfite modification, followed by PCR with specific primers for methylated (*M*) and unmethylated (*UM*) *Wnt3* promoter. The figure is representative of 3 experiments with similar results. +: positive controls with a universal methylated or unmethylated genome sequence, respectively. *bl*: blank.
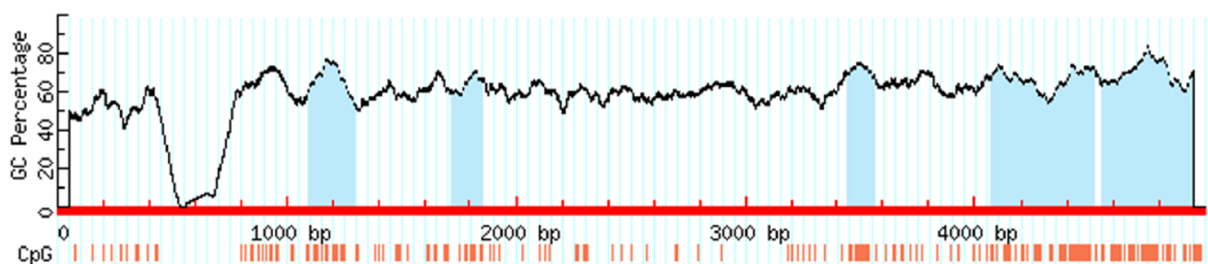
Figure 25. Localization of CpG islands on the promoter of *Wnt3* gene. CpG islands localization on *Wnt3* promoter, according to Methprimer software (http://www.urogene.org/methprimer). As input the promoter sequence (from -5,000 bps to 0 bps) obtained by the UCSC Genome Browser (http://genome.ucsc.edu/) was used.
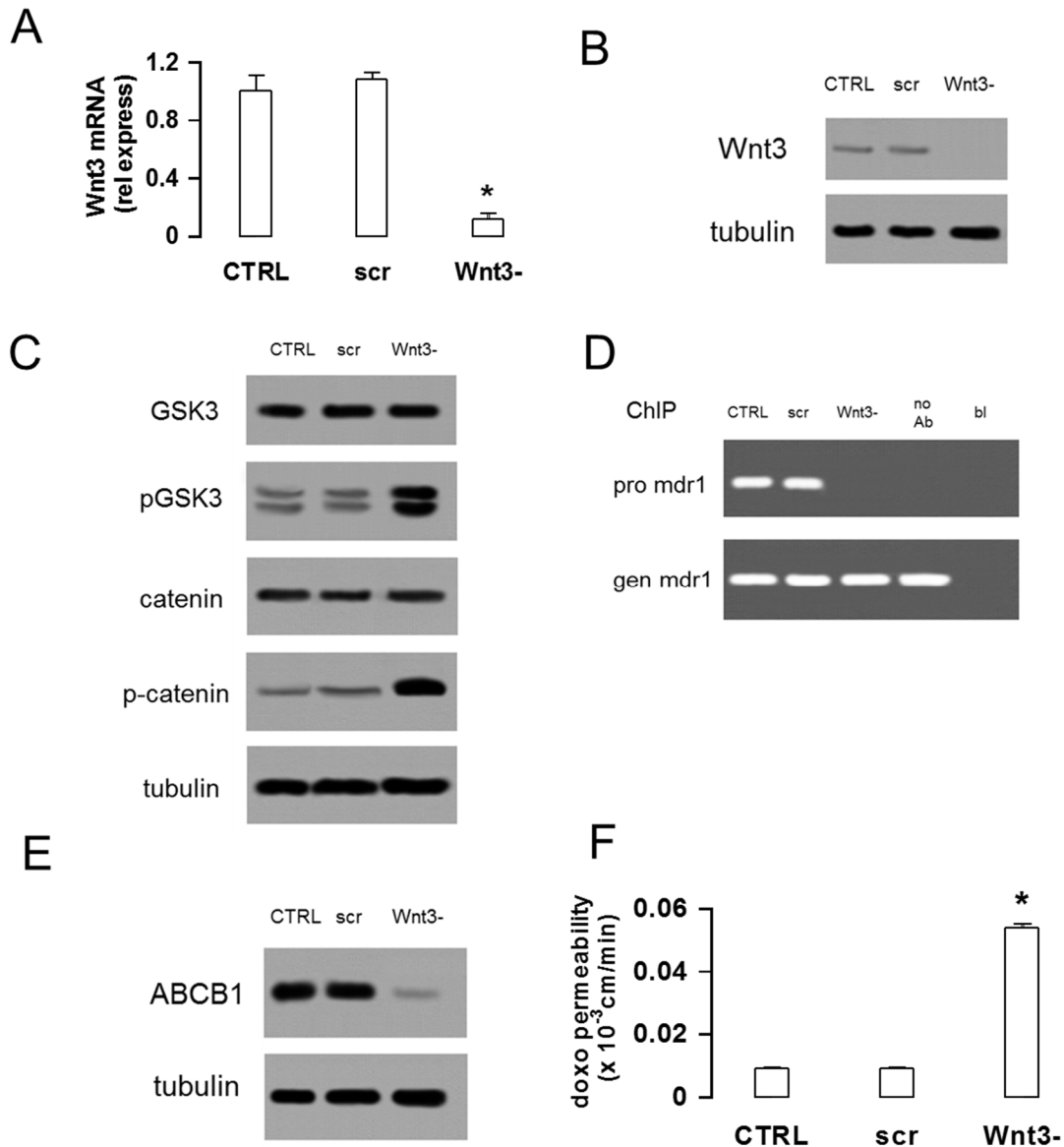
Figure 26. Effects of Wnt3 silencing on *mdr1* expression in hCMEC/D3 cells. Wild-type hCMEC/D3 cells (*CTRL*), cells stably transfected with a non-targeting scrambled shRNA (*scr*) or stably silenced for Wnt3 (*Wnt3-*) were subjected to the following investigations. **A.** Wnt3 qRT-PCR. Total RNA was extracted and reverse-transcribed, the expression of *Wnt3* gene was detected by qRT-PCR. The expression level in untreated cells was considered "1". Data are presented as means $\pm$ SD (n = 3). Vs *CTRL*: * p < 0.001. **B.** Western blot analysis of Wnt3 in whole cell lysates. β-tubulin expression was used as control of equal protein loading. The figure is representative of 3 experiments with similar results. **C.** Western blot analysis of phospho(Tyr216)GSK3, GSK3, phospho(Ser33/37/Thr41)β-catenin, β-catenin in whole cell lysates. β-tubulin expression was used as control of equal protein loading. The figure is representative of 3 experiments with similar results. **D.** ChIP of β-catenin on *mdr1* promoter (*pro*) in hCMEC/D3 cells. *gen*: PCR product from genomic DNA. *no Ab*: precipitated samples without anti-β-catenin antibody. *bl*: blank. The figure is representative of 3 experiments with similar results. **E.** Western blot analysis of Pgp/ABCB1. β-tubulin expression was used as control of equal protein loading. The figure is representative of 3 experiments with similar results. **F.** Doxorubicin permeability. hCMEC/D3 cells were grown for 7 days up to confluence in Transwell inserts, then 5 μmol/l DOX was added in the upper chamber. After 3 h the amount of the drug recovered from the lower chamber was measured fluorimetrically. Permeability coefficient was calculated as reported under Materials and methods. Measurements were performed in duplicate and data are presented as means $\pm$ SD (n = 3). Vs *CTRL*: * p < 0.001.

4.1.6 Temozolomide increases the antitumor efficacy of Pgp substrates in glioblastoma/BBB co-culture models

Since TMZ decreased the amount and activity of Pgp in BBB cells, I next asked the question whether the efficacy of anti-cancer drugs commonly effluxed by this transporter would be improved in BBB/GB co-culture models.

With this goal in mind, I cultured hCMEC/D3 cells, treated or not with TMZ, in Transwell inserts, containing two primary patient-derived GB cells (CV17, 01010627) and the commercial GB U87-MG cell line, all cultured as SCs. DOX was applied in the upper chamber, facing the luminal side of hCMEC/D3 monolayer, which expresses high amounts of Pgp [Tai, 2009]. As expected, the drug was poorly delivered to GB cells in the lower chamber (Figure 27A). Pre-treatment of hCMEC/D3 cells with TMZ significantly increased the intratumor amount of DOX (Figure 27A). The typical nuclear red fluorescence of DOX [Kopecka, 2011] was undetectable in 01010627 GB cells recovered from the lower chamber of the co-cultures, whereas pre-treatment of hCMEC/D3 cells with TMZ restored the nuclear accumulation of DOX in GB cells (Figure 27B). Interestingly, TMZ decreased the expression levels of *mdr1* also in the GB cells cultured in the lower chamber (Figure 28), as it did in hCMEC/D3 cells.

Under the experimental conditions used, neither TMZ nor DOX alone induced detectable cytotoxicity, measured as extracellular release of LDH and activation of Caspase-3 (Figure 27C), in GB cells. The TMZ+DOX combination produced cytotoxic effects in the entire tumor cell lines analyzed (Figure 27C). The rate of proliferation of the three GB cell lines was not affected by the addition of DOX in the upper chamber of the Transwell (Figure 27D). TMZ applied in the upper chamber reduced the proliferation rate of all tumor cell lines in a time-dependent way; of note, its antiproliferative effect was significantly enhanced when TMZ was followed by DOX (Figure 27D). Under these conditions TMZ and DOX, alone or in combination, did not induce any significant cytotoxicity (Figure 29A) and did not affect cell proliferation (Figure 29B) in hCMEC/D3 cells.

The chemosensitizing properties of TMZ were not limited to DOX. In the same co-culture models vinblastine and topotecan, two other substrates of Pgp, did not increase the extracellular LDH (Figure 30A), did not activate the Caspase-3 (Figure 30B) and did not decrease cell proliferation (Figure 30C) of GB SCs, when applied in the upper chamber of the Transwell. Only the pre-treatment of hCMEC/D3 cells with TMZ followed by vinblastine and topotecan exerted significant cytotoxicity (Figure 30A-B) and reduced the proliferation (Figure 30C) of GB cells cultured under the BBB monolayer. The combinations of TMZ +vinblastine or TMZ+topotecan (Figure 30C) were significantly more effective in reducing cell proliferation after 21 and 28 days ($p < 0.02$) than TMZ alone (Figure 27D).

Notably, the same permeabilizing effects induced by TMZ in wild-type BBB cells was obtained after Wnt3 depletion: indeed, Wnt3-silenced hCMEC/D3 monolayer allowed a higher delivery (Figure 27E) and toxicity (Figure 27F) of DOX in the co-cultured 01010627 GB cells.
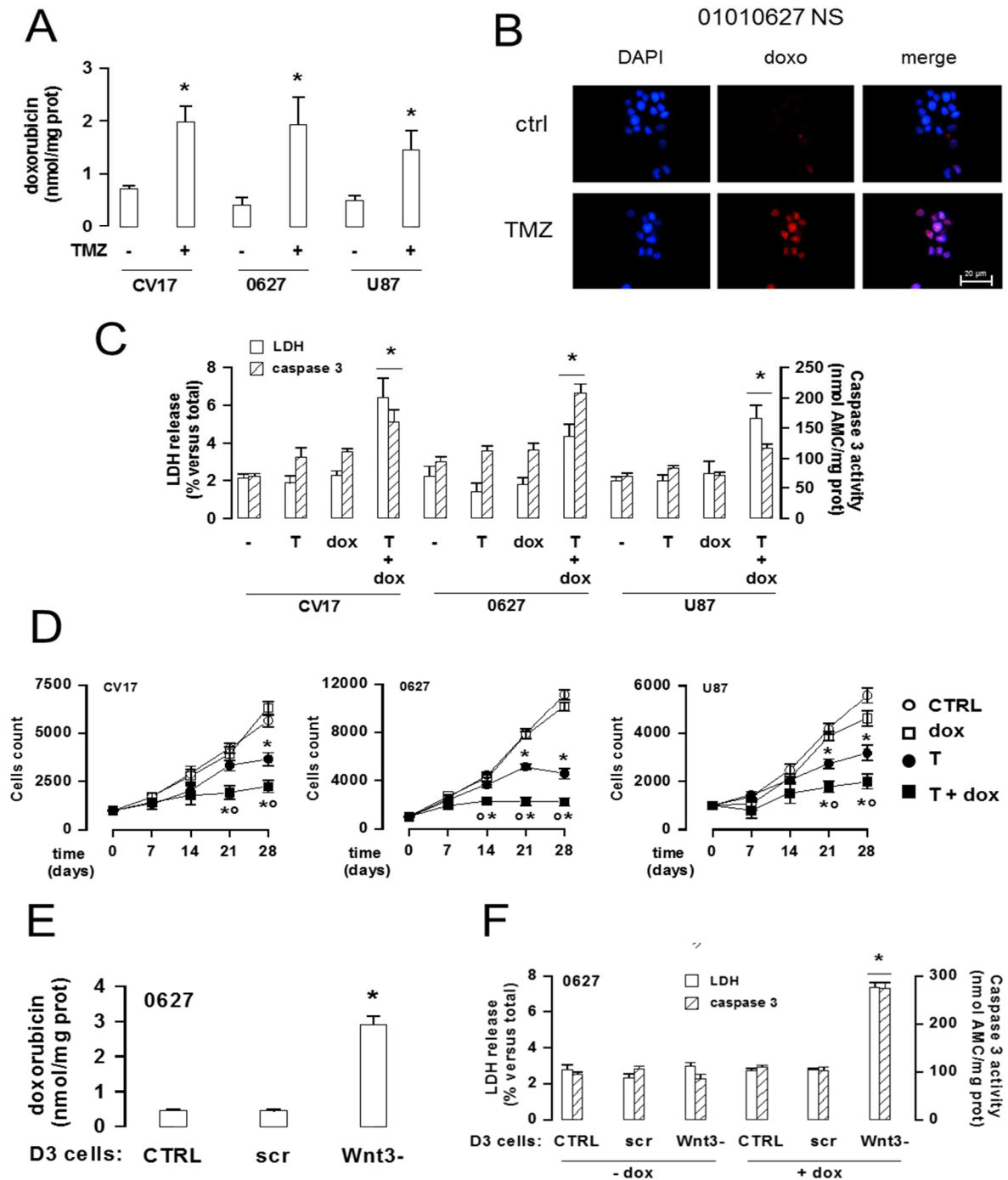
Figure 27. Effects of temozolomide on doxorubicin delivery and cytotoxicity in glioblastoma stem cells co-cultured with hCMEC/D3 cells. hCMEC/D3 cells were grown for 7 days up to confluence in Transwell inserts; CV17, 01010627 and U87-MG SCs (NS) were seeded at day 4 in the lower chamber. After 3 days of co-culture, supernatant in the upper chamber was replaced with fresh medium without (-) or with TMZ (50 µmol/l for 72 h; *TMZ* or *T*). 5 µmol/l DOX (*dox*) was added in the upper chamber in the last 24 h, then the following investigations were performed. **A.** Fluorimetric quantification of intracellular DOX in GB cells. Measurements were performed in duplicate and data are presented as means $\pm$ SD (n = 4). Vs untreated cells: * p < 0.05. **B.** 01010627 cells were seeded on sterile glass coverslips, treated as reported above, then stained with DAPI and analyzed by fluorescence microscopy to detect the intracellular accumulation of doxorubicin. Magnification: 63 x objective (1.4 numerical aperture); 10 x ocular lens. The micrographs are representative of 3 experiments with similar results. **C.** The culture supernatant of GB cells was checked spectrophotometrically for the extracellular activity of LDH (open bars), the cell lysates were analyzed fluorimetrically for the activity of Caspase-3 (hatched bars). Measurements were performed in duplicate and data are presented as means $\pm$ SD (n= 4). Vs untreated cells: * p < 0.05. **D** After 3 days of co-culture, the medium of

the upper chamber was replaced with fresh medium (*open circles*) or medium containing 50 µmol/l TMZ for 72 h (*solid circles*, *T*), 5 µmol/l DOX for 24 h (*open squares*, *dox*), 50 µmol/l TMZ for 72 h plus 5 µmol/l DOX in the last 24 h (*solid squares*, *T + dox*). Drug treatments were repeated every 7 days, as reported in the Materials and methods section. The proliferation of GB cells was monitored weekly by crystal violet staining. Measurements were performed in triplicate and data are presented as means $\pm$ SD (n= 4). Vs untreated cells (*CTRL*): * $p < 0.01$. *T + dox* vs *T* alone: ° $p < 0.05$. **E-F**. Wild-type hCMEC/D3 cells (*CTRL*), cells stably transfected with a non-targeting 29-mer scrambled shRNA (*scr*) or stably silenced for Wnt3 (*Wnt3-*) were grown for 7 days up to confluence in Transwell inserts; 01010627 GB cells were seeded at day 4 in the lower chamber. After 3 days of co-culture, supernatant in the upper chamber was replaced with fresh medium without (- *dox*) or with 5 µmol/l DOX (+ *dox*) for 24 h. The intracellular DOX in GB cells was measured fluorimetrically (panel **E**). Measurements were performed in duplicate and data are presented as means $\pm$ SD (n = 3). Vs untreated cells: * $p < 0.001$. The culture supernatant of GB cells was checked spectrophotometrically for the extracellular activity of LDH (open bars, panel **F**), the cell lysates were analyzed fluorimetrically for the activity of Caspase-3 (hatched bars, panel **F**). Measurements were performed in duplicate and data are presented as means $\pm$ SD (n= 3). Vs untreated cells: * $p < 0.001$.
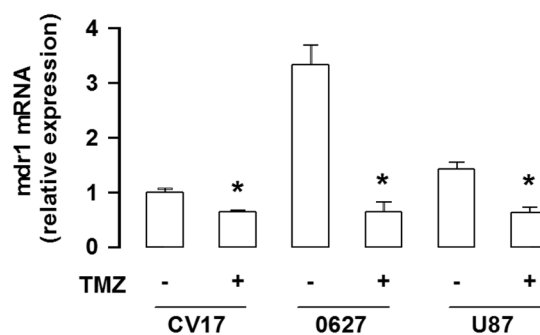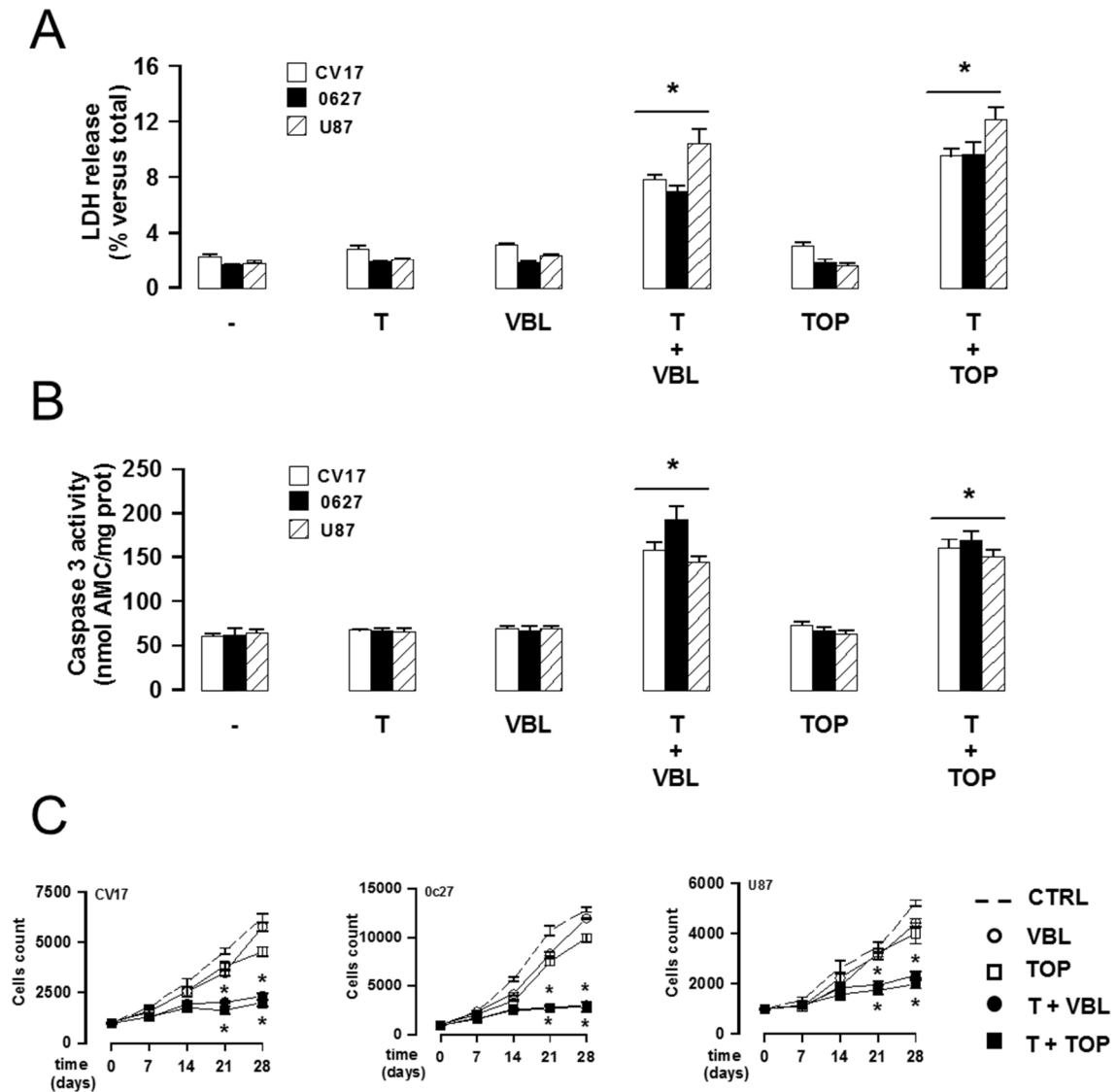

Figure 28. Effects of temozolomide on *mdr1* expression in glioblastoma cells co-cultured with hCMEC/D3 cells.
hCMEC/D3 cells were grown for 7 days up to confluence in Transwell inserts; CV17, 01010627 and U87-MG cells SCs were seeded at day 4 in the lower chamber. After 3 days of co-culture, the supernatant in the upper chamber was replaced with fresh medium without (-) or with TMZ (50 µmol/l for 48 h). Total RNA was extracted and reverse-transcribed, the expression of *mdr1* gene was detected by qRT-PCR. The expression level in untreated CV17 cells was considered "1". Data are presented as means $\pm$ SD (n = 3). Vs untreated cells: * $p < 0.02$.
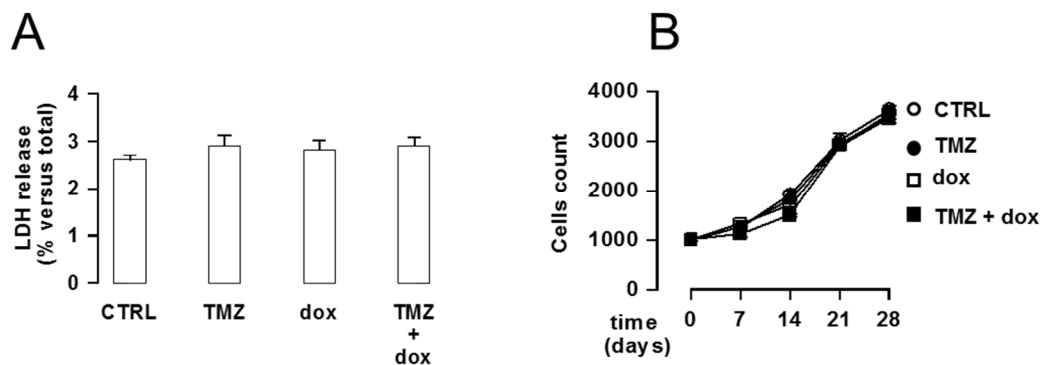
Figure 29. Effects of temozolomide and doxorubicin on cell survival of hCMEC/D3 cells.
A. hCMEC/D3 were cultured 7 days up to confluence, then incubated in fresh medium (CTRL), or medium containing 50 µmol/l TMZ for 72 h, 5 µmol/l DOX for 24 h (*dox*), or 50 µmol/l TMZ for 72 h plus 5 µmol/l DOX in the last 24 h. The culture supernatant of cells was checked spectrophotometrically for the extracellular activity of LDH, taken as an index of cytotoxicity. Measurements were performed in duplicate and data are presented as means $\pm$ SD (n= 3). **B.** 1,000 hCMEC/D3 were seeded at day 0 in 96-wells plates. After 4 days, the medium was replaced with fresh medium (*open circles, CTRL*) or medium containing 50 µmol/l TMZ for 72 h (*solid circles*), 5 µmol/l DOX for 24 h (*open squares, dox*), 50 µmol/l TMZ for 72 h plus 5 µmol/l DOX in the last 24 h (*solid squares, TMZ + dox*). Drug treatments were repeated every 7 days. Cell proliferation was monitored on day 7, 14, 21 and 28 by crystal violet staining. Measurements were performed in triplicate and data are presented as means $\pm$ SD (n= 3)

Figure 30. Effective cytotoxicity of the combination temozolomide plus vinblastine and topotecan on glioblastoma cells co-cultured with hCMEC/D3 cells. hCMEC/D3 cells were grown for 7 days up to confluence in Transwell inserts; CV17, 01010627 and U87-MG SCs were seeded at day 4 in the lower chamber. After 3 days of co-culture, the supernatant in the upper chamber was replaced with fresh medium without (-) or with TMZ (50 µmol/l for 72 h; *T*). 20 nmol/l vinblastine (*VBL*) or 10 µmol/l topotecan (*TOP*) was added in the upper chamber of Transwell in the last 24 h, then the following investigations were performed. **A.** The culture supernatant of GB cells was checked for the extracellular activity of LDH. Measurements were performed in duplicate and data are presented as means $\pm$ SD (n= 4). Vs untreated cells: * p < 0.02. **B.** The activation of Caspase-3 was measured fluorimetrically in GB cells lysates. Measurements were performed in duplicate and data are presented as means $\pm$ SD (n = 4). Vs untreated cells: * p < 0.01. **C.** After 3 days of co-culture, the medium of the upper chamber was replaced with fresh medium (*dashed line*) or medium containing 20 nmol/l vinblastine for 24 h (*open circles*, *VBL*), 10 µmol/l topotecan for 24 h (*open squares*, *TOP*), 50 µmol/l TMZ for 72 h plus 20 nmol/l vinblastine in the last 24 h (*solid circles*, *T + VBL*), 50 µmol/l TMZ for 72 h plus 10 µmol/l topotecan in the last 24 h (*solid squares*, *T + TOP*). Drug treatments were repeated every 7 days, as reported in the Materials and methods section. The proliferation of GB cells was monitored weekly by crystal violet staining. Measurements were performed in triplicate and data are presented as means $\pm$ SD (n= 4). Vs untreated cells (*CTRL*): * p < 0.02.

I then validated the key effects of TMZ in primary cells extracted from human brain microvessels, i.e. HMBECs.

Also in HMBECs, the promoter of *Wnt3* was fully unmethylated; TMZ induced the partial methylation of the promoter (Figure 31A). This was followed by the decrease of *Wnt3* mRNA (Figure 31B) and protein (Figure 31C), the increase of phospho(Tyr216)GSK3 and phospho(Ser33/37-Thr41)β-catenin (Figure 31C), the reduction of the β-catenin binding on *mdr1* promoter (Figure 31D), the decrease of Pgp protein (Figure 31E). In co-cultures of HBMECs and primary GB 01010627 SCs, the intratumor delivery of DOX was low (Figure 31F). Neither DOX or TMZ induced significant cytotoxicity, measured in terms of extracellular release of LDH and activation of the Caspase-3, in GB cells co-cultured with HBMECs (Figure 31G). By contrast, the addition of TMZ on the luminal side of HBMECs, at a concentration that did not induce cytotoxicity (Figure 32A) and did not reduce the proliferation (Figure 32B) of endothelial cells, significantly increased the delivery of DOX and cytotoxicity in GB cells (Figure 31F-G).
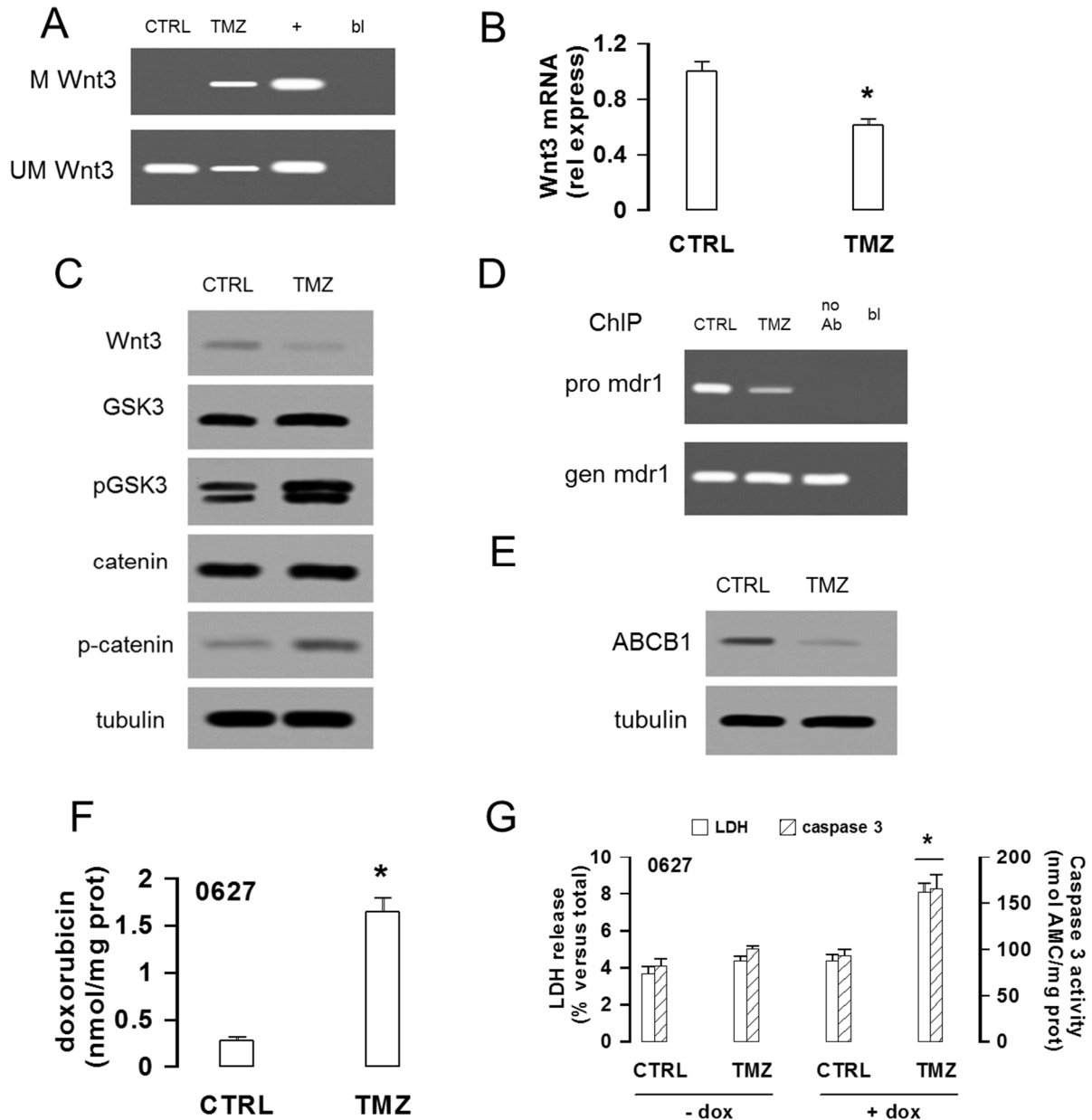
Figure 31. Effects of temozolomide in primary human brain microvascular endothelial cells co-cultured with primary human glioblastoma cells. A. Methylation of *Wnt3* promoter. HBMECs were grown in the absence (*CTRL*) or in the presence of TMZ (50 μmol/l, for 24 h), then genomic DNA was subjected to bisulfite modification, followed by PCR with specific primers for methylated (*M*) and unmethylated (*UM*) *Wnt3* promoter. The figure is representative of 3 experiments with similar results. +: positive controls with a universal methylated or unmethylated genome sequence, respectively. *bl*: blank. **B**. *Wnt3* mRNA levels. Cells were incubated in the absence (*CTRL*) or in the presence of TMZ (50 μmol/l, for 48 h). Total RNA was extracted and reverse-transcribed, the expression of *Wnt3* gene was detected by qRT-PCR. The expression level in untreated cells was considered "1". Data are presented as means ± SD (n = 3). Vs *CTRL*: * p < 0.02. **C.** Western blot analysis of Wnt3-signaling. Cells were incubated as reported in **B**, then lysed and subjected to the Western blot analysis of Wnt3, phospho(Tyr216)GSK3, GSK3, phospho(Ser33/37/Thr41)β-catenin, β-catenin in whole cell lysates. β-tubulin expression was used as control of equal protein loading. The figure is representative of 3 experiments with similar results. **D**. ChIP of β-catenin on *mdr1* promoter (*pro*) in cells incubated as reported in **B**. *gen*: PCR product from genomic DNA. *no Ab*: precipitated samples without anti-β-catenin antibody. *bl*: blank. The figure is representative of 3 experiments with similar results. **E.** Cells were incubated for 72 h without (*CTRL*) or with TMZ (50 μmol/l), then lysed and subjected to Western blot analysis for Pgp/ABCB1. β-tubulin expression was used as control of equal protein loading. The figure is representative of 3

experiments with similar results. **F.** HBMECs were grown for 7 days up to confluence in Transwell inserts; 01010627 GB SCs were seeded at day 4 in the lower chamber. After 3 days of co-culture, supernatant in the upper chamber was replaced with fresh medium without (*CTRL*) or with TMZ (50 µmol/l for 72 h). 5 µmol/l DOX (*dox*) was added in the upper chamber in the last 24 h. GB cells were then collected and analyzed for the intracellular amount of doxorubicin by a fluorimetric assay. Measurements were performed in duplicate and data are presented as means $\pm$ SD (n = 3). Vs untreated cells (*CTRL*): * $p < 0.001$. **G.** Co-cultures of HBMECs and 01010627 cells were set up as detailed in **F**. At the end of the incubation period, the culture supernatant of GB cells was checked spectrophotometrically for the extracellular activity of LDH (open bars), the cell lysates were analyzed fluorimetrically for the activity of Caspase-3 (hatched bars). Measurements were performed in duplicate and data are presented as means $\pm$ SD (n= 3). Vs untreated cells: * $p < 0.005$.
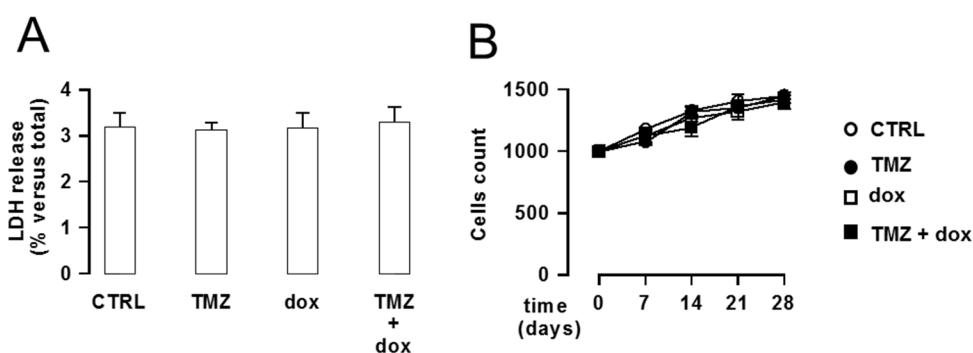
Figure 32. Effects of temozolomide and doxorubicin on cell survival of primary human brain microvascular endothelial cells. A. HBMECs were cultured 7 days up to confluence, then incubated in fresh medium (CTRL), or medium containing 50 µmol/l TMZ for 72 h, 5 µmol/l DOX for 24 h (*dox*), or 50 µmol/l TMZ for 72 h plus 5 µmol/l DOX in the last 24 h. The culture supernatant of cells was checked spectrophotometrically for the extracellular activity of LDH, taken as an index of cytotoxicity. Measurements were performed in duplicate and data are presented as means $\pm$ SD (n= 3). **B.** 1,000 HBMECs were seeded at day 0 in 96-wells plates. After 4 days, the medium was replaced with fresh medium (*open circles, CTRL*) or medium containing 50 µmol/l TMZ for 72 h (*solid circles*), 5 µmol/l DOX for 24 h (*open squares*), 50 µmol/l TMZ for 72 h plus 5 µmol/l DOX in the last 24 h (*solid squares*). Drug treatments were repeated every 7 days. Cell proliferation was monitored on day 7, 14, 21 and 28 by crystal violet staining. Measurements were performed in triplicate and data are presented as means $\pm$ SD (n= 3).

4.2 Aim 2: Influence of interaction between GB and BBB on drug delivery across BBB

4.2.1 Glioblastoma multiforme cells increase blood-brain barrier monolayer permeability

As BBB is disrupted in presence of GB [van Tellingen, 2015], I investigated whether the grade of differentiation and/or stemness of GB cells could influence the expression of ABC transporters on BBB and the drug permeability across BBB.

The permeability to DEXT-70-FITC, DOX and MXR was used as parameter of tight junction integrity, Pgp activity and BCRP activity, respectively [Riganti, 2014], in hCMEC/D3-GB co-cultures. At 24 h and 72 h, the permeability to DEXT, DOX and MXR increased in hCMEC/D3 co-cultured with GB cells respect to hCMEC/D3 alone. The effect was greater in presence of adherent cells (AC) than in the presence of SCs (Figure 33). For the sake of simplicity, the three SC lines and the three AC were pooled together since there were no significant differences within each GB sample that I tested. Also the conditioned medium obtained from a 5-days culture of SCs or AC GB cells and added on hCMEC/D3 cells for 24 h – 72 h, increased the permeability to DOX, MXR and DEXT respect to hCMEC/D3 alone. The conditioned medium of AC induced an higher increase in permeability than the conditioned medium of SCs (Figure 34).

The changes in permeability across BBB were paralleled by changes in BBB uptake of each drug. DOX, MXR, DEXT concentrations in hCMEC/D3 were higher in BBB-SC co-cultures than in BBB-AC co-cultures (Figure 35 A). The trend induced by GB conditioned-medium of SCs or AC was the same (Figure 35 B).
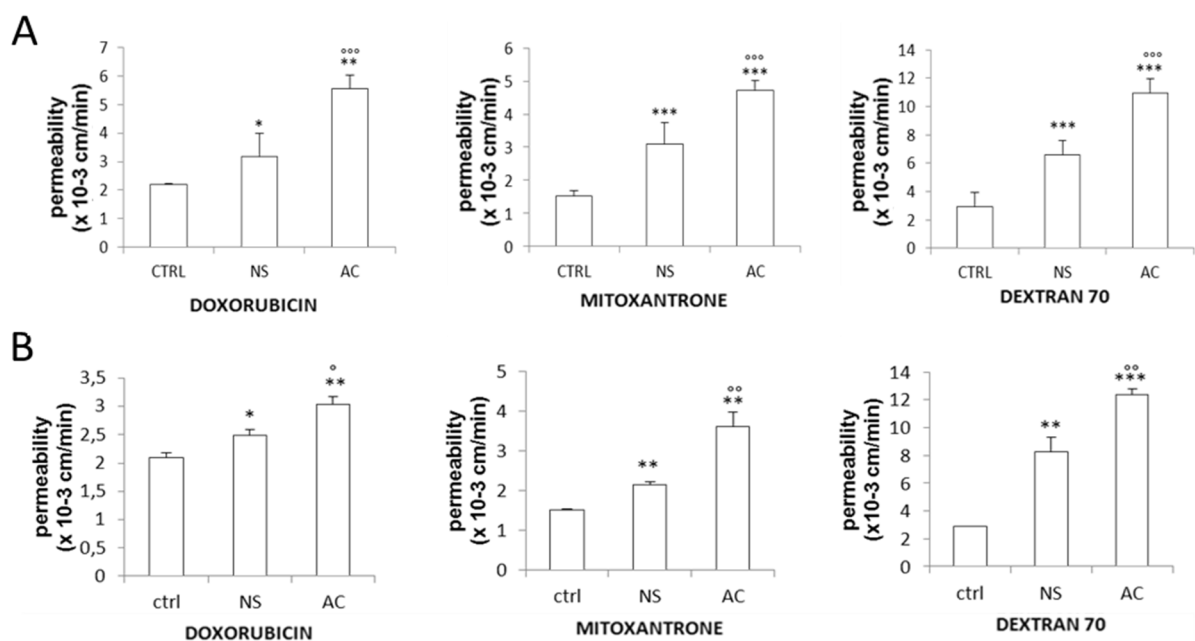
Figure 33. Doxorubicin, mitoxantrone, dextran-FITC permeability in co-culture hCMEC/D3-GB cells. hCMEC/D3 cells were grown for 7 days up to confluence in Transwell inserts (ctrl); when indicated, GB SCs (NS) or AC were seeded at day 7 in the lower chamber for 24 h (**A**) or 72 h (**B**). After 24 h and 72 h co-culture, supernatant in the upper chamber was replaced with medium containing 5 µmol/l DOX, 10 µmol/l MXR and 2 µmol/l DEXT-70-FITC for 3 h. The drug recovered from the lower chamber was measured fluorimetrically. Data are presented as means $\pm$ SD (n = 3); * vs ctrl; ° AC vs NS. * $p < 0.05$ ** $p < 0.01$ ***$p < 0.001$.
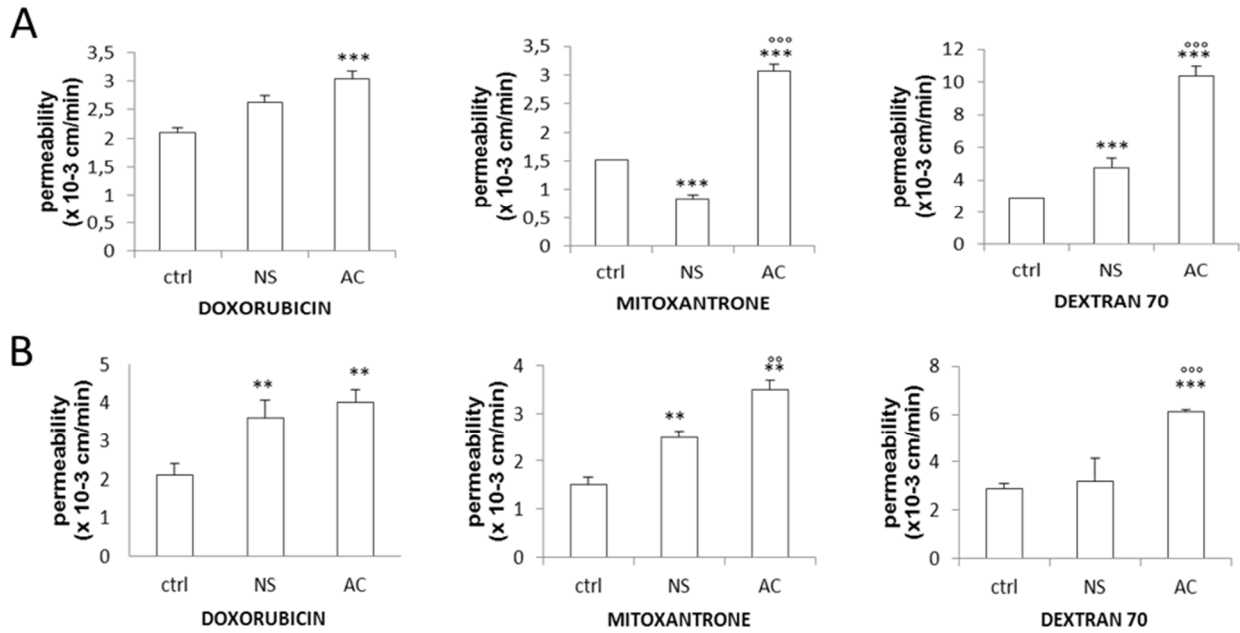
Figure 34. Doxorubicin, mitoxantrone, dextran-FITC permeability in co-culture hCMEC/D3-GB conditioned medium. hCMEC/D3 cells were grown for 7 days up to confluence in Transwell insert ctrl); when indicated, then incubated for 24 h (**A**) or 72 h (**B**) with 5-days conditioned.medium of GB SCs (NS) or AC. After 24 h and 72 h co-culture, supernatant in the upper chamber was replaced with with medium containing 5 µmol/l DOX, 10 µmol/l MXR and 2 µmol/l DEXT-70-FITC for 3 h. The drug recovered from the lower chamber was measured fluorimetrically. Data are presented as means $\pm$ SD (n = 3); * vs ctrl; ° AC vs NS. * p<0.05 ** p< 0.01 ***p< 0.001.
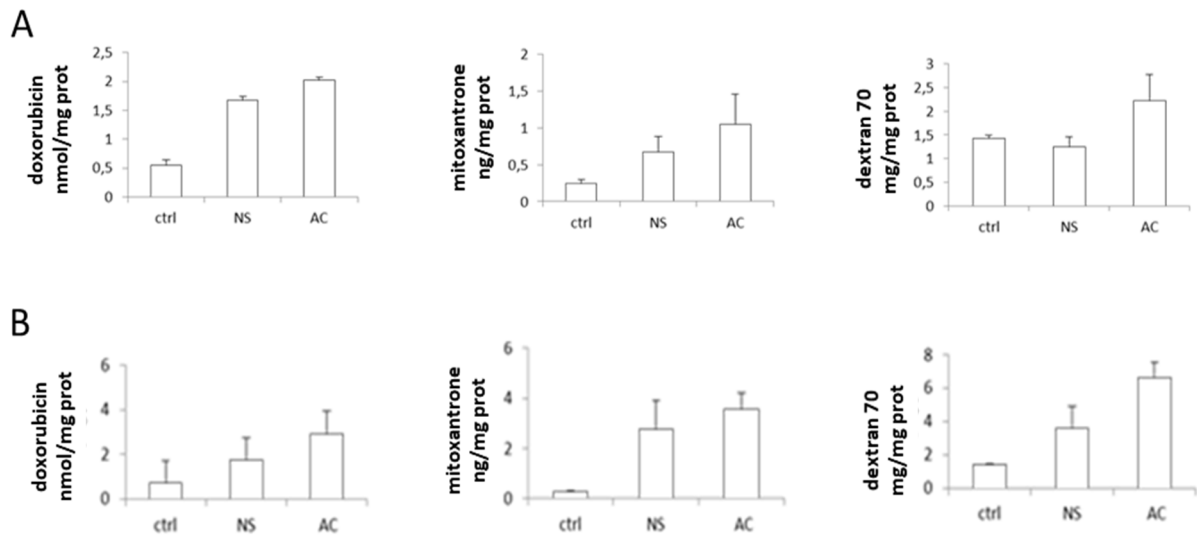
Figure 35. Doxorubicin, Mitoxantrone, Dextran-FITC accumulation in hCMEC/D3. A. hCMEC/D3 cells were grown for 7 days up to confluence in Transwell inserts; GB SCs (NS) or AC were seeded at day 7 in the lower chamber. After 24 h of co-culture, supernatant in the upper chamber was replaced with with medium containing 5 µmol/l DOX, 10 µmol/l MXR and 2 µmol/l DEXT-70-FITC for 3 h. Fluorimetric quantification of intracellular DOX in hCMEC/D3 cells after 3 h. Data are presented as means $\pm$ SD (n= 3). **B**. hCMEC/D3 cells were grown for 7 days up to confluence in Transwell insert, then incubated for 72 h 5-days conditioned.medium of NS or AC GB cells. After 24 h and 72 h co-culture, supernatant in the upper chamber was replaced with with medium containing 5 µmol/l DOX, 10 µmol/l MXR and 2 µmol/l DEXT-70-FITC for 3 h. Fluorimetric quantification of intracellular doxorubicin in hCMEC/D3 cells after 3 h. Data are presented as means $\pm$ SD (n= 3).

4.2.2 Glioblastoma multiforme cells induce changes in ABC transporters and tight junction expression in blood-brain barrier cells

I next investigated the expression levels of ABC transporters involved in DOX and MXR permeability and of TJ proteins in BBB cells co-cultured with GB cells at 24 h and 72 h, to verify whether GB cells or conditioned medium altered the expression of these proteins.

At both time, Pgp, BCRP, occludin and ZO1 were decreased in BBB co-cultured with AC respect to BBB alone and only slightly reduced by the presence of SCs. On the contrary, claudin 3 and 5 were increased by the co-culture with AC and reduced by presence of SCs (Figure 36).

Overall, the changes in the expression levels of ABC transporters were more pronounced after 72 h (Figure 36B), the changes in the expression levels of TJ proteins were already evident after 24 h (Figure 36A). The co-culture with AC markedly decreased the mRNA for Pgp, BCRP, occludin and ZO-1 in BBB cells co-cultured with GB cells at 24 h. Notwithstanding a certian variability for the different mRNA analyzed, SCs produced minor changes: SCs strongly reduced the mRNA level for BCRP, slightly decreased Pgp and increased occludin and ZO-1 mRNA. In keeping with the protein levels, claudin-3 and claudin-5 had an opposite trend than the other mRNAs: they were reduced by SCs and increased by AC respect to the hCMEC/D3 alone (Figure 37). At 72 h the trend was similar to 24 h, except for claudin-3 that increased in both AC and SCs (Figure 37). Conditioned medium form AC or SCs produced the same results (data not shown).
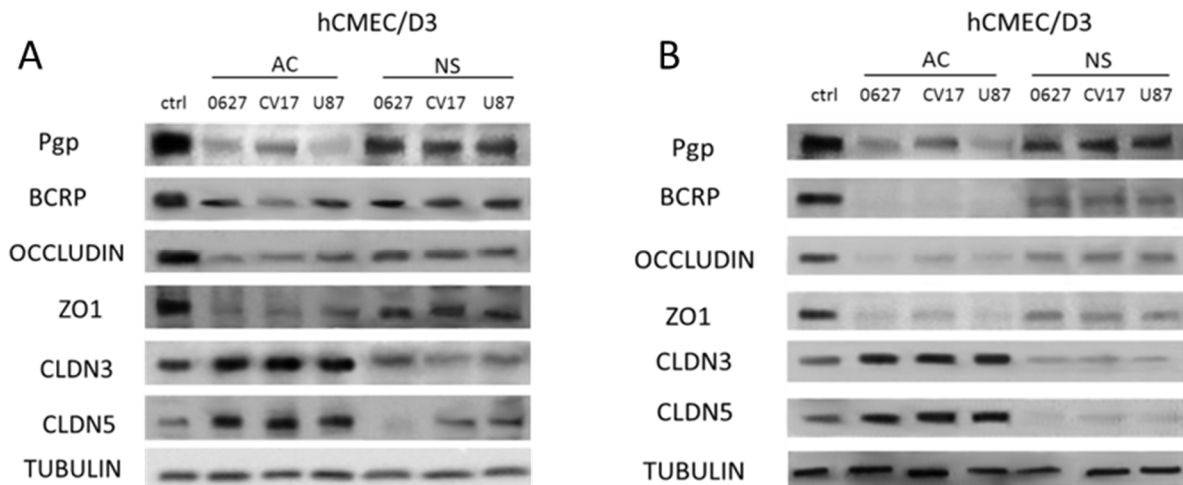
Figure 36. Expression of ABC transporters and tight junctions-related proteins in BBB-GB co-culture. hCMEC/D3 cells were grown for 7 days up to confluence in Transwell insert, then incubated for 24 h (**A**) or 72 h (**B**) in fresh medium (ctrl) or with GB AC or SCs (NS). After 24 h and 72 h hCMEC/D3 cells were lysed and immunoblotted with the indicated antibodies. The expression of tubulin, as housekeeping gene, was used as a control of equal protein loading. The figure is representative of one out of three experiments with similar results. CLDN3: claudin-3; CLDN5: claudin-5.
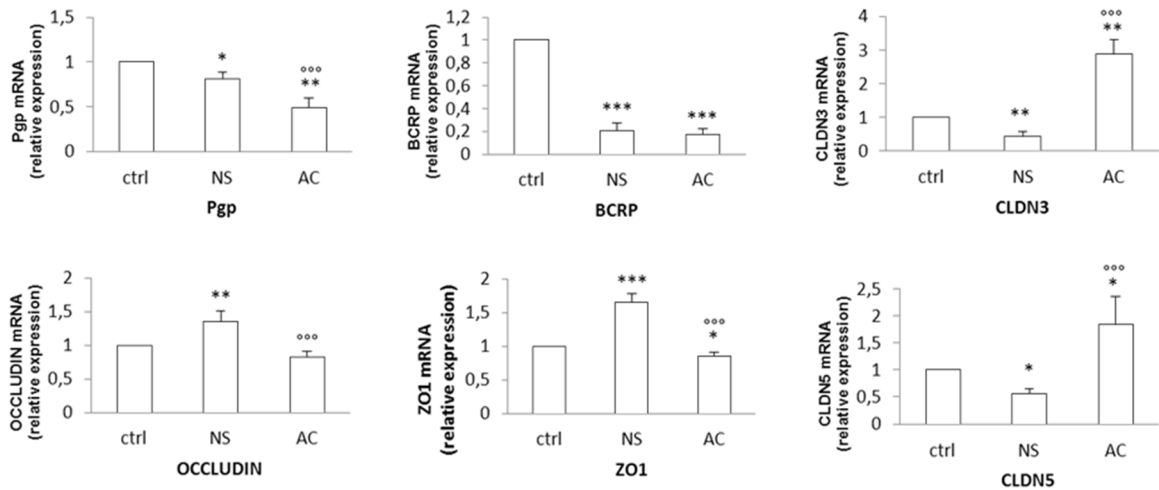
Figure 37. Expression levels of ABC transporters and tight junctions-related gene in BBB-GB co-culture. hCMEC/D3 cells were grown for 7 days up to confluence in Transwell insert, then incubated for 24 h (**A**) or 72 h (**B**) in fresh medium (ctrl) or with SCs (NS) or AC. After 24 h and 72 h, hCMEC/D3 cells were subjected to RNA extraction and qRT-PCR to measure the expression of Pgp, BCRP, claudin-3 (CLDN3), claudin-5 (CLDN5), occludin, ZO1. The expression level of ctrl AC/NS GB was considered "1" and used as the reference for all the other experimental conditions Data are presented as mean ± SD (n=3); * vs CTRL; ° AC vs NS. * $p<0.05$ ** $p<0.01$ ***$p<0.001$

4.2.3 Wnt signaling can modulate blood-brain barrier permeability

In previous works [Riganti, 2013; Riganti, 2014; Pinzón-Daza, 2014], we observed that Wnt3a pathway increseased Pgp expression in GB SCs and Wnt3 increased Pgp in BBB cells. Wnt3a is a soluble factor released by GB in its micro-enviornment. AC do not express Wnt3a, which is instead constitutively expressed in SCs [Riganti, 2013]. I thus investigated if the presence or absence of Wnt in GB can explain the different regulation of ABC transporters and TJ proteins in BBB cells-co-cultured with GB AC or SCs, or exposed to the respective conditioned medium. I generated an AC-derived clone stably overexpressing Wnt3a that acquired the same morphological, functional and chemoresistant profile of SCs [Riganti, 2013], and I co-cultured it with BBB. Wnt3a-overexpressing AC produced a significantly smaller increase in the permeability to DOX, MXR and DEXT compared to the parental AC cells, behaving like SCs at 24 h and 72 h (Figure 38). The stable overexpression of Wnt3a in AC produced the same effects elicited by SCs on ABC transporters and TJ proteins in Western Blot analysis (Figure 39). Indeed, Wnt3a-overexpressing AC cells induced a lower decrease of Pgp, BCRP, occludin and ZO1, as SCs did. Also at transcription level, Wnt3a-overexpressing AC modulated the mRNA levels as SCs did, behaving differently from wild type AC (Figure 40).

These data suggest that Wnt3a released by GB may account for the differential modulation of AC and SCs of at least Pgp in BBB. I am now investigating how the levels of phospho(Tyr216)GSK3 and phospho(Ser33/37/Thr41)-β-catenin, which directly control Pgp amount in BBB cells [Riganti, 2014; Pinzón-Daza, 2014], vary in hCMEC/D3 cells co-cultured with AC, SCs and Wnt3a-overexpressing AC, or their conditioned medium.
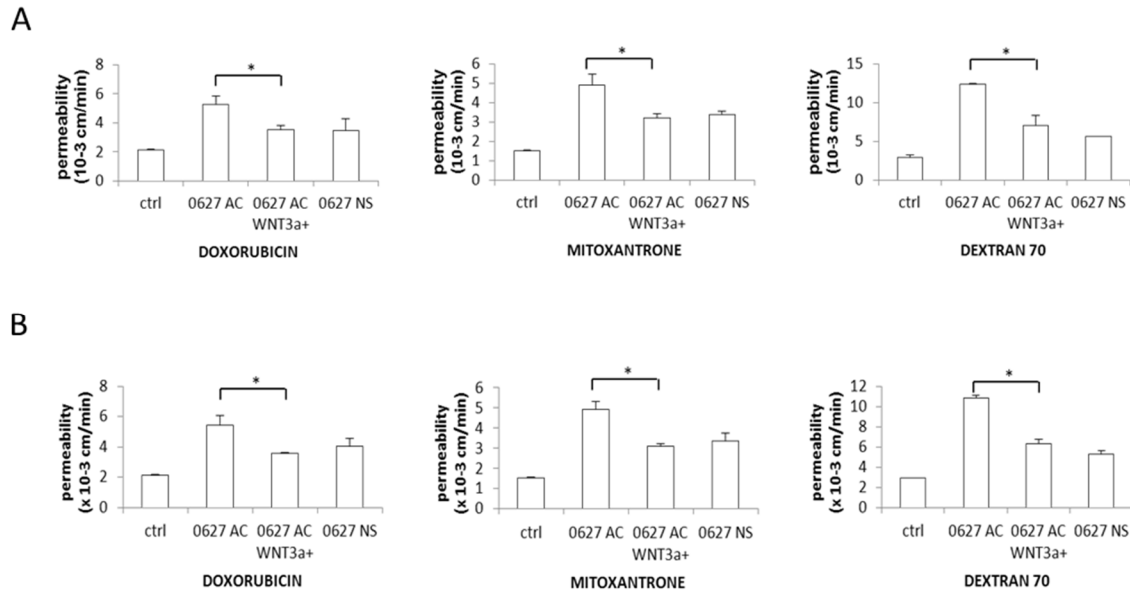
Figure 38. Doxorubicin, mitoxantrone, dextran-FITC permeability in hCMEC/D3 co-cultured with GB AC, AC Wnt3a+, SCs. hCMEC/D3 cells were grown for 7 days up to confluence in Transwell insert, then incubated for 24 h (**A**) or 72 h (**B**) in fresh medium (ctrl), with primary GB 01010627 AC, 01010627 AC stably overexpressing Wnt3a, 01010627 SCs/NS, that constitutively express Wnt3a. After 24 h and 72 h co-culture, supernatant in the upper chamber was replaced with medium containing 5 µmol/l DOX, 10 µmol/l MXR andnd 2 µmol/l DEXT-70-FITC for 3 h. The drug recovered from the lower chamber was measured fluorimetrically. Data are presented as means + SD (n = 3); * vs CTRL; ° AC vs NS. * $p < 0.05$ ** $p < 0.01$ *** $p < 0.001$.
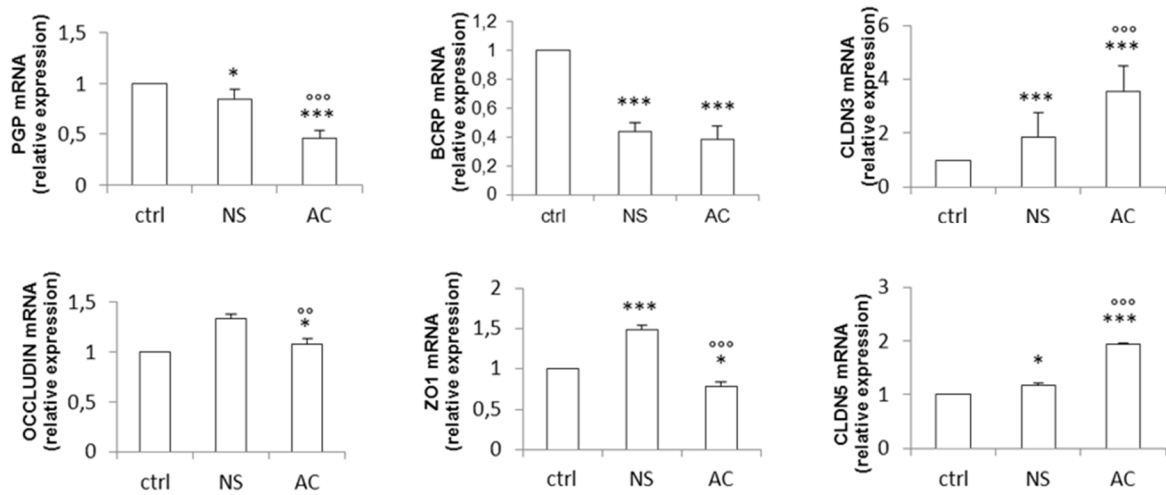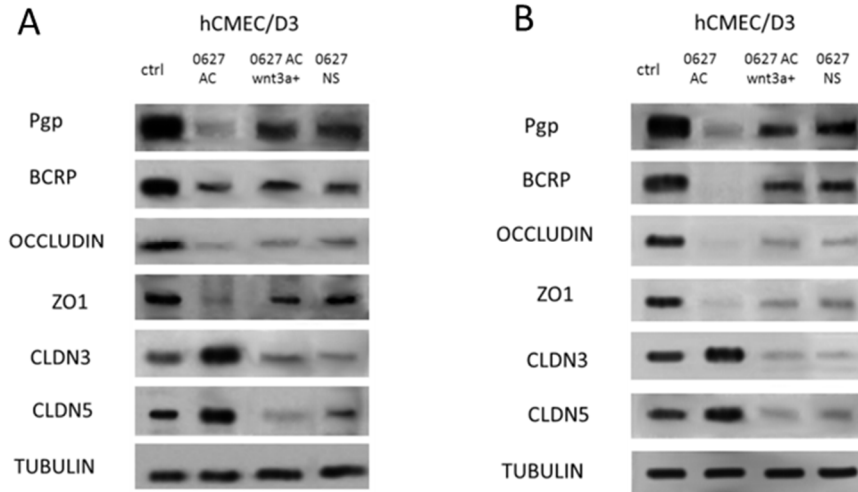
Figure 39. Expression of ABC transporters and tight junctions-related proteins in BBB co-cultured GB AC, AC Wnt3a+, NS. hCMEC/D3 cells were grown for 7 days up to confluence in Transwell insert, then incubated for 24 h (**A**) or 72 h (**B**) in fresh medium (ctrl), or with primary GB 1010627 AC, 01010627 AC stably overexpressing Wnt3a, 01010627 NS/SCs, that constitutively express Wnt3a. After 24 h and 72 h hCMEC/D3 cells were lysed and immunoblotted with the indicated antibodies. The expression of tubulin, as housekeeping gene, was used as a control of equal protein loading. The figure is representative of one out of three experiments with similar results.
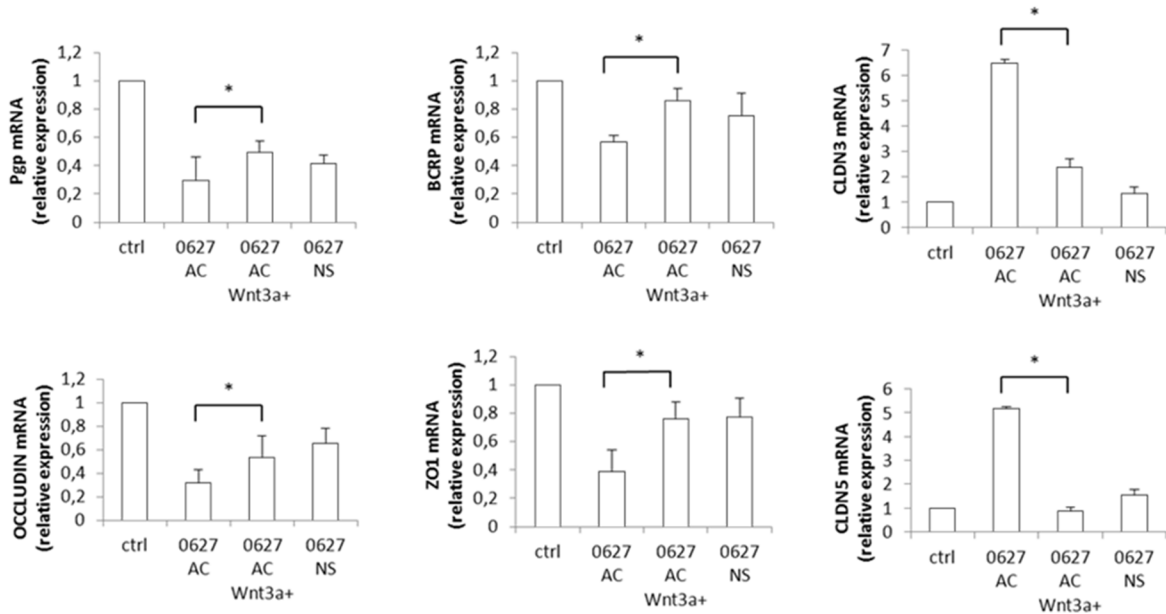
Figure 40. Expression levels of ABC transporters and tight junctions-related genes in BBB co-cultured with GB AC, AC Wnt3a+, NS. hCMEC/D3 cells were grown for 7 days up to confluence in Transwell insert, then incubated for 72 h in fresh medium (ctrl), or primary GB 01010627 AC, 01010627 AC stably overexpressing Wnt3a, 01010627 SCs/NS, that constitutively express Wnt3a. After 72 h, hCMEC/D3 cells were subjected to RNA extraction and qRT-PCR to measure the expression of Pgp, BCRP, claudin-3 (CLDN3), claudin-5 (CLDN5), occludin, ZO1 gene expression. The expression level of ctrl AC/NS GB was considered "1" and used as the reference for all the other experimental conditions Data are presented as mean ± SD (n=3); * vs CTRL; ° AC vs NS. * $p<0.05$ ** $p< 0.01$ ***$p< 0.001$.

4.3 Aim 3: Development of new strategies to improve drug delivery by targeting BBB-dependent mechanisms and GB SCs-dependent mechanisms

4.3.a Aim 3a: Targeting BBB-dependent mechanisms

4.3.a.1 Thiosemicarbazones increase the permeability of Pgp substrates across BBB monolayer

To improve drug delivery across BBB I tested a series of thiosemicarbazone derivatives, originally produced as inducers of collateral sensitivity, i.e. compounds with higher cytotoxicity against Pgp-overexpressing tumors than against Pgp-negative ones [Szakács, 2014], developed by the Department of Pharmacy, University of Bari. In these compounds a metal chelator portion was connected to a moiety targeting both sigma2 receptor, overexpressed on tumor cells, and Pgp, in order to promote the sigma-2 receptors mediated cells death and inhibit Pgp at the same time [Pati, 2015]. Within this library three thiosemicarbazone derivatives, named **8a**, **10a** and **17a**, showed Pgp inhibitory activity at nanomolar concentration, in line with the most potent Pgp blockers such as PSC833 or tariquidar. On the other hand, these compounds were not cytotoxic in this concentration range, having an IC_{50} on cell viability of breast and lung cancer cells in the micromolar range (Figure 41; adapted from Pati, 2015).

After optimising the concentration for inhibiting P-gp and exerting citotoxicity, I used the compounds as potentially safe inhbitors of Pgp on BBB.
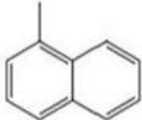
I first evaluated the cytotoxicity of thiosemicarbazone inhibitors on intact BBB. All compounds displayed dose- and time-dependent cytotoxicity on hCMEC/D3 cells monolayer. At 10 and 100 nM - a concentration range compatible with their EC_{50} values on Pgp [Pati, 2015] - they did not damage BBB cells (Figure 42). All the compounds significantly increased the uptake of DOX, chosen as a virtually impermeable compound across BBB being a substrate of Pgp, within hCMEC/D3 cells at 10 nM concentration (Figure 43A). This concentration was chosen for all the subsequent experiments as the lowest concentration that effectively increased the retention of DOX within BBB cells. In line with the higher uptake, the permeability of DOX across hCMEC/D3 cells monolayer was significantly increased (Figure 43B). The effects was selective on Pgp substrates; indeed, the compounds did not increase the permeability of MXR (Figure 43C) and DEXT-70-FITC (Figure 43D), suggesting that the activity of BCRP and the competence of TJs were not altered. Moreover the compounds did not change the expression of Pgp, MRP1, BCRP, three ABC transporters involved in DOX efflux [Agarwal, 2011], and TJ-related protein in these experimental conditions (Figure 44).

4.3.a.2 Thiosemicarbazones increase doxorubicin intratumor delivery and efficacy against primary GB cells co-cultured with BBB

I next investigated if the increased delivery of DOX across BBB monolayer produced an increased delivery of the drug within GB cells growing under BBB. To this aim, I used two primary GB stabilized cell lines, 01010627 and CV17 cells, cultured as AC or SCs populations. As reported above, AC were relatively sensitive to DOX *in vitro* and had low or undetectable expression of Pgp, MRP1 and BCRP, while SCs were DOX-resistant and had a basally high expression of these transporters [Riganti, 2013] (Figure 45). I previously demonstrated that the

presence of a competent BBB strongly reduce the intratumor delivery and efficacy of DOX, for the Pgp-mediated efflux of the drug by BBB cells. In line with these observations, DOX was poorly accumulated in GB cells growing under hCMEC/D3 cells monolayer (Figure 47A-B-E) and did not induce any cytotoxic effect (Figure 47C-D). In both primary GB samples, drug accumulation and toxicity was even lower in SCs than in AC (Figure 46), likely as a consequence of the higher expression of Pgp, MRP1 and BCRP in the former (Figure 45-46). All compounds increased the DOX uptake in GB cells when cultured alone (Figure 47), as well as the intratumor doxorubicin delivery and cytotoxicity in GB growing under hCMEC/D3 cells monolayer. These effects were significantly more pronounced in SCs than in AC (Figure 46; Fgure 47).

Cpd	R	$K_i \pm SEM^a$ (nM)	$EC_{50} \pm SEM^a$ (μM)					
		σ_2	MCF7	MCF7dx	A549	A549dx	Calcein-AM	ATP[b]
1, siramesine		12.6[c]	12.3[c]	5.90[c]	15.4[d]	4.63[d]	1.41[c]	Yes
2		0.04[c]	28.2[c]	17.1[c]	26.4[d]	11.7[d]	0.42[c]	Yes
8a		8.70 ± 1.5	25.9 ± 0.7	22 ± 0.3	20.7 ± 1.2	19.4 ± 1.2	0.075 ± 0.01	No
10a		9.9 ± 1.0	>100	>100	20.6 ± 4.0	13.3 ± 1.9	0.065 ± 0.03	No
17a		7.20 ± 0.16	>100	>100	>100	>100	0.04 ± 0.001	No

[a] Values represent the mean of $n \geq 2$ separate experiments in duplicate ± SEM. [b] 'Yes': ATP is depleted, 'No': ATP is not depleted. [c] From ref. 33. [d] From ref. 34.

Figure 41. Structure and properties of thiosemicarbazone derivatives. 8a, **10a** and **17a** belong to a library of compounds inducers of collateral sensitivity created by Pati et al. [Pati, 2015]. The common moiety is reported in the upper panel. The thiosemicarbazone derivatives inhibit Pgp at nanomolar concentration as detected by Calcein-AM assay and exert cytoxic activity against breast MCF7 cancer cells, lung A549 cancer cells and their Pgp-expressing counterparts (MCF7/dx; A549/dx) at micromolar concentration, measured by EC50 assay.
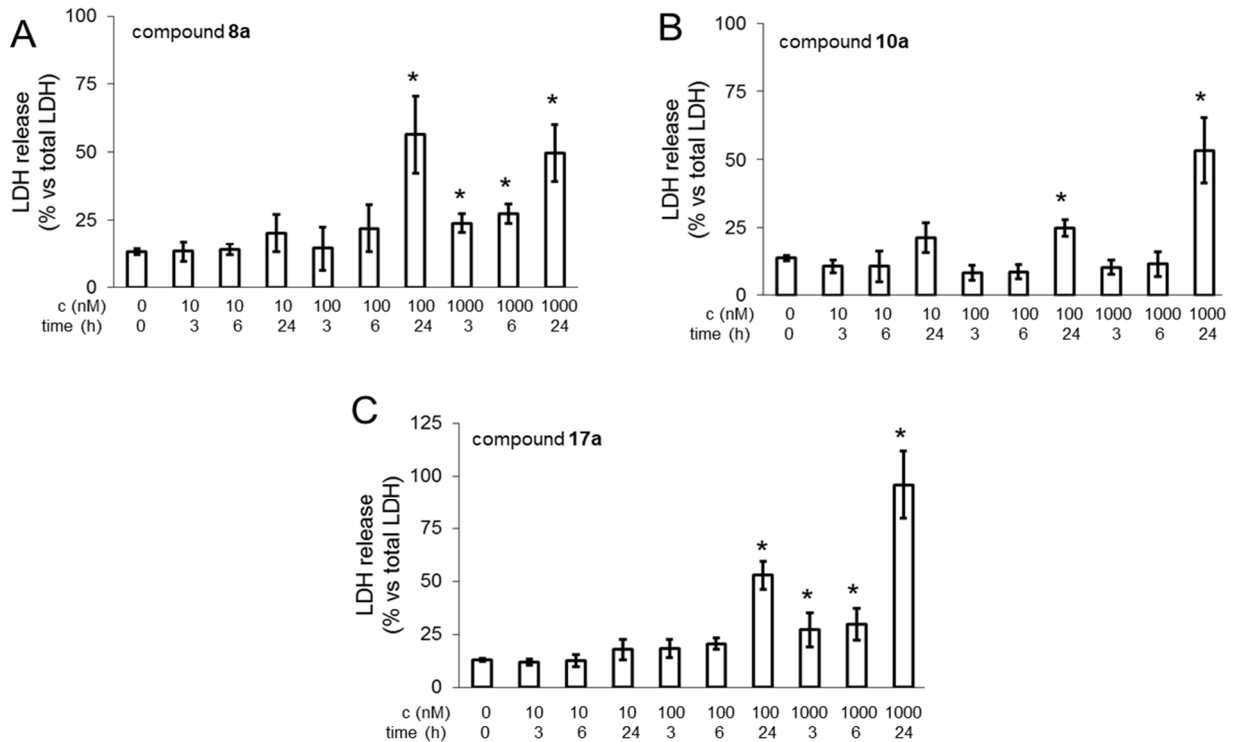
Figure 42. Cytotoxicity of thiosemicarbazone compounds on BBB cells. hCMEC/D3 cells were grown in the absence or in the presence of compounds **8a**, **10a** and **17a** at the indicated times and concentrations. The release of LDH in the extracellular medium was measured spectrophotometrically. Data are presented as means $\pm$ SD (n = 4). *Versus* untreated cells: * p < 0.01.
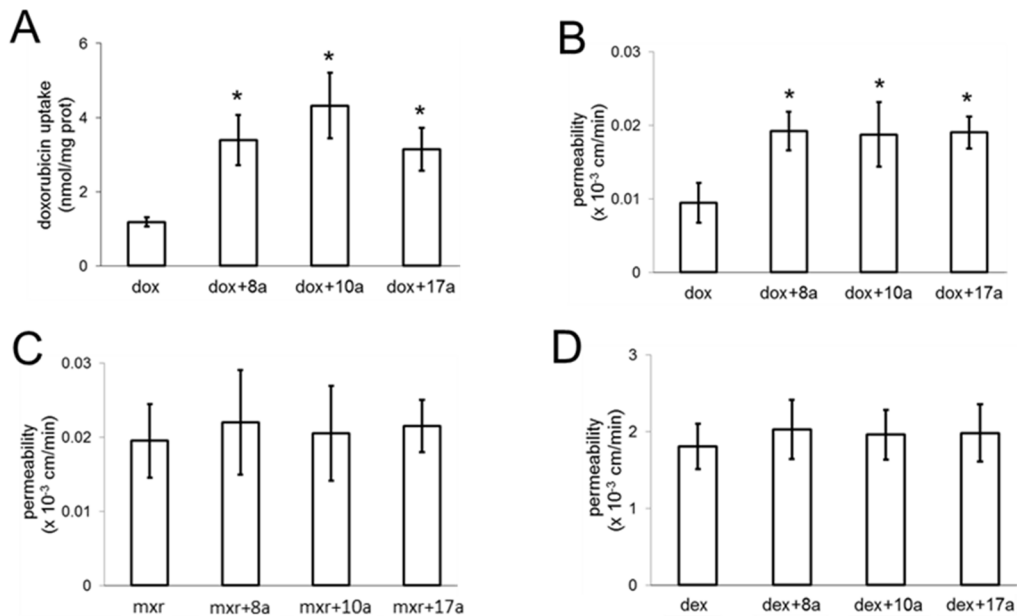
Figure 43. Effects of thiosemicarbazone compounds on BBB permeability. A. hCMEC/D3 cells were grown for 7 days up to confluence in Transwell inserts, then incubated 3 h with 5 μmol/l DOX (dox), alone or in the presence of 10 nmol/l compounds **8a, 10a** and **17a**. The intracellular retention of DOX was measured spectrofluorimetrically. Data are presented as means $\pm$ SD (n = 5). *Versus* dox: * p < 0.001. **B-C-D.** hCMEC/D3 cells were grown for 7 days up to confluence in Transwell inserts, then incubated for 3 h with 5 μmol/l DOX (dox; panel **B**), 10 μmol/l mitoxantrone (mxr; panel **C**), 2 μmol/l DEXT-70-FITC (dex; panel **D**), alone or in the presence of 10 nmol/l compounds **8a, 10a** and **17a**. The drug recovered from the lower chamber was measured fluorimetrically. Data are presented as means $\pm$ SD (n = 3). Vs dox: * p < 0.001.
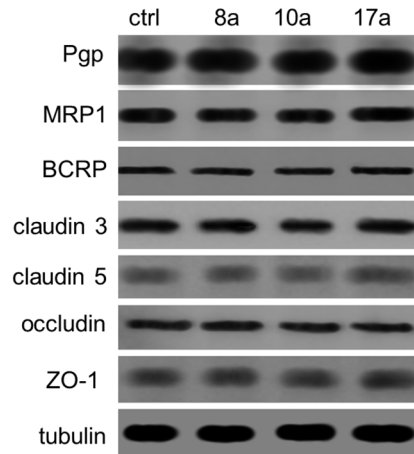
Figure 44. Expression of ABC transporters and tight junctions-related proteins in BBB cells. hCMEC/D3 cells were grown in fresh medium (ctrl) or in medium containing 10 nmol/l compounds **8a**, **10a** and **17a** for 3 h, then lysed and immunoblotted with the indicated antibodies. β-tubulin level was used as control of equal protein loading. The figure is representative of one out of three experiments with similar results.
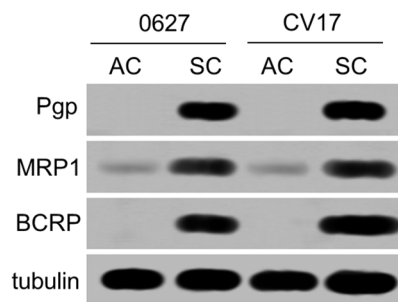
Figure 45. Expression of ABC transporters in glioblastoma cells. 01010627 and CV17 adherent cells (AC) or stem cells (SCs) were lysed and immunoblotted with the indicated antibodies. β-tubulin level was used as control of equal protein loading. The figure is representative of one out of three experiments with similar results.
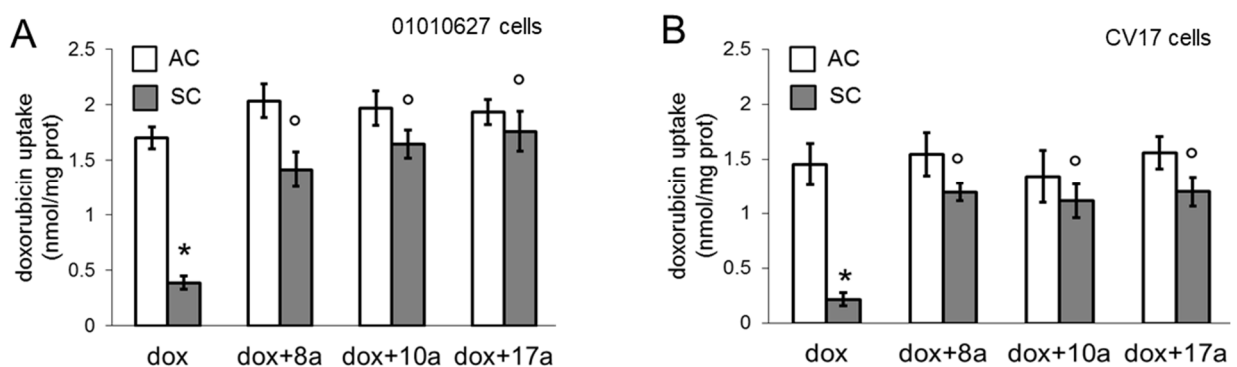
Figure 46. Doxorubicin uptake in glioblastoma cells. 01010627 (panel **A**) and CV17 (panel **B**) adherent cells (AC) or stem cells (SCs) were incubated for 3 h with 5 µmol/l DOX (dox), in the absence or presence of 10 nnol/l compounds **8a, 10a** and **17a**. The intracellular DOX was quantified fluorimetrically. Data are presented as means ± SD (n = 3). Vs AC dox: * $p < 0.001$; vs SCs dox: ° $p < 0.001$.
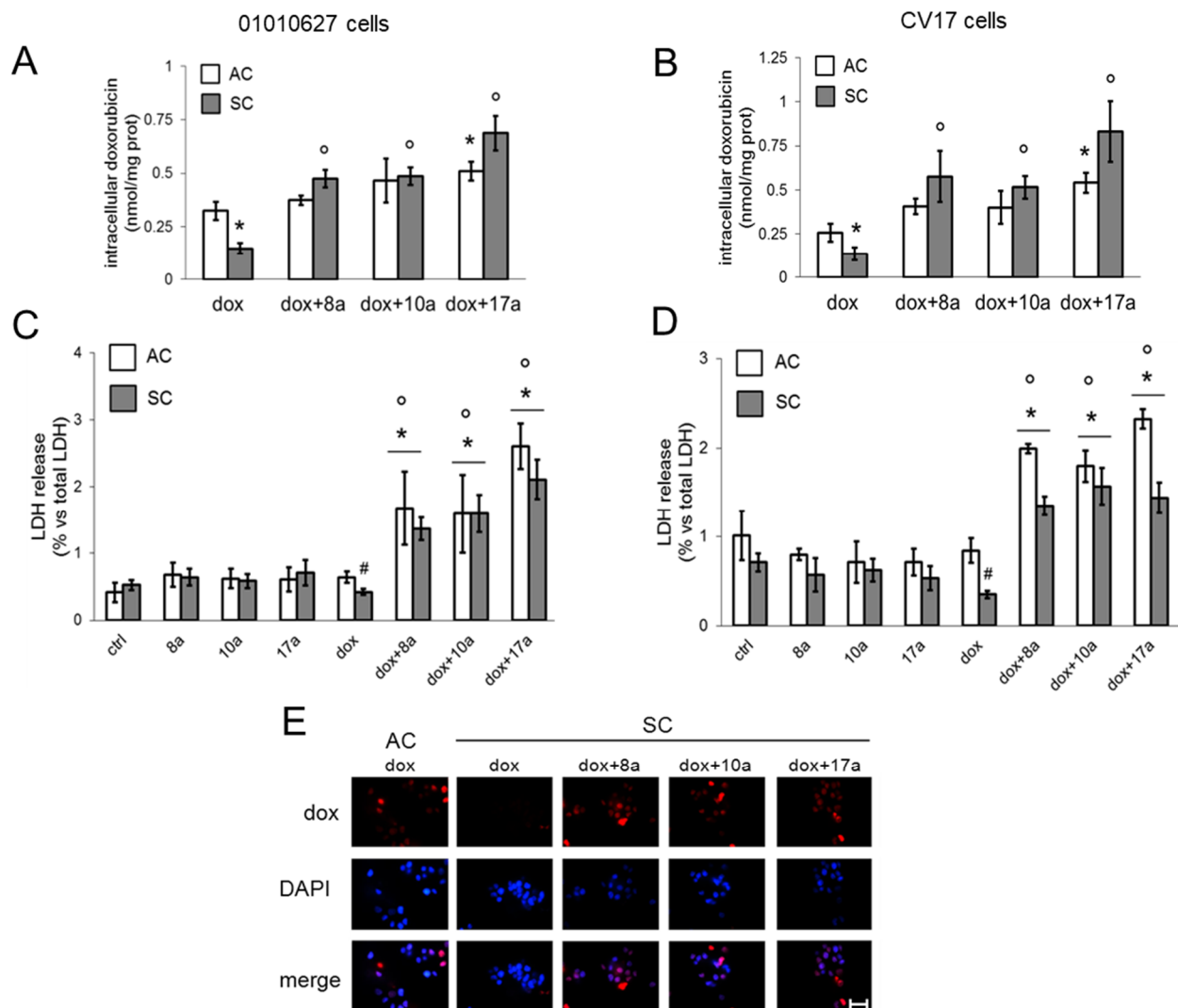
Figure 47. Effects of thiosemicarbazone compounds on doxorubicin delivery and cytotoxicity in glioblastoma cells co-cultured with BBB cells. hCMEC/D3 cells were grown for 7 days up to confluence in Transwell inserts; 01010627 (A, C, E) and CV17 (B, D) adherent cells (AC) or stem cells (SCs) were seeded at day 4 in the lower chamber. After 3 days of co-culture, supernatant in the upper chamber was replaced with fresh medium (ctrl) or with medium containing 5 µmol/l DOX (dox), in the absence or presence of 10 nmol/l compounds **8a, 10a** and **17a**. **A-B**. Fluorimetric quantification of intracellular DOX in GB cells after 3 h. Data are presented as means $\pm$ SD (n = 3). Vs AC dox: * p < 0.005; vs SCs dox: ° p < 0.001. **C-D.** The culture supernatant of GB cells was checked spectrophotometrically for the extracellular activity of LDH after 24 h. Data are presented as means $\pm$ SD (n= 3). Vs AC/SCs ctrl: * p < 0.01; vs AC/SCs dox: ° p < 0.01; SCs dox vs AC dox: # p < 0.05. **E.** 01010627 cells were seeded on sterile glass coverslips, treated as reported above, then stained with DAPI and analyzed by fluorescence microscopy to detect the intracellular accumulation of DOX. Magnification: 63 x objective (1.4 numerical aperture); 10 x ocular lens.Bar 100 µm. The micrographs are representative of 3 experiments with similar results.

4.3.b Aim 3b: Targeting GB SCs-dependent mechanisms

4.3.b.1 Glioblastoma-derived stem cells overexpress CAXII and Pgp

U87-MG SCs and primary cells from three GB patients (UPN1, UPN2, UPN3) expressed higher levels of CAXII and CAIX compared to the corresponding AC. Pgp was present in SCs, but was either undetectable or at very low levels (UPN2 only) in the corresponding AC (Figure 48A). The higher amount of CAXII and Pgp in whole cell lysate was paralleled by a higher amount of both proteins on SC cell surface (Figure 48B). Plasma membrane-associated CAXII co-immunoprecipitated with Pgp in SCs, not in AC. A weak co-immunoprecipitation was detected in UPN2 AC (Figure 48C), the only AC sample with very low detectable Pgp levels (Figure 48A). By contrast, CAIX did not co-immunoprecipitate with Pgp (Figure 48C). The physical association between CAXII and Pgp in SCs - but not in AC - was confirmed in UPN2 sample by proximity-ligation assay (Figure 48D).

4.3.b.2 Inhibitors of CAXII reduce Pgp activity in glioblastoma-derived stem cells, increasing retention and cytotoxicity of Pgp substrates

I next tested the efficacy of CAXII inhibitors, the natural product Psammaplin C (compound **1**) and its derivatives (**2, 3, 4**) as well as control compound lacking CAXII binding (**5**) (Figure 49A), synthesized by the Griffith Institute for Drug Discovery, Griffith University, Brisbane, Australia, on Pgp activity in GB SCs.

Compound **1** (CAXII Ki = 0.79 nM) and compound **3** (CAXII Ki = 43 nM) were the most effective inhibitors of Pgp ATPase activity, followed by compound **4** (CAXII Ki = 219 nM); compound **2** (CAXII Ki = >50,000 nM) and **5** (no CA XII inhibition) were ineffective (Figure 49B-C). As expected, the Pgp substrate DOX accumulated in AC but was poorly retained in SCs (Figure 49C). In line with the low expression of CAXII in AC, CAXII inhibitors did not alter DOX intracellular accumulation in AC (Figure 49C). In contrast, compounds **1** and **3**, which produced the strongest inhibition on Pgp activity (Figure 49B), increased the intracellular DOX in SCs to concentrations comparable to those found in AC (Figure 49C). In accord with the intracellular DOX accumulation and with the different expression levels of CAXII and Pgp, the drug significantly increased the release of LDH from AC, while CAXII inhibitors did not enhance DOX effect (Figure 49D, left panel). DOX was not cytotoxic in SCs, but the addition of CAXII inhibitors **1** and **3** partially restored the release of LDH induced by this drug (Figure 49D, right panel). Again, the effect of compound **4** was less pronounced, while compound **2** and **5** were ineffective, consistent with the relative inhibition constants for compounds. Neutral red staining was used to monitor the cell viability after 72 h-exposure to DOX. As expected, DOX significantly reduced cell viability in AC (Figure 49E, left panel) but not in SCs (Figure 49E, right panel). Again, CAXII inhibitors did not alter the effects of doxorubicin in AC, but restored the anti-proliferative activity of DOX in SCs: maximal efficacy was achieved by both compound **1** and **3** (Figure 49E). The chemosensitizing effects of the test compounds were not drug-specific with similar effects to DOX observed also in AC and SCs treated with other Pgp substrate chemotherapeutic drugs, including etoposide (Figure 50), topotecan (Figure 51) and irinotecan (Figure 52). As compound **1** was the most effective in restoring the anti-tumor effect of all these drugs, it was selected for further characterization in the following experiments.
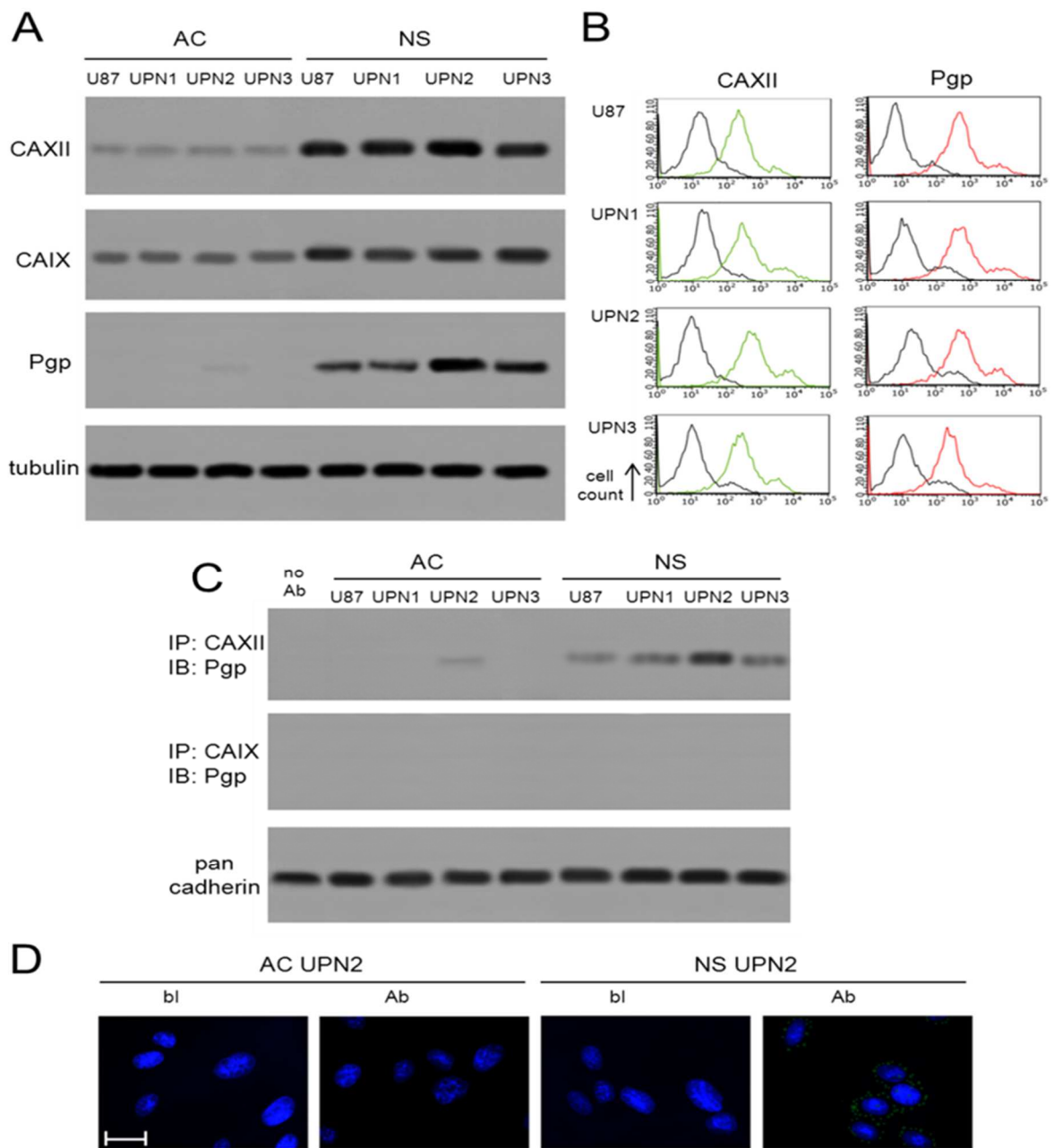
Figure 48. CAXII and Pgp are overexpressed and associated in glioblastoma-derived stem cells. U87-MG cells and three primary GB cultures derived from patients (unknown patients number, UPN1-3) were cultured as AC or SCs/NS, then subjected to the following investigations. **A.** Cells were lysed and immunoblotted for CAXII, CAIX and Pgp. β-tubulin level was used as control of equal protein loading. The figure is representative of one out of three experiments with similar results. **B.** Surface expression of CAXII and Pgp was detected by flow cytometry in duplicate. The histograms are representative of one out of three experiments with similar results. Black line: AC cells; green or red lines: NS cells. **C.** Cells were immunoprecipitated (IP) with anti-CAXII or anti-CAIX antibodies, then immunoblotted (IB) with an anti-Pgp antibody. Pancadherin level was used as control of equal protein loading. no Ab: UPN2 NS sample immunoprecipitated without antibody. The figure is representative of one out of three experiments with similar results. **D.** Proximity-ligation assay (PLA) between CAXII and Pgp in UPN2 AC and NS. Bl: cells incubated without primary antibodies; Ab: cells incubated with primary antibodies. The image is representative of one out of three experiments. Bar: 10 μm.
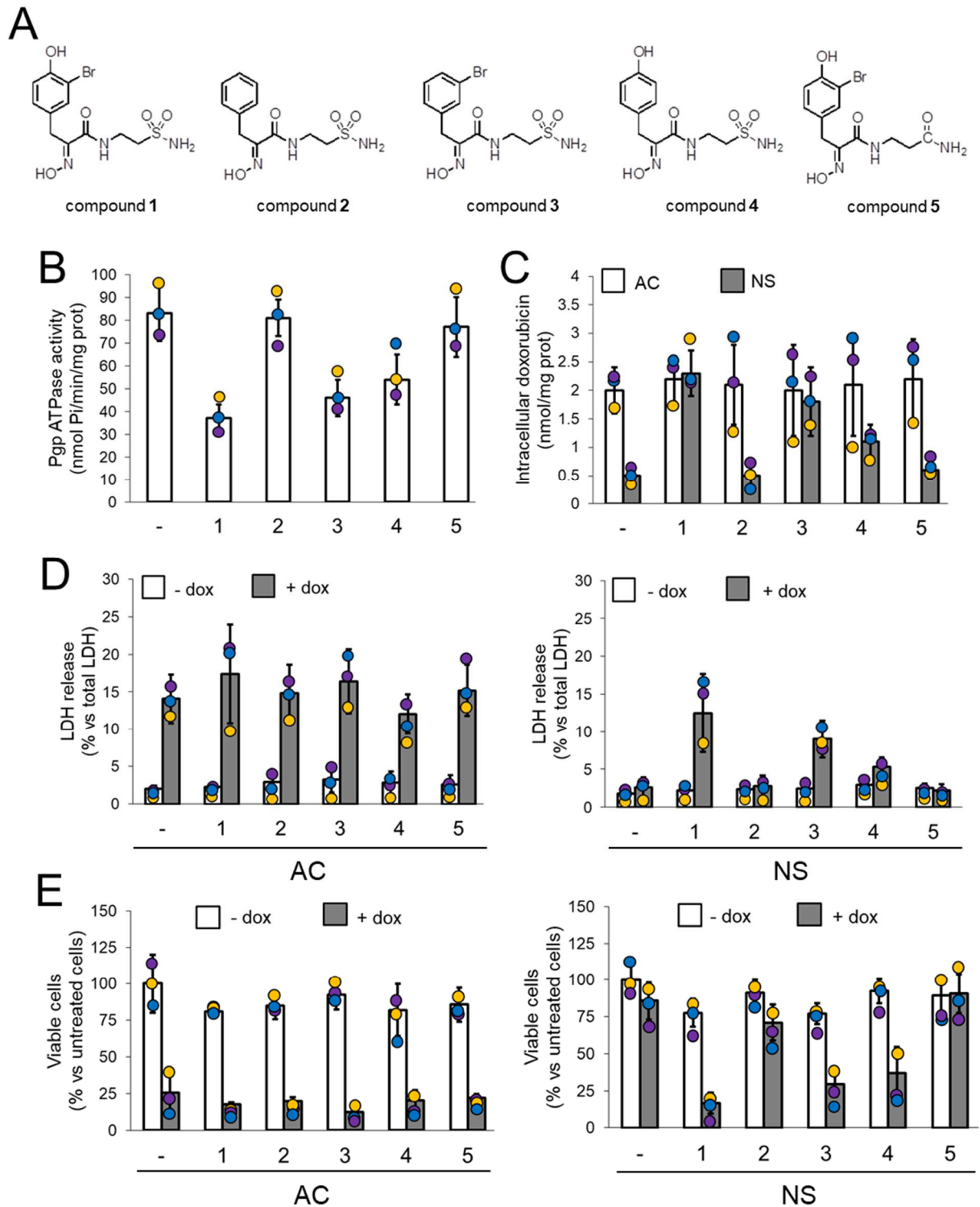
Figure 49. CAXII inhibition reduces Pgp activity and increases cytotoxicity of the Pgp substrate doxorubicin in glioblastoma-derived stem cells. A. Chemical structures of CAXII inhibitors used. **B.** SCs/NS were grown for 24 h in fresh medium (-) or in medium containing 10 nnmol/l compounds **1**, **2**, **3**, **4** and **5**. The Pgp ATPase activity was measured spectrophotometrically on Pgp-rich vesicles extracted from membrane fractions. Data are presented as means $\pm$ SD (n = 3). * p < 0.02: vs. untreated (-) cells. **C.** AC and SCs/NS were grown for 24 h in the presence of 5 μmol/l DOX, alone (-) or in the presence of 10 nmol/l compounds **1**, **2**, **3**, **4** and **5**. The intracellular content of DOX was measured fluorimetrically. Data are presented as means $\pm$ SD (n = 4). * p < 0.001: untreated (-) NS vs AC;° p < 0.002: treated NS *versus* untreated (-) NS. **D.** AC and SCs/NS were grown for 24 h in fresh medium (-) or in medium

containing 10 nmol/l compounds **1**, **2**, **3**, **4** and **5**, in the absence or presence of 5 μmol/l DOX (dox), then the release of LDH in the extracellular medium was measured spetrophotometrically. Data are presented as means $\pm$ SD (n = 4). * $p < 0.001$: vs. untreated (-) cells; ° $p < 0.001$: treated NS *versus* untreated (-) NS. **E.** AC and SCs/NS cells were grown for 72 h in fresh medium (-) or in medium containing 10 nmol/l compounds **1**, **2**, **3**, **4** and **5**, in the absence or presence of 5 μmol/l DOX (dox), then stained with neutral red dye. The absorbance of viable cells was measured spectrophotometrically. Data are presented as means $\pm$ SD (n = 4). * $p < 0.01$: vs. untreated (-) cells; ° $p < 0.005$: treated NS *versus* untreated (-) NS. Violet circle: UPN1; blu circle: UPN2; yellow circle: UPN3.
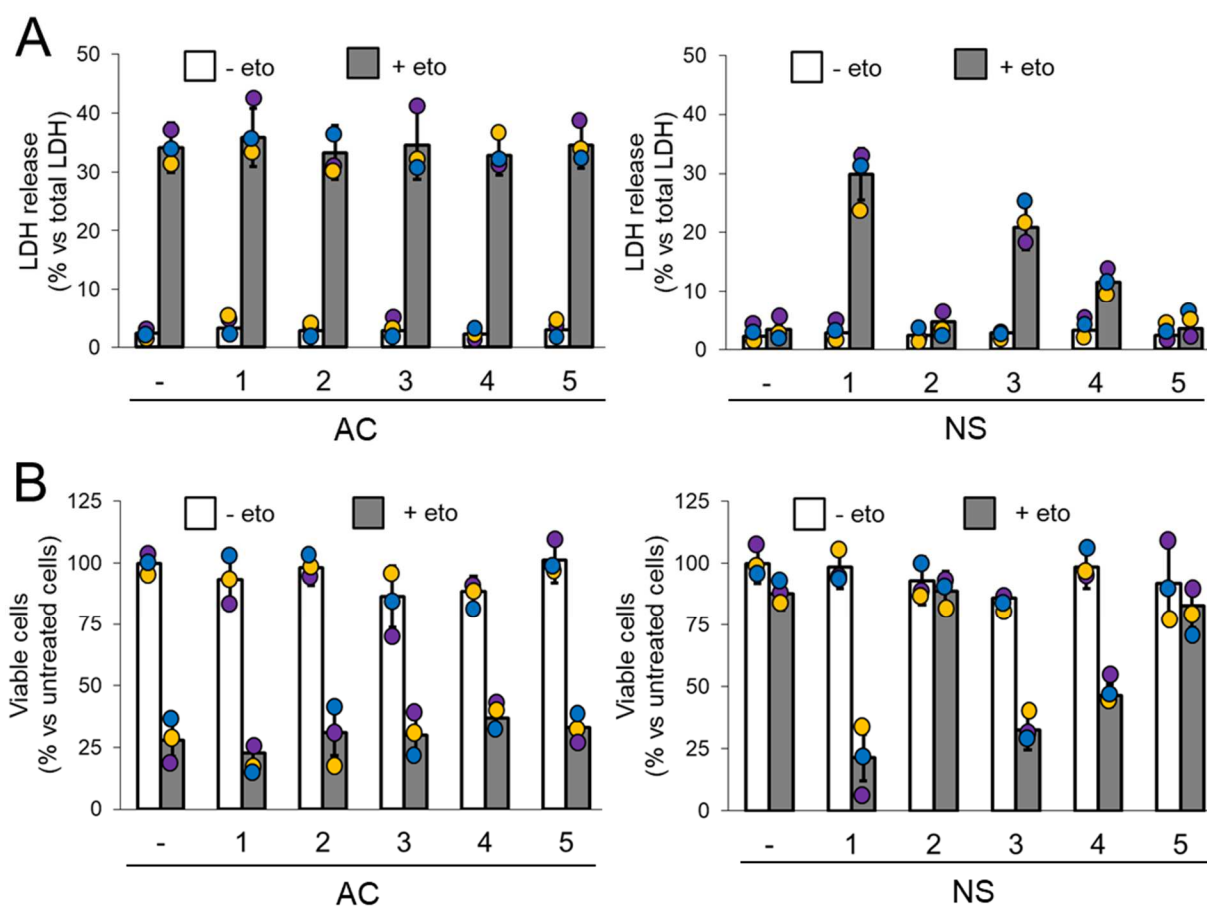
Figure 50. Effects of CAXII inhibitors on etoposide cytotoxicity in glioblastoma cells. AC and SCs/NS were grown for 24 h (panel **A**) or 72 h (panel **B**) in fresh medium (-) or in medium containing 10 nmol/l of compounds **1**, **2**, **3**, **4** and **5**, in the absence or presence of 10 μmol/l etoposide (eto). **A.** The release of LDH in the extracellular medium was measured spectrophotometrically. Data are presented as means $\pm$ SD (n = 4). * $p < 0.001$: vs. untreated (-) cells° $p < 0.001$ vs etoposide-treated cells. **B.** The absorbance of viable cells was measured spectrophotometrically. Data are presented as means $\pm$ SD (n = 4). * $p < 0.001$: vs. untreated (-) cells; ° $p < 0.001$ vs etoposide-treated cells. Violet circle: UPN1; blu circle: UPN2; yellow circle: UPN3.
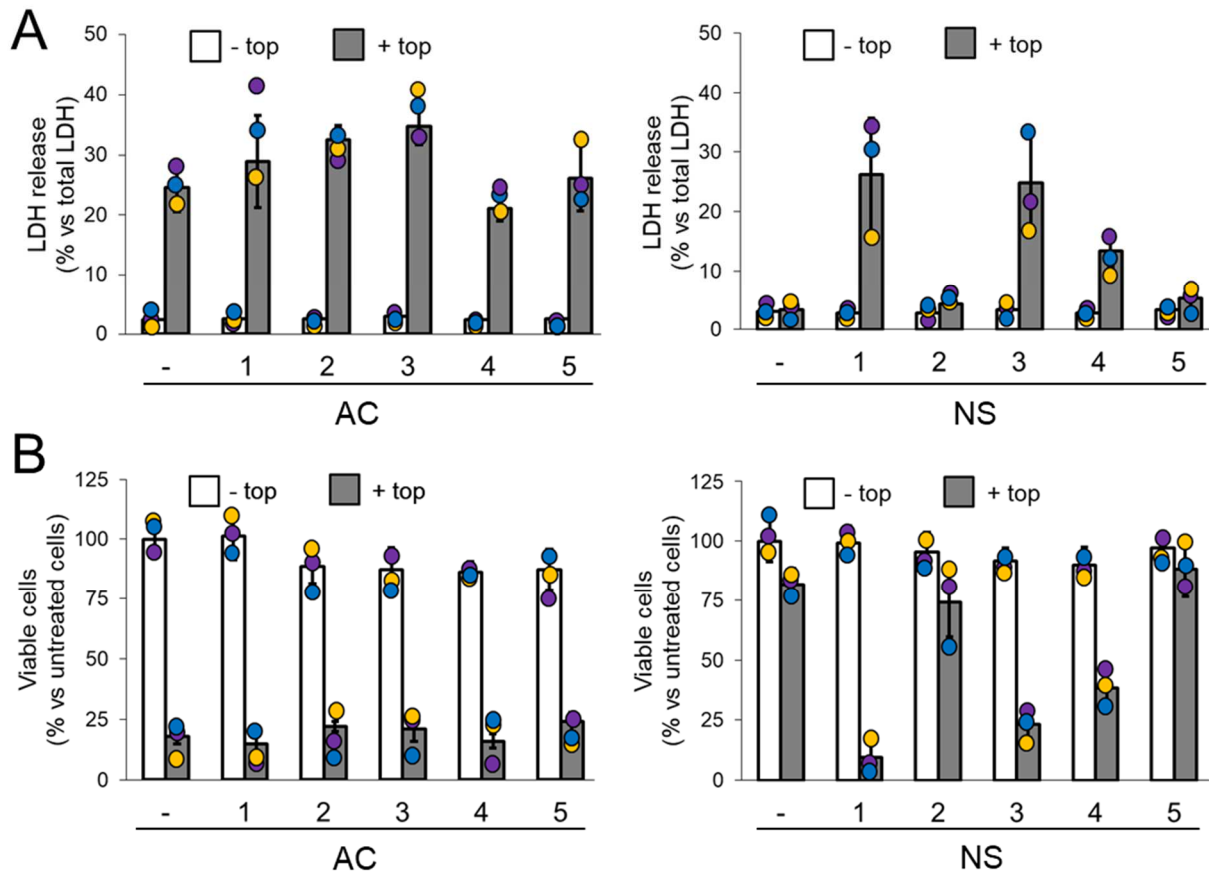
Figure 51. Effects of CAXII inhibitors on topotecan cytotoxicity in glioblastoma cells AC and SCs/NS were grown for 24 h (panel A) or 72 h (panel B) in fresh medium (-) or in medium containing 10 nmol/l of compounds 1, 2, 3, 4 and 5, in the absence or presence of 10 μmol/l topotecan (top). A. The release of LDH in the extracellular medium was measured spectrophotometrically. Data are presented as means $\pm$ SD (n = 4). * p < 0.001: vs. untreated (-) cells; ° p < 0.001 vs topotecan-treated cells. B. The absorbance of viable cells was measured spectrophotometrically. Data are presented as means $\pm$ SD (n = 4). * p < 0.001: vs. untreated cells (-); ° p < 0.001 vs topotecan-treated cells. Violet circle: UPN1; blu circle: UPN2; yellow circle: UPN3.
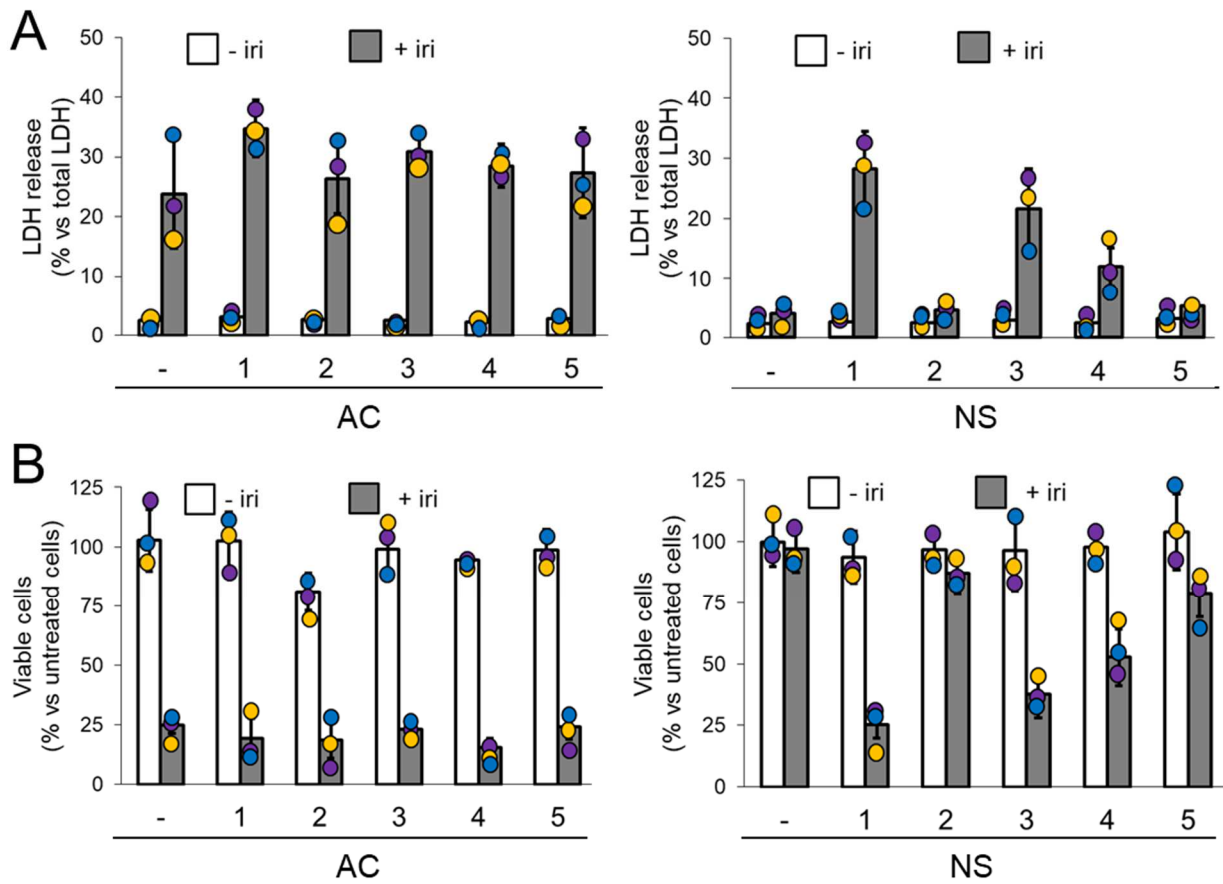
Figure 52. Effects of CAXII inhibitors on topotecan cytotoxicity in glioblastoma cells. UPN2 AC and SCs/NS were grown for 24 h (panel **A**) or 72 h (panel **B**) in fresh medium (-) or in medium containing 10 nmol/l of compounds **1**, **2**, **3**, **4** and **5**, in the absence or presence of 10 μM irinotecan (iri). **A.** The release of LDH in the extracellular medium was measured spectrophotometrically. Data are presented as means $\pm$ SD (n = 4). * p < 0.001: vs. untreated (-) cells; ° p < 0.001 vs irinotecan-treated cells. **B.** The absorbance of viable cells was measured spectrophotometrically. Data are presented as means $\pm$ SD (n = 4). * p < 0.001: vs. untreated (-) cells; ° p < 0.01 vs irinotecan-treated cells. Violet circle: UPN1; blu circle: UPN2; yellow circle: UPN3.

4.3.b.3 CAXII inhibition enhances TMZ cytotoxicity in glioblastoma-derived stem cells by reducing Pgp activity

It has been shown that TMZ downregulates Pgp expression [Munoz, 2015] and activity [Zhang, 2016] in GB cells. I observed a downregulation of Pgp expression in TMZ-treated SCs (Figure 53A-B). Compound **1** did not affect Pgp expression (Figure 53A), but it further reduced Pgp ATPase activity in SCs treated with TMZ (Figure 53B) over TMZ treatment alone. It has been previously reported that TMZ is a substrate of Pgp [Munoz, 2015]. Here TMZ accumulated less in Pgp-expressing SCs than in AC (CAXII^{-ve}) (Figure 53C). Consistently, TMZ did not increase the release of LDH (Figure 53D), did not activate Caspase-3 (Figure 53E) and did not reduce viability in CAXII expressing SCs (Figure 53F). The co-incubation of TMZ with compound **1** increased TMZ accumulation (Figure 53C) and restored its cytotoxic effects in SCs, such that it was as effective as TMZ in AC (Figure 53D-F). To prove that the chemosensitizing effects were mediated by a reduced Pgp activity, I produced SCs clones knocked out for Pgp. Pgp KO did not change CAXII levels (Figure 54), but the SCs knocked out for Pgp had the same response to TMZ than SCs treated with compound **1** (Figure 53C-F). These results suggest that the chemosensitizing effect of compound **1** was mediated by the indirect inhibition of Pgp exerted by CAXII reduced activity.

4.3.b.4 CAXII knocking out restores sensitivity to TMZ in glioblastoma-derived stem cells

CAXII-KO SCs (Figure 55A) had lower Pgp activity than wild-type SCs (Figure 55B), despite Pgp level being the same in both (Figure 55A). TMZ further reduced Pgp activity in CAXII-KO SCs (Figure 55B), again despite Pgp level being the same in CAXII-KO and in wild-type SCs (Figure 55A). Consistently with the reduced Pgp activity in CAXII-KO SCs treated with TMZ, the drug was significantly more retained in these cells (Figure 55C), increased acute cell cytoxicity (Figure 55D) and apoptosis (Figure 55E), and reduced cell viability (Figure 55F), similarly to TMZ-treated AC. These findings suggest that CAXII activity mediated the Pgp-induced resistance to TMZ in SCs and that CAXII inhibition may overcome such resistance.

4.3.b.5 CAXII inhibition enhances the cytotoxic effect of TMZ and Pgp substrates in glioblastoma-derived stem cells subjected to combination treatments

Next, I analyzed the effects of the co-administration of compound **1**, TMZ and chemotherapeutic drugs that are substrates of Pgp, including DOX, etoposide, topotecan and irinotecan. The four drugs alone did not exert any cytotoxic effects in SCs (Figure 56A-C). When either compound **1** or TMZ, was combined with etoposide, topotecan or irinotecan, the release of LDH (Figure 56A), the activation of Caspase-3 (Figure 56B) and the reduction in cell viability (Figure 56C) exerted by the chemotherapeutic agents was restored in the SCs. The triple combination of compound **1**, TMZ and each of these drugs further enhanced the cytotoxic effects of the latter chemotherapeutic drugs than either **1** or TMZ dual combination with the drugs (Figure 56A-C).
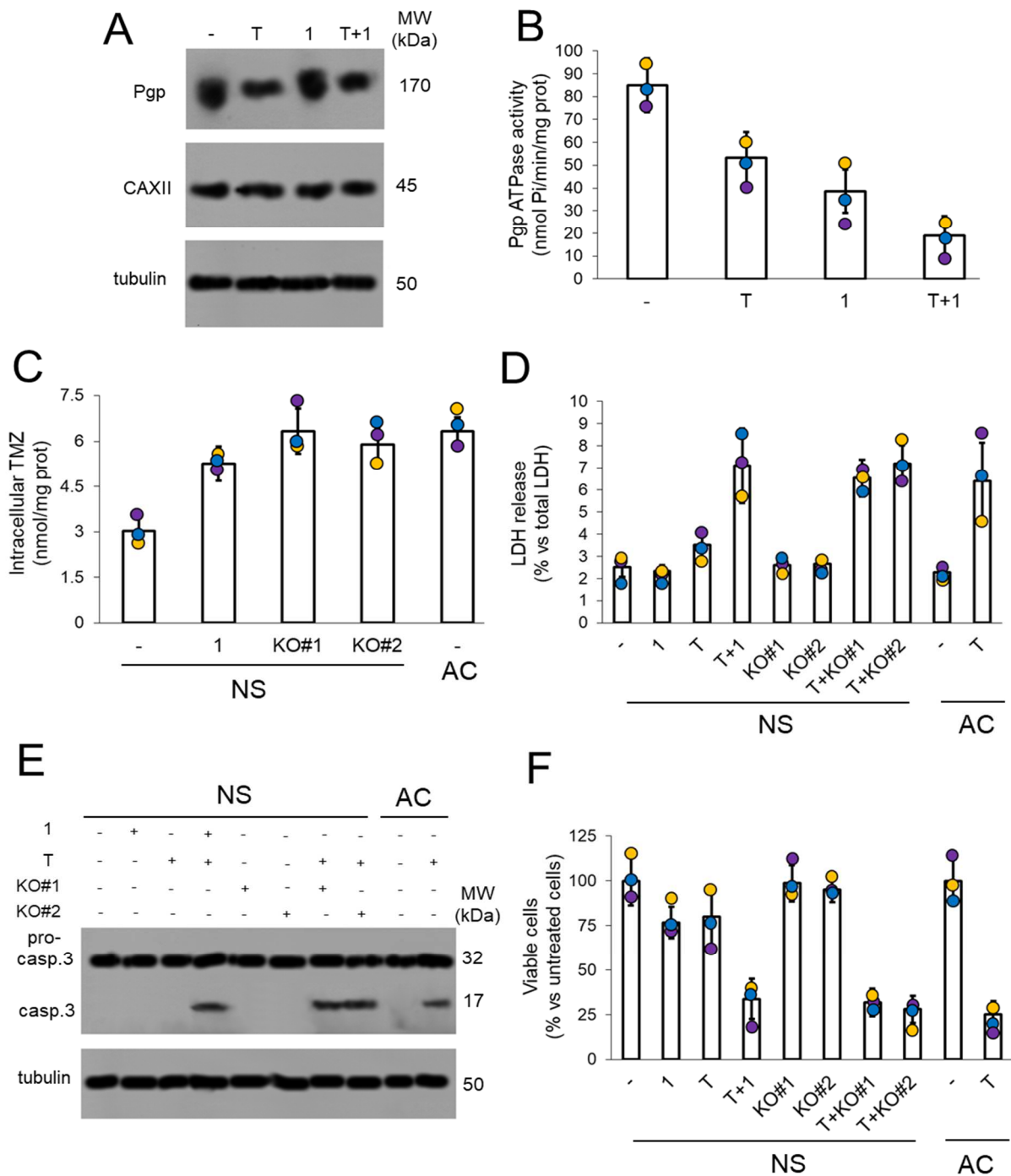
Figure 53. CAXII pharmacological inhibition restores temozolomide cytotoxicity in glioblastoma-derived stem cells. SCs/NS were grown for 48 h (panels **A**-**E**) or 72 h (panel **F**) in fresh medium (-) or in medium containing 50 µmol/l temozolomide (T) or 10 nmol/l compound **1**, alone or in association. **A.** Cells were lysed and immunoblotted for Pgp and CAXII. β-tubulin level was used as control of equal protein loading. The figure is representative of one out of three experiments with similar results, obtained on UPN2. Similar results were obtained in UPN1 and UPN3 (not shown). **B.** The Pgp ATPase activity was measured spectrophotometrically on Pgp-rich vesicles extracted from membrane fractions. Data are presented as means ± SD (n = 3). * p < 0.01: vs. untreated (-) cells; ° p < 0.005: vs. temozolomide-treated cells. **C.** The intracellular content of temozolomide (TMZ) was measured radiometrically. NS knocked out for Pgp (KO#1, KO#2) and AC were included as control of cells with undetectable or very low expression of Pgp. Data are presented as means ± SD (n = 4). * p < 0.001: vs. untreated (-) cells; ° p < 0.001: vs. temozolomide-

treated cells. **D.** The release of LDH in the extracellular medium was measured spectrophotometrically. Data are presented as means $\pm$ SD (n = 4). * p < 0.001: vs. untreated (-) NS or AC. **E.** Cells were lysed and immunoblotted for procaspase and cleaved Caspase-3. β-tubulin level was used as control of equal protein loading. The figure is representative of one out of three experiments with similar results, obtained on UPN2. Similar results were obtained in UPN1 and UPN3 (not shown). **F.** The absorbance of viable cells was measured spectrophotometrically. Data are presented as means $\pm$ SD (n = 4). * p < 0.01: vs. untreated (-) NS or AC; ° p < 0.001: vs. temozolomide-treated cells. Violet circle: UPN1; blu circle: UPN2; yellow circle: UPN3.
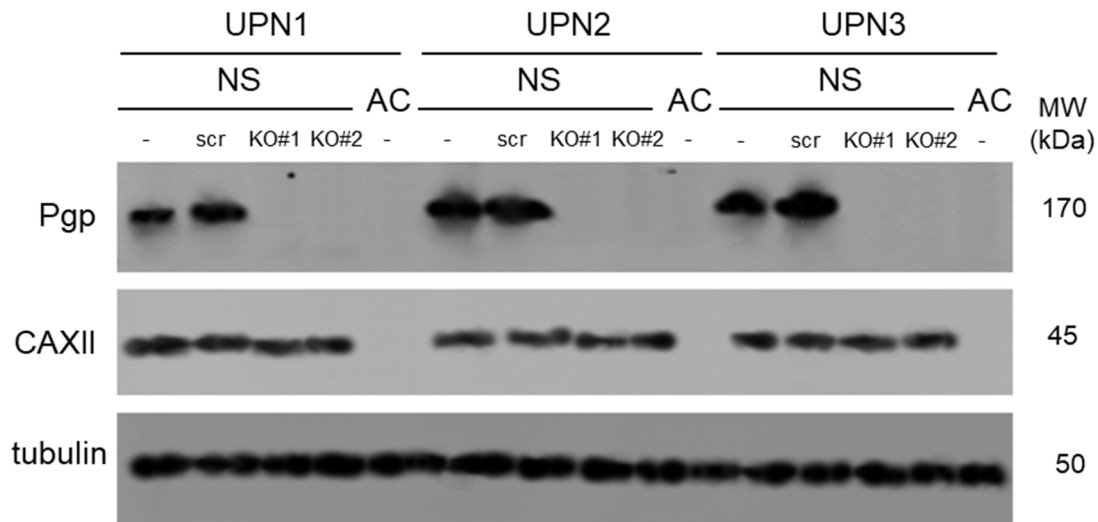
Figure 54. Pgp knocking out in glioblastoma-derived SCs. UPN1, UPN2 and UPN3 SCs/NS were grown in fresh medium (-), transduced with a non-targeting vector (scrambled vector; scr) or with two CRISPR pCas *ABCC1/Pgp*-targeting vectors (KO #1 and #2). AC were included as control of Pgp-lowly expressing cells. Cells were lysed and immunoblotted with the indicated antibodies. The figure is representative of one out of three experiments.
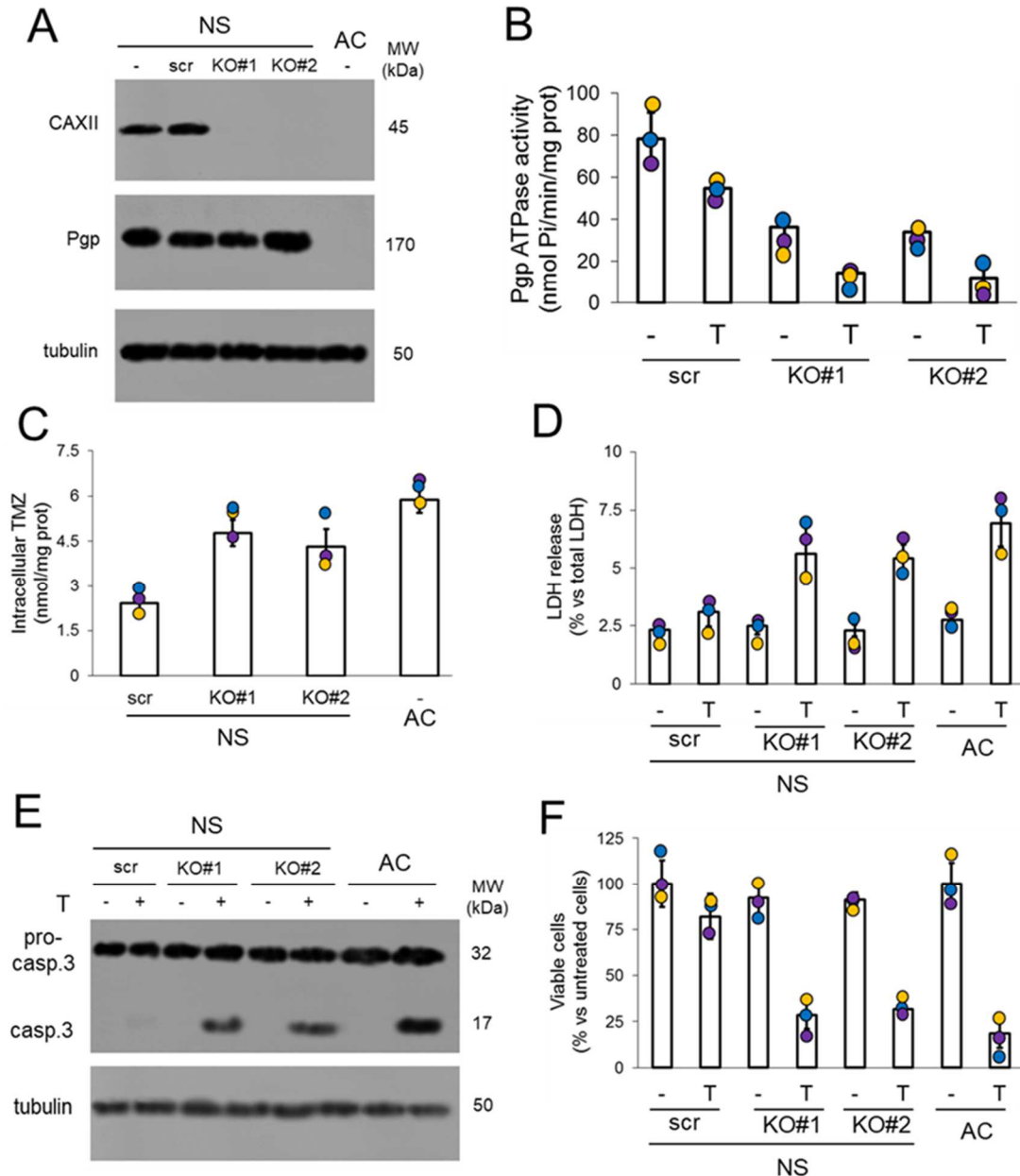
Figure 55. CAXII knock out rescue glioblastoma-derived stem cells sensitivity to temozolomide. SCs/NS were growth in fresh medium (-), transduced with a not-targeting vector (scrambled vector; scr) or with a CRISPR pCas *CAXII*-targeting vector (KOCAXII). When indicated, 50 μmol/l temozolomide (T) was added for 48 h (**panels B**-**E**) or 72 h (panel **F**). AC were included as control of CAXII-lowly expressing cells. **A.** Cells were lysed and immunoblotted for CAXII, CAIX and Pgp. β-tubulin level was used as control of equal protein loading. The figure is representative of one out of three experiments with similar results, obtained on UPN2. Similar results were obstained in UPN1 and UPN3 (not shown). **B.** The Pgp ATPase activity was measured spectrophotometrically on Pgp-rich vesicles extracted from membrane fractions. Data are presented as means $\pm$ SD (n = 3). * p < 0.02: vs. untreated (-) cells;° p < 0.001: *versus* temozolomide-treated cells. **C.** The intracellular content of TMZ was measured radiometrically. Data are presented as means $\pm$ SD (n = 4). * p < 0.001: vs. untreated (-) cells. **D.** The release of LDH in the extracellular medium was measured spectrophotometrically. Data are presented as means $\pm$ SD (n = 4). * p < 0.001: vs. untreated (-) NS or AC; ° p < 0.001: KO CAXII cells *versus* scr cells. **E.** Cells were lysed and immunoblotted for procaspase and cleaved Caspase-3. β-tubulin level was used as control of equal protein loading. The figure is representative of one out of three experiments with similar results, obtained on UPN2. Similar results were obstained in UPN1 and UPN3 (not shown). **F.** The absorbance of viable cells was measured spectrophotometrically. Data are presented as means $\pm$ SD (n = 4). * p < 0.001: vs. untreated (-) NS or AC; ° p < 0.002: KO CAXII cells *versus* scr cells. Violet circle: UPN1; blu circle: UPN2; yellow circle: UPN3.

91
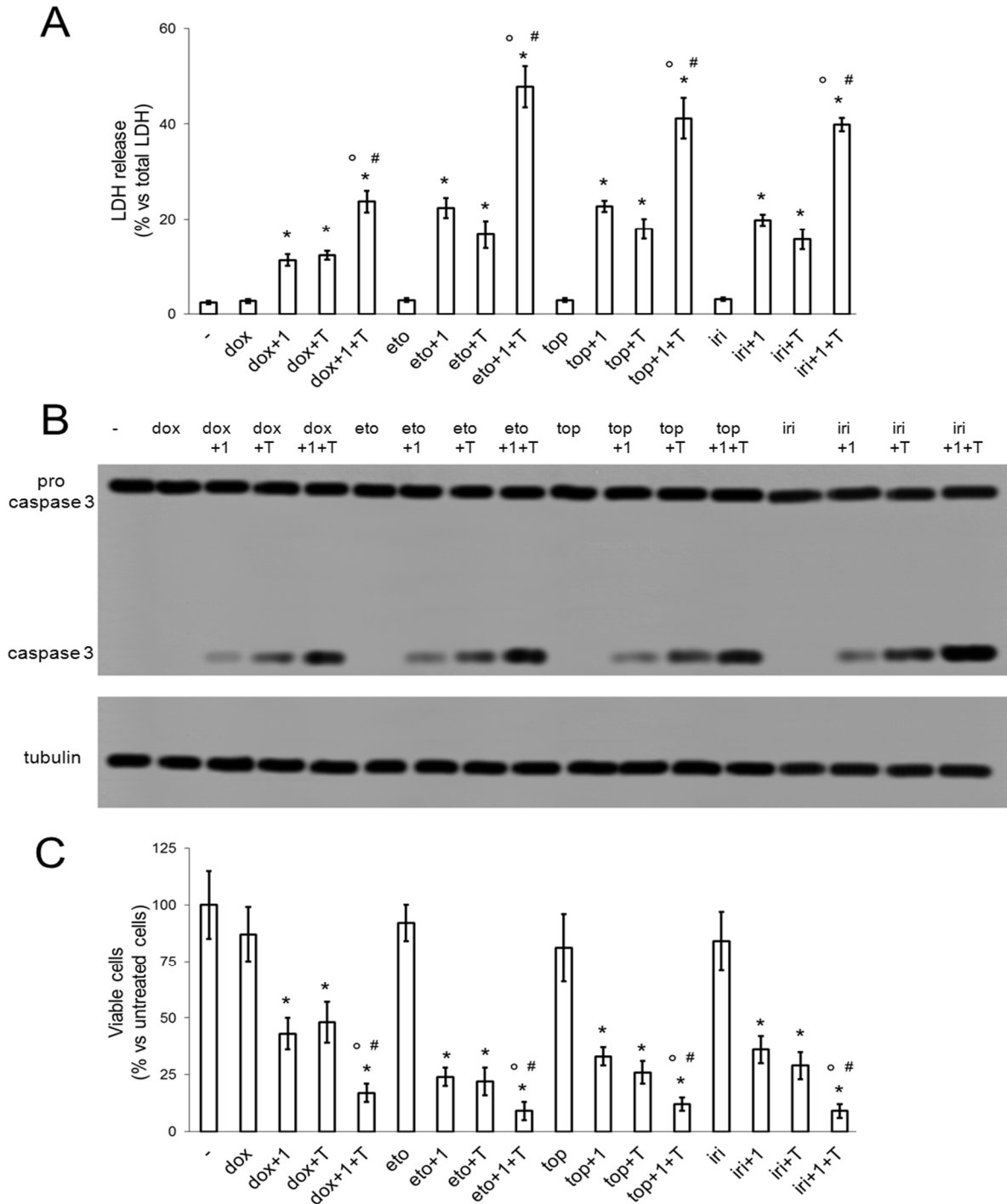
Figure 56. Effects of the combination of CAXII inhibitor, temozolomide and Pgp substrates in glioblastoma-derived stem cells. UPN2 SCs/NS were grown for 48 h (panels **A**-**B**) or 72 h (panel **C**) in fresh medium (-) or in medium containing 10 nmol/l compound **1**, 50 μmol/l temozolomide (T), 5 μmol/l DOX (dox), 10 μmol/l etoposide (eto), 10 μmol/l topotecan (top), 10 μmol/l irinotecan (iri), in different combinations. **A.** The release of LDH in the extracellular medium was measured spectrophotometrically. Data are presented as means ± SD (n = 4). * $p < 0.001$: vs. untreated (-) cells; ° $p < 0.001$: vs. dox/eto/top/iri-treated cells; # $p < 0.001$: vs. cells treated with compound **1** or temozolomide alone. **B.** Cells were lysed and immunoblotted for procaspase and cleaved Caspase-3. β-tubulin level was used as control of equal protein loading. The figure is representative of one out of three experiments with similar results. **C.** The absorbance of viable cells was measured spectrophotometrically. Data are presented as means ± SD (n = 4). * $p < 0.001$: vs. untreated (-) cells; ° $p < 0.002$: vs. dox/eto/top/iri-treated cells; # $p < 0.02$: vs. cells treated with compound **1** or temozolomide alone.

4.3.b.6 CAXII inhibition restores the antitumor efficacy of TMZ in tumors derived from resistant glioblastoma stem cells

Finally, I tested the *in vivo* anti-tumor efficacy of compound **1** in combination with TMZ against GB derived from UPN2 SCs. As different schedules of TMZ administration *per os* have shown different efficacy against GB [Plowman, 1994; Houghton, 2000], I preliminarily compared different protocols. As shown in Figure 57A, oral administration of 50 mg/kg for 2 cycles of 5 consecutive days, separated by a 5-day period of drug suspension, gave the maximal efficacy in reducing tumor growth derived from UPN2 AC implanted subcutaneously. By contrast, this dosage had a significantly lower anti-tumor activity against UPN2 SCs/NS-derived tumors (Figure 57B-C).

Compound **1** was stable in Balb/c mice plasma at 37 °C, with measured concentrations of 1 across the 4 h incubation period being within ±10% of the measured concentrations at time = 5 min. At time = 4 h 94% of compound **1** remained. Additionally, the *in vitro* metabolic stability of compound **1** in mouse liver microsomes, either in the presence or absence of NADPH, revealed good stability, with no measurable degradation of compound **1** in the presence or absence of NADPH. The hepatic blood clearance and E_H were calculated (Table 1): based on E_H compound **1** was classified to have low *in vivo* clearance and a plasma half-life > 240 min.

In a preliminary dose-response experimental set, compound **1** was administered at two dosages, i.e. 38 ng/kg (10 nmol/l final concentration) and 3800 ng/kg (1 µmol/l final concentration) in mice bearing UPN2 SCs implanted subcutaneously. The lower concentration was chosen according to the CAXII K_i; the latter concentration was chosen to maximize the amount of compound **1** that reached the tumor, balancing the hematic and lymphatic clearance. When compound **1** was administered alone it did not reduce SC-derived tumor growth, but when co-administered with TMZ it significantly enhanced the anti-tumor efficacy of TMZ against SC-derived tumors: both dosages were effective, although – as expected – the higher dose maximally reduced tumor growth (Figure 57B-C).

According to the hematochemical parameters of the animals at the time of sacrifice, compound **1** was not toxic for hematopoiesis, liver, kidney and muscles (Table 2). TMZ slightly reduced the number of platelets at the end of the observation period, but the co-administration of compound **1** did not elicit any further decrease of this parameter (Table 2). Since GB AC did not grow orthotopically [Riganti, 2013], I investigated the effects of compound **1** and TMZ in orthotopically implanted patient-derived SC-tumors. When used alone, neither compound **1** nor TMZ reduced tumor growth, as observed by *in vivo* bioluminescence imaging (Figure 58A-B). Tumor growth was significantly reduced only by the combination of TMZ+compound **1** (Figure 58A-B). The decrease in tumor growth was paralleled by a significantly increased in overall survival in all patient-derived xenografts (Figure 58C). Only UPN3 showed a partial response to TMZ, in terms of reduced tumor growth (Figure 58B) and increased overall survival (Figure 58C): this could be due to the MGMT fully methylated status and to the genomic profile of GB cells (Table 2) that are suggestive of increased response to TMZ. Also in this case, however, the addition of compound **1** significantly improved TMZ effects (Figure 58B-C). Furthermore, in SCs-derived tumors - that showed detetctable levels of CAXII - the combination treatment also reduced Pgp expression and cell proliferation, and increased intratumor apoptosis, in contrast to untreated animals or animals treated with compound **1** or TMZ alone (Figure 58D-E).
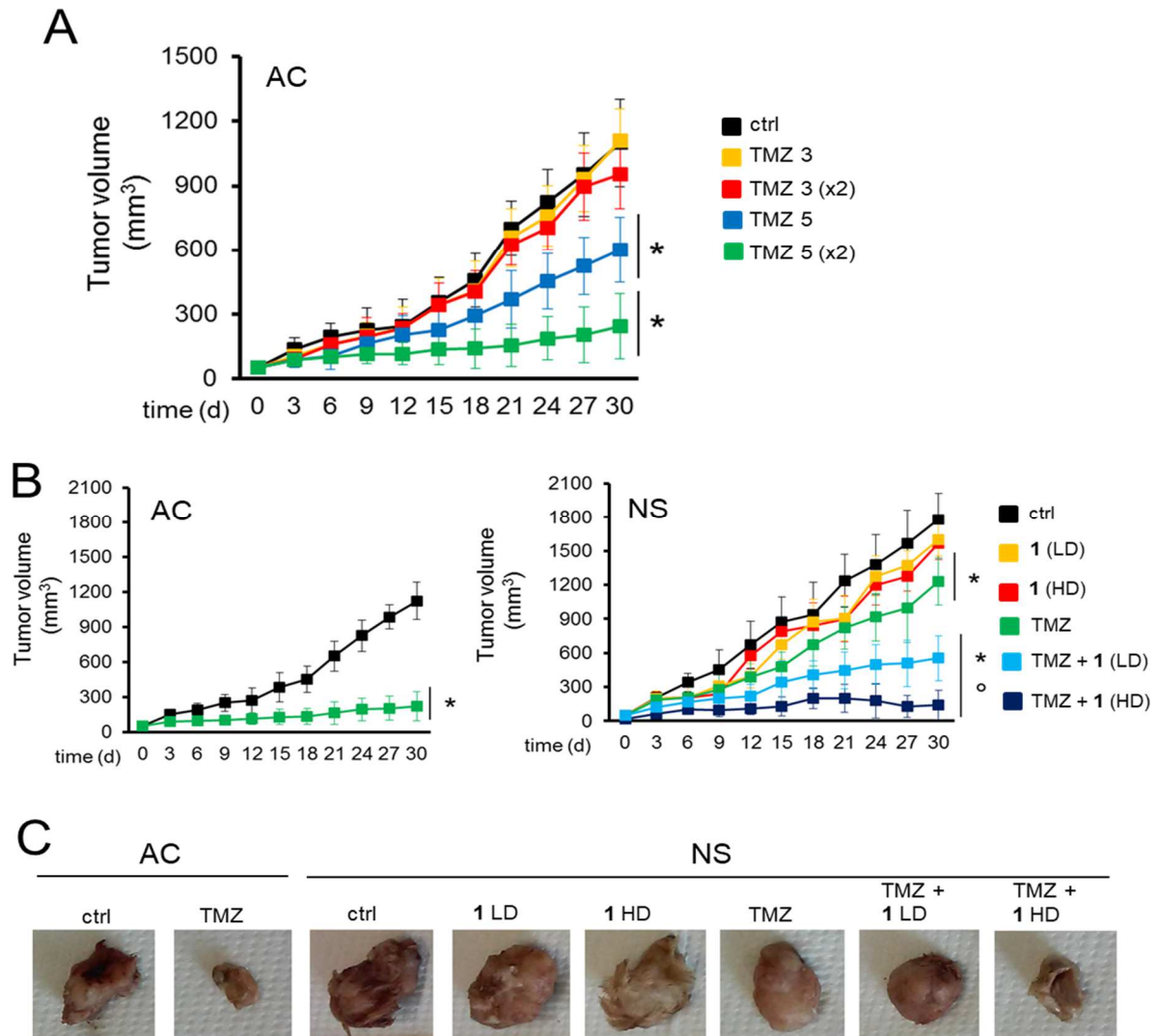
Figure 57. *In vivo* **antitumor activity of different combination of temozolomide and compound 1.** Six week-old female BALB/c *nu/nu* mice were inoculated s.c. with 1×10^6 AC from UPN2. When the tumor reached the volume of 50 mm³, the mice were randomized into the following groups (10 animals/group) and treated as it follows: 1) control (ctrl) group treated with 0.2 ml saline solution i.v., 2 cycles of 5 consecutive days (days: 1-5; 11-15 after randomization); 2) temozolomide (TMZ 3), group treated with 50 mg/kg TMZ p.o., for 3 consecutive days (days: 1-3 after randomization); 3) temozolomide group [TMZ 3 (X2)], treated with 50 mg/kg TMZ p.o., 2 cycles of 3 consecutive days (days: 1-3; 7-9 after randomization); 4) temozolomide group (TMZ 5), treated with 50 mg/kg TMZ p.o., for 5 consecutive days (days: 1-5 after randomization); 5) temozolomide group [TMZ 5 (x2)], treated with 50 mg/kg TMZ p.o., 2 cycles of 5 consecutive days (days: 1-5; 11-15 after randomization). Tumor growth was monitored by caliper measure. Data are presented as means ± SD. * $p < 0.005$: TMZ 5/TMZ 5 (x2) groups vs. ctrl group (days 21-30). **B.** Six week-old female BALB/c *nu/nu* mice were inoculated s.c. with 1×10^6 UPN2 AC or SCs/NS. When the tumor reached the volume of 50 mm³, the mice were randomized into the following groups (10 animals/group) and treated with 2 cycles as it follows: 1) control (ctrl) group, treated with 0.2 ml saline solution i.v. (days: 1-5; 11-15 after randomization); 2) **1** low dose (LD) group, treated with 38 ng/kg compound **1** (in 0.2 ml saline solution; final concentration: 10 nM) i.v.; 3) **1** high dose (HD) group, treated with 3800 ng/kg compound **1** (in 0.2 ml saline solution; final concentration: 1 µM) i.v.; 4) temozolomide (TMZ) group, treated with 50 mg/kg TMZ p.o.; 5) TMZ + **1** LD group, treated with 50 mg/kg TMZ p.o. and 38 ng/kg compound **1** i.v.; 6) TMZ + **1** HD group, treated with 50 mg/kg TMZ p.o. and 3800 ng/kg compound **1** i.v. Tumor growth was monitored by caliper measure. Data are presented as means ± SD. * $p < 0.05$: TMZ/TMZ+**1** (LD)/TMZ+**1** (HD) groups vs. ctrl group (day 30); ° $p < 0.001$: TMZ+**1** (LD)/TMZ+**1** (HD) groups vs. TMZ group (day 30). **C.** Photographs of representative tumors from each treatment group after mice sacrified.

Table 1. *In vitro* **mouse plasma stability and mouse microsome stability data for compound 1.** CL_{int}: *in vitro* clearance; E_H: hepatic extraction ratio.

$CL_{int, in\ vitro}$ (µL/min/mg protein)	Predicted $CL_{int, in\ vivo}$ (mL/min/kg)	Predicted CL_{blood} (mL/min/kg)	Predicted E_H	Clearance classification	Plasma stability half-life (min)
10	26	21	0.18	low	>240

Table 2. **Hematochemical parameters of animals.** Animals (n = 10/group) were treated as reported under Materials and methods and in Figure 57. Blood was collected immediately after euthanasia and analyzed for red blood cells (RBC), hemoglobin (Hb), white blood cells (WBC), platelets (PLT), lactate dehydrogenase (LDH), aspartate aminotransferase (AST), alanine aminotransferase (ALT), alkaline phosphatase (AP), creatinine, creatine phosphokinase (CPK). ctrl: mice treated with saline solution; **1** LD: mice treated with 38 ng/kg compound **1** i.v., 2 cycles of 5 consecutive days (days: 1-5; 11-15); 1HD: mice treated with 3800 ng/kg compound **1** i.v., 2 cycles of 5 consecutive days (days: 1-5; 11-15). TMZ: mice treated with 50 mg/kg temozolomide p.o., 2 cycles of 5 consecutive days (days: 1-5; 11-15). * $p < 0.05$: vs. ctrl group.

	ctrl	**1** LD	**1** HD	TMZ	TMZ+ **1** LD	TMZ+ **1** LD
RBC (x 10^6/µl)	12.34 ± 2.56	13.15 ± 0.99	15.24 ± 3.28	10.11 ± 1.26	11.22 ± 0.83	10.29 ± 1.08
Hb (g/dl)	14.23 ± 2.21	15.24 ± 1.08	13.53 ± 3.21	12.54 ± 2.21	13.21 ± 0.97	12.96 ± 2.04
WBC (x 10^3/µl)	15.98 ± 3.25	16.58 ± 2.91	14.58 ± 4.26	14.05 ± 2.42	15.09 ± 1.47	14.12 ± 3.49
PLT (x 10^3/µl)	1125 ± 241	938 ± 152	1138 ± 215	624 ± 125 *	701 ± 115 *	658 ± 173 *
LDH (U/l)	6123 ± 985	6521 ± 943	5897 ± 1523	6432 ± 552	6458 ± 1182	6284 ± 1025
AST (U/l)	263 ± 52	232 ± 51	268 ± 51	254 ± 58	297 ± 47	256 ± 38
ALT (U/l)	37 ± 11	44 ± 14	39 ± 11	41 ± 8	42 ± 8	49 ± 11
AP (U/l)	97 ± 23	86 ± 15	105 ± 18	91 ± 23	94 ± 14	102 ± 21
Creatinine (mg/l)	0.034 ± 0.008	0.037 ± 0.005	0.028 ± 0.009	0.034 ± 0.009	0.038 ± 0.012	0.031 ± 0.005
CPK (U/l)	302 ± 99	312 ± 115	278 ± 98	325 ± 102	324 ± 58	256 ± 45
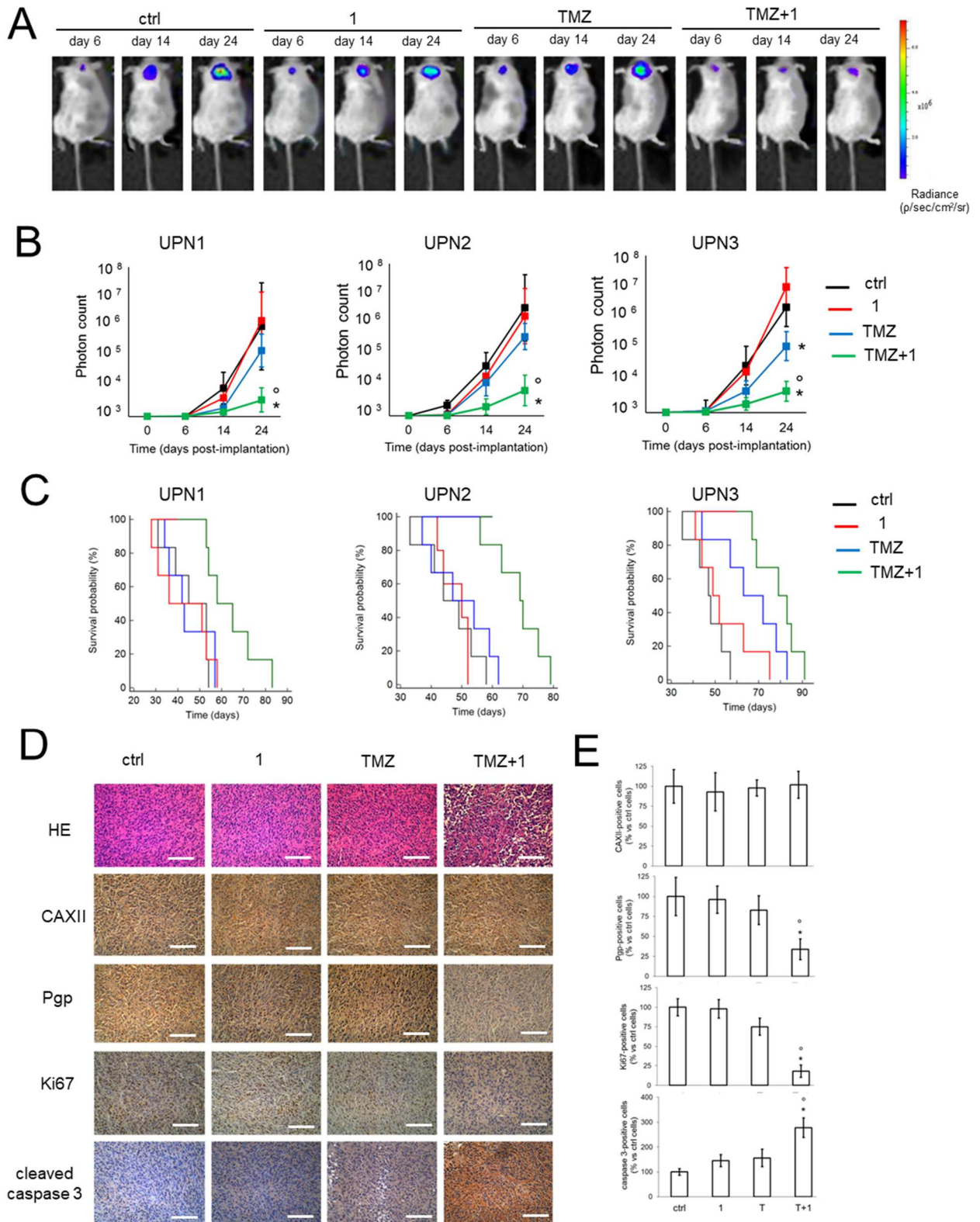
Figure 58. Compound 1 improves temozolomide efficacy against orthotopically implanted glioblastoma neurosphere-derived tumors. A. Representative *in vivo* bioluminescence imaging of orthotopially implanted UPN2 SCs/NS, in animals treated with vehicle (ctrl), compound **1** and temozolomide (TMZ), as indicated in the Materials and methods section (6 animals/group). **B.** Quantification of UPN1-3 NS-derived bioluminescence, taken as index of tumor growth. Data are presented as means±SD (6 animals/group). At day 24, UPN1-3: * p < 0.001: TMZ+**1** group vs. vs. all the other groups of treatment; ° p < 0.01 TMZ+**1** group vs TMZ-group. UPN3: *p< 0.01: TMZ-group vs. ctrl and **1-**group (two-way ANOVA). **C.** Overall survival probability was calculated using the Kaplan-Meier method.

UPN1: p < 0.02: TMZ+**1-**group vs. all the other groups of treatment. UPN2: p < 0.002: TMZ+**1-**group vs. all the other groups of treatment. UPN3: p < 0.001: TMZ+**1-**group vs. ctrl and **1-**group; p < 0.05: TMZ+**1** group vs. TMZ-group; p< 0.01: TMZ-group vs. ctrl and **1-**group (log rank test). **D.** Representative intratumor staining with hematoxylin and eosin (HE) or the indicated antibodies. The photographs are representative of sections from 5 tumors/group of treatment. Bar=10 µm (10× ocular lens, 20× objective). **E.** Quantification of immunohistochemical images, performed on sections with 111-94 nuclei/field. The percentage of proliferating cells was determined by the ratio Ki67-positive nuclei/total number (hematoxylin-positive) of nuclei using ImageJ software (http://imagej.nih.gov/ij/). The ctrl group percentage was considered 100%. The percentage of CAXII, Pgp and Caspase-3-positive cells was determined by Photoshop program. Data are presented as means$\pm$SD. *p< 0.005: vs. ctrl group; °p<0.02 vs TMZ-group (for Pgp-positive cells; *p<0.001: vs. ctrl group; °p<0.001 vs TMZ group (for Ki67-positive cells); *p< 0.001: vs. ctrl group; °p<0.01 vs TMZ group (for cleaved Caspase-3-positive cells).

4.3.c Aim 3c: Targeting BBB-GB interface

4.3.c.1 Functionalization and purification of ddMTX-SLNs

ddMTX-loaded SLNs were prepared with coacervation method [Moura, 2011] by the Department of Drug Science and Technology, University of Turin. Considering the good drug entrapment efficiency (EE) and the promising drug uptake and cytotoxicity in GB/BBB model [Annovazzi, 2017], SLNs were functionalized with a chimeric peptide derived from ApoE (Figure 9 Material and Methods) to have a good biodistribution and clearance by reticuloendothelial system (RES) organs *in vivo* model. This peptide cointains the ApoE-binding site for VLDL receptor and an amphipatic moiety able to anchor the peptide to the lipid surfaces, and allows a better accumulation to the brain, as already demonstrated when conjugated with liposomes [Nikanjam, 2007]. In the formulation development, particular care was taken to evaluate and to select a suitable purification technique for ddMTX-loaded SLNs ApoE, based on molecular size exclusion, in order to maintain the EE of ddMTX and the binding of ApoE to SLNs. Different molecular size cutoffs were used in gel centrifugation (6,000 Da) and gel filtration (100,000 Da) techniques.

Once purified, SLNs functionalized with ApoE were resolved by SDS-PAGE followed by Blue Coomassie staining (Figure 59) to detect the best method of purification. The amount of ApoE bound to SLNs was identified at the top of gel, since it did not run in the gel, because of the high size of nanoparticles compared with the free protein. Human recombinant ApoE had both ApoE monomer and dimers, while SLN formulations showed only monomers. All methods used for purification removed a part of the ddMTX amount used to formulate drug loaded SLNs, but dialysis led to a greater ApoE leakage from nanoparticles compared with gel centrifugation and gel filtration (Figure59; Table 3). Basing on these data, gel filtration was chosen as the purification method for ddMTX-loaded SLNs ApoE in the following experiments.
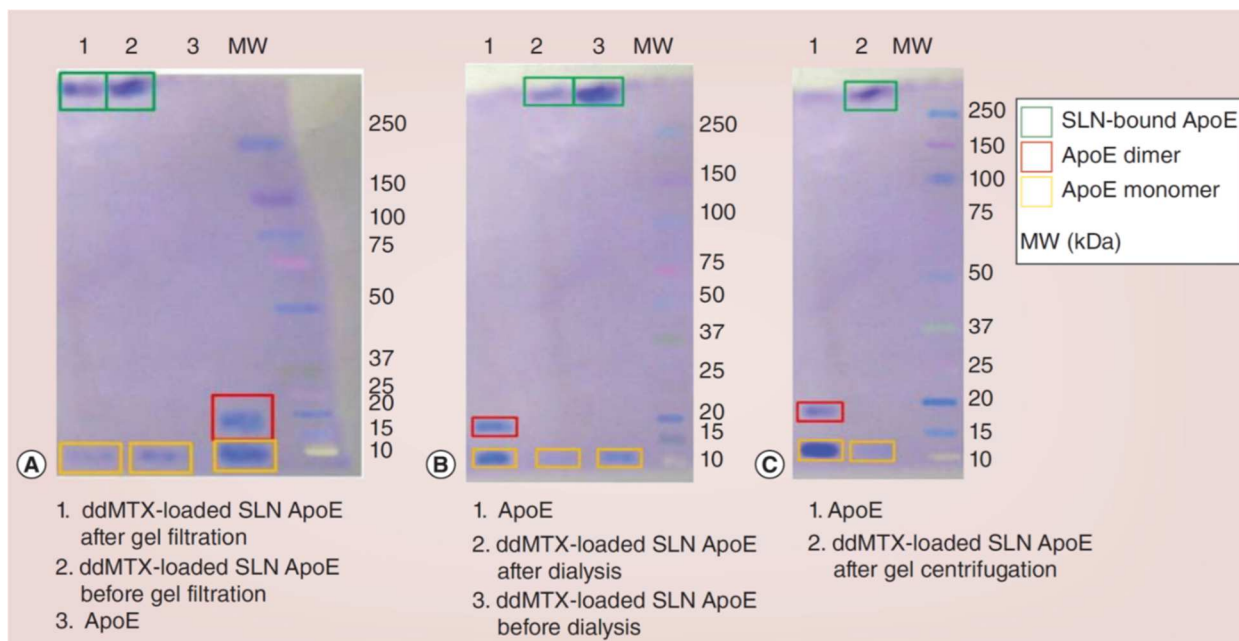
Figure 59. Representative photographs of the solid lipid nanoparticle ApoE after electrophoresis resolution and Coomassie Blue staining. ddMTX-SLNs functionalized with ApoE were purificated from unbound protein by gel filtration, using a matrix of crosslinked agarose (Sepharose CL 4B – size exclusion 100,000 Da; panel A), by gel centrifugation, using crosslinked poliacrylamide (Biogel P-6 – size exclusion 6,000 Da; panel B) and by dialysis (14,000 Da membrane cutoff; panel C). The effective functionalization was assessed by SDS gel electrophoresis (12% poliacrylamide) performed in non-denaturing conditions, followed by staining with Coomassie Blue solution. The amount of ApoE associated with SLNs was quantified at the same time with the BCA kit (Table 3).

Table 3. Physic-chemical feautures of ddMTX-SLNs.

	Diameter (nm)	Polydispersity	ζ Potential (mV)	ddMTX (mg/ml)	EE %	Drug loading (mg drug/mg lipid)	% of ApoE (BCA assay)	Number of ApoE for SLN	Diameter (nm) in normal saline	Polydispersity in normal saline
ddMTX-loaded SLN	322.9 ± 7.8	0.270	-2.44 ± 0.86	0.691	86	0.014	–	–	327 ± 5.0	0.24
ddMTX-loaded SLN ApoE	338.0 ± 10.0	0.287	-7.18 ± 1.92	0.716	89	0.014	100	10,942	–	–
ddMTX-loaded SLN ApoE (gel filtrated)	363.6 ± 2.8	0.288	-7.64 ± 1.50	0.550	69	0.011	65	8810	360 ± 5.8	0.25
ddMTX-loaded SLN ApoE (dialyzed)	370.5 ± 2.5	0.237	-5.64 ± 0.90	0.310	39	0.006	47	6746	–	–
ddMTX-loaded SLN ApoE (gel centrifuged)	296.6 ± 10.4	0.314	-6.64 ± 1.30	0.570	71	0.011	66	4850	–	–

ddMTX: Didoceylmethotrexate; EE: Entrapment efficiency; MTX: Methotrexate; SLN: Solid lipid nanoparticle.

4.3.c.2 ddMTX-SLNs induce cytotoxicity in rat glioma cell

At first I tested the toxicity of ddMTX-SLNs against F98 glioma cells, syngeneic with Fischer rats. Since ApoE is important to improve drug delivery to the brain, SLNs were not functionalized with ApoE for *in vitro* toxicity assay. In the presence of both free and SLN-entrapped ddMTX, the *in vitro* proliferation of F98 cells was inhibited, as previoisly observed for human GB cell lines [Annovazzi, 2017]. After 72-h exposure, F98 cells grew rounded, unable to adhere and with a significant reduction of cell viability at 0.5 μmol/l and even more at 5 μmol/l SLN-loaded ddMTX respect to untreated cells (Figure 60A). At 5 μmol/l concentration, the number of surviving cells was almost negligible with a higher effect respect to that induced by TMZ, used as positive control of first-line drug used in GB treatment (Figure 60A). The exposure of the cells to unloaded SLNs at the highest SLNs concentration used for the study determined only a mild reduction of cell viability, suggesting the safety of SLNs under study (Figure 60A). Then I investigated cell death occurrence in both control and drug-treated tumor cells, by using the immunocytochemical determination of the activated Caspase-3 and the TUNEL assay. Caspase-3 allows detection of cells in the initial stages of apoptosis, whereas TUNEL method reveales the DNA fragmentation that could be a characteristic of apoptotic and/or necrotic process. I observed an enhanced expression of cleaved Caspase-3 after treating the cells with SLN-entrapped ddMTX or free MTX respect to that with TMZ at the same concentration. Moreover free MTX induced a greater apoptotic effect respect to ddMTX-SLNs. With the TUNEL assay, a lower rate of apoptosis was detectable, but the general trend was confirmed (Figure 60B). After 48 h treatment with TMZ the effect on cell death was better evidenced with TUNEL assay, whereas activation of Caspase-3 was more visible after treatment with free and SLN-loaded MTX. This difference was likely due to the different action mechanisms of the two drugs. Probably, TMZ at 50 μmol/l concentration induced a precocious cell death in F98 cells and, already after 48 h, most cells displayed DNA fragmentation detectable with TUNEL. On the contrary, the activation of Caspase-3 resulted higher in MTX-treated cells, compared with untreated cells, indicating that the drug is more prone to induce early apoptosis. Occurrence of apoptosis after treatment with unloaded SLNs was similar to that showed by untreated cells. These results indicated that the toxicity on F98 rat glioma cells, mediated by the induction of apoptotic death of ddMTX-loaded SLNs is due to entrapped MTX and not to the nanosystem, as unloaded SLNs were not cytotoxic (Figure 60B).

A
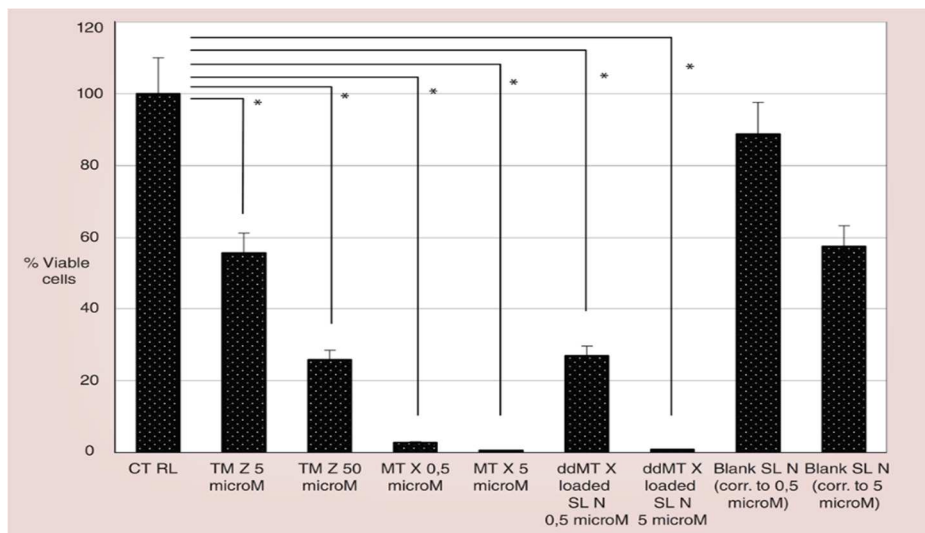
B
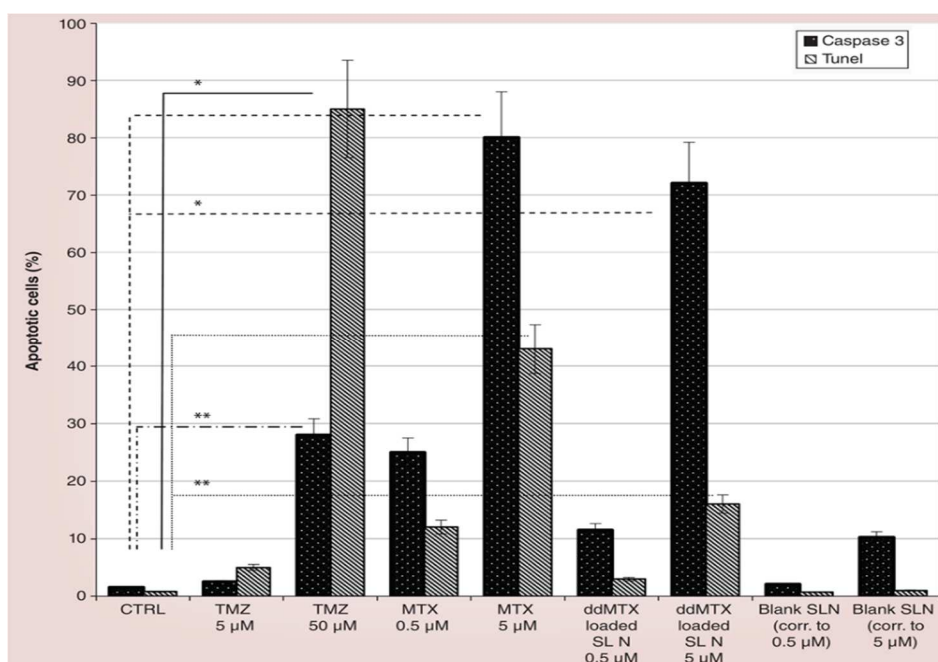
Figure 60. Cytotoxicity of methotrexate and didoceylmethotrexate-loaded solid lipid nanopaticle against F98 cells. F98 cells were plated at a density of 2×10^5 cells for 24 h and then treated with 0.5 -5 µmol/l of MTX (free or ddMTX entrapped in SLN), 5-50 µmol/l of TMZ (positive control) for 72 h (cell viability) or 48h (apoptosis assay). ddMTX was not used as control, because of its very low solubility in the medium. **A**. Cell viability.The number of viable cells was determined by Tripan Blue dye using a TC20 automatedcell counter and was expressed as the number of surviving cells as percentage of control (untreated cells). *p < 0.01 between control and TMZ (5 and 50 µmol/l), control and MTX (0.5 and 5 µmol/l), control and ddMTX-loaded SLNs (0.5 and 5 µmol/l). Unloaded SLNs at the concentration corresponding to that used for entrapped drugs were used to verify the nontoxicity of the carriers.All experiments were performed in quadruplicate. **B.** Apoptosis by using immunocytochemistry ad TUNEL assay. After 48 h of drug exposure, cells were fixed for 30 min with 4% paraformaldehyde at room temperature, and then the immunostaining reaction was performed using a Ventana Full BenchMark® XT automated immunostainer as the detection system. Primary antibody was rabbit anticleaved Caspase-3 (Asp175), or using *in situ* TUNEL assay according to the manufacturer's instructions. Observations were done by fluorescence microscope. Apoptotic indexes were calculated as the mean number of cleaved Caspase-3-positive cells or TUNELpositive cells counted in five randomly selected microscopic fields at 400× magnification; the number of apoptotic cells was expressed as percentages of the total cell number. *p < 0.01 between control and TMZ 50 µmol/l (TUNEL assay), between control and MTX 5 µM and between control and ddMTX-loaded SLNs 5 µmol/l (Caspase-3). **p < 0.05 between control and MTX 5 µmol/l, between control and ddMTX-loaded SLNs 5 µM (TUNEL assay), between control and TMZ 50 µM (Caspase-3).

4.3.c.3 ApoE ddMTX-SLNs reduce the tumor growth *in vivo* glioma model

ddMTX could be a substrate of the Pgp, but the loading in SLN can avoid this feature. Wong et al. demonstrated that SLN might enter the cells by an endocytosis mechanism, bypassing the Pgp system, regardeless of ddMTX is a substrate of the Pgp [Wong, 2007]. *In vivo* biodistribution experiments on healthy Fischer rats I showed drug accumulation in RES organs. However, a significantly lower drug removal from plasma and organs was observed after ddMTX-loaded SLN administration compared with the parental drug (MTX) solution (Figures 61A- 62A). The presence of ApoE on SLN slightly increased drug amount recovered in the brain, especially at longer time after administration (90 min), compared with nonfunctionalized SLN and free drug (Figure 62B). Since the altered BBB in the glioma can increase the uptake of molecules and small NPs [Yu, 2012], similar biodistribution experiments were performed in rat glioma models. No difference was noted compared with healthy rats (Figure 61B-62B), probably because SLN size exceeds the small fenestrations of altered BBB.

The rapid onset and exponential growth of F98 cells orthotopically implanted in Fisher rats makes this glioma model suitable to mimic some of the human GB characteristics. Oral TMZ was employed as positive control [Dagıstan, 2012]. Tumor volume, measured through MRI, increased very fast, starting from 1 week after implantation. Treatment with ddMTX-loaded ApoE SLNs resulted in a significant mean decrease of tumor volume growth at day 11, compared with control and oral TMZ. No free and unfuctionalized SLNs were used because biodistribution data revealed negligible drug brain accumulation (Figure 63).

All GB showed similar histopathological hallmarks, regardless that they belonged to treated or control rats. Tumors were composed of variably sized, irregular, rounded or elongated fusiform cells, nearly always arranged in a lobular pattern. Multifocal necrosis and mitotic figures were present in all the tumors. Parenchymal invasion was abundant and characterized by small to voluminous neoplastic cells abutting adjacent blood vessels and invading the adjacent brain parenchyma. Moderate vascular proliferation was present at the peripheral margin. A very limited and inconstant mononuclear inflammatory reaction was observed around the blood vessels surrounding the tumor masses [Wyne, 1996]. GFAP was strongly expressed by peripheral reactive glia, while a multifocal to diffuse expression of this marker was observed in the neoplastic cells, confirming their glial origin (data not shown).

Ki-67 staining revealed a high proportion of mitotic cells in all the tumors (Figure 64). Of note, Caspase-3 was different on the basis of the treatment: rats treated with ddMTX-loaded SLNs ApoE showed increased apoptosis compared with both negative and positive controls (TMZ) (Figure 65) even if the differences in Caspase-3 quantification were not significant in glioma specimens (Figure 65).

A
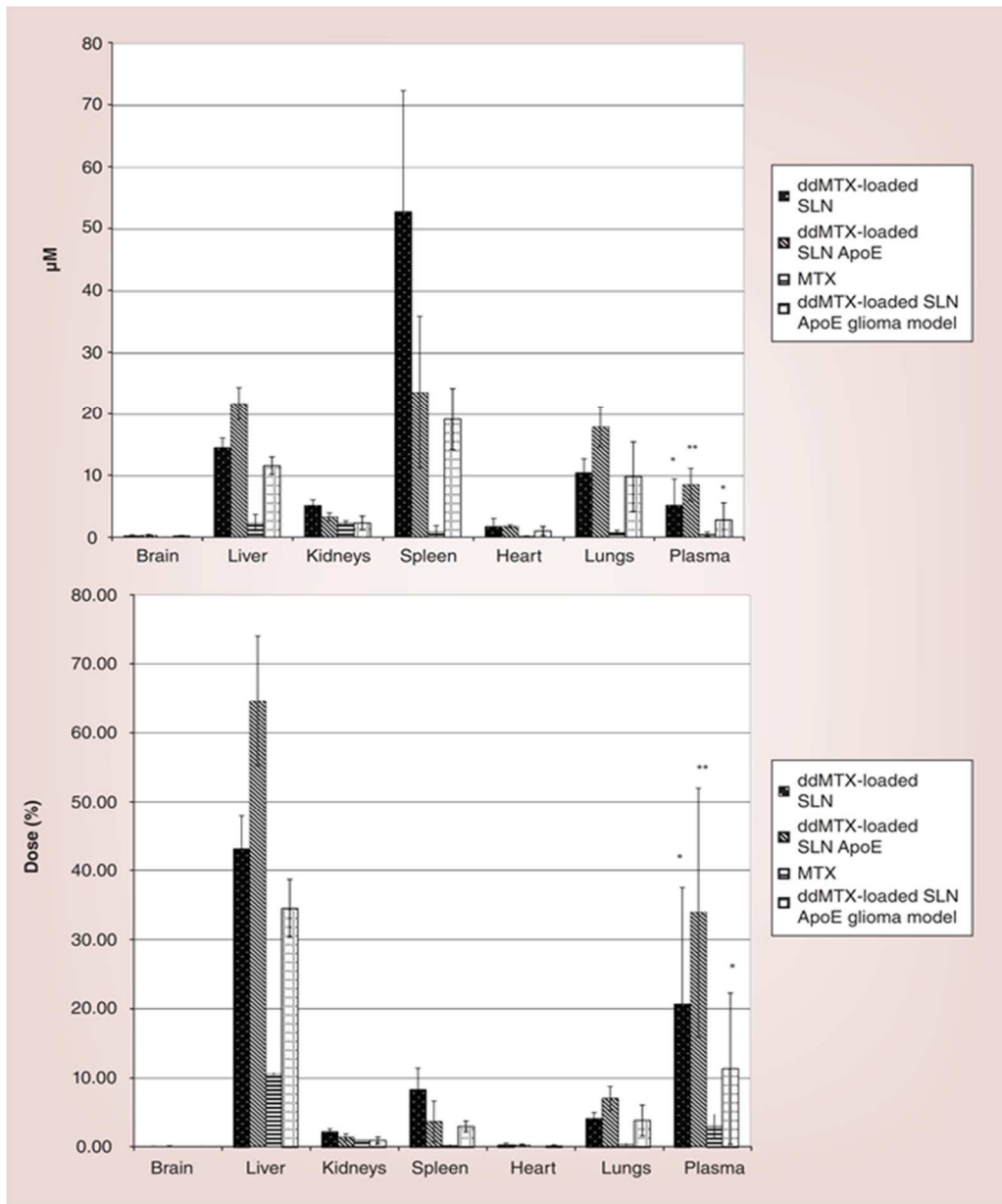
B
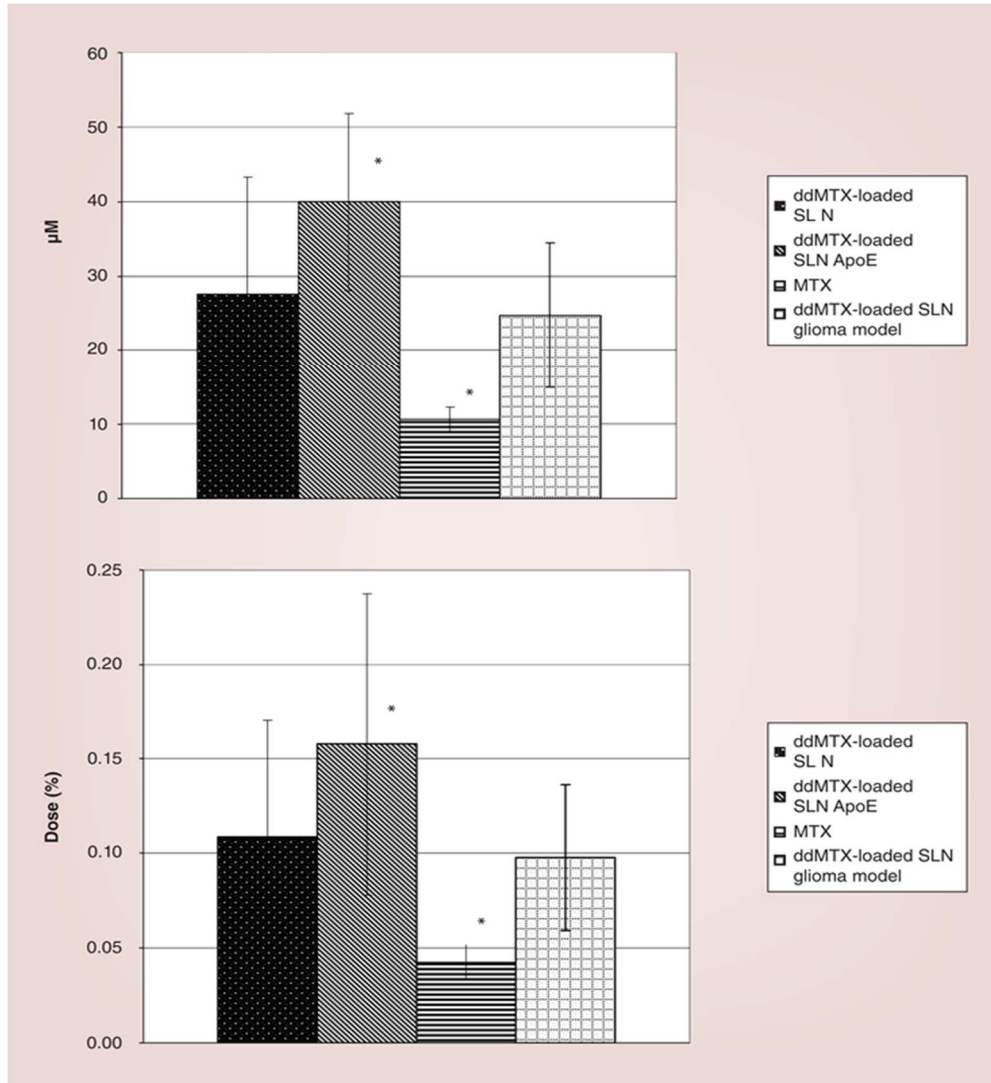
Figure 61. Biodistribution of methotrexate and didoceylmethotrexate-loaded solid lipid nanoparticle 30 min after administration. ddMTX-loaded SLNs, with or without ApoE and ddMTX solution in normal saline were administered through a catheter surgically positioned in the jugular vein of male Fischer healthy rats. ddMTX was not used as control, because of its very low water solubility, that hampers its intravenous administration as a free molecule. At 30 min after administration, rats were sacrificed; plasma was withdrawn, and organs (liver, spleen, kidneys, lungs, heart and brain) were removed surgically. Each experiment was performed with four rats for each sample administered. A pilot biodistribution experiment was also performed by using 7-day implanted glioma models, aiming to detect differences between biodistribution in healthy rats and glioma models. Glioma- model-carrying rats were sacrificed 30 min after administration. Organs were homogenized with UltraTurrax® (IKA, Staufen, Germany) for 5 min in water at a tissue concentration of 125 mg/ml; tissue homogenates and plasma underwent the derivatization reaction prior to fluorimetric HPLC detection. **A**.Organs: *$p < 0.01$ plasma ddMTX-loaded SLNs *versus* MTX and ddMTX-loaded SLNs glioma model *versus* MTX; **$p < 0.05$ plasma ddMTX loaded SLNs ApoE *versus* MTX. **B.** Brain:*$p <0.01$ ddMTX-loaded SLNs ApoE *versus* MTX in brain.

A

B

Figure 62. Biodistribution of methotrexate and didoceylmethotrexate-loaded solid lipid nanoparticle 90 min after administration. ddMTX-loaded SLNs, with or without ApoE and ddMTX solution in normal saline were administered through a catheter surgically positioned in the jugular vein of male Fischer healthy rats. ddMTX was not used as control, because of its very low water solubility, that hampers its intravenous administration as a free molecule. At 30 min after administration, rats were sacrificed; plasma was withdrawn, and organs (liver, spleen, kidneys, lungs, heart and brain) were removed surgically. Each experiment was performed with four rats for each sample administered. A pilot biodistribution experiment was also performed by using 7-day implanted glioma models, aiming to detect differences between biodistribution in healthy rats and glioma models. Glioma- model-carrying rats were sacrificed 30 min after administration. Organs were homogenized with UltraTurrax® (IKA, Staufen, Germany) for 5 min in water at a tissue concentration of 125 mg/ml; tissue homogenates and plasma underwent the derivatization reaction prior to fluorimetric HPLC detection. **A**.Organs: *p < 0.01 plasma ddMTX-loaded SLNs *versus* MTX and ddMTX-loaded SLNs glioma model *versus* MTX; **p < 0.05 plasma ddMTX loaded SLNs ApoE *versus* MTX. **B.** Brain:*p <0.01 ddMTX-loaded SLNs ApoE *versus* MTX in brain.

Figure 63. Glioma growth. Glioma growth was monitored at different times (days 7, 9 and 11 after implantation) through MRI. Rats were anesthetized. Glioma volume was evaluated through Bruker Pharmascan software: the brain was divided in 15 transverse slices of 1.5 mm thickness of, and the area evidenced by gadobenate dimeglumine (tumor) was approximated by the software. Final integration was performed between calculated areas and slice thickness. Data are normalized to day 7.
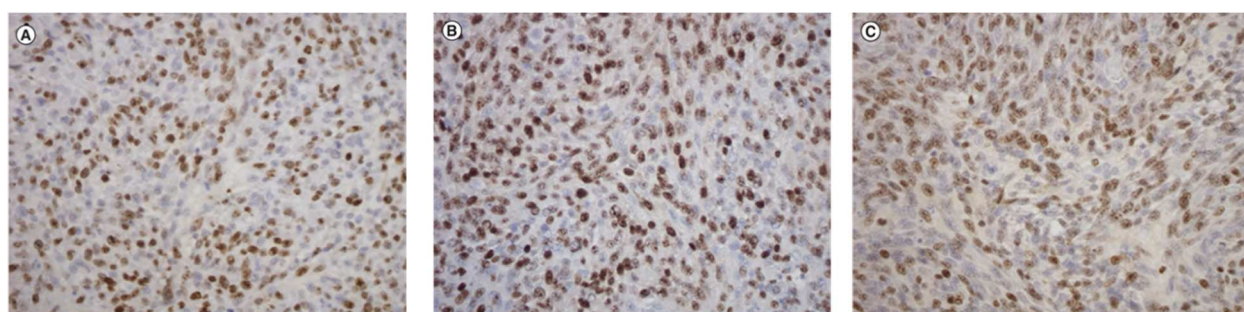
Figure 64. Immunohistochemical staining of Ki-67 in tumor sections. Collected brain from control group **(A)** and rats treated with ddMTX-loaded SLNs **(B)** and TMZ **(C)** were stored in 10% formalin for histological evaluation. Slide sections (5 mm thick) were obtained using a microtome and stained with hematoxylin stain. During brain evaluation, histological features were classified as positive if a tumor mass was present and negative if no tumor was detected. Immunohistochemical staining was also done on selected sections. Decoration with monoclonal antibody Ki-67 was detected using the avidin–biotin– peroxidase technique. Each immunohistochemical marker was evaluated in at least ten different fields, and particularly measuring the numbers of positive cells for Ki-67.
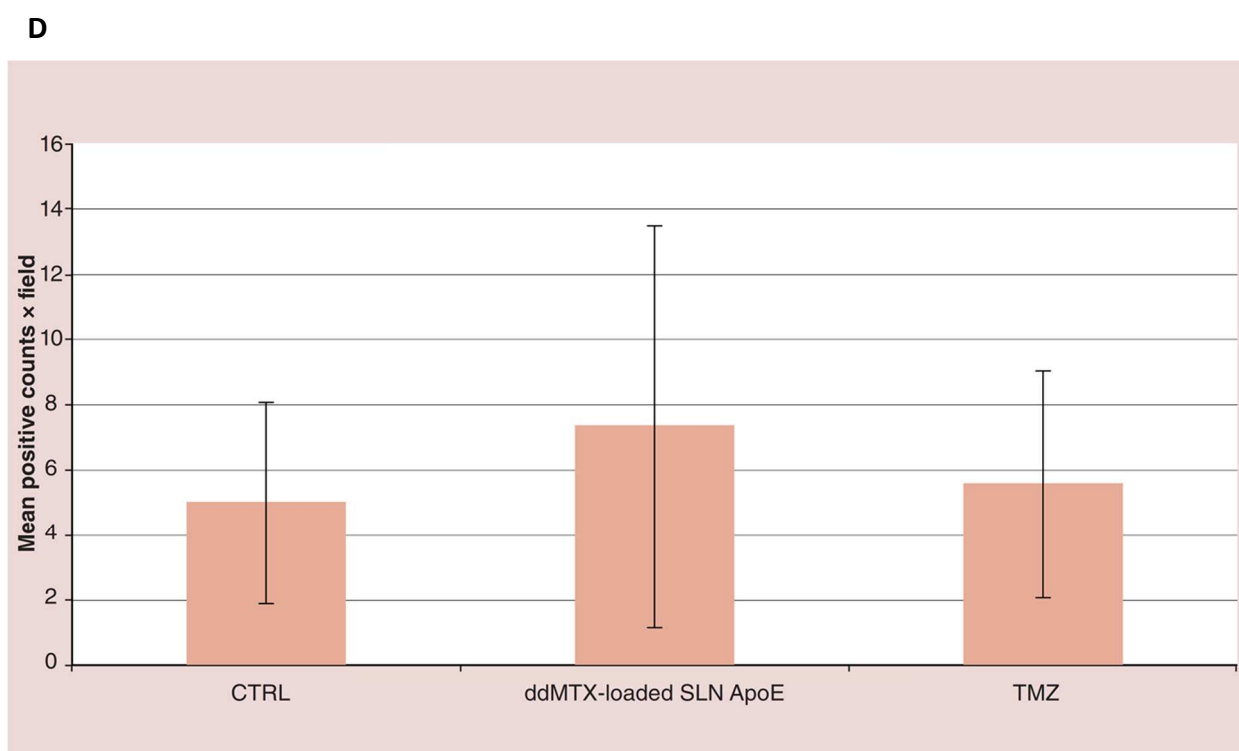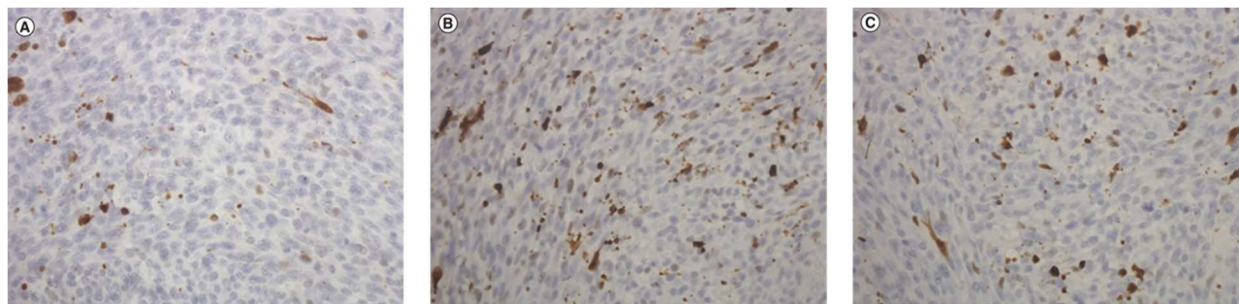
Figure 65. Immunohistochemical staining of Caspase-3 in tumor sections. Collected brain from control group **(A)** and rats treated with ddMTX-loaded SLNs **(B)** and TMZ **(C)** were stored in 10% formalin for histological evaluation. Slide sections (5 mm thick) were obtained using a microtome and stained with hematoxylin stain. During brain evaluation, histological features were classified as positive if a tumor mass was present and negative if no tumor was detected. Immunohistochemical staining was also done on selected sections. Decoration with monoclonal antibody cleaved Caspase-3 was detected using the avidin–biotin–peroxidase technique. **(D)** Quantification of Caspase-3 expression in glioma specimen by using an Image Pro Plus analysis system. Each immunohistochemical marker was evaluated in at least ten different fields, and particularly measuring the numbers of positive cells for cleaved Caspase-3.

5. DISCUSSION

GB chemotherapy often fails because of the chemoresistant phenotype of GB and the low delivery of anti-neoplastic drugs across the BBB. ATP dependent efflux pumps, such as Pgp, abundantly localized on BBB, are physiologically important to protect CNS from xenobiotics and toxic compounds but can result a problem for drug delivery against brain tumors.

My thesis investigates the molecular and cellular basis of BBB and GB interaction in order to know the mechanisms of low drug delivery across BBB and develop new strategies that improve delivery of chemotherapeutic drug against GB.

Aim 1

In the first part I analyzed the molecular mechanisms regulating Pgp at BBB level, demonstrating the central role of Wnt pathway. It is known that Pgp is under the transcriptional control of Wnt/GSK3/β-catenin pathway (i.e. the so-called Wnt-canonical pathway) in BBB cells [Lim, 2008], but it is unknown whether the Wnt non canonical pathway (Wnt/RhoA/ RhoAK axis) is also involved and whether the canonical and non-canonical Wnt pathways cooperate in regulating the Pgp levels in BBB cells.

I observed that the Wnt activation increases at the same time the activity of GSK3 and the activity of RhoA/ RhoAK in hCMEC/D3 cells, while the Wnt inhibition reduced them. The positive cooperation between Wnt/GSK3 and Wnt/RhoA/RhoAK axis, which I detected in BBB cells, has been described in pulmonary aortic endothelial cells: the bone morphogenetic protein 2 increases the activity of GSK3/β-catenin axis and at the same time recruits the Wnt-downstream effector Disheveled, which activates RhoA [de Jesus Perez, 2009]. However, it has not been clarified whether the canonical Wnt pathway controls the activity of the non-canonical Wnt pathways or *viceversa*. In gastric cancer cells, the activation of RhoA in response to Wnt5a is dependent on the activation of the PI3K/Akt/ GSK3 axis [Liu, 2013]. My results demonstrated that an active RhoA decreases the activity of GSK3, prevents the GSK3-mediated phosphorylation of β-catenin, and favors its nuclear translocation and the subsequent transcription of Pgp, whereas the RhoA silencing produces opposite effects. These data suggest that RhoA activity controls the GSK3/β-catenin axis in hCMEC/ D3 cells. This hypothesis is in contrast with results obtained in murine cerebrovascular endothelial cells, where the activation of RhoA promotes the phosphorylation of β-catenin and reduces its transcriptional activity [Chang, 2012]. As murine and human brain microvascular cells have often striking differences in the expression and activity of Pgp, it is not surprising that they also differ in the upstream pathways controlling Pgp expression. For instance, the mechanism by which RhoA modulates GSK3 activity is quite different in murine and human cerebrovascular endothelial cells: in murine cells, RhoA controls the GSK3 activity in a PTEN- and protein kinase Cδ-dependent way and changes the phosphorylation of GSK3 on serine with inhibitory effects [Chang, 2012].

I next looked for putative downstream effectors of RhoA responsible for this effect. I focused on RhoAK, whose activity followed the same trend of RhoA activity in response to activator WntA and inhibitor Dkk-1 in hCMEC/D3 cells. Interestingly, the inhibition of RhoAK by Y27632 quickly decreased the nuclear translocation of β-catenin, with a maximal efficacy after 3 h. At longer time points, nuclear β-catenin progressively re-accumulated in the nucleus, although it remained lower than in untreated cells: this may be due to the short half-life (i.e., less than 12 h) of β-catenin [Bareiss, 2010], which produces a fast re-synthesis of new β-catenin ready to translocate into the nucleus. After 3 h, Y27632 effectively increased the phosphorylation on

tyrosine 216 of GSK3 by inhibiting RhoAK mediated phosphorylation of a tyrosine phosphatase, PTP1B, which recognizes GSK3 as substrate. As a result, the nuclear translocation of β-catenin and its transcriptional activity were reduced, whereas the ubiquitination and proteasomal degradation of β-catenin were increased. Working at proper concentrations and incubation times, the RhoAK inhibitor increased the delivery of DOX, a Pgp substrate with a very low permeability across the BBB [Weksler, 2005].

Fasudil, the clinically prescribed analog of Y27632, is used to prevent vasospasms after subarachnoid hemorrhage [Zoerle, 2012], to improve tissue perfusion during cerebral ischemia [Shin, 2014] and to prevent the progression of cerebral aneurisms [Eldawoody, 2010]. My work suggests that Fasudil might be used to improve the delivery of Pgp substrates through the BBB. In the case of DOX, a drug that is highly effective against GB cells *in vitro* [Hau, 2004] and ineffective in the presence of a competent BBB [Riganti, 2014], the pretreatment of hCMEC/D3 cells with Y27632 fully restored the DOX delivery and cytotoxicity in GB cells. Repeated doses of Y27632 followed by DOX confirmed that this approach effectively reduced the long-term proliferation of GB cells grown under a BBB monolayer. However, Pgp is not the only transporter present on the luminal side of BBB that can efflux DOX; also MRP1 and BCRP which are detectable in the hCMEC/D3 cells [Pinzón-Daza, 2012], meet these requisites, but their expression did not change in cells with constitutively active RhoA, silenced for RhoA or treated with Y27632. I thus hypothesize that the changes in DOX delivery after RhoA activation or inhibition were consequent to the expression change of Pgp in hCMEC/D3 cells. To further quantify the contribution of this transporter in DOX permeability, I treated the hCMEC/D3 cells with the Pgp inhibitor verapamil, which produced the same effects—in terms of DOX delivery and toxicity in GB cells—of Y27632. These results indirectly suggest that Pgp has a major role in limiting DOX delivery in the CNS. Although Pgp tightly cooperates with BCRP in controlling the delivery of several drugs across the BBB [Agarwal, 2011] DOX has high affinity for Pgp, which represents the main transporter of this drug in BBB cells [Qu, 2003].

The downregulation of the canonical Wnt/GSK3/β-catenin pathway is known to reduce Pgp expression and to induce chemosensitization in colon [Siflinger-Birnboim, 1987], GB SCs [Riganti, 2013], neuroblastoma [Flahaut, 2009], chronic myeloid leukemia [Corrêa, 2012] and cholangiocarcinoma [Shen, 2013]. In my work, I showed that downregulation of Pgp by distruption of the canonical Wnt/GSK3/β-catenin pathway increased the drug delivery across BBB cells. The actor of this process is TMZ, i.e. the first-line therapy in GB, whose effects on BBB were not yet investigated before.

The administration of TMZ to hCMEC/D3 increased the permeability of Pgp substrates across the BBB monolayer. Notably, at concentrations found in the blood of patients [Portnow, 2009] TMZ did not induce any detectable cytotoxic effect on BBB cells, but it increased the permeability of Pgp substrates across the BBB monolayer, like DOX and vinblastine. Unlike other permeabilizing strategies [Pinzòn-Daza, 2013], TMZ did not affect the integrity of TJs, as the permeability to DEXT, inulin, and sucrose, as well as the expression of claudin-5, occludin and ZO-1 did not change. TMZ effect was specific for Pgp, since the activity and expression of MRP1 and BCRP were not affected. The decrease of Pgp without changes in other ABC transporters is of particular interest. Indeed, mice knocked down for Pgp have a compensatory increase of BCRP in BBB, suggesting a cooperation between these transporters [Pinzòn-Daza, 2012]. My study was

performed by treating cells with a single dose of TMZ for 72 h; I did not investigate whether different experimental conditions (e.g. repetitive treatments with the drug or longer treatment periods) affected the expression of ABC transporters other than Pgp. The antitumor effects of TMZ, in terms of alkylating efficacy and DNA damages, are significantly stronger when the drug is administered repetitively within the same day than when the drug is administered as single dose [Wick, 2009]. I cannot exclude *a priori* that prolonged or repetitive administrations of TMZ might exert a stronger decrease in Pgp, thereby triggering a progressive increase in BCRP. When BCRP is increased in response to the decrease of Pgp, drugs that are dual substrates of these transporters are not more delivered through the BBB. Notwithstanding, the downregulation of Pgp results in the increased delivery of drugs that have higher affinity for Pgp than for BCRP [Agarwal, 2011]. This is the case of DOX and vinblastine, which were more transported across hCMEC/D3 monolayer upon the downregulation of Pgp induced by TMZ.

Untreated hCMEC/D3 cells and primary brain microvascular endothelial cells HBMECs had β-catenin constitutively bound on the promoter of *mdr1* gene and Pgp constitutively expressed. In contrast, cells treated with TMZ showed increased activity of GSK3 and increased amounts of phosphorylated β-catenin. The phosphorylation-dependent degradation of β-catenin resulted in a decrease of its nuclear translocation and binding on the *mdr1* promoter. The results obtained with activators and inhibitors of the Wnt canonical pathway suggested that TMZ downregulated Pgp acting like a Wnt-pathway inhibitor. Indeed, TMZ acted at transcription level, downregulating the transcription of *Wnt3* gene in BBB cells. Untreated hCMEC/D3 and HBMEC cells expressed a fully unmethylated *Wnt3* promoter, which is consistent with the constitutive transcription of Wnt3. As an alkylating agent, TMZ methylated the promoter of *Wnt3* gene, which is rich in CpG islands and consequently reduced Wnt/GSK3/β-catenin axis and Pgp expression.

Interestingly, TMZ administered on the luminal side of hCMEC/D3 cells also decreased the *mdr1* levels in GB SCs (that constitutively express Pgp [Riganti, 2013]) growing under hCMEC/D3 monolayer: this means that the drug crossed—as expected—the BBB, and acted on both endothelial and tumor cells, increasing at the same time the permeability of BBB cells and the chemosensitivity of GB cells. In GB SCs, TMZ downregulates Pgp with the same type of mechanism, but downregulating the GB isoform Wnt3a [Riganti, 2013]. In view of these results, clinical doses of TMZ may facilitate the subsequent passage of anticancer drugs, not commonly used in the therapy of GB because they are rapidly effluxed through the BBB by Pgp. Using DOX as a prototype, I indeed observed in co-culture models of hCMEC/D3 or HBMEC and GB SCs that the pre-treatment of BBB cells with TMZ significantly increased the delivery of DOX, induced marked cytotoxicity, and reduced the proliferation of GB SCs. The increased permeability of DOX induced by TMZ was likely triggered by the downregulation of the Wnt3/GSK3/β-catenin/Pgp axis in BBB cells, since the same effect was achieved by depleting Wnt3 in hCMEC/D3 cells.

The pharmacokinetics, the pharmacodynamic effects and the side effects of TMZ and DOX are well known, but the combination of TMZ and DOX is new and requires appropriate studies of pharmacokinetics and safety pharmacology.

The same chemosensitizing effects of TMZ that I describe here were obtained with two other Pgp substrates, vinblastine, and topotecan. While the former is not currently used in GB therapy, the latter has received a great deal of interest in the last few years. Although topotecan does not cross the BBB [Lopez, 2011], it has a very low IC50 against GB cells *in vitro* [Carcaboso, 2010] and has been proposed as an effective agent when administered by convection-enhanced delivery

[Lopez, 2011]. The results of the present study are paving the way to other studies on the antitumor efficacy of this new drug combination in orthotopic animal models of human GB. If the results obtained in our co-culture models will be confirmed *in vivo*, this might open the door for new therapeutic protocols based on the pre-treatment with TMZ followed by systemic administration of topotecan. These findings may also explain the clinical observation that the topoisomerase I – topotecan - vinblastine inhibitors produce significant benefits in patients with recurrent gliomas when used in combination with TMZ [Vredenburgh, 2011].

As conclusion of the first part of my thesis, I suggest that TMZ at clinical dose is an active chemotherapeutic agent but also chemosensitizer at both BBB and GB level, able to increase the permeability of drugs substrates of Pgp. These results might have important implications for the eradication of GB cells in the BAT area, where tumor cells lay surrounded by intact BBB, and cannot be completely removed by surgery or radiotherapy, and almost never are reached by effective concentrations of chemotherapeutic drugs. The use of TMZ in association with DOX, topotecan, or vinblastine may become a successful strategy for eradicating GB cells from BAT area and preventing recurrence. Also RhoAK inhibitors might be used as downregulators of Pgp in order to deliver chemotherapeutic agents, but also the passage of drugs used to treat CNS diseases such as infective diseases, neurodegenerative diseases, and epilepsy [Pinzòn-Daza, 2013].

Aim 2

GB induces breakdown of BBB and edema formation contributing to patient morbidity [Rape, 2014]. The molecular and cellular mechanisms underlying GB-induced disruption of the BBB are not clear yet. In the second part of my thesis, in order to investigate the interactions existing between GB and BBB, I set co-culture models of hCMEC/D3 and GB cells, cultured as SCs/NS and as differentiated cells (AC) derived from the same primary GB.

At 24 h and 72 h, BBB cells showed a great permeability to DEXT-70-FITC, which normally cannot cross BBB, in particular in the presence of differentiated compoment. This enhanced paracellular flux was associated with the downregulation of specific TJ components at trascription and protein level: occludin and ZO1 protein were decreased in BBB co-cultured with differentiated cells respect to BBB alone, and only slightly reduced by the presence of SCs. On the contrary, claudin 3 and 5 were increased by the co-culture with differentiated cells, whereas reduced by presence of SCs. These results are in line with previous data showing that occludin, ZO1 and claudin 3 and claudin 5 were found to be significantly downregulated in high grade astrocytoma, rich of SCs [Ishihara, 2008]. Interestingly the conditioned-medium obtained from GB cells culture induced the highest increase in DEXT-70-FITC permeability, suggesting that GB cells release soluble factors that may mediate these changes of BBB permeability. The nature of these factors is unknown to us currently, but from the preliminary data obtained by cytokines and chemokines screening profile on hCMEC/D3 co-cultured with GB cells, probable candidates might include: stromal-derived-factor-1/C-X-C chemokine receptor type 4 (SDF1/CXCR4), monocyte chemoattractant protein-1 (MCP1) and tumor-necrosis factor α (TNFα). I found that the mRNA of these chemokines were more expressed in BBB cells co-culture with differentiated cells respect to BBB/SC co-culture, and I am currently evaluating their protein expression in the supernatants of BBB cells co-cultured with GB. Interestingly, CXCR4 was found to be overexpressed in GB and its ligand SDF-1, as autocrine signals, stimulated receptors on invasive glioma cells and created a permissive microenvironment for malignant progression [Hoelzinger,

2007]. MCP-1 and TNFα are pro-inflammatory chemokines implicated in disruption of the BBB by altering TJs in several models of CNS inflammation [Nishioku, 2010; Dimitrijevic, 2006]. Moreover the microenvironment of hCMEC/D3 co-cultured with U87 MG cell line model presented by Mendes et al. showed a significant increase of MCP-1 and IL-6 production; these cytokines were suggested to induce an increased BBB permeability [Mendes, 2015]. Some proteases (MMP-2, MMP-9), VEGF and scatter factor/hepatocyte growth factor (SF/HGF), transforming growth factor (TGF-β2) have been also suggested to impair the BBB [Ishihara, 2008; Schneider, 2004]. I am expanding the field of investigation to these factors in the BBB/GB co-culture models.

My work differs from the precedent ones for two reasons. The first reason is the aim in approaching BBB/GB co-cultures. In general, BBB/GB co-culture *in vitro* models are designed to prove the ability of drug delivery systems to permeate the BBB monolayer, while here I aim investigating the interaction existing between GB and BBB. In literature, few works report studies of GB/BBB co-culture to clarify this point [Ishihara, 2008; Mendes, 2015], and there are not yet conclusive findings. The second reason is the use of GB SCs and GB differentiated cells from the same patient. It is completely uninvestigated whether the grade of differentiation and/or stemness of GB cells could influence the BBB drug permeability.

Establishing *in vitro* models of the BBB has been a challenging task due to species differences, low availability of human primary brain endothelial cells and poor barrier formation by immortalized human brain microvascular endothelial cells [Ogunshola, 2011]. The primary cell cultures widely used are brain endothelial cells derived from a spectrum of mammals that includes rat, mouse, pig, bovine, or human origin [Wilhelm, 2011]. The establishment of human BBB *in vitro* model is very important to know GB-niche interactions. Here I used the hCMEC/D3 cell line, immortalized brain microvascular human cells, which retains morphological and functional characteristics of brain endothelium [Weksler, 2005]. This BBB model is widely used as a human *in vitro* BBB model but it represents a simplified model, far from mimicking *in vivo* conditions. Although cerebral endothelial cells are the principal components of the BBB, there is increasing evidence of other cell types such as glial cells, pericytes and neurons playing important regulatory roles in the induction and maintenance of the BBB [Ogunshola, 2011]. To give more strength to my data, it will be necessary to confirm my data with other more complex *in vitro* BBB models, e.g. the endothelial cells derived from cord blood-derived CD34+ hematopoietic stem cells co-cultured with brain pericytes that has been proven to be a stringent and competent BBB model [Vandenhaute, 2016].

Besides change in TJ, I also observed that GB cells induces changes in ABC transporters at BBB level. The permeability to DOX and MXR, indexes of Pgp and BCRP activity, increased in GB-hCMEC/D3 co-culture respect to hCMEC/D3 alone, with greater effect in presence of the differentiated cells and their conditioned medium, than in presence of the GB SCs. Unexpectedly, higher was the permeability to DOX, MXR and DEXT-FITC, higher was the amount of each compounds found within BBB cells. Probably the compounds cross BBB monolayer by transcytosis, from the luminal side (bloodstream side) to the basolateral side (brain parenchima side), but time-course experiments monitoring trancytosis process should be performed to clarify the kinetics of entrapment of the compounds within BBB cells and their release toward the basal side.

The expression levels of Pgp and BCRP were decreased in BBB co-cultured with differentiated

cells respect to BBB alone, and only slightly reduced by the presence of SCs. Considering my previous works (part 1 of the thesis) and other works showing that Wnt3 modulates the expression of ABC transporters on BBB [Liebner, 2008], I investigated if Wnt signaling was involved in decreasing in Pgp and BCRP expression in BBB cells. I stably overexpressed Wnt3a in differentiated GB cells, that are known - upon the overexpression of Wnt3a - to acquire the same morphological, functional and chemoresistant profile of SCs/NS [Riganti, 2013]. The overexpression of Wnt3a in differentiated GB cells affected the permeability of BBB in the same way of SCs derived from the same tumor. On the basis of these results, Wnt3a, that has lower activity in differentiated cells than in SCs [Riganti, 2013], could be an additional modulator of BBB permeability and may explain the differential impact of differentiated cells and SCs on BBB cells. To go in depth into this field of investigation, I am analyzing how phospho(Tyr216)GSK3 and phospho(Ser33/37/Thr41)-β-catenin expression in BBB cells change in the presence of differentiated cells and SCs, and how this can modulate the expression of Pgp.

From the data obtained in the second part of my thesis, I propose that GB cells permeabilize BBB, and that more differentiated are the cells, more permeable is the BBB. Further investigations in identifying soluble factors released by GB would contributed to improve the drug delivery across BBB, tailoring it on the basis of the degree of differentiation of GB.

Aim 3:
The presence of Pgp in both BBB and GB creates a "double barrier" that dramatically reduces the success of chemotherapy against this tumor. In the last part of my thesis, I analyzed new types of molecules or formulations able to inhibit Pgp on BBB cells and/or GB cells: thiosemicarbazones compounds, carbonic anidrase XII inhibitors and SLN-carried drugs.

With the aim of targeting Pgp on BBB, I tested a series of thiosemicarbazone derivatives that were ineffective as antitumor agents at nanomolar concentrations, but showed a good inhibition on Pgp of cancer cells [Pati, 2015]. Here I proposed the use of three thiosemicarbazone compounds as effective inhibitors of Pgp acting at BBB level.

Most Pgp inhibitors successfully employed *in vitro* had failed in preclinical and clinical models for their off-target toxicity at the concentrations used to achieve a detectable inhibition of Pgp [Callaghan, 2014]. According to our dose- and time-dependence cytotoxicity assays, the three compounds analyzed were not toxic at 10 nmol/l. This concentration was sufficient to inhibit Pgp, as demonstrated by the increased DOX uptake and permeability across BBB monolayer. At the same concentration, the compounds did not damage GB cells when used alone, confirming that the ability to inhibit Pgp was coupled with the lack of toxicity on BBB and GB cells.

Compared to other Pgp inhibitors, these compounds may be advantageous for multiple reasons. First, thiosemicarbazones increased the permeability of Pgp substrates in a selective way. Indeed, the permeability of substrates of BCRP and the TJs competence were not changed. Such selectivity may limit eventual side-effects due to the broad alterations of BBB functions produced by other strategies. Second, the selective inhibition on Pgp was achieved at nanomolar concentration, in line with the most potent Pgp inhibitors and Pgp tracers used *in vivo* [Bauer, 2012; Bauer, 2015]. Moreover, the increased uptake of DOX in either BBB or GB SCs, when cultured alone, suggest that thiosemicarbazones may inhibit Pgp on both cell types. I could not directly demonstrate that these compounds crossed BBB monolayer, because nanomolar concentrations – that were not toxic

for BBB cells – were under the detection limit of HPLC device, while micromolar concentrations – that are detected by HPLC – damaged the BBB monolayer. However, the increase in DOX uptake was small in differentiated cells (with undetectable Pgp amount) growing under hCMEC/D3 cells monolayer; such increase was more pronounced in SCs, which had high levels of Pgp. If the effect of the compounds was limited to the inhibition of Pgp in BBB cells, I should expect a similar increase in DOX delivery between differentiated cells and SCs co-cultured with BBB cells. I might hypothesize that the huge increase in DOX accumulation and toxicity observed in BBB-GB SCs co-cultures were not the simple consequence of an increased drug delivery across BBB, but it may be due to the simultaneous inhibition of Pgp on endothelial and tumor cells.

Overall, thiosemicarbazones can transform the BBB-impermeable drug DOX into a drug with a good BBB permeability and efficacy even against GB SCs. These results may pave the way to the preclinical application of thiosemicarbazones in combination with DOX and/or other first-line and second-line chemotherapeutic drugs such as topoisomerase I and II inhibitors.

With the aim of targeting Pgp on GB SCs, I used natural inhibitors of CAXII. Previous findings from my group demonstrated that in solid tumors CAXII is necessary to support the activity of Pgp [Kopecka, 2015] and that the selective inhibition of CAXII overcomes Pgp-mediated chemoresistance [Kopecka, 2016]. Here I found that CAXII was highly expressed and physically associated with Pgp in SCs obtained by GB primary tumors. An increased expression of CAXII in SCs derived from U87-MG has been recently reported [Takada, 2016], but my study is the first study showing that CAXII expression is increased in GB SCs derived from primary tumors. Starting from these considerations, I hypothesized that CAXII inhibitors may be exploited to overcome the Pgp-mediated drug-resistance.

I employed a library of selective CAXII inhibitors derived from the natural product sulfonamide Psammaplin C (compound **1**) with different modifications of the bromotyrosine sidechain (compound **2-3-4**). Compound **5** – lacking CAXII binding – was used as negative control [Mujumdar, 2016]. I identified compounds **1** and **3** as the most effective inhibitors of CAXII and Pgp ATPase activity. Accordingly, when administrated with Pgp substrates - DOX, etoposide, topotecan and irinotecan – they rescued the cytotoxic efficacy of these substrates.

TMZ remains the first-line drug in GB treatment, but it often fails to fully eradicate GB SCs. Some reasons for TMZ-resistance in GB SCs is the over-expression of O^6-methylguanine-DNA methyltransferase (MGMT) [Eramo, 2006], altered activity of DNA-repairing systems, aberrant activation of cell survival and anti-apoptotic pathways, microenvironment factors such as hypoxic niches and/or niches rich of growth factors [Beier, 2011]. Recent experimental evidences has demonstrated that TMZ is a substrate of Pgp [Munoz, 2015]: this provides an additional factor that contributes to the failure of TMZ efficacy in GB SCs. These observations, together with the lack of improvement in GB treatment and the alarmingly low survival rate for GB patients, show the necessity to investigate innovative combination treatments based on TMZ with agents that decrease Pgp activity.

Here I propose the combination of CAXII inhibitors with TMZ that allows an increase of intracellular retention of TMZ and subsequent cytotoxicity of this front-line therapy. SCs treated with TMZ and compound **1**- the strongest CAXII inhibitor – had the same amount of Pgp than cells treated with TMZ alone, but exhibited lower Pgp activity. This result suggests that CAXII inhibition does not change Pgp gene transcription but it reduced only catalytic efficacy of Pgp. It

is likely that this reduction is consequent to the altered optimal pH of membrane microenvironment where Pgp works, as observed in most solid tumors [Kopecka, 2015; Kopecka, 2016]. As a consequence, the treatment of SCs with CAXII inhibitors made TMZ as effective as in differentiated GB cells (that have no or very low detectable levels of Pgp) or in SCs knocked out for Pgp. These results are in line with previous findings showing that the less specific CA inhibitor acetazolamide enhances TMZ-induced apoptosis in GB [Das, 2008]. In that study a link between CAXII and reversal of chemoresistance *via* Pgp, and the difference between the effects in GB SCs *versus* differentiated cells were not known. My results suggest that acetazolamide reduces the efflux of TMZ *via* Pgp, increasing the intracellular TMZ retention and the consequent apoptosis elicited by the drug. Compared to acetazolamide, which strongly inhibits many different CA isoforms, compound **1** had an improved potency for CAXII and more selectivity for CAXII over all other CA isozymes. Given the low rate of therapeutic success in GB treatment, combination therapies based on TMZ and a second chemotherapeutic drug are under intensive investigations. Topoisomerase I and II inhibitors have been proposed as good adjuvant agents in TMZ-based regimens or as alternative drugs in TMZ-refractory patients [Carvalho, 2015; Peters, 2015; Reynés, 2016; Tonder, 2014; Mita, 2015; Whittle, 2015]. They are however all substrate of Pgp and their efficacy in killing/eradicating the Pgp-expressing GB SCs is thus limited [Tonder, 2014; Reynés, 2016]. Interestingly, a further notable finding was that the combination of compound **1**, TMZ and inhibitors of topoisomerase I (topotecan, irinotecan) or II (etoposide, doxorubicin) was highly effective in inducing cell death and reducing cell viability of GB SCs. Probably compound **1** increased the retention of TMZ and topoisomerase poisons, thanks to the inhibition exerted on Pgp activity, thus producing synergistic cytotoxic effects between TMZ and topoisomerase I/II inhibitors.

Compound **1** was effective in rescuing TMZ antitumor activity also in *in vivo* model. In xenografts derived from primary TMZ-refractory GB SCs, either a very low (10 nmol/l) dosage - around CAXII Ki - or a 100-fold higher dosage (1 µmol/l) – to prevent lymphatic and blood clearance - systemically administered significantly reduced SCs-derived tumor growth as TMZ-alone did in sensitive GB xenografts derived froms sensitive and differentiated cells. Moreover, at both dosages compound **1** did not elicit liver or kidney toxicity, and did not worsen the platelet reduction elicited by TMZ. *In silico,* analysis predicted a low delivery of compound **1** across the BBB. However the combination of compound **1** and TMZ significantly reduced tumor growth, decreased tumor cell proliferation, increased the intratumor apoptosis and the overall survival of mice with orthotopically implanted TMZ-refractory GB SCs-derived tumors. These data suggest an effective rescue of TMZ efficacy in tumors derived from primary GB that were completely unresponsive to TMZ treatment. These results may form the basis to undertake the preclinical validation of new combinatorial treatments including CAXII-inhibitors, TMZ and topoisomerase I/II inhibitors as effective treatments to eliminate GB SCs.

The compounds tested differ from direct Pgp inhibitors because they did not target the transporter but CAXII, a Pgp-adjuvant protein. CAXII protein is specifically expressed in tumor cells [Kivelä, 2000; Hynninen, 2006; Rafalko, 2010; Monti, 2013] and is usually poorly expressed in most healthy cells [Monti, 2013]. The use of CAXII inhibitors, to indirectly reduce Pgp activity, may provide a selective GB tumor-targeting approach when administered with standard chemotherapeutic drugs to patients with GB, resolving the problem of low specificity and side effects of other Pgp inhibitors [Callaghan, 2014].

Several strategies that increase the transport of anticancer drug across BBB and their delivery to GB based on PEGylated liposomes or BBB-targeting NPs are under intensive investigations [Fakhoury, 2016]. Here I proposed that the use of SLNs, functionalized with ApoE chimera peptide and loaded with ddMTX, the lipophilic ester of MTX, might increase the drug accumulation in the brain *in vivo* model. MTX, a chemotherapeutic agent that is widely used in pediatric neurooncology [Wolff, 2011], is difficult to entrap within SLNs because of its hydrophilicity, but the more lipophilic ddMTX can be easily loaded.

ddMTX-SLNs showed cytotoxic activity against primary human GB cultures and promising uptake by endothelial cells in artificial BBB model [Annovazzi, 2017]. *In vivo* models are more complex than *in vitro* models: biodistribution and clearance by reticuloendothelial system (RES) organs of systemically administered drug-delivery systems can actually influence the drug amount presenting to the BBB. To this aim, ApoE chimera peptide - able to bind the VLDL receptor anchored to the SLNs lipid surface - was used. The receptor-binding sequence in the chimera peptide [Nikanjam, 2007] corresponded to ApoE2, which is the main ligand for VLDL receptor. VLDL receptors are abundantly expressed in heart, muscle adipose tissue and brain, and are barely expressed in the liver, where LDL receptors are expressed abundantly [Takahashi, 2004]; consequently, even if not selectively specific for the brain, the VLDL receptor could be a good compromise to enhance brain accumulation of SLNs. From the biodistribution data obtained in healthy rats, the ApoE-conjugated formulation was more uptaken in brain respect to not functionalized-SLNs or free drug. However, no difference in brain uptake was revealed between healthy rats and glioma models, probably because particle size exceeds fenestrations of glioma altered BBB. The *in vivo* biodistribution of nanoparticles is influenced by different factors, such as size: nanoparticles smaller than 200 nm are considered to be able to exclude splenic filtration, and, if coated by hydrophilic polymers, to avoid opsonization; particles with size in the 200–500 nm range can avoid splenic filtration, owing to surface characteristics and deformability [Liu, 2012]. Long circulation of nanoparticles should be a key point for brain delivery, allowing a prolonged contact with endothelial cells. In this experimental work, 350 nm-diameter SLNs have been engineered. Although I did have not performed yet a pharmacokinetic study, from plasmatic concentrations obtained at 0.5 and 3 h in biodistribution experiments, it can be observed that ddMTX-loaded SLNs show increased plasmatic residence compared with free MTX; this can be probably ascribed to the use of SLNs as carrier and can contribute to brain accumulation.

The main goal obtained from these preliminary biodistribution experiments is the enhancement of drug brain accumulation by SLNs. Treatment with ddMTX-loaded SLNs ApoE resulted in a mean decrease of tumor volume growth and increase apoptosis, compared with control and oral TMZ, used as positive control, since it is the standard of care in chemotherapy of GB patient. Even if these data are not significant, SLNs functionalized with ApoE can be a good strategy to improve drug accumulation in the brain. They could be loaded with pharmacological treatment for brain tumors and other CNS diseases.

6. CONCLUSION AND FUTURE PERSPECTIVES

GB is the most malignant and frequent intra-assial tumor of the CNS and is very resistant to chemotherapy. This resistance is mainly due to GB-cancer SCs, which present high levels of ABC transporters, and to the BBB.

The presence of TJs and ABC transporters on the luminal side of BBB cells limits the delivery of drugs to the CNS. In patients affected by GB, BBB is often disrupted within GB bulk, but it is intact in the so called BAT area, reducing the efficacy of chemotherapy [Argawal, 2011].

Improving the BBB permeability to anticancer drugs is still an unsolved challenge. In my thesis, I approached this problem from different perspectives. After having clarified the molecular mechanism determining low drug permeability across BBB, I have tested some innovative strategy to improve the drug delivery across BBB and the targeting of GB SCs.

From the first part of my thesis, I may suggest the use of RhoAK inhbitors such as Fasudil as agent able to downregulate the Pgp expression and increase BBB permeability to Pgp substrate.

The second "paradoxical" strategy is TMZ, the GB first-line treatment, that acts as downregulator of the expression of Pgp at clinically achievable concentrations on BBB and GB SCs. TMZ, thus, is not only a potent anticancer drug, but also a Pgp chemosensitizers. This result suggests the use of TMZ in association with anticancer drug Pgp substrate to improve drug delivery across BBB and contributes to the eradication of GB SCs in the BAT area, where tumor cells lay surrounded by intact BBB.

GB induce BBB breakdown, but the molecular and cellular mechanisms underlying GB-induced disruption of the BBB are not clear yet. My GB/BBB co-culture system suggests that BBB undergoes alteration of its structure, upon the contact with GB cells and/or the release of soluble factors from the tumor. The grade of differentiation of GB cells influences the permeability of BBB cells at the tumor-BBB interface: differentiated cells produced a more important damage on BBB cells than SCs. Wnt3 modulates the expression of ABC transporters and tight junctions protein [Liebner , 2008] in BBB. Manipulating the expression of Wnt3a in GB differentiated cells and SCs, I found that Wnt3a may be a key actor in controlling BBB competence. Since Wnt3a is abundantly produced by GB SCs, this feature may explain the great difficulty encountered by chemotherapy to fully eradicate SC-enriched GB niches, surrounded by a less leaky BBB than GB rich of differentiated cells. This point is still open to investigations: to identify further soluble factors released by GB that may influence BBB permeability, I have performed a Multiplex screening of chemokines and cytokines and I am planning the analysis of secretome of SCs and differentiated cells in the BBB/GB co-culture system. I will then validate the role of each soluble factors identified by the two approaches, using blocking antibodies or gene silencing, and re-assessing the permeability to TJs- and ABC transporters substrates after these treatment. My final goal is to modulate the GB microenvironment (the so-called "niche") to improve the drug delivery across BBB and the consequent killing of tumor itself.

In the last part of my thesis, I suggested new strategies to improve drug delivery across BBB so that chemotherapeutic drug might reach a higher efficacy against GB, in particular agisnt GB SCs. I identified new compounds (thiosemicarbazone and CAXII inhbitors) and new formulations (ApoE-conjugated SLNs loaded with a chemotherapeutic drug) able to do that.

Thiosemicarbazones takes advantage from their chemical structures that allow them to inhibit Pgp at nanomolar concentration without development of cytotoxicity on BBB cells. Since both BBB and GB SCs are rich of Pgp, thiosemicarbazones can represent a safe and effective strategy to overcome Pgp-mediated chemoresistance and increase the panel of chemotherapeutic drugs

delivered to GB, in particular the drugs used as second-line treatment like topoisomerase I and II inhibitors.

I am now evaluating plasma stability and metabolism of these compounds, in order to plan their administration in preclinical models of orthotopically-implanted patient-derived GB.

Carbonic anidrase XII inhibitors are potent Pgp inhibitors that exploit a new Pgp-chemosensitizer mechanism: they target a Pgp-adjuvant protein, CAXII protein, which is specifically expressed in GB SCs. These molecules rescue TMZ efficacy, a substrate of Pgp itself, against orthotopically-implanted SC-rich GB refractory to the drug. These results may pave the way to the preclinical application of these molecules in combination with TMZ and other substrates of Pgp, such as topoisomerase I and II inhibitors, used as second-line treatment in GB. The use of CAXII inhibitors, to indirectly reduce Pgp activity, may provide a selective GB tumor-targeting approach when administered with standard chemotherapeutic drugs to patients with GB, solving the problem of low specificity and side effects of other Pgp inhibitors. Therein, after filing a patent on these compounds (Carbonic Anhydrase Inhibitors, n° 35100AU1-DMK, 2017 see patent pag.142), I am planning to expand the library of CAXII inhibitors as new drugs for the GB treatment, in particular for GB with a high component of SCs.

A second approach to improve the drug transport across BBB and increase the delivery to CNS is the optimization of the carriers. To this point, I employed SLNs, in particular SLNs-conjugated with ApoE chimeric peptide that are good carrier to cross BBB. From preliminary biodistribution experiments, these ApoE-SLNs loaded with ddMTX enhanced the drug brain accumulation *in vivo* and decreased the growth of tumor volume, suggesting that SLNs functionalized with ApoE can be a good strategy to improve drug accumulation in the brain.

Although the thesis was focused on the mechanisms underlying the low drug delivery across BBB to GB, in particular to GB SCs, mediated by the high expression of Pgp in BBB and GB SCs, the pharmacological strategies proposed to overcome this problem may not be limited to the improvement of GB treatment. Besides recognizing many chemotherapeutic drugs, Pgp limits the delivery to CNS of several analgesics, anti-inflammatory, antiviral and antiepileptic drugs. In a broader perspective, these compounds may find application in the pharmacological treatment of all those CNS diseases where Pgp represents an obstacle, including tumors, epilepsy and neurodegenerative diseases.

8. REFERENCES

Agarwal S, Hartz AM, Elmquist WF, Bauer B. Breast cancer resistance protein and P-glycoprotein in brain cancer: two gatekeepers team up. Curr Pharm Des. 2011;17(26):2793-802.

Akhtar N, Ahad A, Khar RK, Jaggi M, Aqil M, Iqbal Z, Ahmad FJ, Talegaonkar S.The emerging role of Pglycoprotein inhibitors in drug delivery: a patent review. Expert Opin Ther Pat. 2011 Apr;21(4):561-76.

Al-Abd AM, El-Dine RS, El-Halawany AM. P-glycoprotein inhibitors of natural origin as potential tumor chemo-sensitizers: A review. J Adv Res. 2015 Jan;6(1):45-62.

Alifieris C, Trafalis DT. Glioblastoma multiforme: pathogenesis and treatment. Aug;1(52):63-82.

Allen C, Srivastava K, Bayraktutan U. Small GTPase RhoA and its effector rho kinase mediate oxygen glucose deprivation-evoked in *vitro* cerebral barrier dysfunction. Stroke. 2010 Sep;41(9):2056-63.

Anjum K, Shagufta BI, Abbas SQ, Patel S, Khan I, Shah SAA, Akhter N, Hassan SSU. Current status and future therapeutic perspectives of glioblastoma multiforme (GBM) therapy: A review. Biomed Pharmacother. 2017 Aug;9 (2):681-689.

Ankit BS, Gadhwal AK, Sirohi P, Agrawal RP. Reply from Author. J Assoc Physicians India. 2014 Nov;62(11):76-7.

Annovazzi L, Schiffer D, Mellai M et al. Solid lipid nanoparticles loaded with antitumor lipophilic prodrugs aimed to glioblastoma treatment: preliminary studies on cultured cells. J. Nanosci. Nanotechnol 2017 in press.

Auffinger B, Spencer D, Pytel P, Ahmed AU, Lesniak M. The role of glioma stem cells in chemotherapy resistance and glioblastoma multiforme recurrence. Expert Rev Neurother. 2015;15(7):741-52.

Bai RY, Staedke V, Riggins GJ. Molecular targeting of GBM: drug discovery and therapies. Trends Mol Med. 2011 Jun;17(6):301-312.

Banks WA. From blood-brain barrier to blood-brain interface: new opportunities for CNS drug delivery. Nat Rev Drug Discov. 2016 Apr;15(4):275-92.

Bansal T, Akhtar N, Jaggi M, Khar RK, Talegaonkar S. Novel formulation approaches for optimising delivery of anticancer drugs based on P-glycoprotein modulation. Drug Discov Today. 2009 Nov;14(21-22):1067-74.

Bareiss S, Kim K, Lu Q. Delta-catenin/NPRAP: A new member of the glycogen synthase kinase-3beta signaling complex that promotes beta-catenin turnover in neurons..J Neurosci Res. 2010 Aug 15;88(11):2350-63.

Bauer F, Wanek T, Mairinger S, Stanek J, Sauberer M, Kuntner C, Parveen Z, Chiba P, Müller M, Langer O, Erker T. Interaction of HM30181 with P-glycoprotein at the murine blood-brain barrier assessed with positron emission tomography. Eur J Pharmacol. 2012 Dec 5;696(1-3):18-27.

Bauer M, Karch R, Zeitlinger M, Philippe C, Römermann K, Stanek J, Maier-Salamon A, Wadsak W, Jäger W, Hacker M, Müller M, Langer O. Approaching complete inhibition of P-glycoprotein at the human blood-brain barrier: an (R)-[^{11}C]verapamil PET study. J Cereb Blood Flow Metab. 2015 May;35(5):743-6.

Beier D, Schulz JB, Beier CP. Chemoresistance of glioblastoma cancer stem cells—much more complex than expected. Mol Cancer. 2011 Oct 11;10:128.

Bernardi H, Gay S, Fedon Y, Vernus B, Bonnieu A, Bacou F. Wnt4 activates the canonical β-catenin pathway and regulates negatively myostatin: functional implication in myogenesis. 2011 May;300(5):C1122-38.

Bianco J, Bastiancich C, Jankovski A, des Rieux A, Préat V, Danhier F. On glioblastoma and the search for a cure: where do we stand? Cell Mol Life Sci. 2017 Jul;74(13):2451-2466.

Brown TJ, Brennan MC, Li M, Church EW, Brandmeir NJ, Rakszawski KL, Patel AS, Rizk EB, Suki D, Sawaya R, Glantz M. Association of the extent of resection with survival in glioblastoma: a systematic review and meta-analysis. JAMA Oncol. 2016 Nov 1;2(11):1460-1469.

Caldera V, Mellai M, Annovazzi L, Piazzi A, Lanotte M, Cassoni P, Schiffer D. Antigenic and genotypic similarity primary GBMs and their derived neurospheres. J Oncol. 2011;2011:3(1): 4962.

Callaghan R, Luk F, Bebawy M. Inhibition of the multidrug resistance P-glycoprotein: time for a change of strategy? Drug Metab Dispos. 2014 Apr;42(4):623-31.

Carcaboso AM, Elmeliegy MA, Shen J, Juel SJ, Zhang ZM, Calabrese C, Tracey L, Waters CM, Stewart CF.Tyrosine kinase inhibitor gefitinib enhances topotecan penetration of gliomas. Cancer Res. 2010 Jun 1;70(11):4499-508.

Carlsson SK, Brothers SP, Wahlestedt C. Emerging treatment strategies for glioblastoma multiforme. EMBO Mol Med. 2014 Nov;6(11):1359-70.

Carvalho BF, Fernandes AC, Almeida DS, Sampaio LV, Costa A, Caeiro C, Osório L, Castro L, Linhares P, Damasceno M, Vaz RC. Second-Line Chemotherapy in Recurrent Glioblastoma: A 2-Cohort Study. Oncol Res Treat. 2015;38(7-8):348-54.

Chang CC, Lee PS, Chou Y, Hwang LL, Juan SH. Mediating effects of aryl-hydrocarbon receptor and RhoA in altering brain vascular integrity: the therapeutic potential of statins. Am J Pathol. 2012 Jul;181(1):211-21.

Chen Z, Shi T, Zhang L, Zhu P, Deng M, Huang C, Hu T, Jiang L, Li J. Mammalian drug efflux transporters of the ATP binding cassette(ABC) family in multidrug resistance: A review of the past decade. Cancer Lett. 2016 Jan 1;370(1):153-64.

Chikazawa N, Tanaka H, Tasaka T, Nakamura M, Tanaka M, Onishi H, Katano M. Inhibition of Wnt signaling pathway decreases chemotherapy-resistant side-population colon cancer cells. Anticancer Res. 2010 Jun;30(6):2041-8.

Corrêa S, Binato R, Du Rocher B, Castelo-Branco MT, Pizzatti L, Abdelhay E. Wnt/β-catenin pathway regulates ABCB1 transcription in chronic myeloid leukemia. BMC Cancer. 2012 Jul 23;12:303.

Dagıstan Y, Karaca I, Bozkurt ER, Ozar E, Yagmurlu K, Toklu A, Bilir A. Combinationhyperbaric oxygen and temozolomide therapy in c6 rat glioma model. Acta Cir Bras. 2012 Jun;27(6):383-7.

Dalmark M, Storm HH. A Fickian diffusion transport process with features of transport catalysis. Doxorubicin transport in human red blood cells. J Gen Physiol. 1981 Oct;78(4):349-64.

Das A, Banik NL, Ray SK. Modulatory effects of acetazolomide and dexamethasone on temozolomide-mediated apoptosis in human glioblastoma T98G and U87MG cells. Cancer Invest. 2008 May;26(4):352-8.

De Boo S, Kopecka J, Brusa D, Gazzano E, Matera L, Ghigo D, Bosia A, Riganti C. iNOS activity is necessary for the cytotoxic and immunogenic effects of doxorubicin in human colon cancer cells. Mol Cancer. 2009 Nov 19;8:108.

de Jesus Perez VA, Alastalo TP, Wu JC, Axelrod JD, Cooke JP, Amieva M, Rabinovitch M. Bone morphogenetic protein 2 induces pulmonary angiogenesis *via* Wnt-beta-catenin and Wnt-RhoA-Rac1 pathways. J Cell Biol. 2009 Jan 12;184(1):83-99.

Dean M, Fojo T, Bates S. Tumour stem cells and drug resistance. Nat Rev Cancer. 2005 Apr;5(4):275-84.

Dimitrijevic OB, Stamatovic SM, Keep RF, Andjelkovic AV.Effects of the chemokine CCL2 on blood-brain barrier permeability during ischemia-reperfusion injury. J Cereb Blood Flow Metab. 2006 Jun;26(6):797-810.

Dirks PB, Cancer: stem cells and brain tumours. Nature. 2006 Dec 7;444(7120):687-8.

Eldawoody H, Shimizu H, Kimura N, Saito A, Nakayama T, Takahashi A, Tominaga T. Fasudil, a Rho-kinase inhibitor, attenuates induction and progression of cerebral aneurysms: experimental study in rats using vascular corrosion casts. Neurosci Lett. 2010 Feb 5;470(1):76-80.

Ellor SV, Pagano-Young TA, Avgeropoulos NG. Glioblastoma: background, standard treatment paradigms, and supportive care considerations. J Law Med Ethics. 2014 Summer;42(2):171-82.

Eramo A, Ricci-Vitiani L, Zeuner A, Pallini R, Lotti F, Sette G, Pilozzi E, Larocca LM, Peschle C, De Maria R. Chemotherapy resistance of glioblastoma stem cells. Cell Death Differ. 2006 Jul;13(7):1238-41. Fakhoury M. Drug delivery approaches for the treatment of glioblastoma multiforme. Artif Cells Nanomed Biotechnol. 2016 Sep;44(6):1365-73.

Filatova A, Acker T, Garvalov BK. The cancer stem cell niche(s): the crosstalk between glioma stem cells and their microenvironment. Feb;1830(2):2496-508.

Flahaut M, Meier R, Coulon A, Nardou KA, Niggli FK, Martinet D, Beckmann JS, Joseph J-M, Muhlethaler-Mottet A, Gross N. The Wnt receptor FZD1 mediates chemoresistance in neuroblastoma through activation of the Wnt/b-catenin pathway. Oncogene. 2009 Jun 11;28(23):2245-56.

Fu L, Zhang C, Zhang LY, Dong SS, Lu LH, Chen J, Dai Y, Li Y, Kong KL, Kwong DL, Guan XY. Wnt2 secreted by tumor fibroblasts promotes tumor progression in oesophageal cancer by activation of the Wnt/β-catenin signaling pathway. Gut. 2011 Dec;60(12):1635-43.

Galli R, Binda E, Orfanelli U, Cipelletti B, Gritti A, De Vitis S, Fiocco R, Foroni C, Dimeco F, Vescovi A. Isolation and characterization of tumourigenic, stem-like neural precursors from human glioblastoma. Cancer Res. 2004 Oct 1;64(19):7011-21.

Glaser T, Han I, Wu L, Zeng X. Targeted nanotechnology in glioblastoma multiforme. Front Pharmacol. 2017 Mar 31;8:166

Goodwin AM, Sullivan KM, D'Amore PA. Cultured endothelial cells display endogenous activation of the canonical Wnt signaling pathway and express multiple ligands, receptors, and secreted modulators of Wnt signaling. Dev Dyn. 2006 Nov;235(11):3110-20.

Gottesman MM, Fojo T, Bates SE. Multidrug resistance in cancer: role of ATP-dependent transporters. Nat Rev Cancer. 2002 Jan;2(1):48-58.

Guillaume DJ, Doolittle ND, Gahramanov S, Hedrick NA, Delashaw JB, Neuwelt EA. Intra-arterial chemotherapy with osmotic blood-brain barrier disruption for aggressive oligodendroglial tumors: results of a phase I study. Neurosurgery. 2010 Jan;66(1):48-58.

Hau P, Fabel K, Baumgart U, Rümmele P, Grauer O, Bock A, Dietmaier C, Dietmaier W, Dietrich J, Dudel C, Hübner F, Jauch T, Drechsel E, Kleiter I, Wismeth C, Zellner A, Brawanski A, Steinbrecher A, Marienhagen J, Bogdahn U. Pegylated liposomal doxorubicin-efficacy in patients with recurrent high-grade glioma. Cancer. 2004 Mar 15;100(6):1199-207.

Hendricks BK, Cohen-Gadol AA, Miller JC. Novel delivery methods bypassing the blood-brain and blood-tumor barriers. Neurosurg Focus. 2015 Mar;38(3):E10.

Higgins CF, Callaghan R, Linton KJ, Rosenberg MF, Ford RC.Structure of the multidrug resistance P-glycoprotein. Semin Cancer Biol. 1997 Jun;8(3):135-42.

Hoelzinger DB, Demuth T, Berens ME. Autocrine factors that sustain glioma invasion and paracrine biology in the brain microenvironment. J Natl Cancer Inst. 2007 Nov 7;99(21):1583-93.

Hottinger AF, Stupp R, Homicsko K. Standards of care and novel approaches in the management of glioblastoma multiforme. Chin J Cancer. 2014 Jan;33(1):32-9.

Houghton PJ, Stewart CF, Cheshire PJ, Richmond LB, Kirstein MN, Poquette CA, Tan M, Friedman HS, Brent TP. Antitumor activity of temozolomide combined with irinotecan is partly independent of O6-methylguanine-DNA methyltransferase and mismatch repair phenotypes in xenograft models. Clin Cancer Res. 2000 Oct;6(10):4110-8.

Huang Z, Cheng L, Guryanova OA, Wu Q, Bao S. Cancer stem cells in glioblastomaemolecular signaling and therapeutic targeting. Protein Cell. 2010 Jul;1(7):638-55.

Hynninen P, Vaskivuo L, Saarnio J, Haapasalo H, Kivelä J, Pastoreková S, Pastorek J, Waheed A, Sly WS, Puistola U, Parkkila S. Expression of transmembrane carbonic anhydrases IX and XII in ovarian tumours. Histopathology. 2006; 49: 594-602.

Inda MM, Bonavia R, Seoane J. Glioblastoma multiforme: a look inside its heterogeneous nature, Cancers (Basel). 2014 Jan 27;6(1):226-39.

Ishihara H, Kubota H, Lindberg RL, Leppert D, Gloor SM, Errede M, Virgintino D, Fontana A, Yonekawa Y, Frei K. Endothelial cell barrier impairment induced by glioblastomas and transforming growth factor beta2 involves matrix metalloproteinases and tight junction proteins. J Neuropathol Exp Neurol. 2008 May;67(5):435-48.

Ito S, Woodland C, Sarkadi B, Hockmann G, Walker SE, Koren G. Modeling of P-glycoprotein-involved epithelial drug transport in MDCK cells. Am J Physiol. 1999 Jul;277(1 Pt 2):F84-96.

Jahangiri A, Chin AT, Flanigan PM, Chen R, Bankiewicz K, Aghi MK. Convection-enhanced delivery in glioblastoma: a review of preclinical and clinical studies. J Neurosurg. 2017 Jan;126(1):191-200.

Jain A, Jain A, Garg NK, Tyagi RK, Singh B, Katare OP, Webster TJ, Soni V.Surface engineered polymeric nanocarriers mediate the delivery of transferrin-methotrexate conjugates for an improved understanding of brain cancer. Acta Biomater. 2015 Sep;24:140-51.

Jiang P, Mukthavaram R, Chao Y, Bharati IS, Fogal V, Pastorino S, Cong X, Nomura N, Gallagher M, Abbasi T, Vali S, Pingle SC, Makale M, Kesari S. Novel anti-glioblastoma agents and therapeutic combinations identified from a collection of FDA approved drugs. J Transl Med. 2014 Jan 17;12:13.
Jope RS, Johnson GV. The glamour and gloom of glycogen synthase kinase-3. Trends Biochem Sci. 2004 Feb;29(2):95-102.

Jue TR, McDonald KL. The challenges associated with molecular targeted therapies for glioblastoma. J Neurooncol. 2016 May;127(3):427-34.

Juliano RL, Ling V. A surface glycoprotein modulating drug permeability in Chinese hamster ovary cell mutants. Biochim Biophys Acta. 1976 Nov 11;455(1):152-6

Kania KD, Wijesuriya HC, Hladky SB, Barrand MA. Beta amyloid effects on expression of multidrug efflux transporters in brain endothelial cells. Brain Res. 2011 Oct 18;1418:1-11.

Kanzawa T, Germano IM, Komata T, Ito H, Kondo Y, Kondo S. Role of autophagy in temozolomide-induced cytotoxicity for malignant glioma cells. Cell Death Differ. 2004 Apr;11(4):448-57.

Karim R, Palazzo C, Evrard B, Piel G. Nanocarriers for the treatment of glioblastoma multiforme: Current state-of-the-art. J Control Release. 2016 Apr 10;227:23-37.

Katoh M, Katoh M. WNT signaling pathway and stem cell signaling network. Clin Cancer Res. 2007 Jul 15;13(14):4042-5.

Kim SS, Harford JB, Pirollo KF, Chang EH. Effective treatment of glioblastoma requires crossing the blood-brain barrier and targeting tumors including cancer stem cells: the promise of nanomedicine. Biochem Biophys Res Commun. 2015 Dec 18;468(3):485-9.

Kivelä A, Parkkila S, Saarnio J, Karttunen TJ, Kivelä J, Parkkila AK, Waheed A, Sly WS, Grubb JH, Shah G, Türeci O, Rajaniemi H. Expression of a novel transmembrane carbonic anhydrase isozyme XII in normal human gut and colorectal tumors. Am J Pathol. 2000; 156: 577-584.

Kobune M, Chiba H, Kato J, Kato K, Nakamura K, Kawano Y, Takada K, Takimoto R, Takayama T, Hamada H, Niitsu Y. Wnt3/RhoA/ROCK signaling pathway is involved in adhesion-mediated drug resistance of multiple myeloma in an autocrine mechanism. Mol Cancer Ther. 2007 Jun;6(6):1774-84.

Kopecka J, Campia I, Jacobs A, Frei AP, Ghigo D, Wollscheid B, Riganti C. Carbonic anhydrase XII is a new therapeutic target to overcome chemoresistance in cancer cells. Oncotarget. 2015 Mar 30;6(9):6776-93.

Kopecka J, Campia I, Olivero P, Pescarmona G, Ghigo D, Bosia A, Riganti C. A LDL-masked liposomal-doxorubicin reverses drug resistance in human cancer cells. J Control Release. 2011 Jan 20;149(2):196-205.

Kopecka J, Rankin GM, Salaroglio IC, Poulsen SA, Riganti C. P-glycoprotein-mediated chemoresistance is reversed by carbonic anhydrase XII inhibitors. Oncotarget. 2016 Dec 27;7(52):85861-85875.

Liebner S, Corada M, Bangsow T, Babbage J, Taddei A, Czupalla CJ, Reis M, Felici A, Wolburg H, Fruttiger M, Taketo MM, von Melchner H, Plate KH, Gerhardt H, Dejana E. Wnt/beta-catenin signaling controls development of the blood-brain barrierJ Cell Biol. 2008 Nov 3;183(3):409-17.

Lim JC, Kania KD, Wijesuriya H, Chawla S, Sethi JK, Pulaski L, Romero IA, Couraud PO, Weksler BB, Hladky SB, Barrand MA. Activation of β-catenin signaling by GSK-3 inhibition increases p-glycoprotein expression in brain endothelial cells. J Neurochem. 2008 Aug;106(4):1855-65.

Liu HL, Hua MY, Chen PY, Chu PC, Pan CH, Yang HW, Huang CY, Wang JJ, Yen TC, Wei KC. Blood-brain barrier disruption with focused ultrasound enhances delivery of chemotherapeutic drugs for glioblastoma treatment. Radiology. 2010 May;255(2):415-25.

Liu J, Zhang Y, Xu R, Du J, Hu Z, Yang L, Chen Y, Zhu Y, Gu L. PI3K/Akt-dependent phosphorylation of GSK3b and activation of RhoA regulate Wnt5a-induced gastric cancer cell migration. Cell Signal. 2013 Feb;25(2):447-56.

Liu Y, Lu W. Recent advances in brain tumor-targeted nano-drug delivery systems. Expert Opin Drug Deliv. 2012 Jun;9(6):671-86.

Lopez KA, Tannenbaum AM, Assanah MC, Linskey K, Yun J, Kangarlu A, Gil OD, Canoll P, Bruce JN. Convection-enhanced delivery of topotecan into a PDGF-driven model of glioblastoma prolongs survival and ablates both tumor-initiating cells and recruited glial progenitors. Cancer Res. 2011 Jun 1;71(11):3963-71.

Löscher W, Potschka H. Drug resistance in brain diseases and the role of drug efflux transporters. Nat Rev Neurosci. 2005 Aug;6(8):591-602.

Man J, Shoemake JD, Ma T, Rizzo AE, Godley AR, Wu Q, Mohammadi AM, Bao S, Rich JN, Yu JS. Hyperthermia sensitizes glioma stem-like cells to radiation by inhibiting AKT signaling. Cancer Res. 2015 Apr 15;75(8):1760-9.

Mendes B, Marques C, Carvalho I, Costa P, Martins S, Ferreira D, Sarmento B. Influence of glioma cells on a new co-culture in *vitro* blood-brain barrier model for characterization and validation of permeability. Int J Pharm. 2015 Jul 25;490(1-2):94-101.

Miranda A, Blanco-Prieto M, Sousa J, Pais A, Vitorino C. Breaching barriers in glioblastoma. Part I: Molecular pathways and novel treatment approaches. Int J Pharm. 2017 Oct 5;531(1):372-388.

Mita MM, Natale RB, Wolin EM, Laabs B, Dinh H, Wieland S, Levitt DJ, Mita AC. Pharmacokinetic study of aldoxorubicin in patients with solid tumors. Invest New Drugs. 2015 Apr;33(2):341-8.

Mobasher MA, González-Rodriguez A, Santamaría B, Ramos S, Martín MÁ, Goya L, Rada P, Letzig L, James LP, Cuadrado A, Martín-Pérez J, Simpson KJ, Muntané J, Valverde AM. Protein tyrosine phosphatase 1B modulates GSK3b/Nrf2 and IGFIR signaling pathways in acetaminophen-induced hepatotoxicity. Cell Death Dis. 2013 May 9;4:e626.

Moeslein FM, Myers MP, Landreth GE. The CLK family kinases, CLK1 and CLK2, phosphorylate and activate the tyrosine phosphatase, PTP-1B. J Biol Chem. 1999 Sep 17;274(38):26697-704.

Moghimi SM, Hunter AC, Murray JC. Long-circulating and target-specific nanoparticles: theory to practice. Pharmacol Rev. 2001 Jun;53(2):283-318.

Moghimi SM, Porter CJ, Muir IS, Illum L, Davis SS.Non-phagocytic uptake of intravenously injected microspheres in rat spleen: influence of particle size and hydrophilic coating. Biochem Biophys Res Commun. 1991 Jun 14;177(2):861-6.

Monnaert V, Betbeder D, Fenart L, Bricout H, Lenfant AM, Landry C, Cecchelli R, Monflier E, Tilloy S. Effects of γ- and hydroxy propyl- γ -cyclodextrins on the transport of doxorubicin across an in *vitro* model of blood–brain barrier. J Pharmacol Exp Ther. 2004 Dec;311(3):1115-20.

Monti SM, Supuran CT, De Simone G. Anticancer carbonic anhydrase inhibitors: a patent review (2008 - 2013). Expert Opin Ther Pat. 2013;23(6):737-49.

Montine KS, Bassett CN, Ou JJ, Markesbery WR, Swift LL, Montine TJ. Apolipoprotein E allelic influence on human cerebrospinal fluid apolipoproteins. J Lipid Res. 1998 Dec;39(12):2443-51.

Morris JC, Chiche J, Grellier C, Lopez M, Bornaghi LF, Maresca A, Supuran CT, Pouysségur J, Poulsen SA. Targeting hypoxic tumor cell viability with carbohydrate-based carbonic anhydrase IX and XII inhibitors. J Med Chem. 2011; 54:6905–6918

Moura JA, Valduga CJ, Tavares ER, Kretzer IF, Durvanei, Maranhão MRC. Novel formulation of a methotrexate derivative with a lipid nanoemulsion. Int J Nanomedicine. 2011;6:2285-95.

Mujumdar P, Teruya K, Tonissen KF, Vullo D, Supuran CT, Peat TS, Poulsen SA. An unusual natural product primary sulfonamide: synthesis, carbonic anhydrase inhibition, and protein X-ray structures of Psammaplin C. J Med Chem. 2016 Jun 9;59(11):5462-70.

Munoz JL, Walker ND, Scotto KW, Rameshwar P. Temozolomide competes for P-glycoprotein and contributes to chemoresistance in glioblastoma cells. Cancer Lett. 2015 Oct 10;367(1):69-75.

Nakai E, Park K, Yawata T, Chihara T, Kumazawa A, Nakabayashi H, Shimizu K. Enhanced MDR1 expression and chemoresistance of cancer stem cells derived from glioblastoma. Cancer Invest. 2009 Nov;27(9):901-8.

Nelson JA, Harris BA, Decker WJ, Farquhar D. Analysis of methotrexate in human plasma by high-pressure liquid chromatography with fluorescence detection. Cancer Res.1977; 37, 3970–3973.

Nikanjam M, Gibbs AR, Hunt CA, Budinger TF, Forte TM. Synthetic nano-LDL with paclitaxel oleate as a targeted drug delivery vehicle for glioblastoma multiforme. J Control Release. 2007 Dec 20;124(3):163-71. Epub 2007 Sep 26.

Nishioku T, Matsumoto J, Dohgu S, Sumi N, Miyao K, Takata F, Shuto H, Yamauchi A, Kataoka Y. Tumor necrosis factor-alpha mediates the blood-brain barrier dysfunction induced by activated microglia in mouse brain microvascular endothelial cells. J Pharmacol Sci. 2010;112(2):251-4.

Obach RS. Prediction of human clearance of twenty-nine drugs from hepatic microsomal intrinsic clearance data: An examination of in *vitro* half-life approach and nonspecific binding to microsomes. Drug Metab Dispos. 1999 Nov;27(11):1350-9

Ogunshola OO. In *vitro* modeling of the blood-brain barrier: simplicity *versus* complexity. Curr Pharm Des. 2011;17(26):2755-61.

Panigrahi M, Das PK, Parikh PM. Brain tumor and Gliadel wafer treatment Indian J Cancer. 2011 Jan-Mar;48(1):11-7.

Parhi P, Mohanty C, Sahoo SK. Nanotechnology-based combinational drug delivery: an emerging approach for cancer therapy. Drug Discov Today. 2012 Sep;17(17-18):1044-52.

Pati ML, Niso M, Ferorelli S, Abate C, Berardia F. Novel metal chelators thiosemicarbazones with activity at the σ2 receptors and P-glycoprotein: an innovative strategy for resistant tumor treatment. RSC Adv., 2015,5, 103131 –103146.

Peer D, Karp JM, Hong S, Farokhzad OC, Margalit R, Langer R. Nanocarriers as an emerging platform for cancer therapy. Nat Nanotechnol. 2007 Dec;2(12):751-60.

Peters KB, Lou E, Desjardins A, Reardon DA, Lipp ES, Miller E, Herndon JE 2nd, McSherry F, Friedman HS, Vredenburgh JJ. Phase II Trial of upfront bevacizumab, irinotecan, and temozolomide for unresectable glioblastoma. Oncologist. 2015 Jul;20(7):727-8.

Ping YF, Yao XH, Jiang JY, Zhao LT, Yu SC, Jiang T, Lin MC, Chen JH, Wang B, Zhang R, Cui YH, Qian C, Wang Jm, Bian XW. The chemokine CXCL12 and its receptor CXCR4 promote glioma stem cell-mediated VEGF production and tumour angiogenesis via PI3K/AKT signaling. J Pathol. 2011 Jul;224(3):344-54.

Pinzón-Daza M, Garzón R, Couraud P, Romero Ia, Weksler B, Ghigo D, Bosia A, Riganti C. The association of statins plus LDL receptor-targeted liposome-encapsulated doxorubicin increases in *vitro* drug delivery across blood-brain barrier cells. Br J Pharmacol. 2012 Dec;167(7):1431-47.

Pinzón-Daza ML, Campia I, Kopecka J, Garzón R, Ghigo D, Riganti C. Nanoparticle- and liposome-carried drugs: new strategies for active targeting and drug delivery across blood-brain barrier. Curr Drug Metab. 2013 Jul;14(6):625-40.

Plowman J, Waud WR, Koutsoukos AD, Rubinstein LV, Moore TD, Grever MR. Preclinical antitumor activity of temozolomide in mice: efficacy against human brain tumor xenografts and synergism with 1,3-bis(2-chloroethyl)-1-nitrosourea. Cancer Res. 1994 Jul 15;54(14):3793-9.

Poller B, Drewe J, Krähenbühl S, Huwyler J, Gutmann H. Regulation of BCRP (ABCG2) and P-glycoprotein (ABCB1) by cytokines in a model of the human blood-brain barrier. Cell Mol Neurobiol. 2010 Jan;30(1):63-70.

Portnow J, Badie B, Chen M, Liu A, Blanchard S, Synold TW. The neuropharmacokinetics of temozolomide in patients with resectable brain tumors: potential implications for the current approach to chemoradiation. Clin Cancer Res. 2009 Nov 15;15(22):7092-8.

Portnow J, Badie B, Chen M, Liu A, Blanchard S, Synold TW. The neuro-pharmacokinetics of temozolomide in patients with resectable brain tumors: potential implications for the current approach to chemoradiation. Clin Cancer Res. 2009 Nov 15;15(22):7092-8.

Pourgholi F, Hajivalili M, Farhad JN, Kafil HS, Yousefi M. Nanoparticles novel vehicles in treatment of glioblastoma. Biomed Pharmacother. 2016 Feb;77:98-107.

Qu Q, Chu JW, Sharom FJ. Transition state P-glycoprotein binds drugs and modulators with unchanged affinity, suggesting a concerted transport mechanism. Biochemistry. 2003 Feb 11;42(5):1345-53.

Rafalko A, Iliopoulos O, Fusaro VA, Hancock W, Hincapie M. Immunoaffinity enrichment and liquid chromatography-selected reaction monitoring mass spectrometry for quantitation of carbonic anhydrase 12 in cultured renal carcinoma cells. Anal Chem. 2010 Nov 1;82(21):8998-9005.

Rape A, Ananthanarayanan B, Kumar S. Engineering strategies to mimic the glioblastoma microenvironment. Adv Drug Deliv Rev. 2014 Dec 15;79-80:172-83.

Reynés G, Martínez-Sales V, Vila V, Balañá C, Pérez-Segura P, Vaz MA, Benavides M, Gallego O, Palomero I, Gil-Gil M, Fleitas T, Reche E. Phase II trial of irinotecan and metronomic temozolomide in patients with recurrent glioblastoma. Anticancer Drugs. 2016 Feb;27(2):133-7.

Riganti C, Salaroglio I, Caldera V, Campia I, Kopecka J, Mellai M, Annovazzi L, Bosia A, Ghigo D, Schiffer D. (2013) Temozolomide downregulates P-glycoprotein expression in glioblastoma stem cells by interfering with the Wnt3a/glycogen synthase-3 kinase/β-catenin pathway. Neuro Oncol. 2013 Nov;15(11):1502-17.
Riganti C, Salaroglio IC, Pinzòn-Daza ML, Caldera V, Campia I, Kopecka J, Mellai M, Annovazzi L, Couraud PO, Bosia A, Ghigo D, Schiffer D. Temozolomide downregulates P-glycoprotein in human blood-brain barrier cells by disrupting Wnt3 signaling. Cell Mol Life Sci. 2014 Feb;71(3):499-516.

Ring BJ, Chien JY, Adkison KK, Jones HM, Rowland M, Jones RD, Yates JW, Ku MS, Gibson CR, He H, Vuppugalla R, Marathe P, Fischer V, Dutta S, Sinha VK, Björnsson T, Lavé T, Poulin P. PhRMA CPCDC

initiative on predictive models of human pharmacokinetics, part 3: comparative assessement of prediction methods of human clearance. J Pharm Sci. 2011 Oct;100(10):4090-110.

Roggendorf W, Strupp S, Paulus W. Distribution and characterization of microglia/macrophages in human brain tumors. Acta Neuropathol. 1996 Sep;92(3):288-93.

Roos A, Ding Z, Loftus JC, Tran NL. Molecular and microenvironmental determinants of glioma stem-like cell survival and invasion. Front Oncol. 2017 Jun 16;7:120.

Rosowsky A, Forsch RA, Yu CS, Lazarus H, Beardsley GP. Methotrexate analogues. 21. Divergent influence of alkyl chain length on the dihydrofolate reductase affinity and cytotoxicity of methotrexate monoesters. J Med Chem. 1984 May;27(5):605-9.

Rossol-Allison J, Stemmle LN, Swenson-Fields KI, Kelly P, Fields PE, McCall SJ, Casey PJ, Fields TA. Rho GTPase activity modulates Wnt3a/beta-catenin signaling. Cell Signal. 2009 Nov;21(11):1559-68.

Salmaggi A, Boiardi A, Gelati M, Russo A, Calatozzolo C, Ciusani E, Sciacca FL, Ottolina A, Parati EA, La Porta C, Alessandri G, Marras C, Croci D, De Rossi M. Glioblastoma-derived tumorospheres identify a population of tumor stem-like cells with angiogenic potential and enhanced multidrug resistance phenotype. Glia. 2006 Dec;54(8):850-60.

Saneja A, Khare V, Alam N, Dubey RD, Gupta PN. Advances in P-glycoprotein-based approaches for delivering anticancer drugs: pharmacokinetic perspective and clinical relevance. Expert Opin Drug Deliv. 2014 Jan;11(1):121-38.

Schaich M, Kestel L, Pfirrmann M, Robel K, Illmer T, Kramer M, Dill C, Ehninger G, Schackert G, Krex D. A MDR1 (ABCB1) gene single nucleotide polymorphism predicts outcome of temozolomide treatment in GBM patients. Ann Oncol. 2009 Jan;20(1):175-81.

Schiffer D, Annovazzi L, Mazzucco M, Mellai M. The Microenvironment in Gliomas: Phenotypic Expressions. Cancers (Basel). 2015 Dec 3;7(4):2352-9.

Schneider SW, Ludwig, Tatenhorst L, Braune S, Oberleithner H, Senner V, Paulus W. Glioblastoma cells release factors that disrupt blood-brain barrier features Acta Neuropathol (2004) 107 : 272–276.

Schwartzbaum JA, Fisher JL, Aldape KD, Wrensch M. Epidemiology and molecular pathology of glioma. Nat Clin Pract Neurol. 2006 Sep;2(9):494-503.

Séhédic D, Cikankowitz A, Hindré F, Davodeau F, Garcion E. Feature review nanomedicine to overcome radioresistance in glioblastoma stem-like cells and surviving clones. Trends Pharmacol Sci. 2015 Apr;36(4):236-52.
Seidel S, Garvalov BK, Wirta V, von Stechow L, Schänzer A, Meletis K, Wolter M, Sommerlad D, Henze AT, Nistér M, Reifenberger G, Lundeberg J, Frisén J, Acker T. A hypoxic niche regulates glioblastoma stem cells through hypoxia inducible factor 2 alpha. Brain. 2010 Apr;133(Pt 4):983-95.

Serwer LP, James CD. Challenges in drug delivery to tumors of the central nervous system: an overview of pharmacological and surgical considerations. Adv Drug Deliv Rev. 2012 May 15;64(7):590-7.

Shen DY, Zhang W, Zeng X, Liu CQ. Inhibition of Wnt/β-catenin signaling downregulates P-glycoprotein and reverses multi-drug resistance of cholangiocarcinoma. Cancer Sci. 2013 Oct;104(10):1303-8.

Shin HK, Huang PL, Ayata C. Rho-kinase inhibition improves ischemic perfusion deficit in hyperlipidemic mice. J Cereb Blood Flow Metab. 2014 Feb;34(2):284-7.

Siflinger-Birnboim A, Del Vecchio PJ, Cooper JA, Blumenstock FA, Shepard JM, Malik AB. Molecular sieving characteristics of the cultured endothelial monolayer. J Cell Physiol. 1987 Jul;132(1):111-7.

Smoll NR, Schaller K, Gautschi OP. Long-term survival of patients with glioblastoma multiforme (GBM) J Clin Neurosci. 2013 May;20(5):670-5.

Stupp R, Hegi ME, Neyns B, Goldbrunner R, Schlegel U, Clement PM, Grabenbauer GG, Ochsenbein AF, Simon M, Dietrich PY, Pietsch T, Hicking C, Tonn JC, Diserens AC, Pica A, Hermisson M, Krueger S, Picard M, Weller M. Phase I/IIa study of cilengitide and temozolomide with concomitant radiotherapy followed by cilengitide and temozolomide maintenance therapy in patients with newly diagnosed glioblastoma. J Clin Oncol. 2010 Jun 1;28(16):2712-8. Epub 2010 May 3.

Stupp R, Taillibert S, Kanner AA, Kesari S, Steinberg DM, Toms SA, Taylor LP, Lieberman F, Silvani A, Fink KL, Barnett GH, Zhu JJ, Henson JW, Engelhard HH, Chen TC, Tran DD, Sroubek J, Tran ND, Hottinger AF, Landolfi J, Desai R, Caroli M, Kew Y, Honnorat J, Idbaih A, Kirson ED, Weinberg U, Palti Y, Hegi ME, Ram Z. Maintenance therapy with tumor-treating fields plus temozolomide vs temozolomide alone for glioblastoma: a randomized clinical trial. JAMA. 2015 Dec 15;314(23):2535-43.

Szakács G, Hall MD, Gottesman MM, Boumendjel A, Kachadourian R, Day BJ, Baubichon-Cortay H, Di Pietro A.Targeting the Achilles heel of multidrug-resistant cancer by exploiting the fitness cost of resistance. Chem Rev. 2014 Jun 11;114(11):5753-74.

Tai LM, Loughlin AJ, Male DK, Romero IA. P-glycoprotein and breast cancer resistance protein restrict apical-to-basolateral permeability of human brain endothelium to amyloid-β. J Cereb Blood Flow Metab. 2009 Jun;29(6):1079-83.

Takada T, Takata K, Ashihara E. Inhibition of monocarboxylate transporter 1 suppresses the proliferation of glioblastoma stem cells. J Physiol Sci. 2016 Sep;66(5):387-96.

Takahashi S, Sakai J, Fujino T, Hattori H, Zenimaru Y, Suzuki J, Miyamori I, Yamamoto TT. The very low-density lipoprotein (VLDL) receptor: characterization and functions as a peripheral lipoprotein receptor. J Atheroscler Thromb. 2004;11(4):200-8.

Thakkar JP, Dolecek TA, Horbinski C, Ostrom QT, Lightner DD, Barnholtz-Sloan, JS, Villano JL. Epidemiologic and molecular prognostic review of glioblastoma. Cancer Epidemiol Biomarkers Prev. 2014 Oct;23(10):1985-96.

Tolcher AW, Gerson SL, Denis L, Geyer C, Hammond LA, Patnaik A, Goetz AD, Schwartz G, Edwards T, Reyderman L, Statkevich P, Cutler DL, Rowinsky EK. Marked inactivation of O6-alkylguanine-DNA alkyltransferase activity with protracted temozolomide schedules. 2003 Apr 7;88(7):1004-11.

Tonder M, Weller M, Eisele G, Roth P. Carboplatin and Etoposide in Heavily Pretreated Patients with Progressive High-Grade Glioma. Chemotherapy. 2014;60(5-6):375-8.

Triguero D, Buciak J Pardridge WM. Capillary depletion method for quantification of blood–brain barrier transport of circulating peptides and plasma proteins. J Neurochem. 1990 Jun;54(6):1882-8.

Urbanska K, Sokołowska J, Szmidt M, Sysa P. Glioblastoma multiforme – an overview. Contemp Oncol (Pozn). 2014;18(5):307-12.

Uribe D, Torres Á, Rocha JD, Niechi I, Oyarzún C, Sobrevia L, San Martín R, Quezada C. Multidrug resistance in glioblastoma stem-like cells: Role of the hypoxic microenvironment and adenosine signaling. Mol Aspects Med. 2017 Jun;55:140-151.

van Tellingen O, Yetkin-Arik B, de Gooijer MC, Wesseling P, Wurdinger T, de Vries HE. Overcoming the blood–brain tumor barrier for effective glioblastoma treatment.Drug Resist Updat. 2015 Mar;19:1-12.

Vandenhaute E, Drolez A, Sevin E, Gosselet F, Mysiorek C, Dehouck MP. Adapting coculture in *vitro* models of the blood-brain barrier for use in cancer research: maintaining an appropriate endothelial monolayer for the assessment of transendothelial migration. Lab Invest. 2016 May;96(5):588-98.

Vogelbaum MA, Aghi MK. Convection-enhanced delivery for the treatment of glioblastoma. Neuro Oncol. 2015 Mar;17 Suppl 2:ii3-ii8.

Voigt N, Henrich-Noack P, Kockentiedt S, Hintz W, Tomas J, Sabel BA.Surfactants, not size or zeta-potential influence blood-brain barrier passage of polymeric nanoparticles. Eur J Pharm Biopharm. 2014 May;87(1):19-29.

Vredenburgh JJ, Desjardins A, Reardon DA, Peters KB, Herndon JE 2nd, Marcello J, Kirkpatrick JP, Sampson JH, Bailey L, Threatt S, Friedman AH, Bigner DD, Friedman HS. The addition of bevacizumab to standard radiation therapy and temozolomide followed by bevacizumab, temozolomide, and irinotecan for newly diagnosed glioblastoma. Clin Cancer Res. 2011 Jun 15;17(12):4119-24.

Wei J, Barr J, Kong LY, Wang Y, Wu A, Sharma AK, Gumin J, Henry V, Colman H, Sawaya R, Lang FF, Heimberger AB. Glioma-associated cancer-initiating cells induce immunosuppression. Clin Cancer Res. 2010 Jan 15;16(2):461-73.

Wei J, Wu A, Kong LY, Wang Y, Fuller G, Fokt I, Melillo G, Priebe W, Heimberger AB. Hypoxia potentiates glioma-mediated immunosuppression. PLoS One. 2011 Jan 20;6(1):e16195.
Weisgraber KH, Shinto LH. Identification of the disulfidelinked homodimer of apolipoprotein E3 in plasma. Impact on receptor binding activity. J Biol Chem. 1991 Jun 25;266(18):12029-34.

Weksler BB, Subileau EA, Perrière N, Charneau P, Holloway K, Leveque M, Tricoire-Leignel H, Nicotra A, Bourdoulous S, Turowski P, Male DK, Roux F, Greenwood J, Romero IA, Couraud PO. Blood-brain barrier-specific properties of a human adult brain endothelial cell line. FASEB J. 2005 Nov;19(13):1872-4.

Whittle JR, Lickliter JD, Gan HK, Scott AM, Simes J, Solomon BJ, MacDiarmid JA, Brahmbhatt H, Rosenthal MA. First in human nanotechnology doxorubicin delivery system to target epidermal growth factor receptors in recurrent glioblastoma. J Clin Neurosci. 2015 Dec;22(12):1889-94.

Wick W, Platten M, Weller M. New (alternative) temozolomide regimens for the treatment of glioma. Neuro Oncol. 2009 Feb;11(1):69-79.

Wilhelm I, Fazakas C, Krizbai IA. In *vitro* models of the blood-brain barrier. Acta Neurobiol Exp (Wars). 2011;71(1):113-28.

Wolff JE, Kortmann RD, Wolff B, Pietsch T, Peters O, Schmid HJ, Rutkowski S, Warmuth-Metz M, Kramm C. High dose methotrexate for pediatric high grade glioma: results of the HIT-GBM-D pilot study. J Neurooncol. 2011 May;102(3):433-42.

Wong HL, Bendayan R., Rauth AM, Li Y, Wu XY. Chemotherapy with anticancer drugs encapsulated in solid lipid nanoparticles. Adv Drug Deliv Rev. 2007 Jul 10;59(6):491-504. Epub 2007 May 1.

Wu A, Wei J, Kong LY, Wang Y, Priebe W, Qiao W, Sawaya R, Heimberger AB. Glioma cancer stem cells induce immunosuppressive macrophages/microglia. Neuro Oncol. 2010 Nov;12(11):1113-25.

Wyne KL, Pathak RK, Seabra MC, Hobbs HH. Expression of the VLDL receptor in endothelial cells. Arterioscler Thromb Vasc Biol. 1996 Mar;16(3):407-15.

Yamada R, Nakano I. Glioma stem cells: their role in chemoresistance.World Neurosurg. 2012 Feb;77(2):237-40.

Yang L, Guo G, Niu XY, Liu J, Dendritic cell-based immunotherapy treatment for glioblastoma multiforme. Biomed Res Int. 2015;2015:717530.

Yi Y, Hsieh IY, Huang X, Li J, Zhao W. Glioblastoma stem-lke cells: characteristics, microenvironment, and therapy. Front Pharmacol. 2016 Dec 7;7:477.

Yoshida GJ. Therapeutic strategies of drug repositioning targeting autophagy to induce cancer cell death: from pathophysiology to treatment. J Hematol Oncol. 2017 Mar 9;10(1):67.

Yu Liu, Weiyue Lu. Recent advances in brain tumor-targeted nano-drug delivery systems Expert Opin Drug Deliv. 2012 Jun;9(6):671-86.

Zhang R, Saito R, Shibahara I, Sugiyama, S, Kanamori M, Sonoda Y, Tominaga T. Temozolomide reverses doxorubicin resistance by inhibiting P-glycoprotein in malignant glioma cells. J Neurooncol. 2016 Jan;126(2):235-42.

Zhu TS, Costello MA, Talsma CE, Flack CG, Crowley JG, Hamm LL, He X, Hervey-Jumper SL, Heth JA, Muraszko KM, DiMeco F, Vescovi AL, Fan X. Endothelial cells create a stem cell niche in glioblastoma by providing NOTCH ligands that nurture self-renewal of cancer stem-like cells. Cancer Res. 2011 Sep 15;71(18):6061-72.

Zoerle T, Ilodigwe DC, Wan H, Lakovic K, Sabri M, Ai J, Macdonald RL. Pharmacologic reduction of angiographic vasospasm in experimental subarachnoid hemorrhage: systematic review and meta-analysis. J Cereb Blood Flow Metab. 2012 Sep;32(9):1645-58.

9. LIST OF PUBLICATIONS

1) Riganti C, Lingua MF, **Salaroglio IC**, Falcomatà C, Righi L, Morena D, Picca F, Oddo D, Kopecka J, Pradotto M, Libener R, Orecchia S, Bironzo P, Comunanza V, Bussolino F, Novello S, Scagliotti GV, Di Nicolantonio F, Taulli R. Bromodomain inhibition exerts its therapeutic potential in malignant pleural mesothelioma by promoting immunogenic cell death and changing the tumor immune-environment. Oncoimmunology. 2017 Nov 27. e1398874. 10.1080/2162402X.2017.1398874 *(IF = 7.719)*

2) Gazzano E, Rolando B, Chegaev K, **Salaroglio IC**, Kopecka J, Pedrini I, Saponara S, Sorge M, Buondonno I, Stella B, Marengo A, Valoti M, Brancaccio M, Fruttero R, Gasco A, Arpicco S, Riganti. Folate-targeted liposomal nitrooxy-doxorubicin: an effective tool against P-glycoprotein-positive and folate receptor-positive tumors. J Control Release. 2017 Nov 27. pii: S0168-3659(17)31049-0. doi: 10.1016/j.jconrel.2017.11.042. *(IF = 7.786)*

3) **Salaroglio IC**, Panada E, Moiso E, Buondonno I, Provero P, Rubinstein M, Kopecka J, Riganti C. PERK induces resistance to cell death elicited by endoplasmic reticulum stress and chemotherapy. Mol Cancer. 2017 May 12;16(1):91. doi: 10.1186/s12943-017-0657-0. *(IF = 6.202)*

4) Battaglia L, Muntoni E, Chirio D, Peira E, Annovazzi L, Schiffer D, Mellai M, Riganti C, **Salaroglio IC**, Lanotte M, Panciani P, Capucchio MT, Valazza A, Biasibetti E, Gallarate M. Solid lipid nanoparticles by coacervation loaded with a methotrexate prodrug: preliminary study for glioma treatment. Nanomedicine (Lond). 2017 Mar;12(6):639-656. doi: 10.2217/nnm-2016-0380. *(IF = 4.727)*

5) Kopecka J, Rankin GM, **Salaroglio IC**, Poulsen SA, Riganti C. P-glycoprotein-mediated chemoresistance is reversed by carbonic anhydrase XII inhibitors. Oncotarget. 2016 Dec 27;7(52):85861-85875. doi: 10.18632/oncotarget.13040. *(IF = 5.168)*

6) Buondonno I, Gazzano E, Jean SR, Audrito V, Kopecka J, Fanelli M, **Salaroglio IC**, Costamagna C, Roato I, Mungo E, Hattinger CM, Deaglio S, Kelley SO, Serra M, Riganti C. Mitochondria-targeted doxorubicin: a new therapeutic strategy against doxorubicin-resistant osteosarcoma. Mol Cancer Ther. 2016 Nov;15(11):2640-2652. doi: 10.1158/1535-7163.MCT-16-0048. (*IF = 5.764)*

7) **Salaroglio IC**, Campia I, Kopecka J, Gazzano E, Orecchia S, Ghigo D, Riganti C. Zoledronic acid overcomes chemoresistance and immunosuppression of malignant mesothelioma. Oncotarget. 2015 Jan 20;6(2):1128-42. doi:10.18632/oncotarget.2731. *(IF = 5.168)*

8) Pinzón-Daza ML, **Salaroglio IC**, Kopecka J, Garzòn R, Couraud PO, Ghigo D, Riganti C (2014) The cross-talk between canonical and non-canonical Wnt-dependent pathways regulates P-glycoprotein expression in human blood-brain barrier cells. J Cereb Blood Flow Metab. 2014 Aug;34(8):1258-69. doi: 10.1038/jcbfm.2014.100. *(IF = 5.081)*

9) Riganti C, **Salaroglio IC**, Pinzòn-Daza ML, Caldera V, Campia I, Kopecka J, Mellai M, Annovazzi L, Couraud PO, Bosia A, Ghigo D, Schiffer D. Temozolomide downregulates P-glycoprotein in human blood-brain barrier cells by disrupting Wnt3 signaling. Cell Mol Life Sci. 2014 Feb;71(3):499-516. doi: 10.1007/s00018-013-1397-y. *(IF = 7.786)*

10. PhD ACTIVITIES

Congresses:

- 9th International Conference of Anticancer Research, 6-10 October 2014, Sinthonia, Greece. *P-glycoprotein is up-regulated by autocrine Wnt3a in Glioblastoma stem cells.* **Salaroglio IC,** Caldera V, Campia I, Kopecka J, Mellai M, Annovazzi L, Bosia A, Ghigo D, Riganti C. Selected for <u>oral presentation.</u>

- 3th International Michelangelo Conference: Promise and Challenges of Developing new drugs in Oncology, 2 - 3 July 2015, Museo della Scienza e della Tecnologia, Milan.

- Frontiers in Regenerative Medicine, 18-20 February 2015, Molecular Biotechnology Center, Turin.

- 2nd Zing Barriers of The CNS Conference, 27-30 September 2015, Parador de Oropesa, Spain. *The degree of differentiation of glioblastoma cells influences the permeability of blood-brain barrier.* Salaroglio IC, Caldera V, Ghigo D, Couraud PO, Schiffer D, Riganti C.
  Selected for <u>oral presentation.</u>

- Unito-Polito Conference series in cancer: Enabling technologies in 3D cancer organoids, 8-9 March 2016, Molecular Biotechnology Center, Turin.

- 1st Young Scientist Workshop on Stem Cell Niche: From basic science to clinical application, 8-10 May 2016, Pavia, Italy. *Glioblastoma stem cells influence the permeability of blood-brain barrier.* **Salaroglio IC**, Caldera V, Pierre-Olivier Couraud, Davide Schiffer, Riganti C.
  Selected for <u>oral presentation.</u>

- Optimization of Oncology Therapy: Novel Drugs Affecting Multidrug Resistance, University of Siena, 3-4 November 2016, Siena, Italy. *New inhibitors of P-glycoprotein increasing drug delivery across brain-blood barrier.* **Salaroglio IC**, Abate C, Gazzano E, Annovazzi L, Mellai M, Berardi F, Schiffer D, Riganti C.
  Selected for <u>oral presentation.</u>

- 19th Barrier and Transporter meeting, 15-17 May 2017, Bad Herrenalb, Germany. *Glioblastoma stem cells influence the permeability of blood-brain barrier.* **Salaroglio IC**, Kopecka J, Milosevic V, Caldera V, Mellai M, Annovazzi L, Couraud PO, Schiffer D, Riganti C.
  Selected for <u>poster.</u>

- 4th International Michelangelo Conference, 6-7 July 2017, Milan, Italy. *Chemoresistance of glioblastoma-derived stem cells is overcome by anhydrase carbonic XII inhibitors.* **Salaroglio IC**, Mujumdar P, Annovazzi L, Mellai M, Kopecka J, Schiffer D, Poulsen SA, Riganti C.
  Selected for <u>oral presentation.</u>

- 2017 D-Day, University of Turin, 19 September 2017, Molecular Biotechnology Center, Italy. *Chemoresistance of glioblastoma-derived stem cells is overcome by anhydrase carbonic XII inhibitors.* **Salaroglio IC**, Mujumdar P, Annovazzi L, Mellai M, Kopecka J, Schiffer D, Poulsen SA, Riganti C.
  Selected for <u>poster.</u>

- 30th annual Conference of Italian Association of Cell Cultures: Tumor-Immune cell interface in solid and hematological malignancies, November 27-28 November 2017, Milan, Italy.

Attended courses:
- Bibliographic Research, 16-23 September 2014, Torino Esposizione, Turin.
- Meeting on health and safety at workplaces, 13 February 2015, Centro Didattico del Polo Universitario San Luigi Gonzaga, Turin.
- Biostatistics course, June 2015, Molecular Biotechnology Center, Turin.
- Scientific English course (B1/B2 level), November 2015 - March 2016, Molecular Biotechnology Center, Turin.
- General Project Writing, 8 March 2017, Aula Magna del Rettorato, Turin.
- Flow-cytometry course, 18 March 2017, IRCC institute, Candiolo, Turin.
- Management for Scientist, 12-16 June 2017, Molecular Biotechnology Center, Turin.
- Enhancement of PhD skills to help new PhD doctors out of University, 1 October 2017, Aula Magna del Rettorato, Turin.

Research experience:
2015: visiting scientist at Blood-Brain Barrier Laboratory (LBHE) at Univ. Artois, Lens, France; training session for BBB culture model derived from pluripotent stem cells; organotypic cultures.

Awards:
2016: FEBS (Federation of European Biochemical Societies) fellowship to attend the 41° FEBS congress.

Patents:
co-inventor of 1 patent
Title: CARBONIC ANHYDRASE INHIBITORS
Inventors: Riganti Chiara, Salaroglio Iris Chiara, Mujumdar Prashant, Poulsen Sally-Ann
Filed in Brisbane, Australia, 12 May 2017 (n° 35100AU1-DMK)

11. AKNOWLEDGMENTS